MIMO-OFDM for LTE, Wi-Fi and WiMAX

MIMO-OFDM for LTE, Wi-Fi and WiMAX

Coherent versus Non-coherent and Cooperative Turbo Transceivers

L. Hanzo, J. Akhtman, M. Jiang and L. Wang

All of
University of Southampton, UK

WILEY
A John Wiley and Sons, Ltd, Publication

This edition first published 2010

Registered office
John Wiley & Sons Ltd, The Atrium, Southern Gate, Chichester, West Sussex, PO19 8SQ, United Kingdom

For details of our global editorial offices, for customer services and for information about how to apply for permission to reuse the copyright material in this book please see our website at www.wiley.com.

Library of Congress Cataloging-in-Publication Data

Hanzo, Lajos, 1952–
MIMO-OFDM for LTE, WIFI, and WIMAX : coherent versus non-coherent and cooperative turbo-transceivers / by L. Hanzo, J. Akhtman, M. Jiang, L. Wang.
p. cm.
Includes bibliographical references and index.
ISBN 978-0-470-68669-0 (cloth)
1. Orthogonal frequency division multiplexing. 2. MIMO systems. 3. Wireless LANs–Equipment and supplies. 4. IEEE 802.11 (Standard). 5. IEEE 802.16 (Standard) 6. Radio–Transmitter-receivers. I. Akhtman, J. (Jos) II. Wang, L. (Li), 1982- III. Title.
TK5103.484.H36 2010
621.382’16–dc22

2010015324

A catalogue record for this book is available from the British Library.

ISBN 9780470686690 (H/B)

Set in 9/11pt Times by Sunrise Setting Ltd, Torquay, UK.
Printed in Singapore by Markono Print Media Pte Ltd.

We dedicate this monograph to the numerous contributors to this field, many of whom are listed in the Author Index

The MIMO capacity theoretically increases linearly with the number of transmit antennas, provided that the number of receive antennas is equal to the number of transmit antennas. With the further proviso that the total transmit power is increased proportionately to the number of transmit antennas, a linear capacity increase is achieved on increasing the transmit power. However, under realistic conditions the theoretical MIMO-OFDM performance erodes, hence, to circumvent this degradation, our monograph is dedicated to the design of practical coherent, non-coherent and cooperative MIMO-OFDM turbo transceivers…

Contents

[1]This chapter is partially based on ©IEEE Jiang & Hanzo 2006 [1]

[2]This chapter is partially based on ©IET Jiang & Hanzo 2006 [2]

[3]This chapter is partially based on ©IEEE Jiang, Akhtman & Hanzo 2007 [3]

[4] This chapter is partially based on ©IEEE Wang & Hanzo 2007 [4]

[5] This chapter is partially based on ©IEEE Wang & Hanzo 2007 [7]

[6]This chapter is partially based on ©IEEE Wang & Hanzo 2007 [8]

[7]This chapter is partially based on ©IEEE Akhtman, Wolfgang, Chen & Hanzo 2007 [9]

Chapter 12

Multiple-Symbol Differential Sphere Detection for Differentially Modulated Cooperative OFDM Systems

12.1 Introduction [1]

Multiple-antenna-aided transmit diversity arrangements [596] constitute powerful techniques of mitigating the deleterious effects of fading, hence improving the end-to-end system performance, which is usually achieved by multiple co-located antenna elements at the transmitter and/or receiver, as discussed in Chapter 11. However, in cellular communication systems, it is often impractical for the mobile to employ several antennas for the sake of achieving a diversity gain owing to its limited size. Furthermore, owing to the limited separation of the antenna elements, they rarely experience independent fading, which limits the achievable diversity gain and may be further compromised by the detrimental effects of the shadow fading, imposing further signal correlation among the antennas in their vicinity. Fortunately, as depicted in Figure 12.1, in multi-user wireless systems mobiles may cooperatively share their antennas in order to achieve uplink transmit diversity by forming a Virtual Antenna Array (VAA) in a distributed fashion. Thus, so-called cooperative diversity relying on the cooperation among multiple terminals may be achieved [597, 598].

On the other hand, in order to carry out classic coherent detection, channel estimation is required at the receiver, which relies on using training pilot signals or tones and exploits the fact that in general the consecutive CIR taps are correlated in both the time and frequency domains of the OFDM subchannels. However, channel estimation for an M-transmitter, N-receiver MIMO system requires the estimation of $(M \times N)$ CIRs, which imposes both an excessive complexity and a high pilot overhead, especially in mobile environments associated with relatively rapidly fluctuating channel conditions. Therefore, in such situations, differential encoded transmissions combined with non-coherent detection and hence requiring no CSI at the receiver become an attractive design alternative, leading to differential-modulation-assisted cooperative communications [598]. Three different channel models corresponding

[1] This chapter is partially based on ©IEEE Wang & Hanzo 2007 [7]

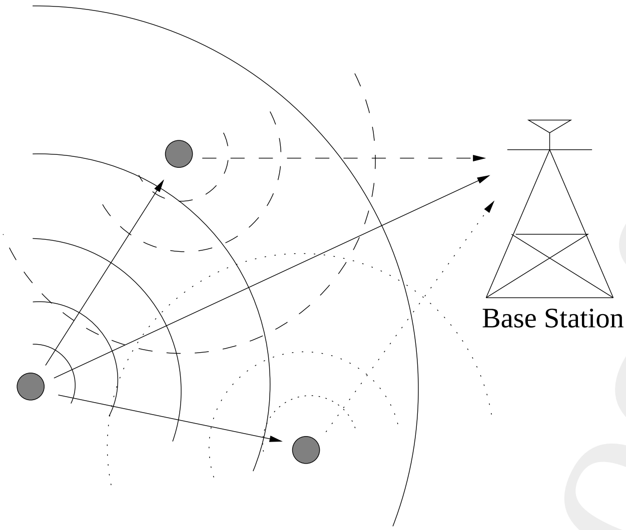

Figure 12.1: Cooperative diversity exploiting cooperation among multiple terminals.

Table 12.1: Channel models considered: sampling frequency $f_s = 10\,\text{MHz}$ and the unit of the power profile is decibels.

Channel models	
Typical urban	Parameter
No. of taps	$N_{taps} = 6$
Power profile	$\boldsymbol{\sigma} = [-7.219\,04 - 4.219\,04 - 6.219\,04 - 10.219 - 12.219 - 14.219]$
Delay profile	$\boldsymbol{\tau} = [0\ 2\ 6\ 16\ 24\ 50]$
Rural area	Parameter
No. of taps	$N_{taps} = 4$
Power profile	$\boldsymbol{\sigma} = [-2.407\,88 - 4.407\,88 - 12.4079 - 22.4079]$
Delay profile	$\boldsymbol{\tau} = [0\ 2\ 4\ 6]$
Hilly terrain	Parameter
No. of taps	$N_{taps} = 6$
Power profile	$\boldsymbol{\sigma} = [-4.053\,25 - 6.053\,25 - 8.053\,25 - 11.0533 - 10.0533 - 16.0533]$
Delay profile	$\boldsymbol{\tau} = [0\ 2\ 4\ 6\ 150\ 172]$

to three distinct communication environments will be considered in this chapter, namely the Typical Urban (TH), the Rural Area (RA) and the Hilly Terrain (HT) scenarios summarized in Table 12.1.

12.1.1 Differential Phase-Shift Keying and Detection

12.1.1.1 Conventional Differential Signalling and Detection

In this section, we briefly review the conventional differential encoding and detection process. Let $\mathcal{M}_c$ denote an M_c-ary PSK constellation which is defined as the set $\{2\pi m/M_c; m = 0, 1, \ldots, M_c - 1\}$, where $v[n] \in \mathcal{M}_c$ represent the data to be transmitted over a slow-fading frequency-flat channel. The differential signalling process commences by transmitting a single reference symbol $s[0]$, which is

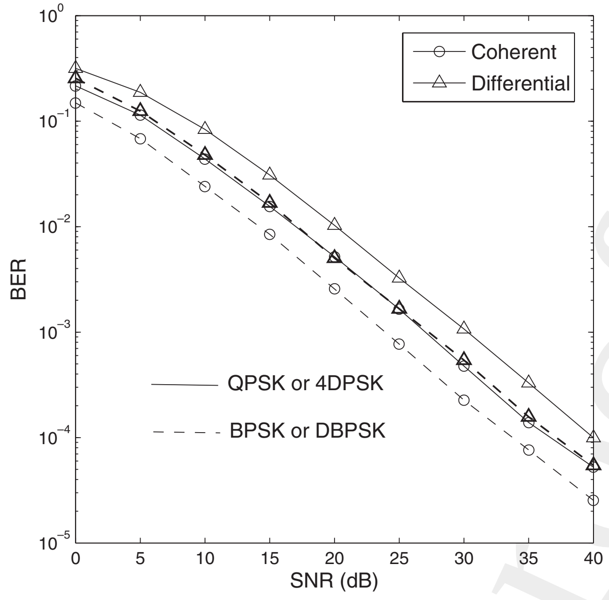

Figure 12.2: BER performance comparison between conventional coherent and differential detection in an SISO system.

normally set to unity, followed by a differential encoding process, which can be expressed as

$$s[n] = s[n-1]v[n], \tag{12.1}$$

where $s[n-1]$ and $s[n]$ represent the symbols transmitted during the $(n-1)$th and nth time slots, respectively.

By representing the signals arriving at the receiver corresponding to the $(n-1)$th and nth transmitted symbols as

$$y[n-1] = h[n-1]s[n-1] + w[n-1], \tag{12.2}$$

$$y[n] = [n]s[n] + w[n], \tag{12.3}$$

respectively, and assuming a slow-fading channel, i.e. $h[n-1] = h[n]$, we arrive at

$$y[n] = h[n-1]s[n-1]v[n] + w[n] \tag{12.4}$$

$$= y[n-1]v[n] + \underbrace{w[n] - w[n-1]v[n]}_{w'[n]}, \tag{12.5}$$

where $w[n-1]$ and $w[n]$ denote the AWGN with a variance of $2\sigma_w^2$ added at the receiver during the two consecutive time slots. Consequently, the differentially encoded data $v[n]$ can be recovered in the same manner as in the conventional coherent detection scheme in a single-input, single-output context by using $y[n-1]$ as the reference signal of the differential detector. This is achieved without any CSI at the expense of a 3 dB performance loss in comparison with its coherent counterpart caused by the doubled noise $w'[n]$ at the decision device, which has a variance of $4\sigma_w^2$. This can be verified by the BER curves of the single-antenna-aided OFDM system characterized in Figure 12.2 for two different throughputs, i.e. for 1 bits per symbol and for 2 bits per symbol, respectively. The other system parameters are summarized in Table 12.2.

Table 12.2: Summary of system parameters for differential-modulation-aided OFDM system.

System parameters	Choice
System	OFDM
Subcarrier BW	$\Delta f = 10\,\text{kHz}$
Number of subcarriers	$D = 1024$
Modulation	DPSK in time domain
Normalized Doppler freq.	$f_d = 0.001$
Channel model	Typical urban, refer to Table 12.1

12.1.1.2 Effects of Time-Selective Channels on Differential Detection

Apart from the 3 dB performance loss suffered by Conventional Differential Detection (CDD) in slow-fading scenarios as discussed in Section 12.1.1, an error floor may be encountered by the CDD in fast-fading channels, if DPSK modulation is carried out in the time direction, i.e. for the same subcarrier of consecutive OFDM symbols, since the fading channel is deemed to be more correlated between the same subcarrier of consecutive OFDM symbols than between adjacent subcarriers of a given OFDM symbol. In other words, the assumption that $h[n-1] = h[n]$ no longer holds, leading to unrecoverable phase information between consecutive transmitted DPSK symbols even in the absence of noise. Furthermore, all the channel models considered in Table 12.1 exhibit temporally Rayleigh-distributed fading for each of the D subcarriers employed by the OFDM system with the autocorrelation function expressed as

$$\varphi_{hh}^{t}[\kappa] \triangleq \mathcal{E}\{h[n+\kappa]h^*[n]\} \tag{12.6}$$

$$= J_0(2\pi f_d \kappa), \tag{12.7}$$

where $J_0(\cdot)$ denotes the zeroth-order Bessel function of the first kind and f_d is the normalized Doppler frequency.

Figure 12.3(a) depicts the magnitude of the temporal correlation function for various normalized Doppler frequencies f_d, while Figure 12.3(b) plots the corresponding BER curves of the DQPSK-modulated CDD-aided OFDM system with the system parameter summarized in Table 12.2. Given a Doppler frequency of $f_d = 0.001$, the BER curves decrease continuously as the SNR increases. However, the BER curve tends to create an error floor when f_d becomes high, which is caused by the relative mobility between the transmitter and the receiver. For example, with a relatively high Doppler frequency of $f_d = 0.03$, the magnitude of the temporal correlation function of the typical urban channel model of Table 12.1 decreases rapidly as κ increases. Therefore, the CDD, which is capable of achieving a desirable performance in slow-fading channels, suffers from a considerable performance loss when the transmit terminal is moving at a high speed relative to the receiver.

12.1.1.3 Effects of Frequency-Selective Channels on Differential Detection

Our discussions in Section 12.1.1.2 were focused on the CDD employing differentially encoded modulation along the Time Domain (TD) – which is referred to here as T-DQPSK modulation – for each of the D subcarriers of an OFDM system. In general, the time- and frequency-domain differential encoding have their own merits. Specifically, the T-DQPSK-modulated OFDM system is advantageous for employment in continuous transmissions, because the effective throughput remains high, since the overhead constituted by the reference symbol $s[0]$ tends to zero in conjunction with a relatively large transmission block/frame size, namely with an increasing transmission frame duration. However, T-DQPSK-aided OFDM is less suitable for burst transmission, when the consecutive OFDM symbols may experience fairly uncorrelated fading. Hence, employment of frequency-domain differentially encoded modulation – which is referred to here as F-DPSK – is preferable for the above-mentioned scenario. Before investigating the impact of the channel's frequency selectivity for the channel models

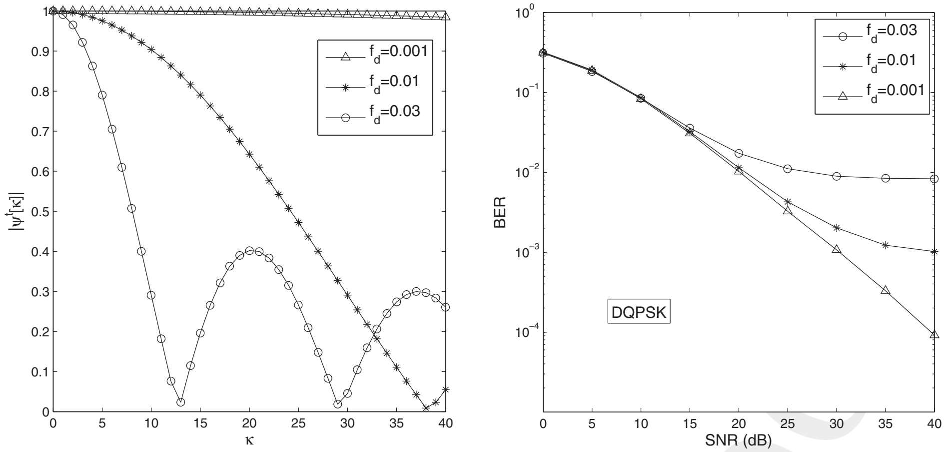

(a) Magnitude of temporal correlation function of Rayleigh fading channels

(b) Effects of Doppler frequency on performance of CDD

Figure 12.3: Impact of mobility on the performance of CDD.

summarized in Table 12.1 on performance of the CDD, we review the frequency-domain (FD) autocorrelation function of OFDM having D active subcarriers and a subcarrier frequency spacing of Δf, which can be expressed as

$$\varphi_{hh}^{f}[\mu] \triangleq \mathcal{E}\{h[k+\mu]h^{*}[k]\}, \tag{12.8}$$

$$= \sum_{l-1}^{N_{taps}} \sigma_l^2 e^{-j2\pi\mu\Delta f \tau_l}, \tag{12.9}$$

where N_{taps}, σ_l and τ_l represent the number of paths, the elements of the power profile $\boldsymbol{\sigma}$ and the delay profile $\boldsymbol{\tau}$ of the channel models given by Table 12.1, respectively.

Accordingly, Figure 12.4(a) depicts the magnitude of the FD autocorrelation function for the three different channel models of Table 12.1, namely the TU, RA and HT channel models, assuming that we have $D = 1024$ and $\Delta f = 10$ kHz. Note that the OFDM symbol duration is

$$T_f = DT_s + T_g, \tag{12.10}$$

where $T_s = 1/(\Delta f D)$ is the OFDM symbol duration and T_g denotes the guard interval. We observe that the magnitude of the spectral correlation of the RA channel model decreases slowly as μ increases, since the maximum path delay τ_{max} is as small as $6T_s$. Thus, a moderately frequency-selective channel is expected, resulting in a gracefully decreasing BER curve, as observed in Figure 12.4(b), where the BER curves corresponding to the TU and HT channel models were also plotted. The latter two BER curves exhibit an error floor as the SNR increases, especially the one corresponding to the HT scenario. This is not unexpected, since we observe a sharp decay in $|\varphi_{hh}^{f}[\mu]|$ during the interval $(\mu = 0, 1, \ldots, 4)$ and a 'strong non-concave' behaviour for $|\varphi_{hh}^{f}[\mu]|$, as seen in Figure 12.4(a). This is caused by the large maximum path delay of $\tau_{max} = 172T_s$.

12.1.2 Chapter Contributions and Outline

As observed in Sections 12.1.1.2 and 12.1.1.3, significant channel-induced performance degradations suffered by the CDD-aided direct-transmission-based OFDM system simply imply that the cooperative diversity gains achieved by the cooperative system may erode as the relative mobile velocities of the

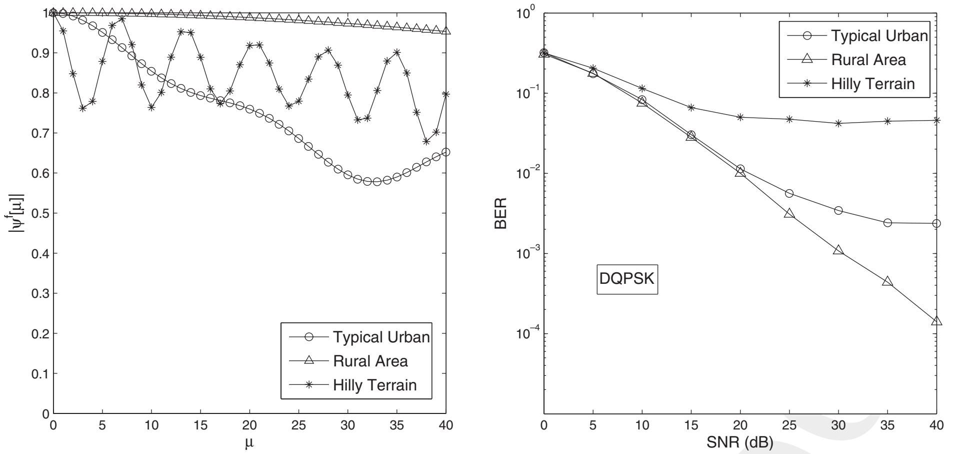

(a) Magnitude of frequency correlation function of Rayleigh fading channels

(b) Effects of frequency-selective channel on performance of CDD

Figure 12.4: Impact of frequency-selective channels on the performance of CDD.

cooperating users with respect to both each other and the BS increase. The detrimental effects of highly time-selective channels imposed on the T-DQPSK-modulated scenario were characterized in Figure 12.3(b), while those of heavily frequency-selective channels on the F-DPSK-modulated system were quantified in Figure 12.4(b). In order to eliminate this performance erosion and still achieve full cooperative diversity in conjunction with differential detection in wideband OFDM-based cooperative systems, in Section 12.2 we will invoke the Multiple-Symbol Differential Sphere Detection (MSDSD) technique, which was proposed by Lutz *et al.* in [599] in order to cope with fast-fading channels in SISO narrowband scenarios. We will demonstrate in Section 12.3 that, although a simple MSDSD scheme may be implemented at the relay, more powerful detection schemes are required at the BS of both the DAF- and DDF-aided cooperative systems in order to achieve a desirable end-to-end performance. Hence, the novel contributions of this chapter are as follows:

- A generalized equivalent multiple-symbol-based system model is constructed for the differentially encoded cooperative system using either the Differential Amplify-and-Forward (DAF) or Differential Decode-and-Forward (DDF) scheme.
- With the aid of the multi-layer search tree mechanism proposed for the SD in Chapter 11 in the context of the SP-modulated MIMO system, the MSDSD is specifically designed for both the DAF- and DDF-aided cooperative systems based on the above-mentioned generalized equivalent multiple-symbol system model. Our design objective is to retain the maximum achievable diversity gains at high mobile velocities, e.g. when T-DQPSK is employed, while imposing a low complexity.

The remainder of this chapter is organized as follows. The principle of the single-path MSDSD, which was proposed for employment in SISO systems, is reviewed in Section 12.2, where we will demonstrate that the MSDSD is capable of significantly mitigating the channel-induced error floor for both T-DQPSK- and F-DPSK-modulated OFDM systems, provided that the second-order statistics of the fading and noise are known at the receiver. Given the duality of the time and frequency dimensions, we will only consider the T-DQPSK-modulated system in Section 12.3, where we focus our attention on the multi-path MSDSD design, which is detailed for both the DAF- and DDF-aided cooperative cellular UL. The construction of the generalized equivalent multiple-symbol cooperative system model is detailed in Section 12.3.3.1. Finally, we provide our concluding remarks in Section 12.4 based on the simulation results of Section 12.3.4.

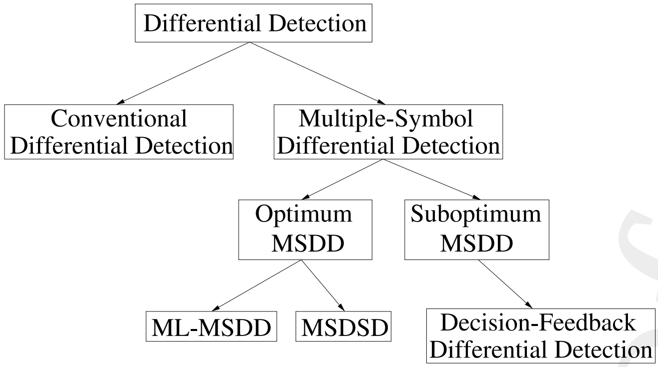

Figure 12.5: Differential detection classification.

12.2 The Principle of Single-Path MSDSD [599]

Differential detection schemes may be broadly divided into two categories, namely CDD and Multiple-Symbol Differential Detection (MSDD), as seen in Figure 12.5. Since a data symbol is mapped to the phase difference between the successive transmitted PSK symbols, CDD estimates the data symbol by directly calculating the phase difference of the two successive received symbols. In contrast to CDD having an observation window size of $N_{wind} = 2$, the MSDD collects $N_{wind} > 2$ consecutively received symbols for joint detection of the $(N_{wind} - 1)$ data symbols. This family may be further divided into two subgroups, namely the optimum maximum-likelihood (ML)-MSDD and suboptimum MSDD schemes, as seen in Figure 12.5. The ML-MSDD is the optimum scheme in terms of performance, but it exhibits a potentially excessive computational complexity in conjunction with a large observation window size N_{wind}. One of the suboptimum approaches that may be employed to achieve a low-complexity near-ML-MSDD is the linear-prediction-based Decision-Feedback Differential Detection (DFDD). Recently, the SD algorithm [562] was also used to resolve the complexity problem imposed by the ML-MSDD without sacrificing the achievable performance [599–602], leading to the so-called MSDSD arrangement, which will be introduced in the forthcoming sections.

12.2.1 ML Metric for MSDD

The basic idea behind ML-MSDD is the exploitation of the correlation between the phase distortions experienced by the consecutive N_{wind} transmitted DPSK symbols [603]. In other words, the receiver makes a decision about a block of $(N_{wind} - 1)$ consecutive symbols based on N_{wind} received symbols, enabling the detector to exploit the statistics of the fading channels. Ideally, the error floor encountered when performing CDD as observed in Figure 12.3 and Figure 12.4 can be essentially eliminated, provided that the value of N_{wind} is sufficiently high.

More explicitly, the MSDD at the receiver jointly processes the ith received symbol vector consisting of N_{wind} consecutively received symbols

$$\mathbf{y}[i_{N_{wind}}] \triangleq [y[(N_{wind}-1)i-(N_{wind}-1)], \ldots, y[(N_{wind}-1)i]]^T, \tag{12.11}$$

where $i_{N_{wind}}$ is the symbol vector index, in order to generate the ML estimate vector $\hat{\mathbf{s}}[i_{N_{wind}}]$ of the corresponding N_{wind} transmitted symbols

$$\mathbf{s}[i_{N_{wind}}] \triangleq [s[(N_{wind}-1)i-(N_{wind}-1)], \ldots, s[(N_{wind}-1)i]]^T. \tag{12.12}$$

Then, when using differential decoding by carrying out the inverse of the differential encoding process of Equation (12.1), the estimated vector $\hat{\mathbf{v}}[i_{N_{wind}}]$ of the corresponding $(N_{wind} - 1)$ differentially encoded data symbols

$$\mathbf{v}[i_{N_{wind}}] \triangleq [v[(N_{wind}-1)i-(N_{wind}-2)],\ldots,v[(N_{wind}-1)i]]^T \tag{12.13}$$

can be attained. Note that, due to differential encoding, consecutive blocks $\mathbf{y}[i_{N_{wind}}]$ overlap by one scalar received symbol [604]. For the sake of representational simplicity, we omit the symbol block index $i_{N_{wind}}$ without any loss of generality.

Under the assumption that the fading is a complex-valued zero-mean Gaussian process with a variance of σ_h^2 and that the channel noise has a variance of $2\sigma_w^2$, the PDF of the received symbol vector $\mathbf{y} = [y_0, y_1, \ldots, y_{N_{wind}-1}]^T$ conditioned on the transmitted symbol vector $\mathbf{s} = [s_0, s_1, \ldots, s_{N_{wind}-1}]^T$ spanning N_{wind} symbol periods is expressed as [599]

$$p(\mathbf{y}|\mathbf{s}) = \frac{\exp(-Tr\{\mathbf{y}^H\Psi^{-1}\mathbf{y}\})}{(\pi^{N_{wind}}det\Psi)}, \tag{12.14}$$

where

$$\Psi = \mathcal{E}\{\mathbf{y}\mathbf{y}^H|\mathbf{s}\} \tag{12.15}$$

denotes the conditional autocorrelation matrix of the Rayleigh fading channel. Then, the ML solution which maximizes the probability of Equation (12.14) can be obtained by exhaustively searching the entire transmitted symbol vector space. Thus, the ML metric of the MSDD can be expressed as [604]

$$\hat{\mathbf{s}}_{ML} = \arg\max_{\check{\mathbf{s}}\in\mathcal{M}_c^{N_{wind}}} p(\mathbf{y}|\check{\mathbf{s}}) \tag{12.16}$$

$$= \arg\min_{\check{\mathbf{s}}\in\mathcal{M}_c^{N_{wind}}} Tr\{\mathbf{y}^H\Psi^{-1}\mathbf{y}\}. \tag{12.17}$$

12.2.2 Metric Transformation

In order to elaborate further on the ML metric of Equation (12.16), we extended the conditional autocorrelation matrix Ψ as [599]:

$$\Psi = \mathcal{E}\{\mathbf{y}\mathbf{y}^H|\mathbf{s}\}, \tag{12.18}$$

$$= \mathrm{diag}(\mathbf{s})\mathcal{E}\{\mathbf{h}\mathbf{h}^H\}\mathrm{diag}(\mathbf{s}^H) + \mathcal{E}\{\mathbf{n}\mathbf{n}^H\}, \tag{12.19}$$

$$= \mathrm{diag}(\mathbf{s})(\mathcal{E}\{\mathbf{h}\mathbf{h}^H\} + 2\sigma_w^2\mathbf{I}_{N_{wind}})\mathrm{diag}(\mathbf{s}^H), \tag{12.20}$$

$$= \mathrm{diag}(\mathbf{s})\,\mathbf{C}\,\mathrm{diag}(\mathbf{s}^H), \tag{12.21}$$

where $\mathcal{E}\{\mathbf{h}\mathbf{h}^H\}$ is the channel's covariance matrix in either the time or the frequency domain, which is determined by the specific domain of the differential encoding. More explicitly, the elements of the covariance matrix $\mathcal{E}\{\mathbf{h}\mathbf{h}^H\}$ can be computed by Equation (12.7), when differential encoding at the transmitter is carried out along the TD. Otherwise, we employ Equation (12.9) to obtain the covariance matrix, when differential encoding is employed in the FD. Furthermore, in the context of Equation (12.21) we define

$$\mathbf{C} \triangleq (\mathcal{E}\{\mathbf{h}\mathbf{h}^H\} + 2\sigma_w^2\mathbf{I}_{N_{wind}}) \tag{12.22}$$

in order to simplify Equation (12.20).

Since we have $\mathrm{diag}(\mathbf{s})^{-1} = \mathrm{diag}(\mathbf{s})^H = \mathrm{diag}(\mathbf{s}^*)$, the ML decision rule of Equation (12.17) can be reformulated as

$$\hat{\mathbf{s}}_{ML} = \underset{\mathbf{s}\in\mathcal{M}_c^{N_{wind}}}{\arg\min}\ \{\mathbf{y}^H \Psi^{-1}\mathbf{y}\} \tag{12.23}$$

$$= \underset{\mathbf{s}\in\mathcal{M}_c^{N_{wind}}}{\arg\min}\ \{\mathbf{y}^H \mathrm{diag}(\mathbf{s})\ \mathbf{C}^{-1}\ \mathrm{diag}(\mathbf{s})^H \mathbf{y}\} \tag{12.24}$$

$$= \underset{\mathbf{s}\in\mathcal{M}_c^{N_{wind}}}{\arg\min}\ \{\mathbf{s}\ \mathrm{diag}(\mathbf{y})^H \mathbf{C}^{-1} \mathrm{diag}(\mathbf{y})\mathbf{s}^*\} \tag{12.25}$$

$$= \underset{\mathbf{s}\in\mathcal{M}_c^{N_{wind}}}{\arg\min}\ \{\mathbf{s}\ \mathrm{diag}(\mathbf{y})^H \mathbf{F}^H \mathbf{F}\ \mathrm{diag}(\mathbf{y})\mathbf{s}^*\}, \tag{12.26}$$

where $\mathbf{F}$ is an upper-triangular matrix obtained using the Cholesky factorization of the inverse matrix $\mathbf{C}^{-1}$, i.e. we have

$$\mathbf{C}^{-1} = \mathbf{F}^H \mathbf{F}. \tag{12.27}$$

Then, by further defining an upper-triangular matrix as

$$\mathbf{U} \triangleq (\mathbf{F}\ \mathrm{diag}(\mathbf{y}))^*, \tag{12.28}$$

we finally arrive at [599]

$$\hat{\mathbf{s}}_{ML} = \underset{\mathbf{s}\in\mathcal{M}_c^{N_{wind}}}{\arg\min}\ \{\|\mathbf{U}\mathbf{s}\|^2\}, \tag{12.29}$$

which completes the process of transforming the ML-MSDD metric of Equation (12.17) to a *shortest-vector* problem [599].

12.2.3 Complexity Reduction Using SD

While the performance of the MSDD improves steadily as N_{wind} is increased, the drawback is its potentially excessive computational complexity, which increases exponentially with N_{wind}. On the other hand, SD algorithms [562, 566, 605] are well known for their efficiency when solving the so-called shortest-vector problem in the context of multi-user, multi-stream detection in MIMO systems. Thus, due to the upper-triangular structure of the $\mathbf{U}$ matrix, the traditional SD algorithm can be employed to solve the shortest-vector problem as indicated by Equation (12.29). Consequently, the ML solution of the ML-MSDD metric of Equation (12.17) can be obtained on a component-by-component basis at a significantly lower complexity. Note that all the SD algorithms discussed in Chapter 9 can be employed to solve the shortest-vector problem of Equation (12.29).

12.2.4 Simulation Results

Monte Carlo simulations are provided in this section in order to characterize the achievable performance and the complexity imposed by the MSDSD for both TD and FD differentially encoded OFDM systems. The simulation parameters are summarized in Table 12.3.

12.2.4.1 Time-Differential-Encoded OFDM System

Let us now consider the application of the MSDSD in the TD differentially encoded OFDM system for three different normalized Doppler frequencies in the presence of the typical urban channel given by Table 12.1. The T-DQPSK modulation scheme is employed at the transmitter, while the MSDSD employing three different observation window sizes N_{wind} is used at the receiver, namely $N_{wind} = 2,\ 6,\ 9$. Note that, as mentioned in Section 12.1.1, when we have $N_{wind} = 2$ the MSDSD actually degenerates to the CDD. Additionally, since T-DQPSK is employed, a relatively short transmission frame length of 101 OFDM symbols is utilized in order to reduce the detection delay imposed by

Table 12.3: Simulation parameters for time-differential-modulation-aided OFDM system.

System parameters	Choice
System	OFDM
Subcarrier BW	$\Delta f = 10\,\text{kHz}$
Number of subcarriers	$D = 1024$
Modulation	T-DQPSK/F-DQPSK
Frame length	101 OFDM symbols
Normalized Doppler freq.	$f_d = 0.001, 0.01, 0.03$
Channel model	Typical urban if not specified

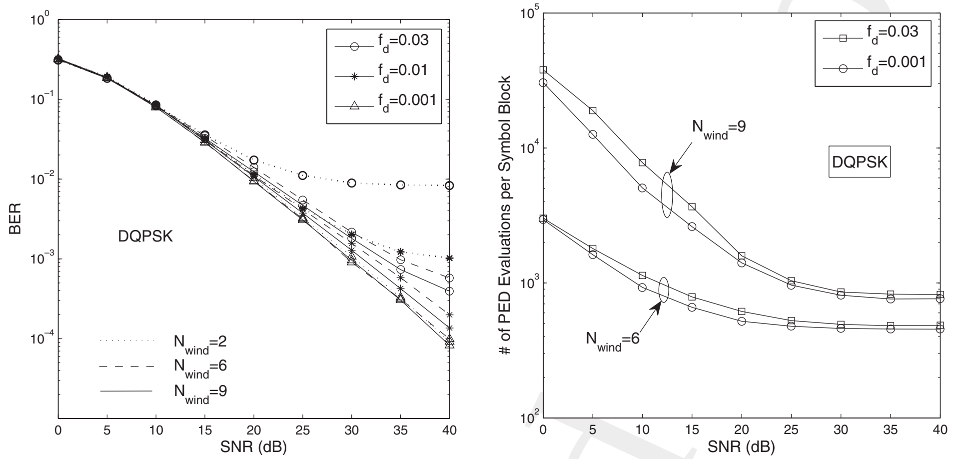

(a) BER performance of a T-DQPSK-modulated OFDM system using MSDSD in Rayleigh fading channels having different normalized Doppler frequencies

(b) Complexity imposed by the MSDSD versus the SNR

Figure 12.6: The application of MSDSD in the time-differential-modulated OFDM system.

the MSDSD. Figure 12.6(a) depicts the BER performance of the MSDSD for normalized Doppler frequencies $f_d = 0.03,\ 0.01,\ 0.001$, where we observe that for the slow-fading channel associated with $f_d = 0.001$, there is no need to employ an observation window size of more than $N_{wind} = 2$, since the CDD does not suffer from an error floor. In other words, the MSDSD is unable to improve the CDD's performance further by increasing N_{wind}. However, when the channel becomes more uncorrelated, i.e. when we have $f_d = 0.03$ or 0.01, the BER curve is shifted downwards by employing an N_{wind} value larger than 2, approaching that observed for $f_d = 0.001$, at the expense of imposing a higher computational complexity. The complexity imposed by the MSDSD versus the SNR is plotted in Figure 12.6(b), where the complexity curves corresponding to $N_{wind} = 9$ are evidently above those corresponding to $N_{wind} = 6$. Moreover, the complexity imposed by the MSDSD decreases steadily as the SNR increases and finally levels out in the high-SNR range. This is not unexpected, since under the assumption of having a reduced noise contamination, it is more likely that the ML solution point $\hat{\mathbf{s}}_{ML}$ is located near the search centre (the origin in this case) of the SD used for finding the MSDD solution. As a result, the SD's search process may converge much more rapidly, imposing a reduced complexity. Again, for more details about the characteristics of SDs, refer to Chapter 9. Furthermore, we can also observe from Figure 12.6(b) that the Doppler frequency has a crucial effect not only on the performance achieved by the MSDSD, but also on its complexity.

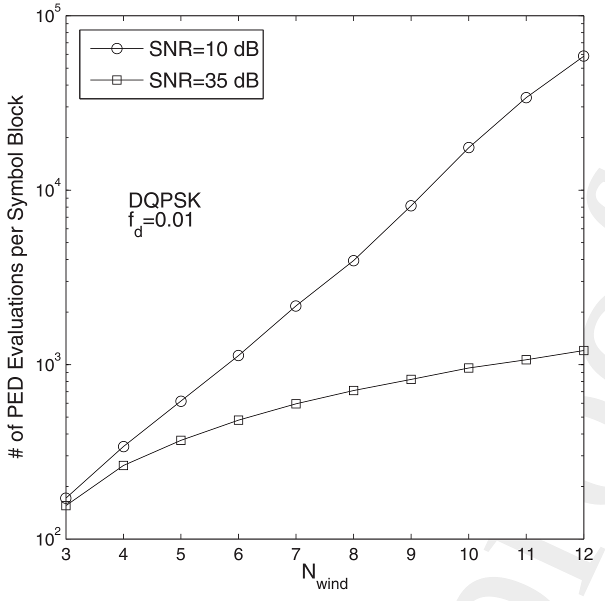

Figure 12.7: Complexity imposed by the MSDSD versus the observation window size N_{wind}.

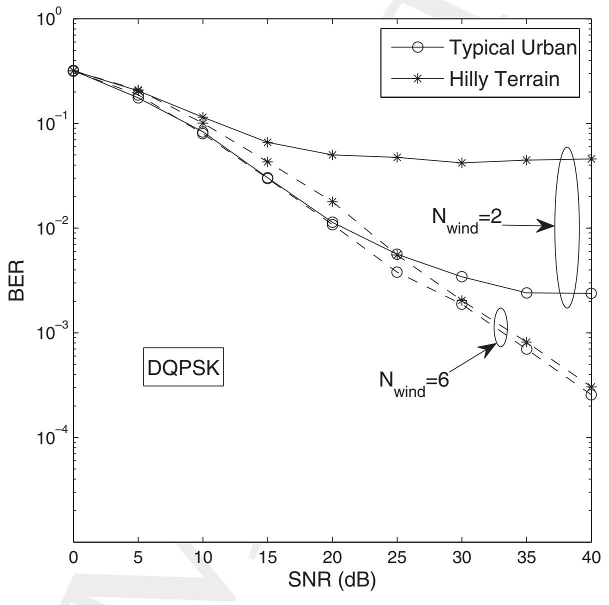

Figure 12.8: BER performance of F-DQPSK-modulated OFDM system using the MSDSD for the different channel models of Table 12.1.

Given a Doppler frequency of $f_d = 0.01$, let us now investigate the complexity of the MSDSD from a different angle by plotting the complexity versus N_{wind} in Figure 12.7, where complexity curves are drawn for two different SNRs. Although both of the curves exhibit an increase upon increasing the value of N_{wind}, the one corresponding to the relatively low SNR of 10 dB rises more sharply than the other one recorded for an SNR of 35 dB.

12.2.4.2 Frequency-Differential-Encoded OFDM System

As discussed in Section 12.1.1.3 for the scenario of burst transmissions or detection-delay-sensitive communications, F-DPSK is preferable to its TD counterpart. However, the channels experienced by the OFDM modem may exhibit a moderate time but a significant frequency selectivity, as exemplified by the TU and HT channel models given in Table 12.1. Therefore, the BER curves corresponding to the TU and HT channel models exhibit an error floor when using the CDD associated with $N_{wind} = 2$, as observed in Figure 12.8, due to the channel's frequency selectivity. Other simulation parameters are summarized in Table 12.3. Similar to the results obtained in the T-DPSK scenario, the error floor can be eliminated with the aid of the MSDSD, where the observation window size was $N_{wind} = 6$. Remarkably, a significant performance improvement is achieved by the MSDSD for the severely frequency-selective HT environment as seen in Figure 12.8. The BER curve associated with the CDD levels out as soon as the SNR increases beyond 20 dB, while the MSDSD using $N_{wind} = 6$ completely removes the error floor, resulting in a steadily decreasing BER curve as the SNR increases.

12.3 Multi-path MSDSD Design for Cooperative Communication

12.3.1 System Model

After the brief review on the principle of the MSDSD designed for single-path channels in Section 12.2, we continue by specifically designing an MSDSD scheme for the cooperative system discussed in Section 12.1. As depicted in Figure 12.9, we consider a U-user cooperation-aided system, where signal transmission involves two transmission phases, namely the broadcast phase and the relay phase, which are also referred to as phase I and II. A user who directly sends his/her own information to the destination is regarded as a *source* node, while the other users who assist in forwarding the information received from the source node are considered as *relay* nodes. In both phases, any of the well-established multiple-access schemes can be employed by the users to guarantee an orthogonal transmission among them, such as Time-Division Multiple Access (TDMA), Frequency-Division Multiple Access (FDMA) or Code-Division Multiple Access (CDMA). In this discussion, TDMA is considered for the sake of simplicity. Furthermore, due to the symmetry of channel allocation among users, as indicated in Figure 12.9, we focus our attention on the information transmission of source terminal T_S seen in Figure 12.10, which potentially employs $(U-1)$ relay terminals $T_{R_1}, T_{R_2}, \ldots, T_{R_{U-1}}$ in order to achieve cooperative diversity by forming a VAA. Without loss of generality, we simply assume the employment of a single antenna for each of the collaborating MSs and that of N receive antennas for the BS. Additionally, a unitary total power P shared by the collaborating MSs for transmitting a symbol is assumed.

Owing to the potential transmission inefficiency and implementational difficulty imposed by the channel estimation in cooperation-aided systems, differential encoding and detection without acquisition of the CSI is preferable to the employment of substantially more complex coherent transmission techniques, as we discussed in Section 12.1. Hence, we assume that in phase I, the source broadcasts its differentially encoded signals, while the destination as well as the relay terminals are also capable of receiving the signal transmitted by the source. In the forthcoming phase II, we consider two possible cooperation protocols which can be employed by the relay nodes: the relay node may either directly forward the received signal to the destination after signal amplification (the

Frequency	Phase I	Phase II		
Ch.1	T_1 transmits	T_2 relays T_1	$\cdots$	T_U relays T_1
Ch.2	T_2 transmits	T_3 relays T_2	$\cdots$	T_1 relays T_2
$\vdots$	$\vdots$	$\vdots$	$\ddots$	$\vdots$
Ch.N	T_U transmits	T_1 relays T_U	$\cdots$	T_{U-1} relays T_U

Time

Figure 12.9: Repetition-based channel allocation scheme.

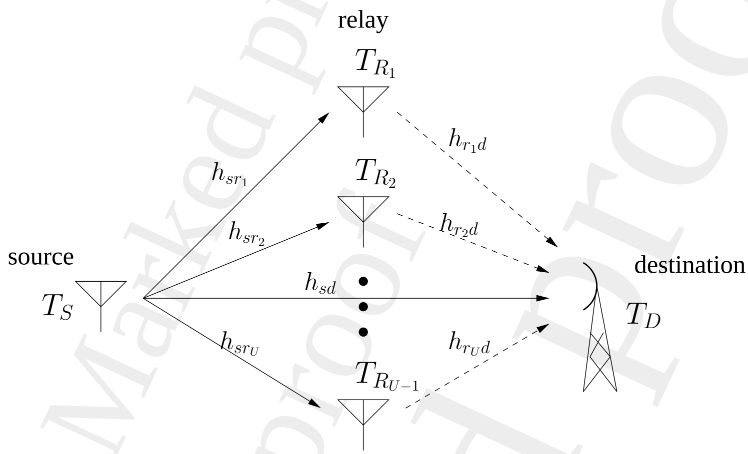

Figure 12.10: Cooperative communication schematic of multiple-relay nodes. ©IEEE Wang & Hanzo 2007 [7]

Amplify-and-Forward (AF) scheme) or differentially decode and re-encode the received signal before its retransmission (the Decode-and-Forward (DF) scheme).

Recall from Section 12.1.1.1 that the information is conveyed in the difference of the phases of two consecutive PSK symbols for differentially encoded transmission. In the context of the user cooperation-aided system of Figure 12.10, the source terminal T_S broadcasts the lth differentially encoded frame $\mathbf{s}^l$ during phase I, which consists of L_f DMPSK symbols $s[n]$ $(n = 1, 2, \ldots, L_f)$ given by Equation (12.1). According to Equation (12.1), the differential encoding process of the source node may be expressed as

$$s_s[n] = s_s[n-1]v_s[n], \tag{12.30}$$

where $v_{sd}[n] \in \mathcal{M}_c = \{e^{j2\pi m/M_c}; m = 0, 1, \ldots, M_c - 1\}$ is the information symbol obtained after bit-to-symbol mapping, and $s_{sd}[n] \in \mathcal{M}_c = \{e^{j2\pi m/M_c}; m = 0, 1, \ldots, M_c - 1\}$ represents the differentially encoded symbols during the nth time slot. We assume a total power of unity, i.e. $P = 1$, for transmitting a DMPSK symbol of the source over the entire user cooperation period and introduce the broadcast transmit power ratio η which is equal to the transmit power P_s employed by the source. Hence, during the forthcoming phase II, the total power consumed by all the $(U-1)$ relay nodes used for transmitting the signal received from the source is $\sum_{u=1}^{U-1} P_{r_u} = 1 - \eta$, where P_{r_u} is the power consumed by the relay terminal T_{R_u} for conveying the signal of the source node. To mitigate the impairments imposed by the time-selective channels on the T-DPSK-modulated transmission, frame-based rather than symbol-based user cooperation is carried out, which is achieved at the expense of both a higher detection delay and increased memory requirements.

Furthermore, according to the cooperative strategy of Figure 12.9, where each of the $(U-1)$ spatially dispersed relay nodes helps forward the signal from the source node to the destination node in $(U-1)$ successive time slots, we construct a *single-symbol system model* for the source node's nth transmit symbol in the context of the TDMA-based user-cooperation-aided system of Figure 12.10 as

$$\mathbf{Y}_n = \mathbf{P}\mathbf{S}_n\mathbf{H}_n + \mathbf{W}_n, \tag{12.31}$$

where the diagonal matrix $\mathbf{P}$ is introduced to describe the transmit power allocation among the collaborating MSs and is defined as

$$\mathbf{P} \triangleq \mathrm{diag}([\sqrt{P_s}\ \sqrt{P_{r_1}} \ldots \sqrt{P_{r_{U-1}}}]). \tag{12.32}$$

Additionally, in Equation (12.31) $\mathbf{S}_n$ and $\mathbf{Y}_n$ represent the *transmitted user-cooperation-based signal matrix* and the received signal matrix at the destination, respectively, during both phase I and phase II. Additionally, $\mathbf{H}_n$ and $\mathbf{W}_n$ denote the channel matrix and the AWGN matrix, respectively. Upon further elaborating of Equation (12.31), we get

$$\begin{aligned}
&\begin{bmatrix} y_{sd_1}[n] & \cdots & y_{sd_N}[n] \\ y_{r_1d_1}[n+1\cdot L_f] & \cdots & y_{r_1d_N}[n+1\cdot L_f] \\ \vdots & \cdots & \vdots \\ y_{r_{U-1}d_1}[n+(U-1)L_f] & \cdots & y_{r_{U-1}d_N}[n+(U-1)L_f] \end{bmatrix}_{U\times N} \\
&= \mathbf{P}\begin{bmatrix} s_s[n] & 0 & \cdots & 0 \\ 0 & s_{r_1}[n+1\cdot L_f] & \cdots & 0 \\ \vdots & \vdots & \ddots & \vdots \\ 0 & 0 & \cdots & s_{r_{U-1}}[n+(U-1)L_f] \end{bmatrix}_{U\times U} \\
&\quad\times \begin{bmatrix} h_{sd_1}[n] & \cdots & h_{sd_N}[n] \\ h_{r_1d_1}[n+1\cdot L_f] & \cdots & h_{r_1d_N}[n+1\cdot L_f] \\ \vdots & \cdots & \vdots \\ h_{r_{U-1}d_1}[n+(U-1)L_f] & \cdots & h_{r_{U-1}d_N}[n+(U-1)L_f] \end{bmatrix}_{U\times N} \\
&\quad+ \begin{bmatrix} w_{sd_1}[n] & \cdots & w_{sd_N}[n] \\ w_{r_1d_1}[n+1\cdot L_f] & \cdots & w_{r_1d_N}[n+1\cdot L_f] \\ \vdots & \cdots & \vdots \\ w_{r_{U-1}d_1}[n+(U-1)L_f] & \cdots & w_{r_{U-1}d_N}[n+(U-1)L_f] \end{bmatrix}_{U\times N},
\end{aligned} \tag{12.33}$$

where the rows and columns of the transmitted user-cooperation-based signal matrix $\mathbf{S}_n$ denote the spatial and temporal dimensions, respectively. Moreover, since the source and multiple relay terminals are assumed to be far apart, the elements of the channel matrix $\mathbf{H}_n$, corresponding to the CIRs between the source and the destination nodes as well as those between the relay node and the destination node, are mutually uncorrelated, but each of them may be correlated along the TD according to the time-selective characteristics of the channel. Additionally, the elements of the AWGN matrix are modelled as independent complex-valued Gaussian random variables with zero mean and a variance of $N_0 = 2\sigma_w^2$.

More specifically, since we have the transmitted symbol $s_s[n] \in \mathcal{M}_c = \{e^{j2\pi m/M_c}; m_s = 0, 1, \ldots, M_c - 1\}$ at the source node, the $(U \times U)$-element transmitted signal matrix $\mathbf{PS}_n$ in the general system model of Equation (12.33) can be reformatted for the DAF-aided cooperative system as

$$\mathbf{PS}_n = \begin{bmatrix} \sqrt{P_s} \cdot e^{j2\pi m_s/M_c} & 0 & \cdots & 0 \\ 0 & f_{AM_{r_1}} y_{sr_1}[n] & \cdots & 0 \\ \vdots & \vdots & \ddots & \vdots \\ 0 & 0 & \cdots & f_{AM_{r_{U-1}}} y_{sr_{U-1}}[n] \end{bmatrix}, \tag{12.34}$$

where $f_{AM_{r_u}}$ is the signal gain employed by the uth relay node to make sure that the average transmitted power of the uth relay is P_{r_u} and

$$\begin{aligned} &y_{sr_u}[n] \\ &\quad = \sqrt{P_s} \cdot s_s[n] h_{sr_u}[n] + w_{sr_u}[n] &(12.35)\\ &\quad = \sqrt{P_s} \cdot e^{j2\pi m_s/M_c} h_{sr_u}[n] + w_{sr_u}[n] \quad (m_s = 0, 1, \ldots, M_c - 1) &(12.36) \end{aligned}$$

represents the signal received at the uth relay node during the broadcast phase I.

As for the DDF-aided user cooperation system, where the relay node differentially detects and re-encodes the signal received from the source node before forwarding it to the destination, the $(U \times U)$-element transmitted signal matrix $\mathbf{PS}_n$ in the general system model of Equation (12.33) can be rewritten as follows under the assumption that the output of the differentially detected relay is error-free:

$$\mathbf{PS}_n = \begin{bmatrix} \sqrt{P_s} \cdot e^{j2\pi m_s/M_c} & 0 & \cdots & 0 \\ 0 & \sqrt{P_{r_1}} \cdot e^{j2\pi m_s/M_c} & \cdots & 0 \\ \vdots & \vdots & \ddots & \vdots \\ 0 & 0 & \cdots & \sqrt{P_{r_{U-1}}} \cdot e^{j2\pi m_s/M_c} \end{bmatrix}. \tag{12.37}$$

12.3.2 Differentially Encoded Cooperative Communication Using CDD

In this section, for the sake of simplicity, we consider two differential-modulation-based two-user cooperative schemes, namely, the DAF and DDF. Both these schemes are amenable to the CDD in fading channels after a linear signal combination process, which will be discussed in our forthcoming discourse.

12.3.2.1 Signal Combining at the Destination for DAF Relaying

For the DAF scheme, the $(U-1)$ relay nodes of Figure 12.10 amplify the signal received from the source node and forward it to the destination node in a preset order over $(U-1)$ successive time slots during phase II. In order to ensure that the average transmit power of the uth relay node remains P_{r_u}, the corresponding amplification factor $f_{AM_{r_u}}$ in Equation (12.34) employed by the uth relay node can be specified as [606]

$$f_{AM_{r_u}} = \sqrt{\frac{P_{r_u}}{P_s \sigma^2_{sr_u} + N_0}}, \tag{12.38}$$

where $\sigma^2_{sr_u}$ is the variance of the channel's envelope spanning between the source and the uth relay node, which can be obtained by long-term averaging of the received signals. Therefore, the signal received at the destination from the uth relay node $y_{r_u d}[n+uL_f]$ in Equation (12.33) can be represented as follows [606]:

$$y_{r_u d}[n + uL_f] = f_{AM_{r_u}} y_{sr_u}[n] h_{r_u d}[n + uL_f] + w_{r_u d}[n + uL_f], \tag{12.39}$$

where $y_{sr_u}[n]$ is the signal received from the source node at the uth relay node during the broadcast phase I, which was given by Equation (12.35).

The destination BS linearly combines the signal at each of the N receive antennas received from the source through the direct link during the broadcast, namely phase I and those at each receive antenna received from all the relay nodes during phase II, followed by the CDD process operating without acquiring any CSI. Based on the multi-channel differential detection principle of [475], we combine the multi-path signal of the U-user cooperation system of Figure 12.10 prior to the CDD process as

$$y = \sum_{i=1}^{N} \left[a_0 (y_{sd_i}[n-1])^* y_{sd_i}[n] + \sum_{u=1}^{U-1} a_u (y_{r_u d_i}[n + uL_f - 1])^* y_{r_u d_i}[n + uL_f] \right], \tag{12.40}$$

where L_f is the length of the frame, while the coefficients a_0 and a_u $(u = 1, 2, \ldots)$ are respectively given by

$$a_0 = \frac{1}{N_0}, \tag{12.41}$$

$$a_u = \frac{P_s \sigma_{sr_u}^2 + N_0}{N_0 (P_s \sigma_{sr_u}^2 + P_{r_u} \sigma_{r_u d}^2 + N_0)}, \tag{12.42}$$

where $\sigma_{sr_u}^2$ and $\sigma_{r_u d}^2$ are the variances of the link between the source and relay nodes as well as of the link between the relay node and the BS, respectively. By assuming that the CIRs h_{sr_u} as well as $h_{r_u d}$ are almost constant over two successive symbol periods, the destination node carries out the CDD based on the combined signal y of Equation (12.40) as

$$e^{j2\pi \hat{m}/M_c} = \underset{\check{m}=0,1,\ldots,M_c-1}{\arg\max} \Re\{e^{-j2\pi \check{m}/M_c} y\}, \tag{12.43}$$

where $\Re\{\cdot\}$ denotes the real component of a complex number.

12.3.2.2 Signal Combining at Destination for DDF Relaying

For the DDF-aided U-user cooperation system of Figure 12.10, each relay node differentially decodes and re-encodes the signal received from the source node, before forwarding it to the BS. Similarly, based on the multi-channel differential detection techniques of [475, 607], the combined signal prior to differential detection by the DDF scheme can be expressed in exactly the same form as that of Equation (12.40) for the DAF scheme, which is repeated here for convenience:

$$y = \sum_{i=1}^{N} \left[a_0 (y_{sd_i}[n-1])^* y_{sd_i}[n] + \sum_{u=1}^{U-1} a_u (y_{r_u d_i}[n + uL_f - 1])^* y_{r_u d_i}[n + uL_f] \right], \tag{12.44}$$

noting that different diversity combining weights of a_0 and a_u $(u = 1, 2, \ldots, U-1)$ are used. Note also that the choice of diversity combining weights may affect the achievable system performance. For example, when the normalized total power of $P = 1$ used for transmitting a symbol during the entire user-cooperation-aided process is equally divided among the source and relay nodes, i.e. when we have $P_s = P_{r_u} = 1/U$ $(u = 1, 2, \ldots, U-1)$, the SNR of the combiner output is maximized by opting for [607]

$$a_0 = a_u = \frac{1}{N_0}, \tag{12.45}$$

provided that the corresponding channel variances are identical. Although the choice of the diversity combining weights is not optimal in general, it is optimal for the case when the SNR of the source–destination link and those of the multiple relay–destination links are the same. Again, by assuming that the CIRs taps h_{sr_u} as well as $h_{r_u d}$ are constant during two successive symbol periods, the CDD process of Equation (12.43) can be carried out by the destination after combining the multi-path signals.

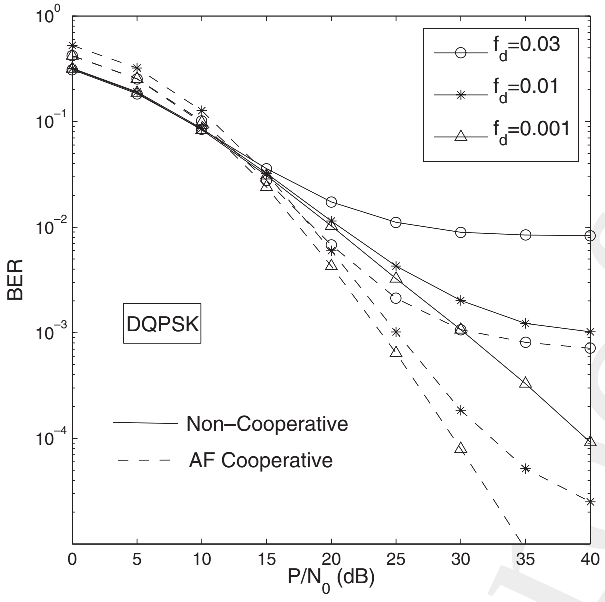

Figure 12.11: BER performance of the DAF-aided DQPSK-modulated two-user cooperative OFDM system in Rayleigh fading channels at different normalized Doppler frequencies. The system parameters were summarized in Table 12.4.

12.3.2.3 Simulation Results

Figure 12.11 depicts the BER performance versus P/N_0 for both the single-user non-cooperative system and the two-user DAF-aided cooperative system, using the simulation parameters summarized in Table 12.4. Note that we consider a scenario where the total power P used for transmitting a differentially encoded symbol during an entire user cooperation process is equally shared between the source and relay nodes, and the SNRs at the receiver of the relay and destination nodes are identical. Additionally, in order to carry out a fair comparison between the non-cooperative and cooperative systems, we assume that the power consumed by the single-user non-cooperative system when transmitting a single T-DQPSK symbol is also equal to $P = 1$, which is identical to that consumed by its user-cooperation-aided counterpart. As observed from Figure 12.11, in the presence of the slowly fading TU channel of Table 12.1 associated with $f_d = 0.001$, the DDF-aided two-user cooperative system is capable of achieving the maximum attainable spatial diversity order of two, resulting in a significant performance gain of 10 dB, given a target BER of 10^{-4}. This high gain is not unexpected, since it is unlikely that both the direct and relay links suffer from a deep fade. However, since the T-DQPSK modulation scheme is employed, the performance achieved by the CDD at the destination node degrades significantly as the normalized Doppler frequency f_d becomes higher. This is due to, for example, the relative mobility of the source and relay nodes with respect to the BS. For the sake of simplicity, here we assume the same normalized Doppler frequency exhibited by all the three links of the two-user cooperative system, namely the source–relay, relay–destination and source–destination links. As shown in Figure 12.11, an error floor is formed by the BER curves corresponding to the more time-selective scenarios associated with an increased normalized Doppler frequency f_d ranging from 0.001 to 0.03, which is an undesirable situation encountered also by the classic single-user non-cooperative benchmark system. However, the lowest achievable end-to-end BER of 10^{-3} exhibited by the CDD operating with the aid of the DAF-aided cooperation scheme is still lower than the BER of 10^{-2} achieved by the non-cooperative system under the assumption of $f_d = 0.03$.

Table 12.4: Summary of system parameters for a T-DQPSK-modulated two-user cooperative OFDM system.

System parameters	Choice
System	Two-user cooperative OFDM
Number of relay nodes	1
Subcarrier BW	$\Delta f = 10\,\text{kHz}$
Number of subcarriers	$D = 1024$
Modulation	T-DQPSK
Frame length L_f	101
CRC	CCITT-6
Normalized Doppler freq.	$f_d = 0.03, 0.01, 0.001$
Channel model	Typical urban, refer to Table 12.1
Channel variances	$\sigma_{sd}^2 = \sigma_{sr}^2 = \sigma_{rd}^2 = 1$
Power allocation	$P_s = P_{r_1} = 0.5P = 0.5$
SNR at relay and destination	$P_s/N_0 = P_{r_1}/N_0$

In comparison with the DAF-aided cooperative system, where the relay node directly forwards the amplified signal to the destination, the differential decoding and re-encoding of the DDF-aided system are carried out by the relay node before forwarding, as discussed in Section 12.3.2.2. The simulation parameters are summarized in Table 12.4, where we can see that a Cyclic Redundancy Check (CRC) code is employed by the relay node in order to determine whether the current decoded signal is correct or not and only the error-free decoded signal is forwarded to the destination. Otherwise, the relay remains silent during phase II. Figure 12.12 plots the BER curves of the DDF-aided two-user cooperative system using the CDD at both the relay and destination nodes in contrast to those of its non-cooperative counterpart. Again, the DDF-aided cooperative scheme is capable of achieving the maximum attainable diversity order of two, leading to a significant performance gain for transmission over a slow-fading channel associated with $f_d = 0.001$. Furthermore, observe by comparing Figure 12.12 that a similarly negative impact is imposed on the end-to-end BER performance by the relative mobility of the source, relay and destination nodes for the DDF scheme as that imposed for the DAF scheme. Moreover, also note in Figure 12.12 that although the DDF-aided cooperative system outperforms its non-cooperative counterpart at the three different values of the normalized Doppler frequency considered, the achievable performance gain becomes more negligible as f_d increases. Specifically, only a slightly lower error floor is exhibited in Figure 12.12 by the DDF-aided system associated with $f_d = 0.03$ than that presented by the classic single-user non-cooperative arrangement. In addition, as observed from both Figure 12.11 and Figure 12.12, both the DAF- and DDF-aided cooperative systems exhibit a worse BER performance than the classic non-cooperative one in the relatively low-SNR range spanning from 0 to 15 dB, which can also be observed for the co-located multiple-transmit-antenna-assisted system. This trend is not unexpected, since the effective SNR experienced at the receiver is halved for the two-transmit-antenna-aided system, and the benefit of diversity is overwhelmed by the deleterious effects of the noise when the SNR is low.

Let us now investigate the benefit of the CRC-based error-detection capability of the relay node on the end-to-end BER performance of a DDF-aided two-user cooperative system in Figure 12.13, where the BER curves corresponding to different CRC codes are plotted in contrast to those of the so-called fixed-relay-based cooperative system as well as to that of the single-user non-cooperative one. Note that, as summarized in Table 12.4, the frame length L_f employed is 101 DQPSK symbols, whereas CCITT-6 was used by the relay node similarly to the previously simulated DDF-aided cooperative system of Figure 12.12, which exhibits a desirable error-detection capability for this relatively short frame length, since a full diversity order of two can be achieved. To improve the achievable transmission efficiency, a CRC code using as few parity bits as possible is preferable, such as CCITT-4. However,

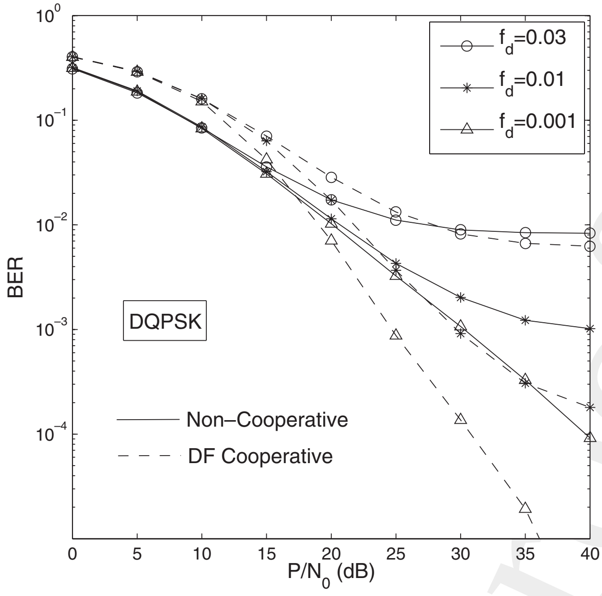

Figure 12.12: BER performance of the DDF-aided DQPSK-modulated cooperative system in Rayleigh fading channels at different normalized Doppler frequencies. The system parameters were summarized in Table 12.4.

as observed in Figure 12.13, the achievable BER performance of the DDF-aided cooperative system gradually degrades as the SNR increases, leading to an approximately 4 dB performance gain reduction at a target BER of 10^{-5} in comparison with the system employing the CCITT-6. Another extreme example worth considering is a fixed-relay-based cooperative system, where the relay forwards the re-encoded differential signal to the destination without checking whether the differentially decoded bits are correct or not. Hence, the achievable transmission efficiency is improved by sacrificing the maximum achievable diversity gain. Specifically, without the aid of the CRC, no spatial diversity gain can be achieved, although an additional transmit antenna provided by the relay node further assists the source by forwarding the signal to the BS. The reason for this trend is that without CRC checking the original diversity gain is eroded by the flawed information delivered by the relay node, which is further combined with the signal received via the direct link at the destination. Hence, a flexible compromise between maintaining a high transmission efficiency and the maximum achievable diversity gain can be struck by employing an appropriate CRC code.

In comparison with the classic co-located multiple-transmit-antenna-assisted system, the performance of the user-cooperation-aided system is affected both by the channel quality of the source–destination and relay–destination links and by that of the source–relay link. This statement is true for both the DAF- and DDF-aided cooperative systems as evidenced by our forthcoming discussions. Figure 12.14 compares the BER performance achieved by the two-user cooperative system employing either the DAF or the DDF scheme in two different scenarios, namely for a noisy source–relay link, as assumed in the scenarios characterized in Figures 12.12 and 12.13, and for a perfect noise-free source–relay link. In other words, the relay is assumed to have perfect knowledge of the source node's transmitted signal in the latter scenario, which can also be regarded as the conventional co-located multiple-transmit-antenna-aided system, if the DDF scheme is employed. Additionally, recall from Figures 12.11 and 12.12 that the maximum diversity order of two can indeed be achieved by the T-DQPSK-modulated two-user cooperative system using the CDD when a quasi-static scenario of a normalized Doppler frequency $f_d = 0.001$ is assumed. Although the maximum achievable diversity

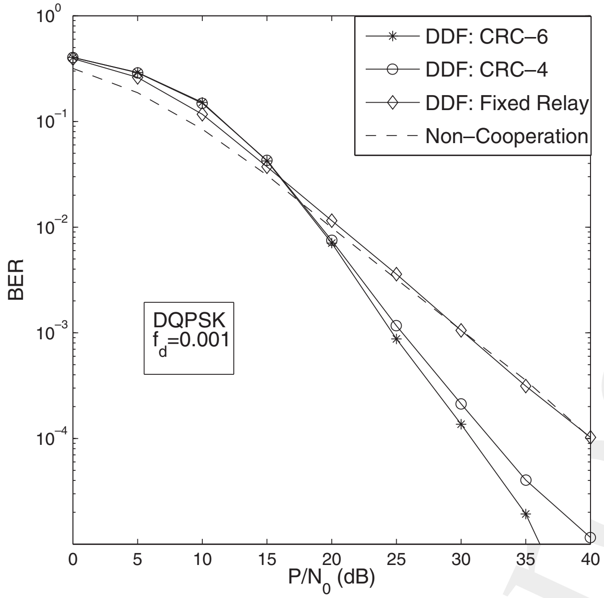

Figure 12.13: Benefits of the CRC-based error-detection capability at the relay node on the end-to-end BER performance of a DDF-aided DQPSK-modulated cooperative system. The system parameters were summarized in Table 12.4.

gain cannot be increased by having a perfect source–relay link, observe in Figure 12.14 that the system's BER performance was indeed improved. To be more specific, a performance gain as high as 5 dB was attained in Figure 12.14 for the system using the DDF scheme by having a perfect source–relay link, whereas only a negligible performance gain was attained in Figure 12.14 by its DAF-aided counterpart. Furthermore, by comparing the performance achieved by the DAF and DDF schemes in Figure 12.14, we observe that the latter is slightly outperformed by the former if the transmissions between the source and relay nodes are carried out over a noisy link having an SNR at the relay node which is equal to that measured at the destination node. However, it is expected that the latter will outperform the former as a benefit of having a better-quality source–relay link, as indicated by the extreme example of having a noise-free source–relay link, which was characterized in Figure 12.14. Therefore, when the source–relay link is of poor quality, it is preferable to employ the DAF scheme, which outperforms the DDF scheme despite its lower complexity, since there is no need to carry out any differential decoding and re-encoding.

12.3.3 Multi-path MSDSD Design for Cooperative Communication

In order to mitigate the potential negative impact induced by strongly time-selective or frequency-selective channels on the conventional T-DQPSK or F-DQPSK scenarios of Section 12.1.1, the single-path MSDSD introduced in Section 12.2 constitutes an attractive scheme for employment by the relay nodes, when differential decoding is carried out at relay nodes using the DF protocol. Figure 12.15 characterizes the achievable performance improvements of the DDF-aided two-user cooperative system attained by the single-path MSDSD scheme at the relay node in time-selective Rayleigh fading channels at different normalized Doppler frequencies. When employing the MSDSD scheme using $N_{wind} = 6$ at the relay node, observe in Figure 12.15 that the error floors encountered in time-selective channels corresponding to $f_d = 0.01$ and $f_d = 0.03$ are significantly mitigated, resulting in a substantial performance gain. For example, given a target BER of 10^{-4}, a performance gain in excess of 5 dB can be

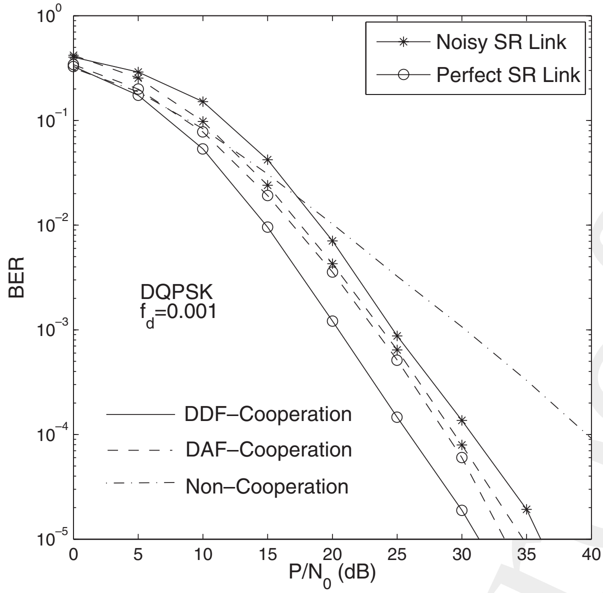

Figure 12.14: Impact of the source–relay link's quality on the end-to-end BER performance of a T-DQPSK-modulated two-user cooperative system. The system parameters were summarized in Table 12.4.

achieved for $f_d = 0.01$ as seen in Figure 12.15. However, since the end-to-end performance of the user cooperative system of Figure 12.10 is determined by the robustness of the differential detection schemes employed at both the relay and destination nodes, the single-path MSDSD-aided relay terminals alone are unable to guarantee a desirable end-to-end performance. Hence, although a significant performance gain can be attained by improving the detection capability at the relay node, there is still a substantial performance gap between the BER curve obtained at $f_d = 0.01$ or $f_d = 0.03$ and that corresponding to $f_d = 0.001$. The maximum diversity order of two is not achieved at $f_d = 0.03$ or $f_d = 0.01$, as indicated by the slope of the BER curve seen in Figure 12.15. Hence, for further improving the performance of the DDF-aided cooperative system or that of the DAF-aided one, a powerful differential detector has to be applied at the destination node, which is robust to the impairments imposed by time-selective channels. Unfortunately, the single-path MSDSD scheme cannot be directly employed by the destination node in order jointly to decode differentially the multi-path signals received from the source and relay nodes. Thus, a potential channel-induced performance degradation may still occur when carrying out conventional differential detection of signals received over the multi-path channel, which is discussed in Section 12.3.2. In the forthcoming sections, based on the principle of the single-path MSDSD, we will propose an MSDSD scheme specifically designed for user-cooperation-aided communication systems, which is capable of jointly detecting differentially the multi-path signals delivered by the source and relay nodes.

12.3.3.1 Derivation of the Metric for Optimum Detection

12.3.3.1.1 Equivalent System Model for the DDF-Aided Cooperative Systems

Following on from the principle of the single-path MSDSD discussed in Section 12.2, the receiver operating without knowledge of the CSI at the destination node collects N_{wind} consecutive user-cooperation-based space–time symbols $\mathbf{S}_n$ $(n = 0, 1, \ldots, N_{wind} - 1)$. These samples are then used jointly to detect a block of $(N_{wind} - 1)$ consecutive symbols $v_s[n]$ $(n = 0, 1, \ldots, N_{wind} - 2)$,

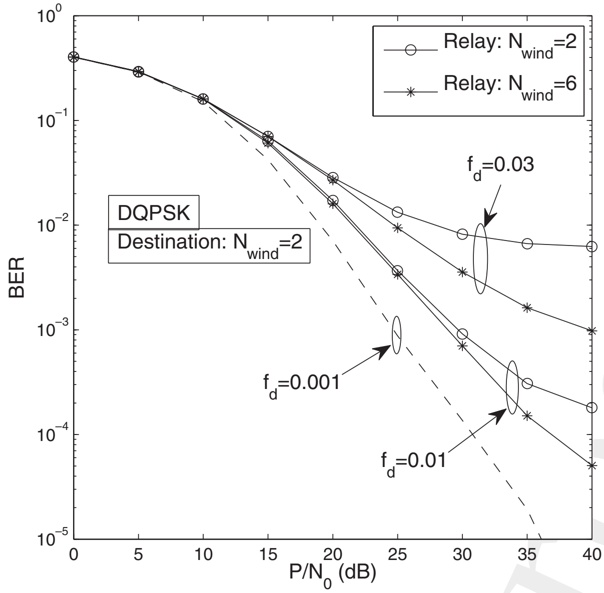

Figure 12.15: BER performance of DDF-aided DQPSK-modulated cooperative system using MSDSD-aided relays in Rayleigh fading channels.

which were differentially encoded by the source during phase I by exploiting the correlation between the phase distortions experienced by the adjacent samples $\mathbf{S}_n$ $(n = 0, 1, \ldots, N_{wind} - 1)$. The nth user-cooperation-based space–time symbol $\mathbf{S}_n$ was defined specifically for the DDF-aided cooperative system in Equation (12.37), which is rewritten here as

$$\mathbf{S}_n = \begin{bmatrix} e^{j2\pi m_s/M_c} & 0 & \cdots & 0 \\ 0 & e^{j2\pi m_s/M_c} & \cdots & 0 \\ \vdots & \vdots & \ddots & \vdots \\ 0 & 0 & \cdots & e^{j2\pi m_s/M_c} \end{bmatrix}, \tag{12.46}$$

where we have $m_s = 0, 1, \ldots, M_c - 1$. Since the total power used for transmitting a single symbol $\mathbf{S}_n$ during the entire user-cooperation process is normalized, we have

$$P_s + \sum_{u=1}^{U-1} P_{r_u} = 1, \tag{12.47}$$

where U is the number of users in the user-cooperation-aided system of Figure 12.10. Moreover, with the aid of Equations (12.33) and (12.37), we can rewrite the generalized single-symbol-based cooperative system model of Equation (12.31) for the DDF-aided cooperative transmission, resulting in the *equivalent single-symbol-based system model* as follows:

$$\begin{aligned} \mathbf{Y}_n &= \mathbf{P}\mathbf{S}_n\mathbf{H}_n + \mathbf{W}_n &(12.48)\\ &= \mathbf{S}_n\mathbf{P}\mathbf{H}_n + \mathbf{W}_n &(12.49)\\ &= \tilde{\mathbf{S}}_n\tilde{\mathbf{H}}_n + \tilde{\mathbf{W}}_n, &(12.50) \end{aligned}$$

where the equivalent user-cooperation transmitted signal's unitary matrix $\tilde{\mathbf{S}}_n$ is represented by

$$\tilde{\mathbf{S}}_n = \mathbf{S}_n = \begin{bmatrix} e^{j2\pi m_s/M_c} & 0 & \cdots & 0 \\ 0 & e^{j2\pi m_s/M_c} & \cdots & 0 \\ \vdots & \vdots & \ddots & \vdots \\ 0 & 0 & \cdots & e^{j2\pi m_s/M_c} \end{bmatrix}, \quad m_s = 0, 1, \ldots, M_c - 1, \quad (12.51)$$

and the equivalent channel matrix $\tilde{\mathbf{H}}_n$ can be expressed as

$$\tilde{\mathbf{H}}_n = \mathbf{P}\mathbf{H}_n \quad (12.52)$$

$$= \begin{bmatrix} \sqrt{P_s} \cdot h_{sd_1}[n] & \cdots & \sqrt{P_s} \cdot h_{sd_N}[n] \\ \sqrt{P_{r_1}} \cdot h_{r_1 d_1}[n + 1 \cdot L_f] & \cdots & \sqrt{P_{r_1}} \cdot h_{r_1 d_N}[n + 1 \cdot L_f] \\ \vdots & \cdots & \vdots \\ \sqrt{P_{r_{U-1}d}} \cdot h_{r_{U-1}d_1}[n + (U-1)L_f] & \cdots & \sqrt{P_{r_{U-1}d}} \cdot h_{r_{U-1}d_N}[n + (U-1)L_f] \end{bmatrix}. \quad (12.53)$$

In addition, according to Equation (12.33) the received signal matrix $\mathbf{Y}_n$ and the equivalent noise matrix $\tilde{\mathbf{W}}_n$ may be written as

$$\mathbf{Y}_n = \begin{bmatrix} y_{sd_1}[n] & \cdots & y_{sd_N}[n] \\ y_{r_1 d_1}[n + 1 \cdot L_f] & \cdots & y_{r_1 d_N}[n + 1 \cdot L_f] \\ \vdots & \cdots & \vdots \\ y_{r_{U-1}d_1}[n + (U-1)L_f] & \cdots & y_{r_{U-1}d_N}[n + (U-1)L_f] \end{bmatrix} \quad (12.54)$$

and

$$\tilde{\mathbf{W}}_n = \mathbf{W}_n = \begin{bmatrix} w_{sd_1}[n] & \cdots & w_{sd_N}[n] \\ w_{r_1 d_1}[n + 1 \cdot L_f] & \cdots & w_{r_1 d_N}[n + 1 \cdot L_f] \\ \vdots & \cdots & \vdots \\ w_{r_{U-1}d_1}[n + (U-1)L_f] & \cdots & w_{r_{U-1}d_N}[n + (U-1)L_f] \end{bmatrix}, \quad (12.55)$$

respectively.

12.3.3.1.2 Equivalent System Model for the DAF-Aided Cooperative System

Similarly, with the aid of Equations (12.33), (12.34) as well as (12.35) and following a number of straightforward manipulations left out here for compactness, we arrive at the *equivalent single-symbol system model* for the DAF-aided cooperation system based on the generalized single-symbol cooperative system model of Equation (12.31) as follows:

$$\mathbf{Y}_n = \tilde{\mathbf{S}}_n \tilde{\mathbf{H}}_n + \tilde{\mathbf{W}}_n, \quad (12.56)$$

where the received signal matrix $\mathbf{Y}_n$ at the BS is expressed identically to that of the DDF-aided system as

$$\mathbf{Y}_n = \begin{bmatrix} y_{sd_1}[n] & \cdots & y_{sd_N}[n] \\ y_{r_1 d_1}[n + 1 \cdot L_f] & \cdots & y_{r_1 d_N}[n + 1 \cdot L_f] \\ \vdots & \cdots & \vdots \\ y_{r_{U-1}d_1}[n + (U-1)L_f] & \cdots & y_{r_{U-1}d_N}[n + (U-1)L_f] \end{bmatrix}, \quad (12.57)$$

and the equivalent user-cooperation transmitted signal matrix $\tilde{\mathbf{S}}_n$ can be written as

$$\tilde{\mathbf{S}}_n = \begin{bmatrix} e^{j2\pi m_s/M_c} & 0 & \cdots & 0 \\ 0 & e^{j2\pi m_s/M_c} & \cdots & 0 \\ \vdots & \vdots & \ddots & \vdots \\ 0 & 0 & \cdots & e^{j2\pi m_s/M_c} \end{bmatrix}, \quad m_s = 0, 1, \ldots, M_c - 1, \tag{12.58}$$

which is identical to the transmitted signal matrix given in Equation (12.51) for the DDF-aided system. However, the resultant equivalent channel matrix $\tilde{\mathbf{H}}_n$ of the DAF-aided system is different from that obtained for its DDF-aided counterpart of Equation (12.52), which is expressed as

$$\tilde{\mathbf{H}}_n = [\tilde{\mathbf{h}}_1\ \tilde{\mathbf{h}}_2 \ldots \tilde{\mathbf{h}}_N], \tag{12.59}$$

where the ith column vector $\tilde{\mathbf{h}}_i$ may be written as

$$\mathbf{h}_i = \begin{bmatrix} \sqrt{P_s} \cdot h_{sd_i}[n] \\ \sqrt{\frac{P_{r_1}}{\sigma^2_{sr_1} + (N_0/P_s)}} h_{sr_1}[n] h_{r_1 d_i}[n + 1 \cdot L_f] \\ \vdots \\ \sqrt{\frac{P_{r_{U-1}}}{\sigma^2_{sr_{U-1}} + (N_0/P_s)}} h_{sr_{U-1}}[n] h_{r_{U-1} d_i}[n + (U-1) \cdot L_f] \end{bmatrix}. \tag{12.60}$$

Moreover, the resultant equivalent noise term $\tilde{\mathbf{W}}_n$ can be represented as

$$\tilde{\mathbf{W}}_n = [\tilde{\mathbf{w}}_1\ \tilde{\mathbf{w}}_2 \ldots \tilde{\mathbf{w}}_N], \tag{12.61}$$

where the ith column vector $\tilde{\mathbf{w}}_i$ may be expressed as

$$\tilde{\mathbf{w}}_i = \begin{bmatrix} w_{sd}[n] \\ \sqrt{\frac{P_{r_1}}{P_s \sigma^2_{sr_1} + N_0}} w_{sr_1}[n] h_{r_1 d_i}[n + 1 \cdot L_f] + w_{r_1 d_i}[n + 1 \cdot L_f] \\ \vdots \\ \sqrt{\frac{P_{r_{U-1}}}{P_s \sigma^2_{sr_{U-1}} + N_0}} w_{sr_{U-1}}[n] h_{r_{U-1} d_i}[n + (U-1) \cdot L_f] + w_{r_{U-1} d_i}[n + (U-1) \cdot L_f] \end{bmatrix}. \tag{12.62}$$

12.3.3.1.3 Optimum Detection Metric

Then, based on Equation (12.50) and Equation (12.56), we can construct the general input–output relation of the channel for multiple differential symbol transmissions for both DAF- and DDF-aided user-cooperative systems, where we have the *equivalent multiple-symbol-based system model* as

$$\underline{\mathbf{Y}} = \underline{\tilde{\mathbf{S}}_d} \underline{\tilde{\mathbf{H}}} + \underline{\tilde{\mathbf{W}}}. \tag{12.63}$$

Note that if $\mathbf{A}$ represents a matrix, then $\underline{\mathbf{A}}$ is a block matrix, $\mathbf{A}_d$ denotes a diagonal matrix, and $\underline{\mathbf{A}}_d$ represents a block diagonal matrix. The block matrix $\underline{\mathbf{Y}}$ hosting the received signal, which contains signals received during N_{wind} successive user-cooperation-based symbol durations corresponding to N_{wind} consecutively transmitted differential symbols $s_s[n]$ $(n = 0, 1, \ldots, N_{wind} - 1)$ of the source node, is defined as

$$\underline{\mathbf{Y}} = [\mathbf{Y}_n^T\ \mathbf{Y}_{n+1}^T \ldots \mathbf{Y}_{n+N_{wind}-1}^T]^T, \tag{12.64}$$

and the block matrix $\underline{\tilde{\mathbf{H}}}$ representing the channel as well as the block matrix $\underline{\tilde{\mathbf{W}}}$ of the AWGN are defined likewise by vertically concatenating N_{wind} matrices $\tilde{\mathbf{H}}_n$ $(n = 0, 1, \ldots, N_{wind} - 1)$ and $\tilde{\mathbf{W}}_n$

$(n = 0, 1, \ldots, N_{wind} - 1)$, respectively. Therefore, we can represent $\underline{\tilde{\mathbf{H}}}$ as

$$\underline{\tilde{\mathbf{H}}} = [\tilde{\mathbf{H}}_n^T \ \tilde{\mathbf{H}}_{n+1}^T \ldots \tilde{\mathbf{H}}_{n+N_{wind}-1}^T]^T, \tag{12.65}$$

and express $\underline{\tilde{\mathbf{W}}}$ as

$$\underline{\tilde{\mathbf{W}}} = [\tilde{\mathbf{W}}_n^T \ \tilde{\mathbf{W}}_{n+1}^T \ldots \tilde{\mathbf{W}}_{n+N_{wind}-1}^T]^T. \tag{12.66}$$

Furthermore, the diagonal block matrix of the transmitted signal is constructed as

$$\underline{\tilde{\mathbf{S}}_d} = \mathrm{diag}(\tilde{\mathbf{S}}_n,\ \tilde{\mathbf{S}}_{n+1},\ \ldots,\ \tilde{\mathbf{S}}_{n+N_{wind}-1}) \tag{12.67}$$

$$= \begin{bmatrix} \tilde{\mathbf{S}}_n & 0 & \cdots & 0 \\ 0 & \tilde{\mathbf{S}}_{n+1} & \cdots & 0 \\ \vdots & \vdots & \ddots & \vdots \\ 0 & 0 & \cdots & \tilde{\mathbf{S}}_{n+N_{wind}-1} \end{bmatrix}, \tag{12.68}$$

where $\tilde{\mathbf{S}}_n$ $(n = 0, 1, \ldots, N_{wind} - 1)$ was given by Equation (12.51) or Equation (12.58).

Note that all the elements in $\tilde{\mathbf{H}}_n$ and $\tilde{\mathbf{W}}_n$ of (12.52) and (12.55) possess a standard Gaussian distribution for the DDF-aided cooperative system, whereas most terms in $\tilde{\mathbf{H}}_n$ and $\tilde{\mathbf{W}}_n$ of (12.59) and (12.61) do not for its DAF-aided counterpart. However, our informal simulation-based investigations suggest that the resultant noise processes are near-Gaussian distributed in the DAF-aided scenario. As a result, the PDF of the corresponding received signal in (12.63) is also near-Gaussian, especially for low SNRs, as seen in Figure 12.16. Hence, under the simplifying assumption that the *equivalent* fading and noise are zero-mean complex-Gaussian processes in the DAF-aided cooperative system, the PDF of the non-coherent receiver's output $\underline{\mathbf{Y}}$ at the BS for both the DAF- and DDF-aided cooperative systems can be obtained based on its counterpart of Equation (12.14) derived for the single-transmit-antenna scenario in Section 12.2 as

$$Pr(\underline{\mathbf{Y}}|\underline{\tilde{\mathbf{S}}_d}) = \frac{\exp(-Tr\{\underline{\mathbf{Y}}^H \underline{\Psi}^{-1} \underline{\mathbf{Y}}\})}{(\pi^{UN_{wind}} \det(\underline{\Psi}))^N}, \tag{12.69}$$

where the conditional autocorrelation matrix is given by

$$\underline{\Psi} = \mathcal{E}\{\underline{\mathbf{Y}\mathbf{Y}}^H | \underline{\tilde{\mathbf{S}}_d}\}, \tag{12.70}$$

$$= \underline{\tilde{\mathbf{S}}_d} \mathcal{E}\{\underline{\tilde{\mathbf{H}}\tilde{\mathbf{H}}}^H\} \underline{\tilde{\mathbf{S}}_d}^H + \mathcal{E}\{\underline{\tilde{\mathbf{W}}\tilde{\mathbf{W}}}^H\}. \tag{12.71}$$

Specifically, for the DDF-aided cooperative system having an equivalent channel matrix $\tilde{\mathbf{H}}_n$ given by Equation (12.52) and a noise matrix given by Equation (12.55), the channel's autocorrelation matrix $\mathcal{E}\{\underline{\tilde{\mathbf{H}}\tilde{\mathbf{H}}}^H\}$ formulated in Equation (12.71) can be further extended as

$$\mathcal{E}\{\underline{\tilde{\mathbf{H}}\tilde{\mathbf{H}}}^H\} = \mathcal{E}\left\{ \begin{bmatrix} \tilde{\mathbf{H}}_n \\ \vdots \\ \tilde{\mathbf{H}}_{n+N_{wind}-1} \end{bmatrix} \begin{bmatrix} \tilde{\mathbf{H}}_n^* & \ldots & \tilde{\mathbf{H}}_{n+N_{wind}-1}^* \end{bmatrix} \right\} \tag{12.72}$$

$$= N \begin{bmatrix} \Gamma_{DF}(0) & \Gamma_{DF}(1) & \cdots & \Gamma_{DF}(N_{wind}-1) \\ \Gamma_{DF}(-1) & \Gamma_{DF}(0) & \cdots & \Gamma_{DF}(N_{wind}-2) \\ \vdots & \vdots & \ddots & \vdots \\ \Gamma_{DF}(1-N_{wind}) & \Gamma_{DF}(2-N_{wind}) & \cdots & \Gamma_{DF}(0) \end{bmatrix}, \tag{12.73}$$

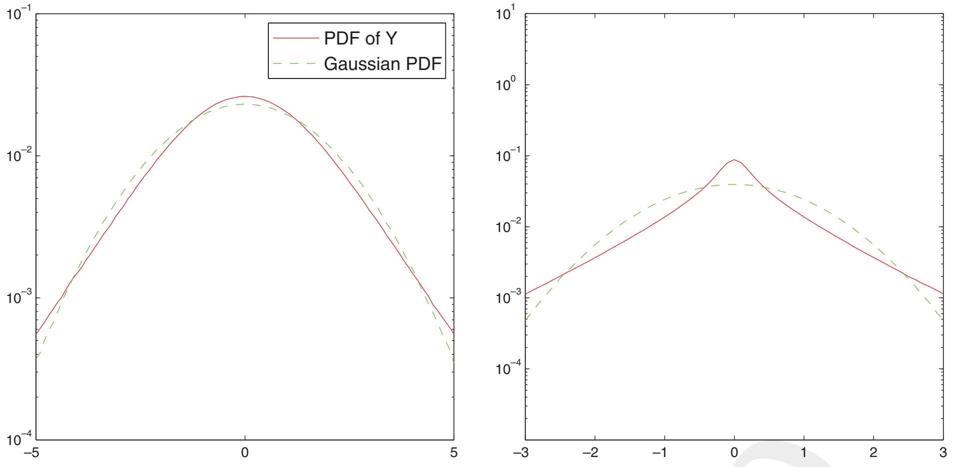

(a) SNR=0 dB (b) SNR=20 dB

Figure 12.16: PDF of the received signal $\underline{\mathbf{Y}}$ of Equation (12.64) in the DAF-aided cooperative system. ©IEEE Wang & Hanzo 2007 [7]

by defining

$$\Gamma_{DF}(\kappa) \triangleq \begin{bmatrix} \varphi^t_{sd}[\kappa] & 0 & \cdots & 0 \\ 0 & \varphi^t_{r_1 d}[\kappa] & \cdots & 0 \\ \vdots & \vdots & \ddots & \vdots \\ 0 & 0 & \cdots & \varphi^t_{r_{U-1} d}[\kappa] \end{bmatrix} \mathbf{P}^2 \tag{12.74}$$

$$= \begin{bmatrix} P_s \varphi^t_{sd}[\kappa] & 0 & \cdots & 0 \\ 0 & P_{r_1}\varphi^t_{r_1 d}[\kappa] & \cdots & 0 \\ \vdots & \vdots & \ddots & \vdots \\ 0 & 0 & \cdots & P_{r_{U-1}}\varphi^t_{r_{U-1} d}[\kappa] \end{bmatrix}, \tag{12.75}$$

where $\mathbf{P}$ is the transmit power allocation matrix given by Equation (12.32), while $\varphi^t_{sd}[\kappa]$ and $\varphi^t_{r_u d}[\kappa]$ respectively represent the channel's autocorrelation function for the direct link and relay–destination link between the uth relay node and the destination BS. Under the assumption of Rayleigh fading channels, the channel's autocorrelation function can be expressed as

$$\varphi^t[\kappa] \triangleq \mathcal{E}\{h[n+\kappa]h^*[n]\} \tag{12.76}$$

$$= J_0(2\pi f_d \kappa), \tag{12.77}$$

with $J_0(\cdot)$ denoting the zeroth-order Bessel function of the first kind and as usual f_d representing the normalized Doppler frequency. Furthermore, under the assumption of an identical noise variance observed at each terminal, $\mathcal{E}\{\underline{\tilde{\mathbf{W}}}\underline{\tilde{\mathbf{W}}}^H\}$ of the DDF-aided system can be expressed with the aid of the equivalent noise matrix given by Equation (12.55) as

$$\mathcal{E}\{\underline{\tilde{\mathbf{W}}}\underline{\tilde{\mathbf{W}}}^H\} = N_0 N \mathbf{I}_{UN_{wind}}, \tag{12.78}$$

where N and N_0 respectively denote the number of receive antennas employed at the BS and the Gaussian noise variance, while $I_{UN_{wind}}$ is a $(UN_{wind} \times UN_{wind})$-element identity matrix.

On the other hand, when considering the DAF-aided user-cooperative system having an equivalent channel matrix $\tilde{\mathbf{H}}_n$ given by Equation (12.59) and a noise matrix given by Equation (12.61), the channel's autocorrelation matrix $\mathcal{E}\{\underline{\tilde{\mathbf{H}}\tilde{\mathbf{H}}}^H\}$ can be expressed as

$$\mathcal{E}\{\underline{\tilde{\mathbf{H}}\tilde{\mathbf{H}}}^H\} = \mathcal{E}\left\{ \begin{bmatrix} \tilde{\mathbf{H}}_n \\ \vdots \\ \tilde{\mathbf{H}}_{n+N_{wind}-1} \end{bmatrix} \begin{bmatrix} \tilde{\mathbf{H}}_n^* & \ldots & \tilde{\mathbf{H}}_{n+N_{wind}-1}^* \end{bmatrix} \right\} \tag{12.79}$$

$$= N \begin{bmatrix} \Gamma_{AF}(0) & \Gamma_{AF}(1) & \cdots & \Gamma_{AF}(N_{wind}-1) \\ \Gamma_{AF}(-1) & \Gamma_{AF}(0) & \cdots & \Gamma_{AF}(N_{wind}-2) \\ \vdots & \vdots & \ddots & \vdots \\ \Gamma_{AF}(1-N_{wind}) & \Gamma_{AF}(2-N_{wind}) & \cdots & \Gamma_{AF}(0) \end{bmatrix}, \tag{12.80}$$

where

$$\Gamma_{AF}(\kappa) \triangleq \begin{bmatrix} \varphi_{sd}^t[\kappa] & 0 & \cdots & 0 \\ 0 & \varphi_{sr_1}^t[\kappa]\varphi_{r_1 d}^t[\kappa] & \cdots & 0 \\ \vdots & \vdots & \ddots & \vdots \\ 0 & 0 & \cdots & \varphi_{sr_{U-1}}^t[\kappa]\varphi_{r_{U-1}d}^t[\kappa] \end{bmatrix} \mathbf{P}^2\mathbf{F}_{AM}^2 \tag{12.81}$$

$$= \begin{bmatrix} P_s\varphi_{sd}^t[\kappa] & 0 & \cdots & 0 \\ 0 & \frac{P_{r_1}\varphi_{sr_1}^t[\kappa]\varphi_{r_1 d}^t[\kappa]}{\sigma_{sr_1}^2+(N_0/P_s)} & \cdots & 0 \\ \vdots & \vdots & \ddots & \vdots \\ 0 & 0 & \cdots & \frac{P_{r_{U-1}}\varphi_{sr_{U-1}}^t[\kappa]\varphi_{r_{U-1}d}^t[\kappa]}{\sigma_{sr_{U-1}}^2+(N_0/P_s)} \end{bmatrix} \tag{12.82}$$

with the diagonal matrix $\mathbf{F}_{AM}$ is defined as

$$\mathbf{F}_{AM} = \begin{bmatrix} 1 & 0 & \cdots & 0 \\ 0 & f_{AM_{r_1}} & \cdots & 0 \\ \vdots & \vdots & \ddots & \vdots \\ 0 & 0 & \cdots & f_{AM_{r_{U-1}}} \end{bmatrix}, \tag{12.83}$$

which contains all the signal gain factors $f_{AM_{r_u}}(u = 1, 2, \ldots, N_{wind} - 1)$ of Equation (12.38) employed by the $(U-1)$ relay nodes, respectively, in the U-user-cooperation-aided communication system of Figure 12.10. Moreover, with the aid of the equivalent noise matrix given by Equation (12.61) for the DAF-aided system, we can express $\mathcal{E}\{\underline{\tilde{\mathbf{W}}\tilde{\mathbf{W}}}^H\}$ as

$$\mathcal{E}\{\underline{\tilde{\mathbf{W}}\tilde{\mathbf{W}}}^H\} = N\mathbf{I}_{N_{wind}} \otimes \begin{bmatrix} N_0 & 0 & \cdots & 0 \\ 0 & \left(\frac{P_{r_1}\sigma_{r_1 d}^2}{P_s\sigma_{sr_1}^2+N_0}+1\right)N_0 & \cdots & 0 \\ \vdots & \vdots & \ddots & \vdots \\ 0 & 0 & \cdots & \left(\frac{P_{r_{U-1}}\sigma_{r_{U-1}d}^2}{P_s\sigma_{sr_{U-1}}^2+N_0}+1\right)N_0 \end{bmatrix}, \tag{12.84}$$

where N represents the number of receive antennas employed at the BS, while $\mathbf{I}_{N_{wind}}$ denotes an $(N_{wind} \times N_{wind})$-element identity matrix. Note that $\otimes$ denotes the Kronecker product. Hence, the noise autocorrelation matrices $\mathcal{E}\{\underline{\tilde{\mathbf{W}}\tilde{\mathbf{W}}}^H\}$, which were given by Equations (12.78) and (12.84) for the DDF-and DAF-aided systems, respectively, are diagonal due to the temporally and spatially uncorrelated nature of the AWGN.

Although the basic idea behind the ML detector is that of maximizing the a posteriori probability of the received signal block matrix $\underline{\mathbf{Y}}$, this problem can be readily shown to be equivalent to maximizing the a priori probability of Equation (12.69) with the aid of Bayes' theorem [548]. Thus, based on the ML detection rule, an exhaustive search has to be carried out over the entire transmitted signal vector space in order to find the specific solution which maximizes the a priori probability of Equation (12.69). Thus, the ML metric of the multi-path MSDD can be expressed as

$$\underline{\hat{\mathbf{S}}}_{ML} = \arg\max_{\underline{\tilde{\mathbf{S}}}_d \rightarrow \tilde{\mathbf{s}} \in \mathcal{M}_c^{N_{wind}}} Pr(\underline{\mathbf{Y}}|\underline{\tilde{\mathbf{S}}}_d) \tag{12.85}$$

$$= \arg\min_{\underline{\tilde{\mathbf{S}}}_d \rightarrow \tilde{\mathbf{s}} \in \mathcal{M}_c^{N_{wind}}} Tr\{\underline{\mathbf{Y}}^H \underline{\Psi}^{-1} \underline{\mathbf{Y}}\}, \tag{12.86}$$

where $\mathbf{s}$ is a column vector hosting all the diagonal elements of the diagonal matrix $\underline{\tilde{\mathbf{S}}}_d$. Note that although $\mathbf{s}$ has UN_{wind} elements, each of which is chosen from an identical constellation set of $\mathcal{M}_c$, we have $\mathbf{s} \in \mathcal{M}_c^{N_{wind}}$ instead of $\mathbf{s} \in \mathcal{M}_c^{UN_{wind}}$, since all the U diagonal elements of our derived equivalent U-user-cooperation transmitted signal $\tilde{\mathbf{S}}_n$ of Equation (12.51) or (12.58) have the same symbol value as that of the nth signal transmitted from the source in the broadcast phase I. More specifically, $\tilde{\mathbf{s}}$ may be expressed as

$$\tilde{\mathbf{s}} = [\underbrace{\tilde{s}_1\ \tilde{s}_2 \ldots \tilde{s}_U}_{\tilde{\mathbf{s}}_1} \ldots \underbrace{\tilde{s}_{(n-1)U+1} \ldots \tilde{s}_{nU}}_{\tilde{\mathbf{s}}_n} \ldots \underbrace{\tilde{s}_{N_{wind}U+1} \ldots \tilde{s}_{N_{wind}U}}_{\tilde{\mathbf{s}}_{N_{wind}}}]^T, \tag{12.87}$$

where the subvector $\tilde{\mathbf{s}}_n$ is a column vector containing all the diagonal elements of the matrix $\tilde{\mathbf{S}}_n$.

12.3.3.2 Transformation of the ML Metric

Again, in a user-cooperation-aided system, the noise contributions imposed at the relay and destination nodes are both temporally and spatially uncorrelated, thus we have diagonal noise autocorrelation matrices for both the DDF-aided and DAF-aided systems, as observed in Equations (12.78) and (12.84), respectively. Additionally, the equivalent transmitted signal matrix $\underline{\tilde{\mathbf{S}}}_d$ of the user-cooperation-aided system as constructed in either Equation (12.51) or Equation (12.58) for the above-mentioned two systems is a unitary matrix, hence we have

$$\underline{\tilde{\mathbf{S}}}_d^{\,-1} = \underline{\tilde{\mathbf{S}}}_d^{\,H}. \tag{12.88}$$

Then, we can further extend Equation (12.71) as

$$\underline{\Psi} = \underline{\tilde{\mathbf{S}}}_d \mathcal{E}\{\underline{\tilde{\mathbf{H}}\tilde{\mathbf{H}}}^H\} \underline{\tilde{\mathbf{S}}}_d^{\,H} + \mathcal{E}\{\underline{\tilde{\mathbf{W}}\tilde{\mathbf{W}}}^H\} \tag{12.89}$$

$$= \underline{\tilde{\mathbf{S}}}_d (\mathcal{E}\{\underline{\tilde{\mathbf{H}}\tilde{\mathbf{H}}}^H\} + \mathcal{E}\{\underline{\tilde{\mathbf{W}}\tilde{\mathbf{W}}}^H\}) \underline{\tilde{\mathbf{S}}}_d^{\,H} \tag{12.90}$$

$$= \underline{\tilde{\mathbf{S}}}_d \mathbf{C} \underline{\tilde{\mathbf{S}}}_d^{\,H}, \tag{12.91}$$

where we have

$$\mathbf{C} \triangleq \mathcal{E}\{\underline{\tilde{\mathbf{H}}\tilde{\mathbf{H}}}^H\} + \mathcal{E}\{\underline{\tilde{\mathbf{W}}\tilde{\mathbf{W}}}^H\}, \tag{12.92}$$

which is defined as the $(UN_{wind} \times UN_{wind})$-element *channel-noise autocorrelation* matrix. Now, the ML metric of Equation (12.86) generated for the multi-path MSDD can be reformulated by substituting Equation (12.91) characterizing Ψ into Equation (12.86) as

$$\underline{\hat{\mathbf{S}}}_{ML} = \arg\min_{\underline{\tilde{\mathbf{S}}}_d \rightarrow \tilde{\mathbf{s}} \in \mathcal{M}_c^{N_{wind}}} Tr\{\underline{\mathbf{Y}}^H \underline{\Psi}^{-1} \underline{\mathbf{Y}}\} \tag{12.93}$$

$$= \arg\min_{\underline{\tilde{\mathbf{S}}}_d \rightarrow \tilde{\mathbf{s}} \in \mathcal{M}_c^{N_{wind}}} Tr\{\underline{\mathbf{Y}}^H (\underline{\tilde{\mathbf{S}}}_d \mathbf{C} \underline{\tilde{\mathbf{S}}}_d^{\,H})^{-1} \underline{\mathbf{Y}}\}. \tag{12.94}$$

Furthermore, since the $\underline{\tilde{\mathbf{S}}}_d$ is unitary, we get

$$\underline{\hat{\mathbf{S}}}_{ML} = \underset{\underline{\tilde{\mathbf{S}}}_d \rightarrow \tilde{\mathbf{s}} \in \mathcal{M}_c^{N_{wind}}}{\arg\min} \; Tr\{\underline{\mathbf{Y}}^H \underline{\tilde{\mathbf{S}}}_d \mathbf{C}^{-1} \underline{\tilde{\mathbf{S}}}_d{}^H \underline{\mathbf{Y}}\}. \tag{12.95}$$

Now we define two matrix transformation operators, namely $\mathcal{F}_y(\cdot)$ and $\mathcal{F}_s(\cdot)$, for the received signal matrix $\underline{\mathbf{Y}}$ of Equation (12.54) or (12.57) and the transmitted signal matrix $\underline{\tilde{\mathbf{S}}}_d$ of Equation (12.51) or (12.58), respectively, in the scenario of a differentially modulated U-user cooperative system employing N receive antennas at the BS and jointly detecting differentially N_{wind} received symbols. Specifically, the operator $\mathcal{F}_y(\cdot)$ is defined as follows:

$$\mathcal{F}_y(\underline{\mathbf{Y}}) \triangleq \begin{bmatrix} \overrightarrow{\mathbf{y}}_1 & \mathbf{0} & \cdots & \mathbf{0} \\ \mathbf{0} & \overrightarrow{\mathbf{y}}_2 & \cdots & \mathbf{0} \\ \vdots & \vdots & \ddots & \vdots \\ \mathbf{0} & \mathbf{0} & \cdots & \overrightarrow{\mathbf{y}}_{UN_{wind}} \end{bmatrix}, \tag{12.96}$$

where $\overrightarrow{\mathbf{y}}_i$ is the ith row of the matrix $\underline{\mathbf{Y}}$ and the resultant matrix is a $(UN_{wind} \times UNN_{wind})$-element matrix. On the other hand, the operator $\mathcal{F}_s(\cdot)$, which is applied to the diagonal transmitted signal matrix $\underline{\mathbf{S}}_d$, is defined as

$$\mathcal{F}_s(\underline{\tilde{\mathbf{S}}}_d) \triangleq \begin{bmatrix} \tilde{s}_1 \mathbf{I}_N \\ \tilde{s}_2 \mathbf{I}_N \\ \vdots \\ \tilde{s}_{UN_{wind}} \mathbf{I}_N \end{bmatrix}, \tag{12.97}$$

where $\tilde{s}_i$ is the ith element of the column vector $\tilde{\mathbf{s}}$ of Equation (12.87) hosting all the UN_{wind} diagonal elements of the diagonal matrix $\underline{\tilde{\mathbf{S}}}_d$. Thus, the resultant matrix is of $(UNN_{wind} \times N)$ dimension.

Consequently, we exploit the transformation operators $\mathcal{F}_y(\cdot)$ defined in Equation (12.96) and $\mathcal{F}_s(\cdot)$ defined in Equation (12.97), which allow us further to reformulate the ML solution expression of Equation (12.95) as

$$\underline{\hat{\mathbf{S}}}_{ML} = \underset{\underline{\tilde{\mathbf{S}}}_d \rightarrow \tilde{\mathbf{s}} \in \mathcal{M}_c^{N_{wind}}}{\arg\min} \; Tr\{\underline{\mathbf{Y}}^H \underline{\tilde{\mathbf{S}}}_d \mathbf{C}^{-1} \underline{\tilde{\mathbf{S}}}_d{}^H \underline{\mathbf{Y}}\} \tag{12.98}$$

$$= \underset{\underline{\mathbf{S}}_{\mathcal{F}} \rightarrow \tilde{\mathbf{s}} \in \mathcal{M}_c^{N_{wind}}}{\arg\min} \; Tr\{\underline{\mathbf{S}}_{\mathcal{F}}^T \underline{\mathbf{Y}}_{\mathcal{F}}^H \mathbf{C}^{-1} \underline{\mathbf{Y}}_{\mathcal{F}} \underline{\mathbf{S}}_{\mathcal{F}}^*\}, \tag{12.99}$$

where we have

$$\underline{\mathbf{Y}_{\mathcal{F}}} = \mathcal{F}_y(\underline{\mathbf{Y}}) \tag{12.100}$$

and

$$\underline{\mathbf{S}_{\mathcal{F}}} = \mathcal{F}_s(\underline{\tilde{\mathbf{S}}}_d) = \begin{bmatrix} \tilde{s}_1 \mathbf{I}_N \\ \tilde{s}_2 \mathbf{I}_N \\ \vdots \\ \tilde{s}_{UN_{wind}} \mathbf{I}_N \end{bmatrix} = \begin{bmatrix} \underline{\mathbf{S}_{\mathcal{F}}}_1 \\ \underline{\mathbf{S}_{\mathcal{F}}}_2 \\ \vdots \\ \underline{\mathbf{S}_{\mathcal{F}}}_{N_{wind}} \end{bmatrix}, \tag{12.101}$$

where the $(UN \times N)$-dimensional matrix $\underline{\mathbf{S}_{\mathcal{F}}}_i$ represents the ith submatrix of the block matrix $\underline{\mathbf{S}_{\mathcal{F}}}$, which may be expressed as

$$\underline{\mathbf{S}_{\mathcal{F}}}_i = \begin{bmatrix} \tilde{s}_{U(i-1)+1} \mathbf{I}_N \\ \tilde{s}_{U(i-1)+2} \mathbf{I}_N \\ \vdots \\ \tilde{s}_{Ui} \mathbf{I}_N \end{bmatrix}_{UN \times N}, \tag{12.102}$$

where all the non-zero elements have an identical symbol value, which corresponds to the ith symbol transmitted from the source during the broadcast phase I.

12.3.3.3 Channel-Noise Autocorrelation Matrix Triangularization

Let us now generate the $(UN_{wind} \times UN_{wind})$-element upper-triangular matrix $\mathbf{F}$, which satisfies $\mathbf{F}^H\mathbf{F} = \mathbf{C}^{-1}$ with the aid of Cholesky factorization. Then we arrive at

$$\underline{\hat{\mathbf{S}}}_{ML} = \arg\min_{\underline{\mathbf{S}_{\mathcal{F}}} \to \tilde{\mathbf{s}} \in \mathcal{M}_c^{N_{wind}}} Tr\{\underline{\mathbf{S}_{\mathcal{F}}}^T \underline{\mathbf{Y}_{\mathcal{F}}}^H \mathbf{F}^H \mathbf{F} \underline{\mathbf{Y}_{\mathcal{F}}} \underline{\mathbf{S}_{\mathcal{F}}}^*\}. \tag{12.103}$$

Then, by further defining a $(UN_{wind} \times UNN_{wind})$-element matrix $\mathbf{U}$ as

$$\mathbf{U} \triangleq (\mathbf{F}\underline{\mathbf{Y}_{\mathcal{F}}})^* \tag{12.104}$$

$$= \begin{bmatrix} \mathbf{U}_{1,1} & \mathbf{U}_{1,2} & \cdots & \mathbf{U}_{1,N_{wind}} \\ \mathbf{0} & \mathbf{U}_{2,2} & \cdots & \mathbf{U}_{2,N_{wind}} \\ \vdots & \vdots & \ddots & \vdots \\ \mathbf{0} & \mathbf{0} & \cdots & \mathbf{U}_{N_{wind},N_{wind}} \end{bmatrix}, \tag{12.105}$$

where we have

$$\mathbf{U}_{i,j} \triangleq \begin{bmatrix} u_{U(i-1)+1,UN(j-1)+1} & u_{U(i-1)+1,UN(j-1)+2} & \cdots & u_{U(i-1)+1,UNj} \\ u_{U(i-1)+2,UN(j-1)+1} & u_{U(i-1)+2,UN(j-1)+2} & \cdots & u_{U(i-1)+2,UNj} \\ \vdots & \vdots & \ddots & \vdots \\ u_{Ui,UN(j-1)+1} & u_{Ui,UN(j-1)+2} & \cdots & u_{Ui,UNj} \end{bmatrix}_{U \times UN}, \tag{12.106}$$

we finally arrive at

$$\underline{\hat{\mathbf{S}}}_{ML} = \arg\min_{\underline{\mathbf{S}_{\mathcal{F}}} \to \tilde{\mathbf{s}} \in \mathcal{M}_c^{N_{wind}}} \|\mathbf{U}\underline{\mathbf{S}_{\mathcal{F}}}\|^2, \tag{12.107}$$

which completes the process of transforming the multi-path ML-MSDD metric of Equation (12.86) to a *shortest-vector* problem.

12.3.3.4 Multi-dimensional Tree-Search-Aided MSDSD Algorithm

Although the problem of finding an optimum solution for the ML-MSDD has been transformed into the so-called *shortest-vector* problem of Equation (12.107), the multi-path ML-MSDD designed for user-cooperation-aided systems may impose a potentially excessive computational complexity when aiming at finding the solution which minimizes Equation (12.107), especially when a high-order differential modulation scheme and/or a high observation window size N_{wind} are employed. Fortunately, in light of the SD algorithms discussed in Chapter 9, the computational complexity imposed may be significantly reduced by carrying out a tree search within a reduced-size hypersphere confined by either the search radius C for the depth-first SD or the maximum number of candidates K retained at each search tree level for the breadth-first SD. In our following discourse, we consider the depth-first SD algorithm as an example and demonstrate how to reduce the complexity imposed by the ML-MSSD.

In order to search for the ML solution of Equation (12.107) in a confined hypersphere, an initial search radius C is introduced. Thus, we obtain the metric relevant for the multi-path MSDSD scheme as

$$\underline{\hat{\mathbf{S}}}_{ML} = \arg\min_{\underline{\mathbf{S}_{\mathcal{F}}} \to \tilde{\mathbf{s}} \in \mathcal{M}_c^{N_{wind}}} \|\mathbf{U}\tilde{\mathbf{s}}\|^2 \leq C^2 \tag{12.108}$$

$$= \arg\min_{\underline{\mathbf{S}_{\mathcal{F}}} \to \tilde{\mathbf{s}} \in \mathcal{M}_c^{N_{wind}}} \left\| \begin{bmatrix} \mathbf{U}_{1,1} & \mathbf{U}_{1,2} & \cdots & \mathbf{U}_{1,N_{wind}} \\ \mathbf{0} & \mathbf{U}_{2,2} & \cdots & \mathbf{U}_{2,N_{wind}} \\ \vdots & \vdots & \ddots & \vdots \\ \mathbf{0} & \mathbf{0} & \cdots & \mathbf{U}_{N_{wind},N_{wind}} \end{bmatrix} \begin{bmatrix} \underline{\mathbf{S}_{\mathcal{F}}}_1 \\ \underline{\mathbf{S}_{\mathcal{F}}}_2 \\ \vdots \\ \underline{\mathbf{S}_{\mathcal{F}}}_{N_{wind}} \end{bmatrix} \right\|^2 \leq C^2 \tag{12.109}$$

$$= \arg\min_{\underline{\mathbf{S}_{\mathcal{F}}} \to \tilde{\mathbf{s}} \in \mathcal{M}_c^{N_{wind}}} \left\| \sum_{n=1}^{N_{wind}} \left(\sum_{m=n}^{N_{wind}} \mathbf{U}_{n,m} \underline{\mathbf{S}_{\mathcal{F}}}_m \right) \right\|^2 \leq C^2. \tag{12.110}$$

Since the tree search is carried out commencing from $n = N_{wind}$ to $n = 1$, the accumulated PED between the candidate $\underline{\mathbf{S}_{\mathcal{F}}}$ and the origin can be expressed as

$$\mathcal{D}_n = \underbrace{\left\| \mathbf{U}_{n,n}\underline{\mathbf{S}_{\mathcal{F}}}_n + \sum_{m=n+1}^{N_{wind}} \mathbf{U}_{n,m}\underline{\mathbf{S}_{\mathcal{F}}}_m \right\|^2}_{\delta_n} + \underbrace{\left\| \sum_{l=n+1}^{N_{wind}} \left(\sum_{m=l}^{N_{wind}} \mathbf{U}_{l,m}\underline{\mathbf{S}_{\mathcal{F}}}_m \right) \right\|^2}_{\mathcal{D}_{n+1}} \leq C^2. \tag{12.111}$$

Furthermore, due to the employment of a differential modulation scheme, the information is encoded as the phase difference between the consecutively transmitted symbols. Hence, in light of the multi-layer tree search proposed for the SD in Section 11.3.2.3, the MSDSD scheme can start the search from $n = (N_{wind} - 1)$ by choosing a trial submatrix for $\underline{\mathbf{S}_{\mathcal{F}}}_{N_{wind}-1}$ satisfying

$$\mathcal{D}_{N_{wind}-1} \leq C^2 \tag{12.112}$$

from the legitimate candidate pool, after simply assuming that the N_{wind}th symbol transmitted by the source is $s_s = 1$. That is, according to Equation (12.102) we have

$$\underline{\mathbf{S}_{\mathcal{F}}}_{N_{wind}} = \underbrace{[\mathbf{I}_N\ \mathbf{I}_N \ldots \mathbf{I}_N]^T}_{U \text{ identity submatrices}}. \tag{12.113}$$

Given the trial submatrix $\underline{\mathbf{S}_{\mathcal{F}}}_{N_{wind}-1}$ satisfying Equation (12.112), the search continues and a candidate matrix is selected for $\underline{\mathbf{S}_{\mathcal{F}}}_{N_{wind}-2}$ based on the criterion that the value of the resultant PED computed using Equation (12.111) does not exceed the squared radius, i.e.

$$\mathcal{D}_{N_{wind}-2} \leq C^2. \tag{12.114}$$

This recursive process will continue until n reaches 1, i.e. when we choose a trial value for $\tilde{\mathrm{s}}_1$ within the computed range. Then the search radius C is updated by calculating the Euclidean distance between the newly obtained signal point $\underline{\mathbf{S}_{\mathcal{F}}}$ and the origin and a new search is carried out within a reduced compound confined by the newly obtained search radius. The search then proceeds in the same way, until no more legitimate signal points can be found in the increasingly reduced search area. Consequently, the last legitimate signal point $\underline{\mathbf{S}_{\mathcal{F}}}$ found this way is regarded as the ML solution of Equation (12.107). Therefore, in comparison with the multi-path ML-MSDD algorithm of Equation (12.107), the MSDSD algorithm may achieve a significant computational complexity reduction, as does its single-path counterpart, as observed in Section 12.2. For more details on the principle of SD algorithms refer to Chapter 9 and on the idea of multi-layer tree search to Chapter 11.

12.3.4 Simulation Results

12.3.4.1 Performance of the MSDSD-Aided DAF-User-Cooperation System

As discussed in Section 12.3.2.3, the relative mobility among users imposes a performance degradation on the user-cooperation-aided system. Thus, the multi-path MSDSD scheme proposed in Section 12.3.3, which relies on the exploitation of the correlation between the phase distortions experienced by the N_{wind} consecutive transmitted DPSK symbols, is employed in order to mitigate the channel-induced error floor encountered by the CDD characterized in Figure 12.17. The system parameters used in our simulations are summarized in Table 12.5.

Figure 12.17 depicts the BER performance improvement achieved by the MSDSD employed at the destination node for the DAF-aided two-user cooperative system in the presence of three different normalized Doppler frequencies, namely $f_d = 0.03$, 0.01 and 0.001. With the aid of the MSDSD employing $N_{wind} = 6$ at the destination node, both the error floors experienced in Rayleigh channels having normalized frequencies of $f_d = 0.03$ and 0.01 are significantly mitigated. Specifically, the

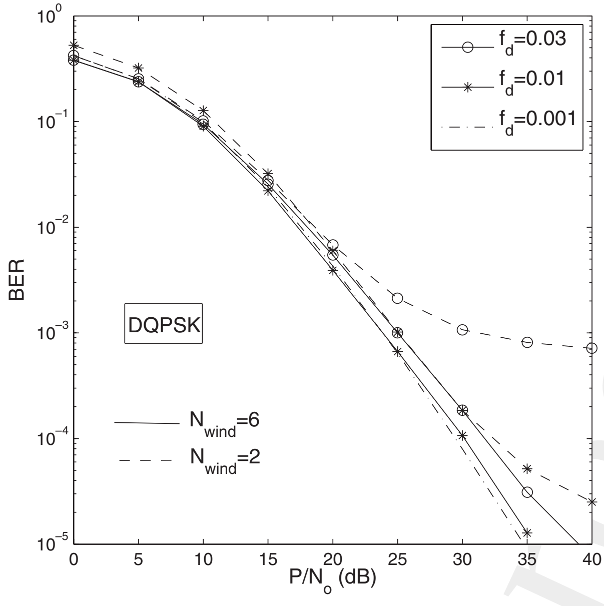

Figure 12.17: BER performance improvement achieved by the MSDSD employing $N_{wind} = 6$ for the DAF-aided T-DQPSK-modulated cooperative system in time-selective Rayleigh fading channels. All other system parameters are summarized in Table 12.5.

Table 12.5: Summary of system parameters used for the T-DQPSK-modulated two-user cooperative OFDM system.

System parameters	Choice
System	Two-user cooperative OFDM
Number of relay nodes	1
Subcarrier BW	$\Delta f = 10\,\text{kHz}$
Number of subcarriers	$D = 1024$
Modulation	T-DQPSK
Frame length L_f	101
CRC	CCITT-6
Normalized Doppler frequency	If it is not specified, $f_{d,sd} = f_{d,sr} = f_{d,rd} = f_d$
Channel model	Typical urban, refer to Table 12.1
Channel variances	$\sigma_{sd}^2 = \sigma_{sr}^2 = \sigma_{rd}^2 = 1$
Power allocation	$P_s = P_{r_1} = 0.5P = 0.5$
SNR at relay and destination	$P_s/N_0 = P_{r_1}/N_0$

BER curve corresponding to the normalized Doppler frequency $f_d = 0.01$ almost coincides with that associated with $f_d = 0.001$, indicating a performance gain of about 10 dB over the system dispensing with the MSDSD. Remarkably, in the scenario of a fast-fading channel having $f_d = 0.03$, the BER curve obtained when the CDD is employed at the destination node levels out just below 10^{-3}, as the SNR increases. By contrast, with the aid of the MSDSD the resultant BER curve decreases steadily,

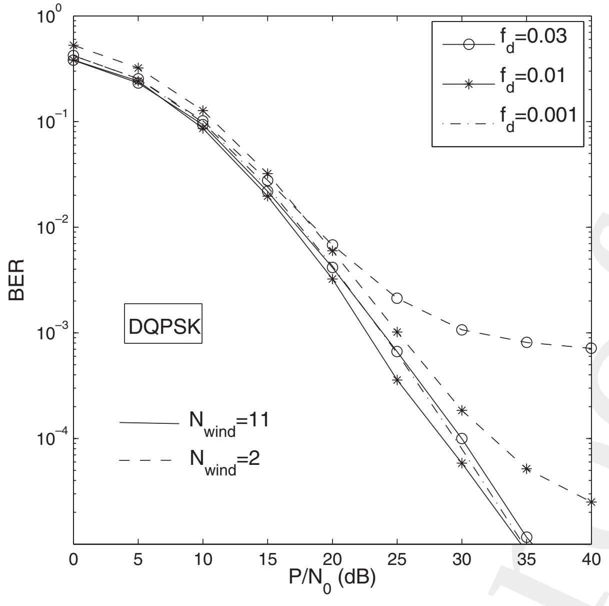

Figure 12.18: BER performance improvement achieved by the MSDSD scheme employing $N_{wind} = 11$ for the DAF-aided T-DQPSK-modulated cooperative system in time-selective Rayleigh fading channels. All other system parameters are summarized in Table 12.5.

suffering a modest performance loss of only about 4 dB at the target BER of 10^{-5} in comparison with the curve associated with $f_d = 0.001$. Hence, the more time selective the channel, the more significant the performance improvement achieved by the proposed MSDSD scheme.

For further reducing the detrimental impact induced by the time-selective channel on the DAF-aided user-cooperative system, an observation window size of $N_{cand} = 11$ is employed by the MSDSD arrangement at the destination node at the expense of a higher detection complexity. As seen in Figure 12.18, the MSDSD using $N_{wind} = 11$ is capable of eliminating the error floor encountered by the system employing the CDD, even when the channel is severely time selective, i.e. for $f_d = 0.03$. In other words, the BER curve corresponding to the MSDSD-aided system in Figure 12.18 and obtained for $f_d = 0.03$ coincides with that of its CDD-aided counterpart recorded for $f_d = 0.001$. Furthermore, the MSDSD-aided system with $N_{wind} = 11$ in a fast-fading channel associated with $f_d = 0.01$ is able to outperform the system employing $N_{wind} = 2$, even if the latter is operating in a slow-fading channel having $f_d = 0.001$. Therefore, even in the presence of a severely time-selective channel, the DAF-aided user-cooperative system employing the MSDSD is capable of achieving an attractive performance by jointly detecting differentially a sufficiently high number of consecutively received user-cooperation-based joint symbols $\mathbf{S}_n$ $(n = 0, 1, \ldots, N_{wind} - 1)$ of Equation (12.58) by exploiting knowledge of the equivalent channel autocorrelation matrix $\mathcal{E}\{\underline{\tilde{\mathbf{H}}\tilde{\mathbf{H}}}^H\}$ of Equation (12.79), which characterizes the CIR statistics of both the direct and relay links.

All the previously described simulations were carried out under the assumption that an identical normalized Doppler frequency is exhibited by each link of the user-cooperation system, i.e. that we have $f_{d,sd} = f_{d,sr} = f_{d,rd} = f_d$. However, a more realistic scenario is the one where the relative speeds of all the cooperative users as well as of the destination terminal are different from each other, leading to a different Doppler frequency for each link. Thus, in order to investigate the impact of different relative speeds among all the nodes on the attainable end-to-end performance of the DAF-aided system, Monte Carlo simulations were carried out for the three different scenarios summarized in Table 12.6. In all the

Table 12.6: Normalized Doppler frequency of three different scenarios.

	$f_{d,sd}$	$f_{d,sr}$	$f_{d,rd}$
Scenario I (S moves, R&D relatively immobile)	0.03	0.03	0.001
Scenario II (R moves, S&D relatively immobile)	0.001	0.03	0.03
Scenario III (D moves, S&R relatively immobile)	0.03	0.001	0.03

three situations, only one of the three nodes in the two-user cooperation-aided system is supposed to move relative to the other two nodes at a speed resulting in a normalized Doppler frequency of 0.03, while the latter two remain stationary relative to each other, yielding a normalized Doppler frequency of 0.001.

In Figure 12.19 the BER curves corresponding to the three different scenarios of Table 12.6 are bounded by the two dashed–dotted BER curves having no legends, which were obtained by assuming an identical normalized Doppler frequency of $f_d = 0.03$ and $f_d = 0.001$ for each link in the user-cooperation-aided system, respectively. This is not unexpected, since the two above-mentioned BER bounds correspond to the least and most desirable time-selective channel conditions considered in this chapter, respectively. The channel quality of the direct link characterized in terms of its grade of time selectivity predetermines the achievable performance of the DAF-aided user-cooperation-assisted system employing the MSDSD. Hence, it is observed in Figure 12.19 that the system is capable of attaining a better BER performance in Scenario II ($f_{d,sd} = 0.001$) than in the other two scenarios ($f_{d,sd} = 0.03$). However, as seen in Figure 12.19, due to the high speed of the relay node observed in Scenario II relative to the source and destination nodes, the MSDSD employing $N_{wind} = 6$ remains unable to eliminate completely the impairments induced by the time-selective channel, unless a higher N_{wind} value is employed. Therefore, a modest performance degradation occurs in comparison with the $f_d = 0.001$ scenario. On the other hand, the MSDSD-aided system exhibits a similar performance in Scenario I and Scenario III, since the source–relay and relay–destination links are symmetric and thus they are exchangeable in the context of the DAF scheme, as observed in Equation (12.81).

12.3.4.2 Performance of the MSDSD-Aided DDF User-Cooperation System

Despite the fact that the performance degradation experienced by the conventional DDF-aided user-cooperation system employing the CDD in severely time-selective channels can be mitigated by utilizing the single-path MSDSD at the relay node, a significant performance loss remains unavoidable due to the absence of a detection technique at the destination node, which is robust to the time-selective channel, as previously seen in Figure 12.15. Fortunately, the multi-path-based MSDSD designed for the user-cooperation-aided system devised in Section 12.3.3 can be employed at the destination node in order to mitigate further the channel-induced performance degradation of the DDF-aided system.

Figure 12.20 demonstrates a significant performance improvement attained by the multi-path-based MSDSD design employing $N_{wind} = 6$ at the destination node of the DDF-aided two-user cooperative system over its counterpart dispensing with MSDSD at the destination at both $f_d = 0.03$ and $f_d = 0.001$ for each link, respectively. The more severely time selective the channel, the higher the end-to-end performance gain that can be achieved by the MSDSD-assisted DDF-aided system. Specifically, for a given target BER of 10^{-3}, a performance gain as high as 9 dB is achieved at $f_d = 0.03$, whereas only negligible performance improvement is attained at $f_d = 0.01$. On the other hand, by comparing the simulation results of Figure 12.17 and Figure 12.20, we observe that the performance gains achieved by the MSDSD employed at the destination node of the DDF-aided system is significantly lower than those recorded for its DAF-aided counterpart. Even though $N_{wind} = 11$ is employed, there is still a conspicuous gap between the BER curves corresponding to high values of f_d and the one obtained at $f_d = 0.001$ in the context of the DDF-aided system, as shown in Figure 12.21. This trend is not

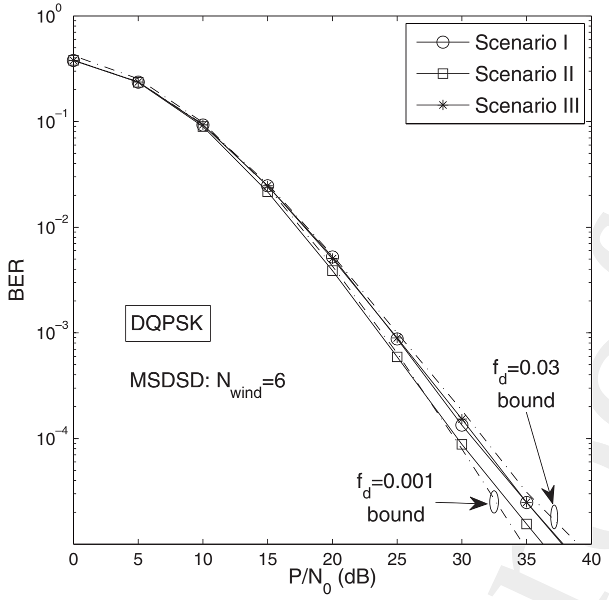

Figure 12.19: The impact of the relative mobility among the source, relay and destination nodes on the BER performance of the DAF-aided T-DQPSK-modulated cooperative system employing MSDSD at the destination node in Rayleigh fading channels. All other system parameters are summarized in Tables 12.5 and 12.6.

unexpected owing to the fact that the design of the multi-path MSDSD used in the DDF-aided user-cooperation-assisted system is carried out under the assumption of an idealized perfect reception-and-forward process at the relay node, while actually the relay will keep silent when it fails to detect the received signal correctly, as detected by the CRC check. In other words, the MSDSD employed at the destination simply assumes that the relay node has knowledge of the signal transmitted by the source node as implied by the system model of Equation (12.37) describing the DDF-aided system, operating without realizing that sometimes only noise is presented to the receive antenna during the relay phase II.

In comparison with its DAF-aided counterpart, the end-to-end performance of the DDF-aided system is jointly determined by the robustness of the differential detection technique to time-selective channels at the destination node, as well as by that at the relay node. Previously, we employed the same observation window size N_{wind} for the MSDSDs used at both the relay and destination nodes. However, in reality there exist situations where the affordable overall system complexity is limited and hence a low value of N_{wind} has to be used at both the relay and destination nodes. Thus, it is beneficial to characterize the importance of the detection technique employed at the relay and destination nodes to determine the system's required complexity. Figure 12.22 plots the BER curve of the DDF-aided two-user cooperative system for $N_{wind} = 6$ at the relay node and for $N_{wind} = 2$ at the destination node versus that generated by reversing the N_{wind} allocation, i.e. by having $N_{wind} = 2$ and $N_{wind} = 6$ at the relay and destination nodes, respectively. Observe in Figure 12.22 that the system having a more robust differential detector at the relay node slightly outperforms the other in the high-SNR range at both $f_d = 0.03$ and $f_d = 0.01$. This is because a less robust detection scheme employed at the relay node may erode the benefits of relaying in the DDF-aided user-cooperation-assisted system. Naturally, this degrades the achievable performance of the MSDSD at the destination, which carries out the detection based on the assumption of a reliable relayed signal. Hence, in the context of the DDF-aided user-cooperation-assisted system employing the MSDSD, a higher complexity should be invested at the relay node in the interest of achieving an enhanced end-to-end performance.

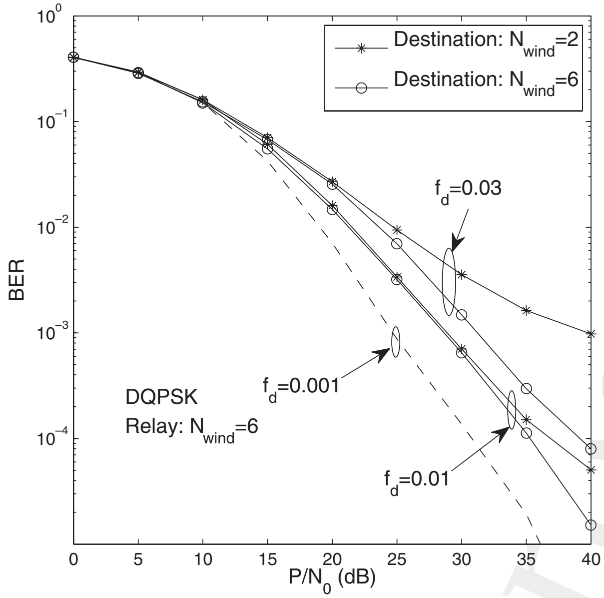

Figure 12.20: BER performance improvement achieved by the multi-path-based MSDSD scheme employing $N_{wind} = 6$ at the destination node of the DDF-aided T-DQPSK-modulated cooperative system in Rayleigh fading channels. All other system parameters are summarized in Table 12.5.

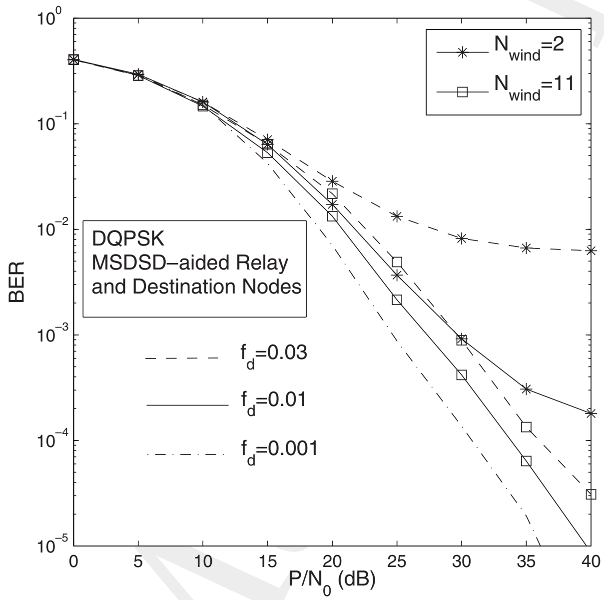

Figure 12.21: BER performance improvement achieved by the multi-path MSDSD employing $N_{wind} = 11$ at the destination node of the DDF-aided T-DQPSK-modulated cooperative system in Rayleigh fading channels. All other system parameters are summarized in Table 12.5.

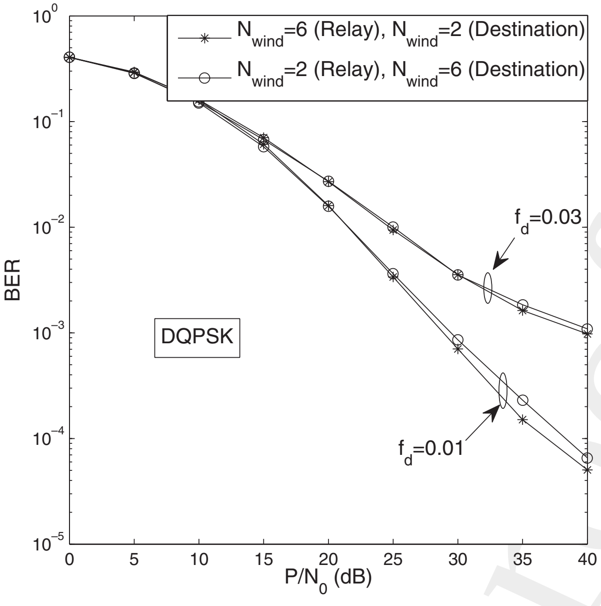

Figure 12.22: BER performance of the DDF-aided T-DQPSK-modulated cooperative system employing MSDSD in conjunction with different detection-complexity allocations in Rayleigh fading channels. All other system parameters are summarized in Table 12.5.

Let us now investigate the effect of the relative mobility of the source, relay and destination nodes on the achievable BER performance of the DDF-aided two-user cooperative system by considering the BER curves corresponding to the three scenarios of Table 12.6, in Figure 12.23. Based on our previous discussions, we understand that the performances of the detection schemes employed at both the relay and destination nodes are equally important factors in determining the achievable end-to-end system performance, which are mainly affected by the Doppler frequency characteristics of both the source–relay link and the source–destination link in the DDF-aided user-cooperation-assisted system. In Scenario I of Table 12.6 the system exhibits the worst BER performance, which is roughly the same as the $f_d = 0.03$ performance bound, since the benefits brought about by a high-quality, near-stationary relay–destination link may be eroded by a low-quality, high-Doppler source–relay link dominating the achievable performance of the MSDSD scheme at the relay node, which in turn substantially degrades the achievable end-to-end system performance. In Scenario II of Table 12.6, we assumed that the source and destination nodes experience a low Doppler frequency in the direct link ($f_{d,sd} = 0.001$), which is one of the two above-mentioned dominant links in the DDF-aided system. Thus, for a given target BER of 10^{-4}, the system achieves a performance gain as high as 5 dB in Scenario II over that attained in the benchmark scenario having an identical Doppler frequency of $f_d = 0.03$ for each link, as observed in Figure 12.23. Moreover, the achievable performance gain can be almost doubled if the system is operating in Scenario III, where in turn the other important link, namely the source–relay link, becomes a slow-fading channel associated with $f_d = 0.001$. Remarkably, the performance achieved in Scenario III is comparable with that attained by the same system in the benchmark scenario, where we have $f_d = 0.001$ for each of the three links. More specifically, the system operating in Scenario III only suffers a performance loss of about 1 dB at a target BER of 10^{-4} in comparison with that associated with the slow-fading benchmark scenario.

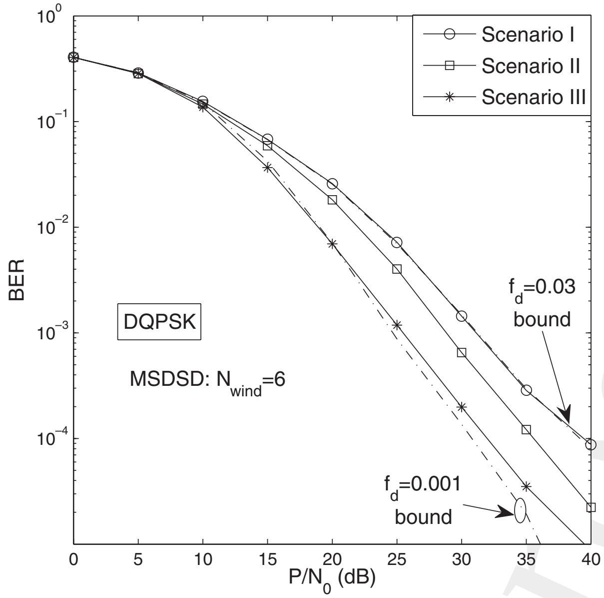

Figure 12.23: The impact of the relative mobility among the source, relay and destination nodes on the BER performance of the DDF-aided T-DQPSK-modulated cooperative system employing MSDSD at both the relay and destination nodes in Rayleigh fading channels. All other system parameters are summarized in Tables 12.5 and 12.6.

12.4 Chapter Conclusions

Cooperative diversity, emerging as an attractive diversity-aided technique to circumvent the cost and size constraints of implementing multiple antennas on a pocket-sized mobile device with the aid of antenna sharing among multiple cooperating single-antenna-aided users, is capable of effectively combating the effects of channel fading and hence improving the attainable performance of the network. However, the user-cooperation mechanism may result in a complex system when using coherent detection, where not only the BS but also the cooperating MSs would require channel estimation. Channel estimation would impose both an excessive complexity and a high pilot overhead. This situation may be further aggravated in mobile environments associated with relatively rapidly fluctuating channel conditions. Therefore, the consideration of cooperative system design without assuming knowledge of the CSI at transceivers becomes more realistic, which inspires the employment of differentially encoded modulation at the transmitter and that of non-coherent detection dispensing with both the pilots and channel estimation at the receiver. However, as discussed in Section 12.1.1, the performance of the low-complexity CDD-aided direct-transmission-based OFDM system may substantially degrade in highly time-selective or frequency-selective channels, depending on the domain in which the differential encoding is carried out. Fortunately, as argued in Section 12.2, the single-path MSDSD, which has been contrived to mitigate the channel-induced error floor encountered by differentially encoded single-input, single-output transmission, jointly detects differentially multiple consecutively received signals by exploiting the correlation among their phase distortions. Hence, inspired by the proposal of the single-path MSDSD, our main objective in this chapter is specifically to design a multi-path MSDSD which is applicable to the differentially encoded cooperative systems in order to make the overall system robust to the effects of the hostile wireless channel. To this end, in Section 12.3.3.1 we constructed a generalized equivalent multiple-symbol system model for the cooperative system employing either the DAF or DDF scheme, which facilitated the process of

Table 12.7: Performance summary of the MSDSD investigated in Chapter 12. The system parameters were given by Table 12.5. Note that 'N/C' means the target BER is not achievable, regardless of the SNR, while 'N/A' means the data are not available.

Performance of the single-relay-aided cooperative system						
			BER			
			P/N_0 (dB)		Gain (dB)	
	f_d	N_{wind}	10^{-3}	10^{-4}	10^{-3}	10^{-4}
Non-cooperative system	$f_{d,sd} = f_{d,sr} = f_{d,rd} = 0.001$	2	30	40	—	—
		6	30	40	0.0	0.0
	$f_{d,sd} = f_{d,sr} = f_{d,rd} = 0.01$	2	40	N/C	—	—
		6	32	N/A	8	N/A
	$f_{d,sd} = f_{d,sr} = f_{d,rd} = 0.03$	2	N/C	N/C	—	—
		6	35	N/A	∞	N/A
DAF cooperative system	$f_{d,sd} = f_{d,sr} = f_{d,rd} = 0.001$	2	23.5	29	—	—
		6	23.5	29	0.0	0.0
	$f_{d,sd} = f_{d,sr} = f_{d,rd} = 0.01$	2	25	33	—	—
		6	23.5	30	1.5	3
	$f_{d,sd} = f_{d,sr} = f_{d,rd} = 0.03$	2	32.5	N/C	—	—
		6	25	32	7.5	∞
	$f_{d,sd} = f_{d,sr} = 0.03$, $f_{d,rd} = 0.001$	6	24	31	—	—
	$f_{d,sr} = f_{d,rd} = 0.03$, $f_{d,sd} = 0.001$	6	23	30	1	1
	$f_{d,sd} = f_{d,rd} = 0.03$, $f_{d,sr} = 0.001$	6	24	31	0.0	0.0
DDF cooperative system	$f_{d,sd} = f_{d,sr} = f_{d,rd} = 0.001$	R: 2, D: 2	24.5	31	—	—
		R: 6, D: 2	24.5	31	0.0	0.0
		R: 2, D: 6	24.5	31	0.0	0.0
		R: 6, D: 6	24.5	31	0.0	0.0
	$f_{d,sd} = f_{d,sr} = f_{d,rd} = 0.01$	R: 2, D: 2	30	58	—	—
		R: 6, D: 2	29	37	1	21
		R: 2, D: 6	30	38	0	20
		R: 6, D: 6	29	35.5	1	22.5
	$f_{d,sd} = f_{d,sr} = f_{d,rd} = 0.03$	R: 2, D: 2	N/C	N/C	—	—
		R: 6, D: 2	40	N/C	∞	0
		R: 2, D: 6	41	N/C	∞	0
		R: 6, D: 6	31.3	41	∞	∞
	$f_{d,sd} = f_{d,sr} = 0.03$, $f_{d,rd} = 0.001$	R, D: 6	31	40	—	—
	$f_{d,sr} = f_{d,rd} = 0.03$, $f_{d,sd} = 0.001$	R, D: 6	29	36	2	4
	$f_{d,sd} = f_{d,rd} = 0.03$, $f_{d,sr} = 0.001$	R, D: 6	25.5	32	5.5	8

transforming the optimum detection metric to a shortest-vector problem, as detailed in Section 12.3.3.2. Then, it was shown in Section 12.3.3.4 that the resultant shortest-vector problem may be efficiently solved by a multi-layer tree search scheme, which is similar to that proposed in Section 11.3.2.3. This procedure relies on the channel-noise autocorrelation matrix triangularization procedure of Section 12.3.3.3.

Our Monte Carlo simulation results provided in Section 12.3.4.1 demonstrated that the resultant multi-path MSDSD employed at the BS is capable of completely eliminating the performance loss encountered by the DAF-aided cooperative system, provided that a sufficiently high value of N_{wind} is used. For example, observe in Figure 12.18 that, given a target BER of 10^{-3}, a performance gain of about 10 dB can be attained by the proposed MSDSD employing $N_{wind} = 11$ for a DQPSK-modulated two-user cooperative system in a relatively fast-fading channel associated with a normalized Doppler frequency of 0.03. In contrast to the DAF-aided cooperative system, it was shown in Figure 12.21 of

Section 12.3.4.2 that, although a significant performance improvement can also be achieved by the multi-path MSDSD at the BS in highly time-selective channels for the DDF-aided system, the channel-induced performance loss was not completely eliminated, even when $N_{wind} = 11$ was employed. This was because the MSDSD employed at the BS simply assumed a guaranteed perfect decoding at the relay, operating without taking into account that sometimes only noise is presented to the receive antenna during the relay's phase II, i.e. when the relay keeps silent owing to the failure of recovering the source's signal. Furthermore, our investigation of the proposed MSDSD in the practical Rayleigh fading scenario, where a different Doppler frequency is assumed for each link, demonstrated that the channel quality of the direct source–destination link characterized in terms of its grade of time selectivity predetermines the achievable performance of the DAF-aided cooperative system. By contrast, the source–relay and relay–destination links are symmetric and thus they may be interchanged without affecting the end-to-end performance. By contrast, observe in Figure 12.23 that the achievable performance of the DDF-aided system employing the MSDSD is dominated by the source–relay link. This is not unexpected, since a high-quality, near-stationary source–relay link enhances the performance of the MSDSD at the BS, making its assumption of a perfect decoding at the relay more realistic. Finally, based on the simulation results obtained in this chapter, we quantitatively summarize the performance gains achieved by the MSDSD for the direct-transmission-based non-cooperative system as well as for both the DAF- and DDF-aided cooperative systems in Table 12.7.

Chapter 13

Resource Allocation for the Differentially Modulated Cooperation-Aided Cellular Uplink in Fast Rayleigh Fading Channels

13.1 Introduction [1]

13.1.1 Chapter Contributions and Outline

It was observed in Chapter 12 that the differentially modulated user-cooperative uplink systems employing either the DAF scheme of Section 12.3.2.1 or the DDF scheme of Section 12.3.2.2 were capable of achieving cooperative diversity gain while circumventing the cost and size constraints of implementing multiple antennas in a pocket device. Additionally, by avoiding the challenging task of estimating all the $(N_t \times N_r)$ CIRs of multi-antenna-aided systems, the differentially encoded cooperative system may exhibit a better performance than its coherently detected, but non-cooperative, counterpart, since the CIRs cannot be perfectly estimated by the terminals. The CIR estimation becomes even more challenging when the MS travels at a relatively high speed, resulting in a rapidly fading environment. On the other hand, although it was shown in Chapter 12 that a full spatial diversity can usually be achieved by the differentially modulated user-cooperative uplink system, the achievable end-to-end BER performance may significantly depend on the specific choice of the cooperative protocol employed and/or on the quality of the relay channel. Therefore, in the scenario of differentially modulated cooperative uplink systems, where multiple cooperating MSs are roaming in the area between a specific MS and the BS seen in Figure 13.1, an appropriate Cooperative-Protocol Selection (CPS) as well as a matching Cooperating-User Selection (CUS) becomes necessary in order to maintain a desirable end-to-end performance. Motivated by the above-mentioned observations, the novel contributions of this chapter are as follows:

[1] This chapter is partially based on ©IEEE Wang & Hanzo 2007 [8]

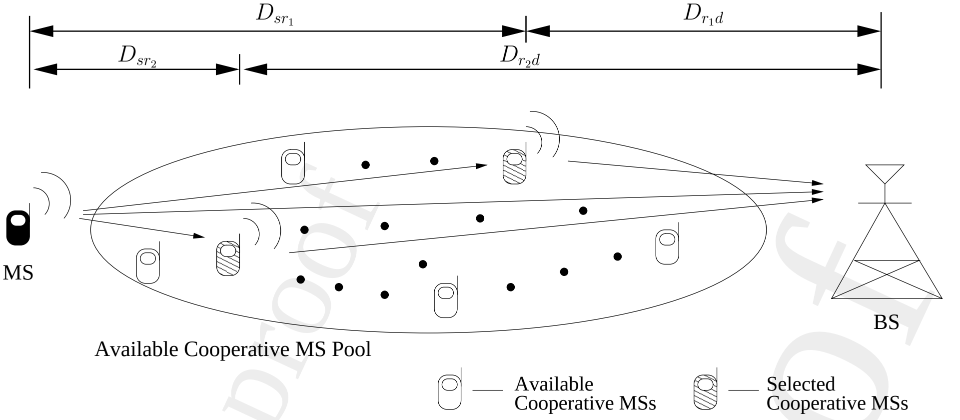

Figure 13.1: Cooperation-aided uplink systems using relay selection. ©IEEE Wang & Hanzo 2007 [8]

- The achievable end-to-end performance is theoretically analysed for both the DAF- and DDF-aided cooperative systems.
- Based on the above-mentioned analytical results, both CUS schemes and Adaptive Power Control (APC) schemes are proposed for the above two types of cooperative system in the interest of achieving the best possible performance.
- Intensive comparative studies of the most appropriate resource allocation in the context of both DAF- and DDF-assisted cooperative systems are carried out.
- In order to make the most of the complementarity of the DAF- and DDF-aided cooperative systems, a more flexible resource-optimized adaptive hybrid cooperation-aided system is proposed, yielding a further improved performance.

The remainder of this chapter is organized as follows. In Section 13.2 we first theoretically analyse the achievable end-to-end performance of both the DAF- and DDF-assisted cooperative systems. Then, based on the BER performance analysis of Section 13.2, in Sections 13.3.1 and 13.3.2 we will propose appropriate CUS schemes for both the above-mentioned two types of cooperative systems, along with an optimized power control arrangement. Additionally, in order to improve further the achievable end-to-end performance of the cooperation-aided UL of Figure 13.1 and to create a flexible cooperative mechanism, in Section 13.4 we will also investigate the CPS of the UL in conjunction with the CUS as well as the power control, leading to a resource-optimized adaptive cooperation-aided system. Finally, our concluding remarks will be provided in Section 13.5.

13.1.2 System Model

To be consistent with the system model employed in Chapter 12, the U-user TDMA UL is considered for the sake of simplicity. Again, due to the symmetry of channel allocation among users, as indicated in Figure 12.9, we focus our attention on the information transmission of a specific source MS seen in Figure 13.1, which potentially employs M_r out of the $\mathcal{P}_{cand} = (U-1)$ available relay stations in order to achieve cooperation-aided diversity by forming a VAA. Without loss of generality, we simply assume the employment of a single antenna for each terminal. For simple analytical tractability, we assume that the sum of the distances D_{sr_u} between the source MS and the uth RS, and that between the uth RS and the destination BS, which is represented by D_{r_ud}, is equal to the distance D_{sd} between the source MS and the BS. Equivalently, as indicated by Figure 13.1, we have

$$D_{sr_u} + D_{r_ud} = D_{sd}, \quad u = 1, 2, \ldots, U-1. \tag{13.1}$$

Furthermore, by considering a path-loss exponent of v [608], the average power $\sigma^2_{i,j}$ at the output of the channel can be computed according to the internode distance $D_{i,j}$ as follows:

$$\sigma^2_{i,j} = C \cdot D^{-v}_{i,j}, \quad i,j \in \{s, r_u, d\}, \tag{13.2}$$

where C is a constant which can be normalized to unity without loss of generality and the subscripts s, r_u and d represent the source, the uth relay and the destination, respectively. Thus, Equation (13.2) can be expressed as

$$\sigma^2_{i,j} = D^{-v}_{i,j}, \quad i,j \in \{s, r_u, d\}. \tag{13.3}$$

Additionally, under the assumption of having a total transmit power of P and assuming that M_r cooperating MSs are activated out of a total of $\mathcal{P}_{cand}$, we can express the associated power constraint as

$$P = P_s + \sum_{m=1}^{M_r} P_{r_m}, \tag{13.4}$$

where P_s and P_{r_m} $(m = 1, 2, \ldots, M_r)$ are the transmit power employed by the source MS and the mth RS, respectively.

13.2 Performance Analysis of the Cooperation-Aided UL

In this section, we commence analysing the error probability performance of both the DAF-aided and DDF-aided systems, where the MSDSD devised in Chapter 12 is employed in order to combat the effects of fast fadings caused by the relative mobility of the MSs and BS in the cell. Recall from Chapter 12 that the Doppler-frequency-induced error floor encountered by the CDD (or equivalently by the MSDSD using $N_{wind} = 2$) is expected to be significantly eliminated by jointly detecting $N_{wind} > 2$ consecutive received symbols with the aid of the MSDSD, provided that N_{wind} is sufficiently high. Therefore, under the assumption that the associated performance degradation can be mitigated by the MSDSD in both the DAF-aided and DDF-aided cooperative systems, it is reasonable to expect that the BER performance exhibited by the cooperation-assisted system employing the MSDSD in a relatively rapidly fading environment can be closely approximated by that achieved by the CDD in slow-fading channels. Hence, in the ensuing two sections our performance analysis is carried out without considering the detrimental effects imposed by the mobility of the MSs, since these effects are expected to be mitigated by employment of the MSDSD of Section 12.3. Consequently, our task may be interpreted as the performance analysis of a CDD-assisted differentially modulated cooperative system operating in slow-fading channels.

13.2.1 Theoretical Analysis of Differential Amplify-and-Forward Systems

13.2.1.1 Performance Analysis

First of all, without loss of accuracy, we drop the time index n and rewrite the signal of Equation (12.35) received at the mth cooperating MS and that of Equation (12.39) from the mth RS at the BS as follows:

$$y_{sr_m} = \sqrt{P_s} s_s h_{sr_m} + w_{sr_m}, \tag{13.5}$$
$$y_{r_m d} = f_{AM_{r_m}} y_{sr_m} h_{r_m d} + w_{r_m d}, \tag{13.6}$$

where the amplification factor $f_{AM_{r_m}}$ employed by the mth relay node can be specified as [606]

$$f_{AM_{r_m}} = \sqrt{\frac{P_{r_m}}{P_s \sigma^2_{sr_m} + N_0}}, \tag{13.7}$$

with N_0 being the variance of the AWGN imposed at all cooperating MSs as well as at the BS. Then, we can further reformat Equation (13.6) with the aid of Equation (13.5) in order to express the signal received at the destination BS from the RS as

$$y_{r_m d} = f_{AM_{r_m}} h_{r_m d}(\sqrt{P_s} h_{sr_m s_s} + w_{sr_m}) + w_{r_m d} \tag{13.8}$$
$$= f_{AM_{r_m}} \sqrt{P_s} h_{r_m d} h_{sr_m} s_s + f_{AM_{r_m}} h_{r_m d} w_{sr_m} + w_{r_m d}. \tag{13.9}$$

Hence, we can calculate the received SNR per symbol at the BS for both the direct and the relaying links, respectively, as

$$\gamma_{sd}^s = \frac{P_s |h_{sd}|^2}{N_0}, \tag{13.10}$$
$$\gamma_{r_m d}^s = \frac{P_s P_{r_m} |h_{sr_m}|^2 |h_{r_m d}|^2}{N_0 (P_s \sigma_{sr_m}^2 + P_{r_m} |h_{r_m d}|^2 + N_0)}. \tag{13.11}$$

Furthermore, MRC is assumed to be employed at the BS prior to the CDD scheme for the system using the DAF arrangement characterized in Equation (12.40) of Section 12.3.2.1, which is rewritten here for convenience:

$$y = a_0 (y_{sd}[n-1])^* y_{sd}[n] + \sum_{m=1}^{M_r} a_m (y_{r_m d}[n + mL_f - 1])^* y_{r_m d}[n + mL_f], \tag{13.12}$$

where L_f is the length of the transmission packet, while the coefficients a_0 and a_m $(m = 1, 2, \ldots, M_r)$ are given by

$$a_0 = \frac{1}{N_0}, \tag{13.13}$$
$$a_m = \frac{P_s \sigma_{sr_m}^2 + N_0}{N_0 (P_s \sigma_{sr_m}^2 + P_{r_m} |h_{r_m d}|^2 + N_0)}. \tag{13.14}$$

According to the basic property of the MRC scheme, the SNR at the MRC's output can be expressed as

$$\gamma^s = \gamma_{sd}^s + \sum_{m=1}^{M_r} \gamma_{r_m d}^s. \tag{13.15}$$

Equivalently, we can express the SNR per bit at the output of the MRC as

$$\gamma^b = \frac{\gamma_{sd}^s}{\log_2 M_c} + \sum_{m=1}^{M_r} \frac{\gamma_{r_m d}^s}{\log_2 M_c}$$
$$= \gamma_{sd}^b + \sum_{m=1}^{M_r} \gamma_{r_m d}^b, \tag{13.16}$$

where M_c is the constellation size of a specific modulation scheme.

On the other hand, the end-to-end BER expression conditioned on the SNR per bit at the combiner's output, namely γ^b of Equation (13.16), for the DAF-aided system activating M_r RSs for a specific source MS can be expressed as [609]

$$P_{BER|\gamma^b}^{DAF}(a, b, M_r) = \frac{1}{2^{2(M_r+1)}\pi} \int_{-\pi}^{\pi} f(a, b, M_r + 1, \theta) e^{-\alpha(\theta)\gamma^b} \, d\theta, \tag{13.17}$$

where [609]

$$f(a,b,L,\theta) = \frac{b^2}{2\alpha(\theta)} \sum_{l=1}^{L} \binom{2L-1}{L-l} [(\beta^{-l+1} - \beta^{l+1}) \cos((l-1)(\phi + \pi/2)) \\ - (\beta^{-l+2} - \beta^{l}) \cos(l(\phi + \pi/2))], \tag{13.18}$$

$$\alpha(\theta) = \frac{b^2(1 + 2\beta \sin\theta + \beta^2)}{2} \tag{13.19}$$

and

$$\beta = a/b. \tag{13.20}$$

In Equation (13.17) the parameters a and b are the modulation-dependent factors defined in [475]. Specifically, $a = 10^{-3}$ and $b = \sqrt{2}$ for DBPSK modulation, while $a = \sqrt{2-\sqrt{2}}$ and $b = \sqrt{2+\sqrt{2}}$ for DQPSK modulation using Gray coding. Additionally, the parameter β, which is defined as Equation (13.20), can be calculated according to the specific modulation scheme employed [475]. Moreover, the parameter L of Equation (13.18) denotes the number of diversity paths. For example, when M_r cooperating MSs are activated, we have $L = M_r + 1$, assuming that the BS combines the signals received from all the M_r RSs as well as that from the direct link.

On the other hand, since a non-dispersive Rayleigh fading channel is considered here, the PDF of the channel's fading amplitude r can be expressed as [608]

$$p_r(r) = \begin{cases} \frac{2r}{\Omega} e^{-r^2/\Omega}, & 0 \leq r \leq \infty \\ 0, & r < 0, \end{cases} \tag{13.21}$$

where $\Omega = \overline{r^2}$ represents the mean square value of the fading amplitude. Hence, the PDF of the instantaneous received SNR per bit at the output of the Rayleigh fading channel is given by the so-called Γ distribution [608]

$$p_{\gamma^b}(\gamma) = \begin{cases} \frac{1}{\overline{\gamma^b}} e^{-\gamma/\overline{\gamma^b}}, & \gamma \geq 0 \\ 0, & \gamma < 0 \end{cases} \tag{13.22}$$

where $\overline{\gamma^b}$ denotes the average received SNR per bit, which can be expressed as

$$\overline{\gamma^b} = \frac{P_{t,bit} \cdot \Omega}{N_0} \tag{13.23}$$

$$= \frac{P_{t,symbol} \cdot \Omega}{N_0 \cdot \log_2 \mathcal{M}_c}, \tag{13.24}$$

with $P_{t,bit}$ and $P_{t,symbol}$ representing the transmit power per bit and per symbol, respectively.

Now, the unconditional end-to-end BER of the DAF-aided cooperative system can be calculated by averaging the conditional BER expression of Equation (13.17) over the entire range of received SNR per bit values by weighting it according to its probability of occurrence represented with the aid of its PDF in Equation (13.22) as follows [609, 610]:

$$P_{BER}^{DAF}(a,b,M_r) = \int_{-\infty}^{+\infty} P_{BER|\gamma^b}^{DAF} \cdot p_{\gamma^b}(\gamma)\, d\gamma \tag{13.25}$$

$$= \frac{1}{2^{2(M_r+1)}\pi} \int_{-\pi}^{\pi} f(a,b,M_r+1,\theta) \int_{-\infty}^{+\infty} e^{-\alpha(\theta)\gamma} p_{\gamma^b}(\gamma)\, d\gamma\, d\theta \tag{13.26}$$

$$= \frac{1}{2^{2(M_r+1)}\pi} \int_{-\pi}^{\pi} f(a,b,M_r+1,\theta) \mathcal{M}_{\gamma^b}(\theta)\, d\theta, \tag{13.27}$$

where the joint Moment Generating Function (MGF) [610] of the received SNR per bit γ^b given by Equation (13.16) is defined as

$$\mathcal{M}_{\gamma^b}(\theta) = \int_{-\infty}^{+\infty} e^{-\alpha(\theta)\gamma} p_{\gamma^b}(\gamma)\, d\gamma \tag{13.28}$$

$$= \underbrace{\int_{-\infty}^{+\infty} \cdots \int_{-\infty}^{+\infty}}_{(M_r+1)\text{-fold}} e^{-\alpha(\theta)(\gamma_{sd}+\sum_{m=1}^{M_r}\gamma_{r_m d})} p_{\gamma^b_{sd}}(\gamma_{sd})$$

$$\times \prod_{m=1}^{M_r} p_{\gamma^b_{r_m d}}(\gamma_{r_m d})\, d\gamma_{sd}\, d\gamma_{r_1 d} \ldots d\gamma_{r_{M_r} d} \tag{13.29}$$

$$= \mathcal{M}_{\gamma^b_{sd}}(\theta) \prod_{m=1}^{M_r} \mathcal{M}_{\gamma^b_{r_m d}}(\theta), \tag{13.30}$$

with $\mathcal{M}_{\gamma^b_{sd}}(\theta)$ and $\mathcal{M}_{\gamma^b_{r_m d}}(\theta)$ representing the MGF of the received SNR per bit γ^b_{sd} of the direct link and that of the received SNR per bit $\gamma^b_{r_m d}$ of the mth relay link. Specifically, with the aid of Equation (13.22) we have [606, 610]

$$\mathcal{M}_{\gamma^b_{sd}}(\theta) = \frac{1}{1+k_{sd}(\theta)}, \tag{13.31}$$

$$\mathcal{M}_{\gamma^b_{r_m d}}(\theta) = \frac{1}{1+k_{sr_m}(\theta)} \left(1 + \frac{k_{sr_m}(\theta)}{1+k_{sr_m}(\theta)} \frac{P_s\sigma^2_{sr_m}+N_0}{P_{r_m}} \frac{1}{\sigma^2_{r_m d}} Z_{r_m}(\theta)\right), \tag{13.32}$$

where

$$k_{sd}(\theta) \triangleq \frac{\alpha(\theta)P_s\sigma^2_{sd}}{N_0}, \tag{13.33}$$

$$k_{sr_m}(\theta) \triangleq \frac{\alpha(\theta)P_s\sigma^2_{sr_m}}{N_0} \tag{13.34}$$

and

$$Z_{r_m}(\theta) \triangleq \int_0^{\infty} \frac{e^{-(u/\sigma^2_{r_m d})}}{u+R_{r_m}(\theta)}\, du, \tag{13.35}$$

with

$$R_{r_m}(\theta) \triangleq \frac{P_s\sigma^2_{sr_m}+N_0}{P_{r_m}[1+k_{sr_m}(\theta)]}. \tag{13.36}$$

According to Equations (3.352.2) and (8.212.1) of [611], Equation (13.35) can be further extended as

$$Z_{r_m}(\theta) = -e^{R_{r_m}(\theta)/\sigma^2_{r_m d}} \left(\zeta + \ln \frac{R_{r_m}(\theta)}{\sigma^2_{r_m d}} + \int_0^{R_{r_m}(\theta)/\sigma^2_{r_m d}} \frac{e^{-t}-1}{t}\, dt\right), \tag{13.37}$$

where $\zeta \triangleq 0.577\,215\,664\,90\ldots$ denotes the Euler constant. In order to circumvent the integration, Equation (13.37) can be expressed with aid of the Taylor series as

$$Z_{r_m}(\theta) = -e^{R_{r_m}(\theta)/\sigma^2_{r_m d}} \left(\zeta + \ln \frac{R_{r_m}(\theta)}{\sigma^2_{r_m d}} + \sum_{n=1}^{\infty} \frac{(-R_{r_m}(\theta)/\sigma^2_{r_m d})^n}{n \cdot n!}\right) \tag{13.38}$$

$$\approx -e^{R_{r_m}(\theta)/\sigma^2_{r_m d}} \left(\zeta + \ln \frac{R_{r_m}(\theta)}{\sigma^2_{r_m d}} + \sum_{n=1}^{N_n} \frac{(-R_{r_m}(\theta)/\sigma^2_{r_m d})^n}{n \cdot n!}\right), \tag{13.39}$$

where the parameter N_n is introduced to control the accuracy of Equation (13.39). Since the Taylor series in Equation (13.38) converges quickly, the integration in Equation (13.37) can be approximated by the sum of the first N_n elements in Equation 13.39. Consequently, the average BER of the DAF-aided cooperative system where the desired source MS relies on M_r cooperating MSs activated in order to form a VAA can be expressed as

$$P_{BER}^{DAF}(a,b,M_r) = \frac{1}{2^{2(M_r+1)}\pi}\int_{-\pi}^{\pi}\frac{f(a,b,M_r+1,\theta)}{1+k_{sd}(\theta)}\prod_{m=1}^{M_r}\frac{1}{1+k_{sr_m}(\theta)} \times\left(1+\frac{k_{sr_m}(\theta)Z_{r_m}(\theta)}{1+k_{sr_m}(\theta)}\frac{P_s\sigma_{sr_m}^2+N_0}{P_{r_m}\sigma_{r_m d}^2}\right)d\theta. \tag{13.40}$$

Using the same technique as in [606], the BER expression of Equation (13.40) can be upper-bounded by bounding $Z_{r_m}(\theta)$ of Equation (13.35), to simplify the exact BER expression of Equation (13.40). Specifically, $R_{r_m}(\theta)$ of Equation (13.36) reaches its minimum value when $\alpha(\theta)$ of Equation (13.19) is maximized at $\theta = \pi/2$, which in turn maximizes $Z_{r_m}(\theta)$ of Equation (13.35). Thus, the error probability of Equation (13.40) may be upper-bounded as

$$P_{BER}^{DAF}(a,b,M_r) \lessapprox \frac{1}{2^{2(M_r+1)}\pi}\int_{-\pi}^{\pi}\frac{f(a,b,M_r+1,\theta)}{1+k_{sd}(\theta)}\prod_{m=1}^{M_r}\frac{1}{1+k_{sr_m}(\theta)} \times\left(1+\frac{k_{sr_m}(\theta)Z_{r_m,max}}{1+k_{sr_m}(\theta)}\frac{P_s\sigma_{sr_m}^2+N_0}{P_{r_m}\sigma_{r_m d}^2}\right)d\theta, \tag{13.41}$$

where

$$Z_{r_m,max} \triangleq -e^{R_{r_m,min}/\sigma_{r_m d}^2}\left(\zeta+\ln\frac{R_{r_m,min}}{\sigma_{r_m d}^2}+\sum_{n=1}^{N_n}\frac{(-R_{r_m,min}/\sigma_{r_m d}^2)^n}{n\cdot n!}\right), \tag{13.42}$$

in which

$$R_{r_m,min} \triangleq \frac{P_s\sigma_{sr_m}^2+N_0}{P_{r_m}[1+P_s\sigma_{sr_m}^2 b^2(1+\beta)^2/2N_0]}. \tag{13.43}$$

Similarly, the average BER of Equation (13.40) can be lower-bounded by minimizing $Z_{r_m}(\theta)$ of Equation (13.35) at $\theta = -\pi/2$. Specifically, from Equation (13.40) we arrive at the error probability expression of

$$P_{BER}^{DAF}(a,b,M_r) \gtrapprox \frac{1}{2^{2(M_r+1)}\pi}\int_{-\pi}^{\pi}\frac{f(a,b,M_r+1,\theta)}{1+k_{sd}(\theta)}\prod_{m=1}^{M_r}\frac{1}{1+k_{sr_m}(\theta)} \times\left(1+\frac{k_{sr_m}(\theta)Z_{r_m,min}}{1+k_{sr_m}(\theta)}\frac{P_s\sigma_{sr_m}^2+N_0}{P_{r_m}\sigma_{r_m d}^2}\right)d\theta, \tag{13.44}$$

where

$$Z_{r_m,min} \triangleq -e^{R_{r_m,max}/\sigma_{r_m d}^2}\left(\zeta+\ln\frac{R_{r_m,max}}{\sigma_{r_m d}^2}+\sum_{n=1}^{N_n}\frac{(-R_{r_m,max}/\sigma_{r_m d}^2)^n}{n\cdot n!}\right), \tag{13.45}$$

in which

$$R_{r_m,max} \triangleq \frac{P_s\sigma_{sr_m}^2+N_0}{P_{r_m}[1+P_s\sigma_{sr_m}^2 b^2(1-\beta)^2/2N_0]}. \tag{13.46}$$

For further simplifying the BER expressions of Equations (13.41) and (13.44), we can neglect all the additive terms of ‘1’ in the denominators of both of the above-mentioned BER expressions by considering the relatively high-SNR region. Consequently, after some further manipulations, the

Table 13.1: Summary of system parameters.

System parameters	Choice
System	User-cooperative cellular uplink
Cooperative protocol	DAF
Number of relay nodes	M_r
Number of subcarriers	$D = 1024$
Modulation	DPSK
Packet length	$L_f = 128$
Normalized Doppler frequency	$f_d = 0.008$
Path-loss exponent	Typical urban area, $v = 3$ [608]
Channel model	Typical urban, refer to Table 12.1
Relay location	$D_{sr_m} = D_{sd}/2, m = 1, 2, \ldots, M_r$
Power control	$P_s = P_{r_m} = P/(M_r + 1), m = 1, 2, \ldots, M_r$
Noise variance at MS and BS	N_0

approximated high-SNR BER upper bound and its lower-bound counterpart respectively can be expressed as follows:

$$P_{BER,high-snr}^{DAF}(a, b, M_r) \lessapprox \frac{F(a, b, M_r + 1)N_0^{M_r+1}}{P_s\sigma_{sd}^2} \prod_{m=1}^{M_r} \frac{P_{r_m}\sigma_{r_m,d}^2 + P_s\sigma_{sr_m}^2 Z_{r_m,max}}{P_s P_{r_m}\sigma_{sr_m}^2\sigma_{r_m d}^2} \quad (13.47)$$

$$P_{BER,high-snr}^{DAF}(a, b, M_r) \gtrapprox \frac{F(a, b, M_r + 1)N_0^{M_r+1}}{P_s\sigma_{sd}^2} \prod_{m=1}^{M_r} \frac{P_{r_m}\sigma_{r_m,d}^2 + P_s\sigma_{sr_m}^2 Z_{r_m,min}}{P_s P_{r_m}\sigma_{sr_m}^2\sigma_{r_m d}^2}, \quad (13.48)$$

where

$$F(a, b, L) = \frac{1}{2^{2L}\pi} \int_{-\pi}^{\pi} \frac{f(a, b, L, \theta)}{\alpha^L(\theta)}\, d\theta. \quad (13.49)$$

Then $R_{r_m,min}$ of Equation (13.43) and $R_{r_m,max}$ of Equation (13.46) can be approximated as

$$R_{r_m,min} \approx \frac{2N_0}{b^2(1+\beta)^2 P_{r_m}}, \quad (13.50)$$

$$R_{r_m,max} \approx \frac{2N_0}{b^2(1-\beta)^2 P_{r_m}}, \quad (13.51)$$

respectively. Importantly, both the BER upper and lower bounds of Equations (13.47) and (13.48) imply that a DAF-aided cooperative system having M_r selected cooperating users is capable of achieving a diversity order of $L = (M_r + 1)$, as indicated by the exponent L of the noise variance N_0.

13.2.1.2 Simulation Results and Discussion

Let us now consider a DAF-aided cooperative cellular uplink system using M_r relaying MSs in an urban area having a path-loss exponent of $v = 3$. Without loss of generality, all the activated relaying MSs are assumed to be located about half-way between the source MS and the BS, while the total power used for transmitting a single modulated symbol is equally shared among the source MS and the M_r RSs. To be more specific, we have $D_{sr_m} = D_{sd}/2$, $P_s = P_{r_m} = P/(M_r + 1)$, $m = 1, 2, \ldots, M_r$. Moreover, the normalized Doppler frequency is set to $f_d = 0.01$ under the assumption that multiple MSs are randomly moving around in the same cell. The system parameters considered in this section are summarized in Table 13.1.

The theoretical BER curves of Equation (13.40) versus the SNR received for slow-fading channels are depicted in Figure 13.2 in comparison with the results obtained by our Monte Carlo simulations, where the MSDSD of Section 12.3 using $N_{wind} = 8$ is employed at the BS to eliminate the performance

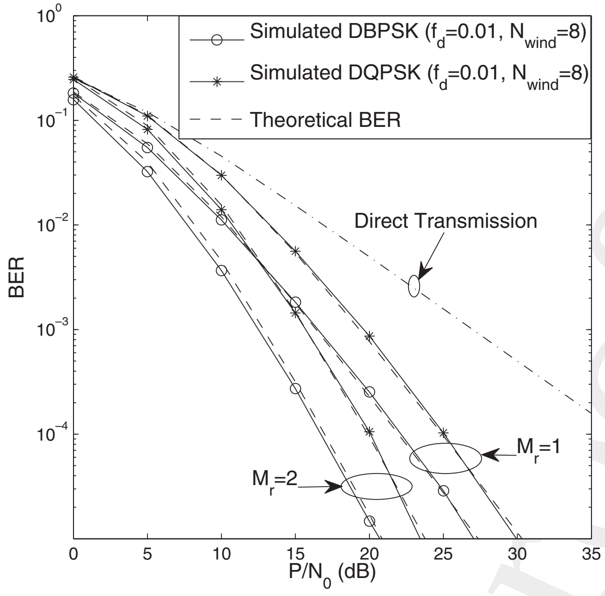

Figure 13.2: BER performance versus SNR for DAF-aided cooperative cellular systems, where there are M_r activated cooperating MSs, each having fixed transmit power and location. The MSDSD using $N_{wind} = 8$ is employed at the BS. All other system parameters are summarized in Table 13.1.

loss imposed by the relative mobility of the cooperating MSs, which is again modelled by a normalized Doppler frequency of $f_d = 0.01$. As suggested previously in Section 13.2.1.1, the Taylor series in Equation (13.38) converges rapidly and hence we employ $N_n = 5$ in Equation (13.39) to reduce the computational complexity, while maintaining the required accuracy. Observe in Figure 13.2 that all theoretical BER curves, corresponding to different numbers of activated cooperating MSs and to DBPSK and DQPSK modulation schemes, match well with the BER curves obtained by our Monte Carlo simulations. Therefore, with the aid of the MSDSD of Section 12.3 employed at the BS, a full diversity order of $L = (M_r+1)$ can be achieved by the DAF-aided cooperative system in rapidly fading channels, where the achievable BER performance can be accurately predicted using Equation (13.40).

Additionally, the BER upper and lower bounds of Equations (13.41) and (13.44) derived for both DBPSK- and DQPSK-modulated DAF-aided cooperative systems are plotted in Figures 13.3(a) and 13.3(b), respectively, versus the theoretical BER curve of Equation (13.40). Both the lower and upper bounds are tight in comparison with the exact BER curve of Equation (13.40) when the DBPSK modulation scheme is used, as observed in Figure 13.3(a). On the other hand, a relatively loose upper bound is obtained by invoking Equation (13.41) for the DQPSK-modulated system, while the lower bound associated with Equation (13.44) still remains very tight. Therefore, it is sufficiently accurate to approximate the BER performance of the DAF-aided cooperative system using the lower bound of Equation (13.44).

Furthermore, in order to simplify the lower-bound expression of Equation (13.41), the integration term of Equation (13.37) is omitted completely, assuming that we have $N_n = 0$ in Equation (13.45). The corresponding BER curves are depicted in Figure 13.4 versus those obtained when $N_n = 5$. It can be seen that the lower bound obtained after discarding the integration term in Equation (13.37) still remains accurate and tight in the relatively high-SNR region. More specifically, the resultant BER lower bound remains tight over a wide span of SNRs and only becomes inaccurate when the SNR of P/N_0 dips below 5 dB and 10 dB for the DBPSK- and DQPSK-modulated cooperative systems, respectively.

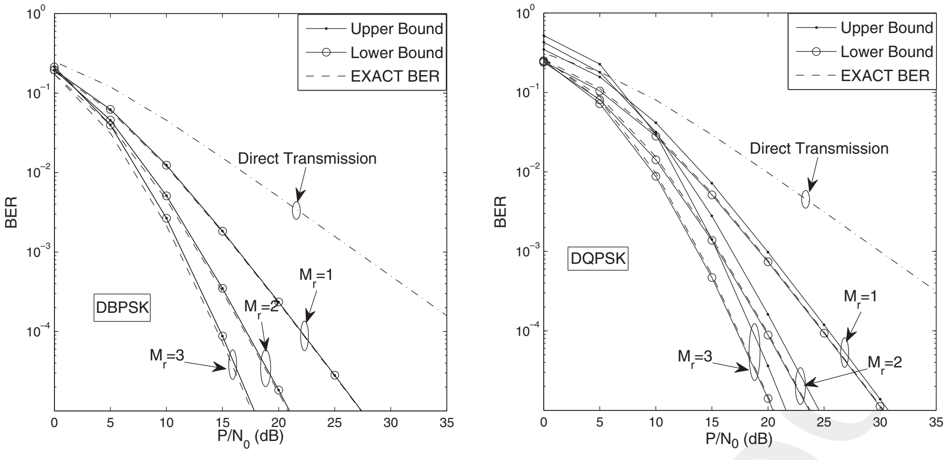

(a) DBPSK (b) DQPSK

Figure 13.3: BER lower and upper bounds versus SNR for DAF-aided cooperative cellular systems where there are M_r activated cooperating MSs, each having fixed transmit power and location. All other system parameters are summarized in Table 13.1.

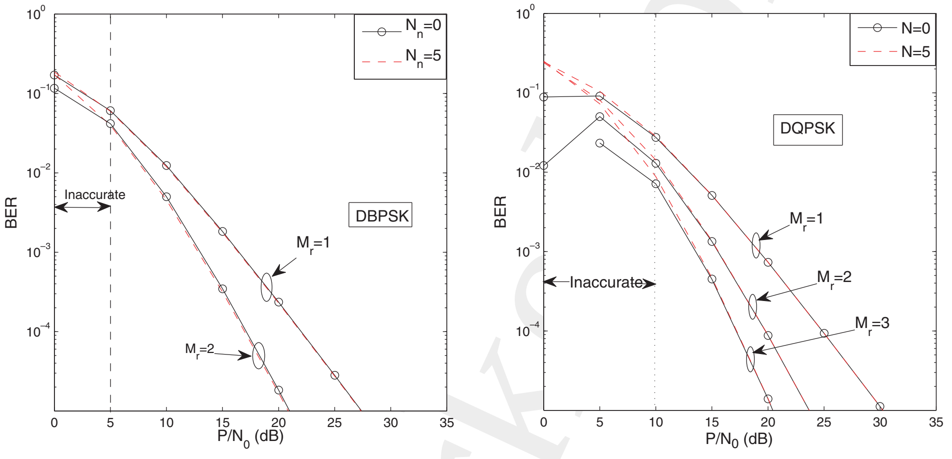

(a) DBPSK (b) DQPSK

Figure 13.4: Impact of N_n of Equation (13.45) on the BER lower bounds versus SNR for DAF-aided cooperative cellular systems, where there are M_r activated cooperating MSs, each having fixed transmit power and location. All other system parameters are summarized in Table 13.1.

When the SNR is sufficiently high and hence employment of the high-SNR-based lower bound of Equation (13.48) can be justified, its validity is verified by the BER curves of Figures 13.5(a) and 13.5(b) for the DBPSK- and DQPSK-modulated systems, respectively. Specifically, the simplified high-SNR-based BER lower bound of Equation (13.48) having $N_n = 0$ in Equation (13.45) is capable of accurately predicting the BER performance achieved by the DAF-aided cooperative cellular uplink, provided that the transmitted SNR expressed in terms of P/N_0 is in excess of 15 dB for both the DBPSK and DQPSK modulation schemes considered.

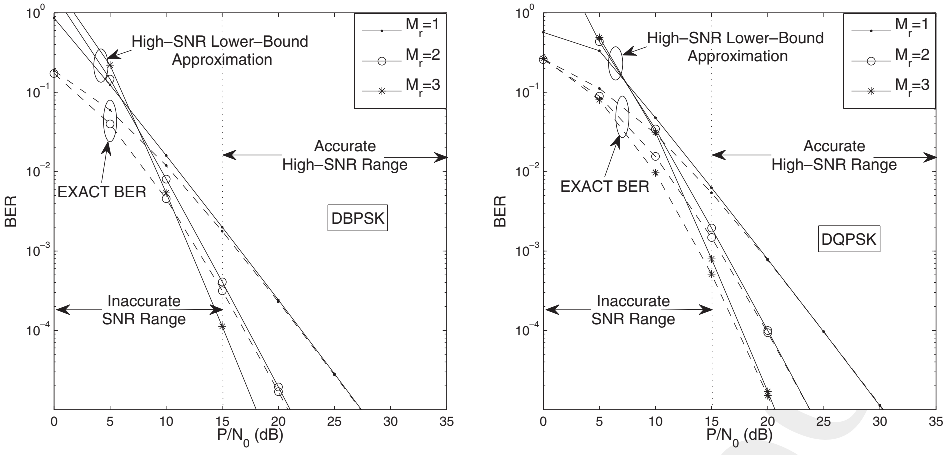

(a) DBPSK (b) DQPSK

Figure 13.5: High-SNR-based BER lower bounds versus SNR for DAF-aided cooperative cellular systems, where there are M_r activated cooperating MSs, each having transmit power and location. All other system parameters are summarized in Table 13.1.

13.2.2 Theoretical Analysis of DDF Systems

13.2.2.1 Performance Analysis

In the following discourse, the analytical BER performance expressions will be derived for a DDF-aided cooperative cellular system in order to facilitate our resource allocation to be outlined in Section 13.3.2. In contrast to its DAF-aided counterpart of Section 13.2.1, the M_r cooperating MSs selected will make sure that the information contained in the frame or packet received from the source MS can be correctly recovered by differentially decoding the received signal with the aid of CRC checking, prior to forwarding it to the BS. In other words, some of the M_r cooperating MSs selected may not participate during the relaying phase, to avoid potential error propagation due to the imperfect signal recovery. By simply assuming that the packet length is sufficiently high with respect to the channel's coherent time, the worst-case Packet Loss Ratio (PLR) at the mth cooperating MS can be expressed as

$$P_{PLR_m,upper} = 1 - (1 - P_{SER_m})^{L_f}, \tag{13.52}$$

for a given packet length L_f, where P_{SER_m} represents the symbol error rate at the mth cooperating MS, which can be calculated as [612]

$$P_{SER_m} = \frac{M_c - 1}{M_c} + \frac{|\rho_m| \tan(\pi/M_c)}{\xi(\rho_m)} \left[\frac{1}{\pi} \arctan\left(\frac{\xi(\rho_m)}{|\rho_m|} \right) - 1 \right], \tag{13.53}$$

where ρ_m and the function $\xi(x)$, respectively, can be written as follows:

$$\rho_m = \frac{P_s \sigma_{sr_m}^2 / N_0}{1 + (P_s \sigma_{sr_m}^2 / N_0)}, \tag{13.54}$$

$$\xi(x) = \sqrt{1 - |x|^2 + \tan^2(\pi/M_c)}. \tag{13.55}$$

Then, based on the $P_{PLR_m,upper}$ expression of Equation (13.52), the average end-to-end BER upper bound of a DDF-aided cooperative system can be obtained. Explicitly, in the context of a system where only $M_r = 1$ cooperating user is selected to participate in relaying the signal from the source MS to the

BS, the average end-to-end BER upper bound $P_{BER,upper}^{DDF}$ is obtained by the summation of the average BERs of two scenarios as

$$P_{BER,upper}^{DDF} = (1 - P_{PLR_1,upper})P_{BER}^{\Phi_1} + P_{PLR_1,upper}P_{BER}^{\Phi_2}, \tag{13.56}$$

where Φ_1 is defined as the first scenario when the cooperating MS perfectly recovers the information received from the source MS and thus transmits the differentially remodulated signal to the BS. By contrast, Φ_2 is defined as the second scenario, when the cooperating MS fails to decode correctly the signal received from the source MS and hence remains silent during the relaying phase. Therefore, the scenarios Φ_1 and Φ_2 can be simply represented as follows, depending on whether the transmit power P_{r1} of the cooperating MS is zero or not during the relaying phase. Thus, we can represent Φ_1 and Φ_2 as

$$\Phi_1 \triangleq \{P_{r_1} \neq 0\}, \tag{13.57}$$

$$\Phi_2 \triangleq \{P_{r_1} = 0\}, \tag{13.58}$$

respectively. Recall our BER analysis carried out for the DAF-aided system in Section 13.2.1.1, where the end-to-end BER expression of a cooperative system conditioned on the received SNR per bit γ^b can be written as

$$P_{BER|\gamma^b}(a,b,L) = \frac{1}{2^{2L}\pi}\int_{-\pi}^{\pi} f(a,b,L,\theta)e^{-\alpha(\theta)\gamma^b}\,d\theta, \tag{13.59}$$

where $f(a,b,L,\theta)$ given by Equation (13.18) is a function of the number of multi-path components L and is independent of the received SNR per bit γ^b. The parameters a and b are modulation dependent, as defined in [475]. Consequently, the unconditional end-to-end BER, $P_{BER}^{\Phi_i}$, corresponding to the scenario Φ_i can be expressed as

$$P_{BER}^{\Phi_i} = \int_{-\infty}^{\infty} P_{BER|\gamma_{\Phi_i}^b} \cdot p_{\gamma_{\Phi_i}^b}(\gamma)\,d\gamma, \tag{13.60}$$

where $p_{\gamma_{\Phi_i}^b}(\gamma)$ represents the PDF of the received SNR per bit after diversity combining at the BS in the scenario Φ_i of Equations (13.57) and (13.58).

On the other hand, since the MRC scheme is employed at the BS to combine the signals potentially forwarded by multiple cooperating MSs and the signal transmitted from the source MS as characterized by Equation (12.44) using the combining weights of Equation (12.45), the received SNR per bit after MRC combining is simply the sum of that of each combined path, which is expressed as

$$\gamma_{\Phi_1}^b = \gamma_{sd}^b + \gamma_{r_1d}^b, \tag{13.61}$$

$$\gamma_{\Phi_2}^b = \gamma_{sd}^b. \tag{13.62}$$

Therefore, the unconditional BER of the scenario Φ_1 can be computed as

$$\begin{aligned} P_{BER}^{\Phi_1} &= \frac{1}{2^{2L}\pi}\int_{-\pi}^{\pi} f(a,b,L=2,\theta)\int_{-\infty}^{\infty} e^{-\alpha(\theta)\gamma_{\Phi_1}^b} p_{\gamma_{\Phi_1}^b}(\gamma)\,d\gamma\,d\theta & (13.63)\\ &= \frac{1}{2^{2L}\pi}\int_{-\pi}^{\pi} f(a,b,L=2,\theta)\mathcal{M}_{\gamma_{\Phi_1}^b}(\theta)\,d\theta, & (13.64) \end{aligned}$$

where the joint MGF of the received SNR per bit recorded at the BS for the scenario Φ_1 is expressed as

$$\begin{aligned} \mathcal{M}_{\gamma_{\Phi_1}^b}(\theta) &= \int_{-\infty}^{\infty} e^{-\alpha(\theta)\gamma_{\Phi_1}^b} p_{\gamma_{\Phi_1}^b}(\gamma)\,d\gamma & (13.65)\\ &= \int_{-\infty}^{\infty}\int_{-\infty}^{\infty} e^{-\alpha(\theta)(\gamma_{sd}^b+\gamma_{r_1d}^b)} p_{\gamma_{sd}^b}(\gamma_{sd}) p_{\gamma_{r_1d}^b}(\gamma_{r_1d})\,d\gamma_{sd}\,d\gamma_{r_1d} & (13.66)\\ &= \mathcal{M}_{\gamma_{sd}^b}(\theta)\mathcal{M}_{\gamma_{r_1d}^b}(\theta) & (13.67)\\ &= \frac{N_0^2}{(N_0+\alpha(\theta)P_s\sigma_{sd}^2)(N_0+\alpha(\theta)P_{r_1}\sigma_{r_1d}^2)}, & (13.68) \end{aligned}$$

with $p_{\gamma^b_{sd}}(\gamma_{sd})$ and $p_{\gamma^b_{r_1 d}}(\gamma_{r_1 d})$, respectively, denoting the PDF of the received SNR per bit for the direct link and for the RD relay link. Both of these expressions were given by Equation (13.22). In parallel, the unconditional BER corresponding to the scenario Φ_2 can be obtained as

$$P^{\Phi_2}_{BER} = \frac{1}{2^{2L}\pi}\int_{-\pi}^{\pi} f(a,b,L=1,\theta)\int_{-\infty}^{\infty} e^{-\alpha(\theta)\gamma^b_{\Phi_2}} p_{\gamma^b_{\Phi_2}}(\gamma)\, d\gamma\, d\theta \tag{13.69}$$

$$= \frac{1}{2^{2L}\pi}\int_{-\pi}^{\pi} f(a,b,L=1,\theta)\mathcal{M}_{\gamma^b_{\Phi_2}}(\theta)\, d\theta, \tag{13.70}$$

where the MGF of the received SNR per bit recorded at the BS for the scenario Φ_2 is written as

$$\mathcal{M}_{\gamma^b_{\Phi_2}}(\theta) = \int_{-\infty}^{\infty} e^{-\alpha(\theta)\gamma^b_{\Phi_2}} p_{\gamma^b_{\Phi_2}}(\gamma)\, d\gamma \tag{13.71}$$

$$= \int_{-\infty}^{\infty} e^{-\alpha(\theta)\gamma^b_{sd}} p_{\gamma^b_{sd}}(\gamma_{sd})\, d\gamma_{sd} \tag{13.72}$$

$$= \frac{N_0}{N_0 + \alpha(\theta)P_s\sigma^2_{sd}}. \tag{13.73}$$

Similarly, the BER upper bound can also be attained for cooperative systems relying on $M_r > 1$ cooperating users. For example, when $M_r = 2$, the average end-to-end BER upper bound $P^{DDF}_{BER,upper}$ becomes the sum of the average BERs of four scenarios expressed as

$$\begin{aligned} P^{DDF}_{BER,upper} &= (1 - P_{PLR_1,upper})(1 - P_{PLR_2,upper})P^{\Phi_1}_{BER} + P_{PLR_1,upper}(1 - P_{PLR_2,upper})P^{\Phi_2}_{BER} \\ &\quad + (1 - P_{PLR_1,upper})P_{PLR_2,upper}P^{\Phi_3}_{BER} + P_{PLR_1,upper}P_{PLR_2,upper}P^{\Phi_4}_{BER}, \end{aligned} \tag{13.74}$$

where the four scenarios are defined as follows:

$$\Phi_1 = \{P_{r_1} \neq 0, P_{r_2} \neq 0\}, \tag{13.75}$$

$$\Phi_2 = \{P_{r_1} = 0, P_{r_2} \neq 0\}, \tag{13.76}$$

$$\Phi_3 = \{P_{r_1} \neq 0, P_{r_2} = 0\}, \tag{13.77}$$

$$\Phi_4 = \{P_{r_1} = 0, P_{r_2} = 0\}. \tag{13.78}$$

13.2.2.2 Simulation Results and Discussion

Under the assumption of a relatively rapidly Rayleigh fading channel associated with a normalized Doppler frequency of $f_d = 0.008$ and a packet length of $L_f = 16$ DQPSK-modulated symbols, the BER curves corresponding to DDF-aided cooperative systems with $M_r = 1$ and $M_r = 2$ cooperating MSs are plotted in comparison with the worst-case theoretical BERs of Equations (13.56) and (13.74) in Figure 13.6(a). Since the worst-case BER expression derived in Section 13.2.2.1 for the DDF-aided system does not take into account the negative impact of the time-selective channel, the resultant asymptotic line may not be capable of accurately approximating the true achievable BER performance of a DDF-aided system employing the CDD in the context of a rapidly fading environment. However, with the aid of the MSDSD of Section 12.3 using $N_{wind} > 2$, the performance loss induced by the relative mobility of the cooperating terminals and the BS can be significantly eliminated. Thus, as revealed by Figure 13.6(a), the worst-case BER bound closely captures the dependency of the system's BER on the P/N_0 ratio. On the other hand, the BER curves of DDF-aided cooperative systems employing the MSDSD using different packet lengths L_f are plotted together with the corresponding worst-case theoretical BER bound in Figure 13.6(b). Likewise, the theoretical BER bound based on Equation (13.56) closely captures the dependency of the MSDSD-aided system's BER on the packet length L_f employed in the scenario of a rapidly fading channel associated with a normalized Doppler frequency of $f_d = 0.008$.

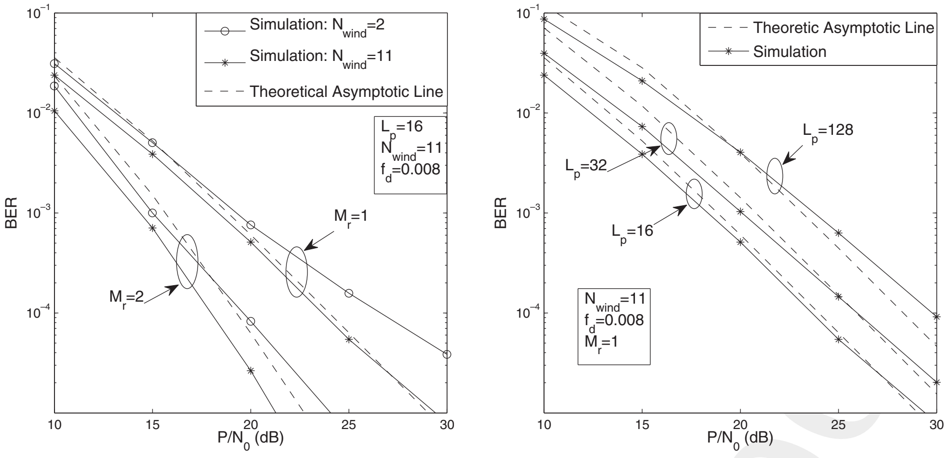

(a) Different numbers of cooperating MSs M_r

(b) Different frame lengths L_f

Figure 13.6: BER performance versus SNR for DDF-aided cooperative cellular systems, where there are M_r activated cooperating MSs, each having fixed transmit power and location. The MSDSD using $N_{wind} = 11$ is employed at the BS. All other system parameters are summarized in Table 13.2.

Table 13.2: Summary of system parameters.

System parameters	Choice
System	User-cooperative cellular uplink
Cooperative protocol	DDF
Number of relay nodes	M_r
Number of subcarriers	$D = 1024$
Modulation	DQPSK
Packet length	L_f
CRC	CCITT-4
Normalized Doppler freq.	$f_d = 0.008$
Path-loss exponent	Typical urban area, $v = 3$ [608]
Channel model	Typical urban, refer to Table 12.1
Relay location	$D_{sr_m} = D_{sd}/2, m = 1, 2, \ldots, M_r$
Power control	$P_s = P_{r_m} = P/(M_r + 1), m = 1, 2, \ldots, M_r$
Noise variance at MS and BS	N_0

13.3 CUS for the Uplink

User-cooperation-aided cellular systems are capable of achieving substantial diversity gains by forming VAAs constituted by the concerted action of distributed mobile users, while eliminating the space and cost limitations of the shirt-pocket-sized mobile phones. Hence, the cost of implementing user cooperation in cellular systems is significantly reduced, since there is no need specifically to set up additional RSs. On the other hand, it is challenging to realize user cooperation in a typical coherently detected cellular system, since $(N_t \times N_r)$ CIRs have to be estimated. For eliminating the implementationally complex channel estimation, in particular at the RSs, it is desirable to employ differentially detected modulation schemes in conjunction with the MSDSD scheme of Section 12.3. Furthermore, even if the Doppler-frequency-induced degradations are eliminated by employing the MSDSD, another major problem is how to choose the required number of cooperating users from the pool of P_{cand} available candidates, which may significantly affect the end-to-end performance of the cooperative system. These effects have been observed in our previous simulation results shown in Figure 12.14 in Section 12.3.2.3, where we indicated that the quality of the source–relay link quantified in terms of the SNR, which is dominated by the specific location of the cooperating users, plays a vital role in determining the achievable end-to-end performance of a cooperative system. Moreover, the employment of Adaptive Power Control (APC) among the cooperating users is also important in order to maximize the achievable transmission efficiency. Hence, we will commence our discourse on the above-mentioned two schemes, namely the CUS and the APC schemes, in the context of the cooperative uplink, which will be based on the end-to-end performance analysis carried out in Section 13.2. More specifically, we will propose a CUS scheme combined with APC for the DAF-aided cooperative system employing the MSDSD of Section 12.3 and its DDF-aided counterpart in Sections 13.3.1 and 13.3.2, respectively.

13.3.1 CUS Scheme for DAF Systems with APC

13.3.1.1 APC for DAF-Aided Systems [610]

As discussed in Section 13.1.2, for the sake of simplicity and analytical tractability, we assume that the source MS is sufficiently far away from the BS and the available cooperating MSs can be considered to be moving along the direct Line-Of-Sight (LOS) path between them, as specified by Equation (13.1) of Section 13.1.2. Explicitly, Equation (13.1) can be rewritten by normalizing D_{sd} to 1, as follows:

$$D_{sr_u} + D_{r_u d} = D_{sd} = 1, \quad u = 1, 2, \ldots, \mathcal{P}_{cand}, \tag{13.79}$$

where $\mathcal{P}_{cand}$ is the RS pool size. This simplified model is readily generalized to a more realistic geography by taking into account the angle between the direct link and the relaying links. Furthermore, given a path-loss exponent of v, the average power $\sigma_{i,j}^2$ of the channel fading coefficient can be computed according to Equation (13.3), which is repeated here for convenience:

$$\sigma_{i,j}^2 = D_{i,j}^{-v}, \quad i, j \in \{s, r_u, d\}. \tag{13.80}$$

Then, by defining

$$d_m \triangleq \frac{D_{sr_u}}{D_{sd}}, \tag{13.81}$$

we can represent $\sigma_{sr_u}^2$ and $\sigma_{r_u d}^2$ respectively as

$$\sigma_{sr_u}^2 = \sigma_{sd}^2 \cdot d_m^v = d_m^v, \tag{13.82}$$

$$\sigma_{r_u d}^2 = \sigma_{sd}^2 \cdot (1 - d_m)^v = (1 - d_m)^v. \tag{13.83}$$

It was found in Section 13.2.1.2 that the simpler high-SNR-based BER lower-bound expression of Equation (13.48) associated with $N_n = 0$ in Equation (13.45) is tight over a wide range of SNRs of interest, e.g. for SNRs in excess of 15 dB for both the uncoded DBPSK- and DQPSK-modulated DAF-aided cooperative systems, as observed in Figure 13.5. Therefore, a power control scheme taking into account the location of the selected cooperating mobile users can be formulated, in order to minimize the BER of Equation (13.48) under the total transmit power constraint of Equation (13.4), i.e. when we have $P = P_s + \sum_{m=1}^{M_r} P_{r_m}$.[2] Thus, we arrive at

$$
\begin{aligned}
&[\hat{P}_s, \{\hat{P}_{r_m}\}_{m=1}^{M_r} \mid \{d_m\}_{m=1}^{M_r}] \\
&= \underset{\check{P}_s, \{\check{P}_{r_m}\}_{m=1}^{M_r}}{\arg\min} \left\{ \frac{F(a,b,M_r+1)N_0^{Mr+1}}{\check{P}_s \sigma_{sd}^2} \prod_{m=1}^{M_r} \frac{\check{P}_{r_m}\sigma_{r_m,d}^2 + \check{P}_s \sigma_{sr_m}^2 Z_{r_m,min}}{\check{P}_s \check{P}_{r_m} \sigma_{sr_m}^2 \sigma_{r_m d}^2} \right\} && (13.84) \\
&= \underset{\check{P}_s, \{\check{P}_{r_m}\}_{m=1}^{M_r}}{\arg\min} \left\{ \frac{F(a,b,M_r+1)N_0^{Mr+1}}{\check{P}_s \sigma_{sd}^2} \prod_{m=1}^{M_r} \frac{\check{P}_{r_m}\sigma_{sd}^2(1-d_m)^v + \check{P}_s \sigma_{sd}^2 d_m^v Z_{r_m,min}}{\check{P}_s \check{P}_{r_m} \sigma_{sd}^4 d_m^v (1-d_m)^v} \right\} && (13.85) \\
&= \underset{\check{P}_s, \{\check{P}_{r_m}\}_{m=1}^{M_r}}{\arg\min} \left\{ \frac{1}{\check{P}_s^{M_r+1}} \prod_{m=1}^{M_r} \frac{\check{P}_{r_m}(1-d_m)^v + \check{P}_s d_m^v \tilde{Z}_{r_m,min}}{\check{P}_{r_m}} \right\}, && (13.86)
\end{aligned}
$$

which is subjected to the power constraint of $P = P_s + \sum_{m=1}^{M_r} P_{r_m}$ and $P_{r_m} > 0\,(m = 1, 2, \ldots, M_r)$. The variable $\tilde{Z}_{r_m,min}$ in Equation (13.86) is defined as

$$\tilde{Z}_{r_m,min} \triangleq -e^{\tilde{R}_{c_m}}(\zeta + \ln \tilde{R}_{c_m}), \qquad (13.87)$$

where we have

$$
\begin{aligned}
\tilde{R}_{c_m} &\triangleq \frac{R_{r_m,max}}{(1-d_m)^v} && (13.88) \\
&= \frac{2N_0}{(1-d_m)^v b^2 (1-\beta)^2 P_s c_m}. && (13.89)
\end{aligned}
$$

In order to find the solution of the minimization problem formulated in Equation (13.86) with the aid of the Lagrangian method, we first define the function $f(Ps, c_m)$ by taking the logarithm of the right hand side of Equation (13.86) as

$$
\begin{aligned}
f(P_s, c_m) &\triangleq \ln\left(\frac{1}{P_s^{M_r+1}} \prod_{m=1}^{M_r} \frac{c_m(1-d_m)^v + d_m^v \tilde{Z}_{r_m,min}}{c_m} \right) && (13.90) \\
&= -(M_r+1)\ln P_s - \sum_{m=1}^{M_r} \ln c_m + \sum_{m=1}^{M_r} \ln(c_m(1-d_m)^v - d_m^v \tilde{Z}_{r_m,min}), && (13.91)
\end{aligned}
$$

where

$$c_m \triangleq \frac{P_{r_m}}{P_s}. \qquad (13.92)$$

Furthermore, we define the function $g(Ps, c_m)$ based on the transmit power constraint of Equation (13.4) as follows:

$$g(P_s, c_m) \triangleq \mathbf{c}^T \mathbf{1} - \frac{P}{P_s}, \qquad (13.93)$$

where

$$\mathbf{c} \triangleq [1, c_1, \ldots, c_{M_r}]^T, \qquad (13.94)$$

[2] In this context we note that here we effectively assume that perfect power control is used when a specific mobile is transmitting its own data as well when it is acting as an RS. Naturally, the associated transmit power may be rather different in these two modes.

and $\mathbf{1}$ represents an $(M_r \times 1)$-element column vector containing all ones. Then, the Lagrangian function Λ can be defined as

$$\Lambda(P_s, c_m, \lambda) \triangleq f(P_s, c_m) + \lambda g(P_s, c_m) \tag{13.95}$$

$$= -(M_r + 1)\ln P_s - \sum_{m=1}^{M_r} \ln c_m + \sum_{m=1}^{M_r} \ln(c_m(1-d_m)^v - d_m^v \tilde{Z}_{r_m,min}) + \lambda\left(\mathbf{c}^T\mathbf{1} - \frac{P}{P_s}\right), \tag{13.96}$$

where λ is the Lagrangian multiplier. Hence, the first-order conditions for the optimum solution can be found by setting the partial derivatives of Equation (13.96) with respect to both P_s and c_m to zero:

$$\frac{\partial\Lambda(P_s, c_m, \lambda)}{\partial P_s} = -\frac{M_r + 1}{P_s} + \lambda\frac{P}{P_s^2} + \sum_{m=1}^{M_r} \frac{d_m^v \frac{e^{\tilde{R}_{c_m}}}{P_s}[\tilde{R}_{c_m}(\zeta + \ln \tilde{R}_{c_m}) + 1]}{c_m(1-d_m)^v - d_m^v e^{\tilde{R}_{c_m}}(\zeta + \ln \tilde{R}_{c_m})} = 0, \tag{13.97}$$

$$\frac{\partial\Lambda(P_s, c_m, \lambda)}{\partial c_m} = \lambda - \frac{1}{c_m} + \frac{(1-d_m)^v + d_m^v\left[\frac{\tilde{R}_{c_m}e^{\tilde{R}_{c_m}}}{c_m}(\zeta + \ln \tilde{R}_{c_m}) + \frac{e^{\tilde{R}_{c_m}}}{c_m}\right]}{c_m(1-d_m)^v - d_m^v e^{\tilde{R}_{c_m}}(\zeta + \ln \tilde{R}_{c_m})} = 0, \tag{13.98}$$

$$\frac{\partial\Lambda(P_s, c_m, \lambda)}{\partial \lambda} = \mathbf{c}^T\mathbf{1} - \frac{P}{P_s} = 0. \tag{13.99}$$

Consequently, by combining Equations (13.97) and (13.98), after a few further manipulations we obtain

$$\frac{(M_r + 1)P_s}{P} - \frac{1}{c_m} + \frac{(1-d_m)^v + d_m^v\left[\frac{2N_0}{b^2(1-\beta^2)(1-d_m)^v P_s c_m^2} e^{\tilde{R}_{c_m}(\zeta + \ln \tilde{R}_{c_m}) + \frac{e^{\tilde{R}_{c_m}}}{c_m}}\right]}{c_m(1-d_m)^v - d_m^v e^{\tilde{R}_{c_m}}(\zeta + \ln \tilde{R}_{c_m})} - \frac{1}{P}\sum_{m=1}^{M_r} \frac{\frac{2N_0 d_m^v e^{\tilde{R}_{c_m}}}{b^2(1-\beta)^2(1-d_m)^v}\left(\zeta + \ln \tilde{R}_{c_m} + \frac{1}{\tilde{R}_{c_m}}\right)}{c_m[c_m(1-d_m)^v - d_m^v e^{\tilde{R}_{c_m}}(\zeta + \ln \tilde{R}_{c_m})]} = 0. \tag{13.100}$$

Therefore, the optimum power control can be obtained by finding the specific values of c_m $(m = 1, 2, \ldots, M_r)$ that satisfy both Equation (13.99) and (13.100), which involves an $L = (M_r + 1)$-dimensional search as specified in the summation of Equation (13.100) containing the power control of each of the M_r cooperating users. Hence, a potentially excessive computational complexity may be imposed by the search for the optimum power control solution. To reduce the search space significantly, the summation in the last term of Equation (13.100) may be removed, leading to

$$\frac{(M_r + 1)P_s}{P} - \frac{1}{c_m} + \frac{(1-d_m)^v + d_m^v\left[\frac{2N_0}{b^2(1-\beta^2)(1-d_m)^v P_s c_m^2} e^{\tilde{R}_{c_m}(\zeta + \ln \tilde{R}_{c_m}) + \frac{e^{\tilde{R}_{c_m}}}{c_m}}\right]}{c_m(1-d_m)^v - d_m^v e^{\tilde{R}_{c_m}}(\zeta + \ln \tilde{R}_{c_m})} - \frac{1}{P} \frac{\frac{2N_0 d_m^v e^{\tilde{R}_{c_m}}}{b^2(1-\beta)^2(1-d_m)^v}\left(\zeta + \ln \tilde{R}_{c_m} + \frac{1}{\tilde{R}_{c_m}}\right)}{c_m[c_m(1-d_m)^v - d_m^v e^{\tilde{R}_{c_m}}(\zeta + \ln \tilde{R}_{c_m})]} = 0, \tag{13.101}$$

so that the resultant Equation (13.101) depends only on the specific c_m value of interest. In other words, the original $(M_r + 1)$-dimensional search is reduced to a single-dimensional search, resulting in a substantially reduced power control complexity, while the resultant power control is close to that corresponding to Equation (13.100).

13.3.1.2 CUS Scheme for DAF-Aided Systems

Since the quality of the relay-related channels, namely the source–relay and the relay–destination links, dominates the achievable end-to-end performance of a DAF-aided cooperative system, the appropriate choice of cooperating users from the candidate pool of MSs roaming between the source MS and the BS as depicted in Figure 13.1 appears to be important in the scenario of cellular systems. In parallel with the APC scheme designed for the DAF-aided cooperative system discussed in Section 13.3.1.1, the CUS scheme is devised based on the minimization problem of Equation (13.84), which can be further simplified as

$$[\{\hat{d}_m\}_{m=1}^{M_r} \mid P_s, \{P_{r_m}\}_{m=1}^{M_r}] = \arg\min_{\{\check{d}_m\}_{m=1}^{M_r}} \left\{ \prod_{m=1}^{M_r} \frac{P_{r_m}\sigma_{sd}^2(1-\check{d}_m)^v + P_s\sigma_{sd}^2\check{d}_m^v Z_{r_m,min}}{\sigma_{sd}^4\check{d}_m^v(1-\check{d}_m)^v} \right\} \tag{13.102}$$

$$= \arg\min_{\{\check{d}_m\}_{m=1}^{M_r}} \left\{ \prod_{m=1}^{M_r} \frac{P_{r_m}(1-\check{d}_m)^v + P_s\check{d}_m^v \tilde{Z}_{r_m,min}}{\check{d}_m^v(1-\check{d}_m)^v} \right\}, \tag{13.103}$$

which is subjected to the physical constraint of having a normalized relay location of $0 < d_m < 1$ $(m = 1, 2, \ldots, M_r)$ measured from the source.

Although Equation (13.103) can be directly solved numerically, it is difficult to get physically tangible insights from a numerical solution. To simplify further the minimization problem of Equation (13.103), we define the function $f(d_m)$ by taking the logarithm of the right hand side of Equation (13.103), leading to

$$f(d_m) \triangleq \ln\left(\prod_{m=1}^{M_r} \frac{P_{r_m}(1-d_m)^v + P_s d_m^v \tilde{Z}_{r_m,min}}{d_m^v(1-d_m)^v} \right) \tag{13.104}$$

$$= -v\sum_{m=1}^{M_r} \ln(d_m(1-d_m)) + \sum_{m=1}^{M_r} \ln(P_{r_m}(1-d_m)^v + P_s d_m^v \tilde{Z}_{r_m,min}). \tag{13.105}$$

Then, by differentiating Equation (13.105) with respect to the normalized relay locations d_m $(m = 1, 2, \ldots, M_r)$ and equating the results to zero, we get

$$\frac{\partial f_{d_m}}{\partial d_m} = \frac{v(2d_m - 1)}{d_m(1-d_m)} + \frac{-P_{r_m}v(1-d_m)^{v-1} + P_s v d_m^{v-1}\tilde{Z}_{r_m,min} + P_s d_m^v \frac{v(e^{\tilde{R}_{c_m}} - \tilde{Z}_{r_m,min}\tilde{R}_{c_m})}{1-d_m}}{P_{r_m}(1-d_m)^v + P_s d_m^v \tilde{Z}_{r_m,min}} = 0. \tag{13.106}$$

Hence, the optimum normalized relay distance of d_m for a specific power control can be obtained by finding the specific d_m values which satisfy Equation (13.106). Consequently, the original M_r-dimensional search of Equation (13.103) is broken down into M_r single-dimensional search processes.

Although the optimized location of the cooperating users can be calculated for a given power control, the resultant location may not be the global optimum in terms of the best achievable BER performance. In other words, to attain the globally optimum location and then activate the available cooperating candidates that happen to be closest to the optimum location, an iterative power versus RS location optimization process has to be performed. To be more specific, the resultant global optimization steps are as follows:

Step 1: Initialize the starting point $(\{c_m\}_{m=1}^{M_r}, \{d_m\}_{m=1}^{M_r})$ for the search in the $2M_r$-dimensional space, hosting the M_r powers and RS locations.

Step 2: Calculate the locally optimum location $\{d_{m,local}\}_{m=1}^{M_r}$ of the cooperating users for the current power control, $\{c_m\}_{m=1}^{M_r}$.

Step 3: If we have $\{d_{m,local}\}_{m=1}^{M_r} \neq \{d_m\}_{m=1}^{M_r}$, then let $\{d_m\}_{m=1}^{M_r} = \{d_{m,local}\}_{m=1}^{M_r}$. Otherwise, stop the search, since the globally optimum solution has been found: $\{d_{m,global}\}_{m=1}^{M_r} = \{d_{m,local}\}_{m=1}^{M_r}$ and $\{c_{m,global}\}_{m=1}^{M_r} = \{c_m\}_{m=1}^{M_r}$.

Step 4: Calculate the locally optimum power control $\{c_{m,local}\}_{m=1}^{M_r}$ of the cooperating RSs for the current location, $\{d_m\}_{m=1}^{M_r}$.

Step 5: If we have $\{c_{m,local}\}_{m=1}^{M_r} \neq \{c_m\}_{m=1}^{M_r}$, then let $\{c_m\}_{m=1}^{M_r} = \{c_{m,local}\}_{m=1}^{M_r}$ and continue to **Step 1**. Otherwise, stop the search, since the globally optimum solution has been found: $\{d_{m,global}\}_{m=1}^{M_r} = \{d_{m,local}\}_{m=1}^{M_r}$ and $\{c_{m,global}\}_{m=1}^{M_r} = \{c_m\}_{m=1}^{M_r}$.

Furthermore, it is worth emphasizing that the above optimization process requires an ‘offline’ operation. Hence, its complexity does not contribute to the complexity of the real-time CUS scheme. As mentioned previously in this section, since it is likely that no available cooperating MS candidate is situated in the exact optimum location found by the offline optimization, the proposed CUS scheme simply chooses the available MS that roams closest to the optimum location and then adaptively adjusts the power control. The rationale of the CUS scheme is based on the observation that the achievable BER is proportional to the distance between the cooperating MS and the optimum location, as will be seen in Section 13.3.1.3.

13.3.1.3 Simulation Results and Discussion

Both the APC and CUS schemes designed for the DAF-aided cooperative system, which were devised in Sections 13.3.1.1 and 13.3.1.2, respectively, are based on the high-SNR-related BER lower bound of Equation (13.48), which was shown to be a tight bound for a wide range of SNRs in Figure 13.5. In order to characterize further the proposed APC and CUS schemes and to gain insights into the impact of power control as well as that of the cooperating user’s location on the end-to-end BER performance of the DAF-aided uplink supporting different number of cooperating users, the BER lower bounds are plotted versus P_s/P and d_m in Figures 13.7(a) and 13.7(b), respectively, in comparison with the exact BER of Equation (13.40) and with its upper bound of Equation (13.47). DQPSK modulation is assumed to be used here. Furthermore, in order to cope with the effects of the rapidly fluctuating fading channel, the MSDSD scheme of Section 12.3 is employed at the BS. For the sake of simplicity, we assume that an equal power is allocated to all activated cooperating MSs, which are also assumed to be located at the same distance from the source MS. All the other system parameters are summarized in Table 13.3. Observe from both Figures 13.7(a) and 13.7(b) that at a moderate SNR of $15\,$dB the lower bounds remain tight across the entire horizontal axes, i.e. regardless of the specific values of P_s/P and d_m. By contrast, the upper bound of Equation (13.47) fails to predict accurately the associated BER trends, especially when the number of activated cooperating MSs, M_r, is high. Therefore, despite using the much simpler optimization metrics of Equations (13.86) and (13.103), which are based on the high-SNR-related BER lower bound of Equation (13.48), the APC and CUS schemes of Sections 13.3.1.1 and 13.3.1.2 are expected to remain accurate for quite a wide range of SNRs.

Furthermore, both the power control strategy and the specific location of the cooperating MSs play a vital role in determining the achievable BER performance of the DAF-aided cooperative system. Specifically, as shown in Figure 13.7(a), under the assumption that all the activated cooperating users are located about half-way between the source MS and the BS, i.e. for $d_m = 0.5$ $(m = 1, 2, \ldots, M_r)$, and for an equal power allocation among the cooperating users, i.e. for $P_{r_m} = (P - P_s)/M_r$ $m = 1, 2, \ldots, M_r)$, the minimum of the BER curve is shifted to the left when an increased number of cooperating MSs participate in signal relaying. This indicates that the transmit power employed by the source MS should be decreased in order to attain the best achievable end-to-end BER performance. On the other hand, under the assumption of an equal power allocation among the source MS and all the cooperating MSs, i.e. where we have $P_s = P_{r_m} = P/M_r$ $(m = 1, 2, \ldots, M_r)$, we observe from Figure 13.7(b) that the shape of the BER curves indicates a stronger sensitivity of the system’s performance to the location of the cooperating users. This trend becomes even more dominant as the number of cooperating MSs, M_r, increases. However, in contrast to the phenomenon observed in Figure 13.7(a), the position of the BER minimum remains nearly unchanged, as observed in Figure 13.7(b), indicating that the optimum location of the cooperating users remains unaffected for this specific system arrangement, regardless of M_r.

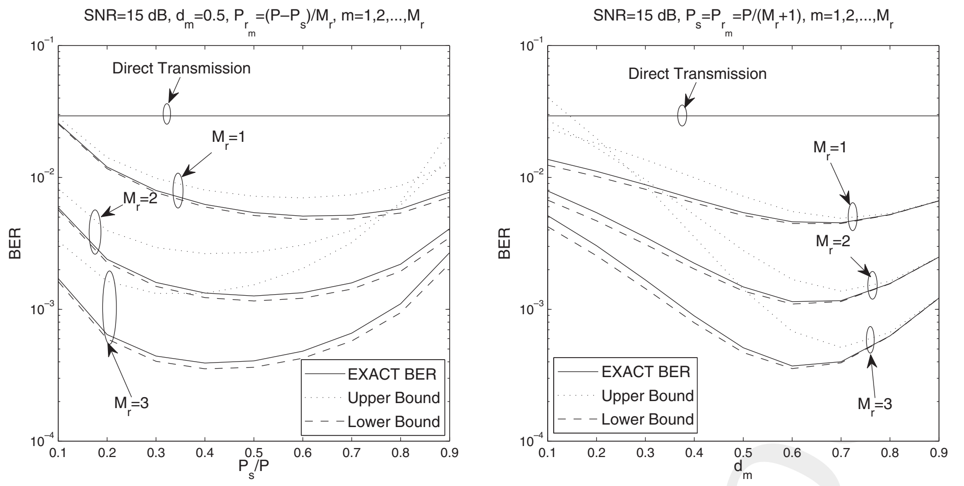

(a) Effects of the power control (b) Effects of the cooperating MS's locations

Figure 13.7: Effects of the power control and of the cooperating MS's location on the BER performance of DQPSK-modulated DAF-aided cooperative cellular systems having M_r activated cooperating MSs. All other system parameters are summarized in Table 13.3.

Table 13.3: Summary of system parameters.

System parameters	Choice
System	User-cooperative cellular uplink
Cooperative protocol	DAF
Number of relay nodes	M_r
Number of subcarriers	$D = 1024$
Modulation	DQPSK
Detection	MSDSD ($N_{wind} = 11$)
Packet length	$L_f = 128$
Normalized Doppler freq.	$f_d = 0.008$
Path-loss exponent	Typical urban area, $v = 3$ [608]
Channel model	Typical urban, refer to Table 12.1
Noise variance at MS and BS	N_0

Importantly, the horizontal coordinate of the BER minimum represents the optimum MS location for the equal power allocation arrangement employed. Therefore, the achievable BER seen in Figure 13.7(b) is proportional to the distance between the RS and the optimum location, which provides the rationale for our distance-based CUS scheme.

In order to examine the tightness of the high-SNR-based BER lower bound of Equation (13.48) for the DAF-aided cooperative system at different transmit SNRs of P/N_0, the BER lower bounds corresponding to three distinct values of P/N_0 versus different power controls and relay locations are depicted in Figures 13.8(a) and 13.8(b), respectively. Let us assume that $M_r = 2$ cooperating MSs are activated. With an SNR as high as 20 dB, the lower bound is tight, as seen in both Figures 13.8(a) and 13.8(b). As the SNR decreases, the lower bound becomes increasingly loose, but remains capable of accurately predicting the BER trends and the best achievable performance in the vicinity of a moderate SNR level of 15 dB. However, when the SNR falls to as low a value as 10 dB, the lower bound remains

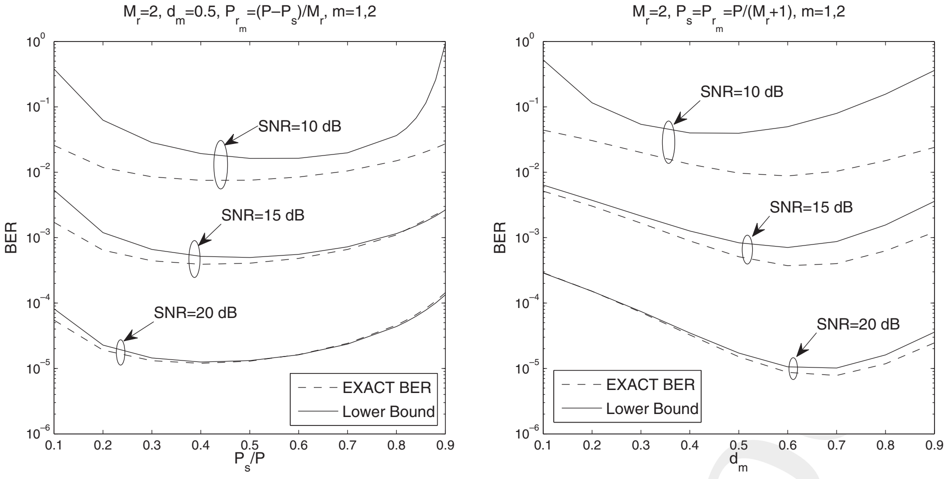

(a) BER versus P_s/P (b) BER versus d_m

Figure 13.8: Effects of the SNR on the tightness of the high-SNR-based BER lower bound for the DQPSK-modulated DAF-aided cooperative cellular uplink having two activated cooperating MSs. All other system parameters are summarized in Table 13.3.

no longer tight to approximate the exact BER, thus the APC and CUS schemes devised under the assumption of a high SNR may not hold the promise of an accurate solution. Nevertheless, since the low SNR range corresponding to high BER levels, such as for example 10^{-2}, is not within our range of interest, the proposed APC and CUS schemes of Sections 13.3.1.1 and 13.3.1.2 are expected to work appropriately for a wide range of SNRs.

Let us now continue by investigating the performance improvements achieved by the optimization of the power control and the cooperating user's location. In Figure 13.9(a) the BER performance of the DAF-aided cooperative system employing the APC scheme of Section 13.3.1.1 is depicted versus the cooperating user's location, d_m, in comparison with that of the system dispensing with the APC scheme. Again, we simply assume that multiple activated cooperating users are located at the same distance from the source user. Observe in Figure 13.9 that significant performance improvements can be achieved by the APC scheme when the cooperating user is situated closer to the BS than to the source MS. Hence the attainable BER is expected to be improved as the cooperating user moves increasingly closer to the BS. For example, the single cooperating user ($M_r = 1$) DAF-aided cooperative system using the APC scheme is capable of attaining its lowest possible BER at $\mathrm{SNR} = 15\,\mathrm{dB}$, when we have $d_1 = D_{sr_1}/D_{sd} = 0.8$. Therefore, the performance improvement achieved by the APC scheme largely depends on the specific location of the cooperating users. Furthermore, the performance gains attained by the APC scheme for a specific arrangement of d_m is also dependent on the number of activated cooperating MSs, M_r. More specifically, when we have $M_r = 3$, a substantially larger gap is created between the BER curve of the system dispensing with the APC scheme and that of its APC-aided counterpart than that observed for $M_r = 1$, as seen in Figure 13.9(a).

At the same time, the BER performance of the DAF-aided system using relay location optimization is plotted in Figure 13.9(b) in comparison with that of the cooperative system, where the multiple activated cooperating users roam midway between the source MS and the BS. Similarly, a potentially substantial performance gain can be achieved by optimizing the location of the cooperating users, although, naturally, this gain depends on the specific power control regime employed as well as on the number of activated cooperating users. To be specific, observe in Figure 13.9(b) that it is desirable to assign the majority of the total transmit power to the source MS in favour of maximizing the achievable

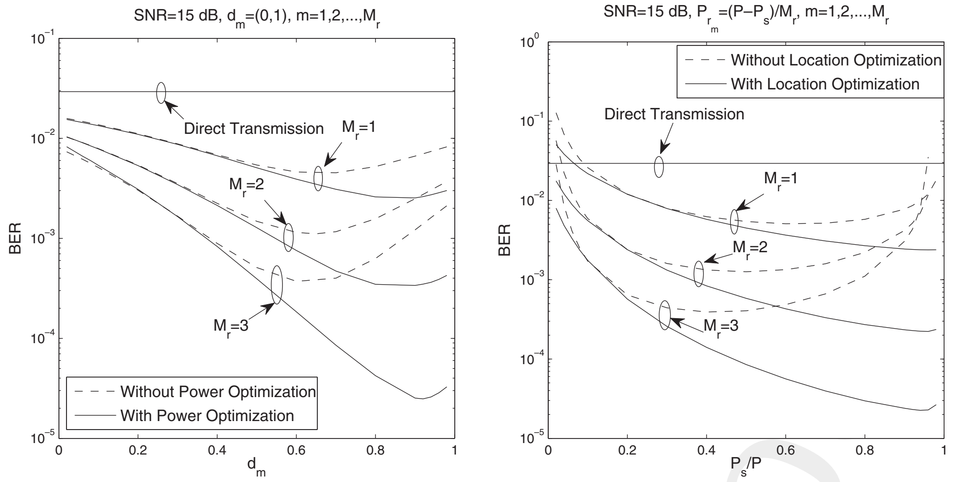

(a) Adaptive power control

(b) Relay location optimization

Figure 13.9: Power and relay location optimization for DQPSK-modulated DAF-aided cooperative cellular systems having M_r activated cooperating MSs. All other system parameters are summarized in Table 13.3. ©IEEE Wang & Hanzo 2007 [8]

performance gain by location optimization. Moreover, the more the cooperating users are activated, the higher the performance enhancement attained. Importantly, in the presence of a deficient power control regime, e.g. when less than 10% of the overall transmit power is assigned to the source MS, the DAF-aided system may suffer from a severe performance loss, regardless of the location of the cooperating users. This scenario results in an even worse performance than that of the non-cooperative system. Therefore, by observing Figures 13.9(a) and 13.9(b) we infer that for the DAF-aided cooperative uplink, it is beneficial to assign the majority of the total transmit power to the source MS and choose the specific cooperating users roaming in the vicinity of the BS in order to enhance the achievable end-to-end BER performance.

The above observations concerning the cooperative resource allocation of the DAF-aided system can also be inferred by depicting the three-dimensional BER surface versus both the power control and the cooperating MS's location in Figure 13.10(a) for a single-RS-aided cooperative system ($M_r = 1$). Indeed, the optimum solution is located in the area where both P_s/P and d_1 have high values. In order to reach the optimum operating point, the iterative optimization process discussed in Section 13.3.1.2 has to be invoked. The resultant optimization trajectory is depicted in Figure 13.10(b) together with the individual power-optimization- and location-optimization-based curves. The intersection point of the latter two lines represents the globally optimum joint power–location solution. As seen in Figure 13.10(b), by commencing the search from the centre of the two-dimensional power–location plane, the optimization process converges after four iterations between the power and location optimization phases, as the corresponding trajectory converges on the above-mentioned point of intersection.

Let us now consider a DAF-aided DQPSK-modulated cooperative cellular system employing both the CUS and APC schemes of Sections 13.3.1.1 and 13.3.1.2, where $M_r = 3$ cooperating MSs are activated in order to amplify and forward the signal received from the source MS to the BS, which are selected from $\mathcal{P}_{cand} = 9$ candidates roaming between the latter two. Without loss of generality, we simply assume that the locations of all the cooperating candidates are independent and uniformly distributed along the direct LOS link connecting the source MS and the BS, which are expected to change from time to time. Figure 13.11 depicts the performance of the DAF-aided cooperative

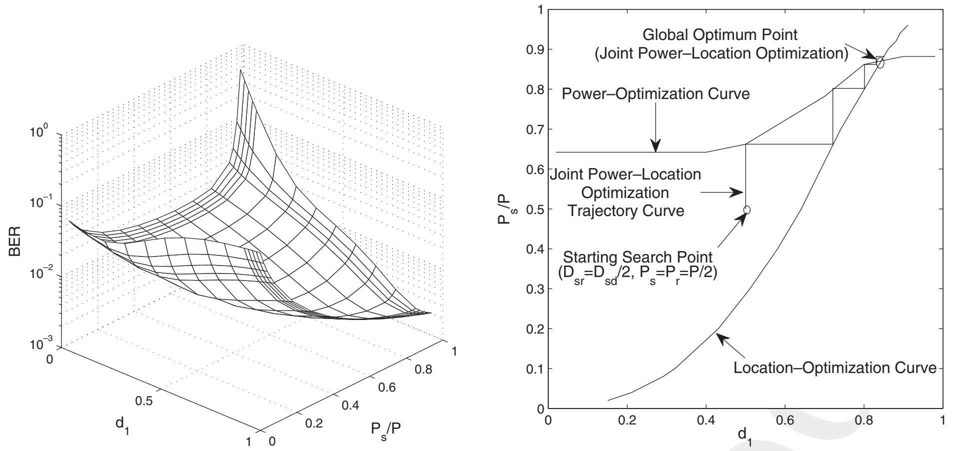

(a) BER surface (b) Search trajectory

Figure 13.10: Optimum cooperative resource allocation for DQPSK-modulated DAF-aided cooperative cellular systems having a single activated cooperating MS at SNR $= 15$ dB. All other system parameters are summarized in Table 13.3.

system employing the CUS and APC schemes of Sections 13.3.1.1 and 13.3.1.2 in comparison with both that exhibited by its counterpart dispensing with the above-mentioned techniques and that of the direct-transmission-based system operating without user cooperation in Rayleigh fading channels associated with different normalized Doppler frequencies. Figure 13.11 demonstrates that the DAF-aided cooperative system is capable of achieving a significantly better performance than the non-cooperative system. Observe in Figure 13.11 that a further significant performance gain of 10 dB can be attained by invoking the CUS and APC schemes for a cooperative system employing the CDD of Section 12.1.1 ($N_{wind} = 2$), at a BER target of 10^{-5} and a normalized Doppler frequency of $f_d = 0.008$. Furthermore, employment of the CUS combined with the APC makes the cooperative cellular system more robust to the deleterious effects of time-selective channels. Indeed, observe in Figure 13.11 that an error floor is induced by a normalized Doppler frequency of $f_d = 0.03$ at a BER of 10^{-3} for the cooperative system dispensing with the CUS and APC arrangements, while the BER curve corresponding to the system carrying out cooperative resource allocation only starts to level out at a BER of 10^{-5}. For the sake of further eliminating the BER degradation caused by severely time-selective channels, the MSDSD employing $N_{wind} > 2$ can be utilized at the BS. As observed in Figure 13.11, for a target BER level of 10^{-5}, a P/N_0 degradation of about 7 dB was induced by increasing f_d from 0.008 to 0.03 for the CDD-aided system, while it was reduced to 1 dB by activating the MSDSD scheme of Section 12.3 using $N_{wind} = 11$.

Let us now consider the BER performance of DAF-aided cooperative systems dispensing with at least one of the two above-mentioned schemes, which is plotted in Figure 13.12(a). To be more specific, given a target BER of 10^{-5}, performance gains of 6 and 2.5 dB can be achieved respectively by employment of the CUS and APC over the benchmark system, where three cooperating users are randomly selected from the available nine RS candidates and the total transmit power is equally divided between the source and the relaying MSs. Hence, the distance-based CUS scheme of Section 13.3.1.2 performs well as a benefit of activating the RS candidates closest to the predetermined optimum locations, even in conjunction with a relatively small cooperating RS candidate pool, where it is more likely that none of the available RS candidates is situated in the optimum locations. In order further to enhance the achievable end-to-end performance, the APC is carried out based on the cooperating users' location as activated by the CUS and results in a performance gain as high as about 9.5 dB over

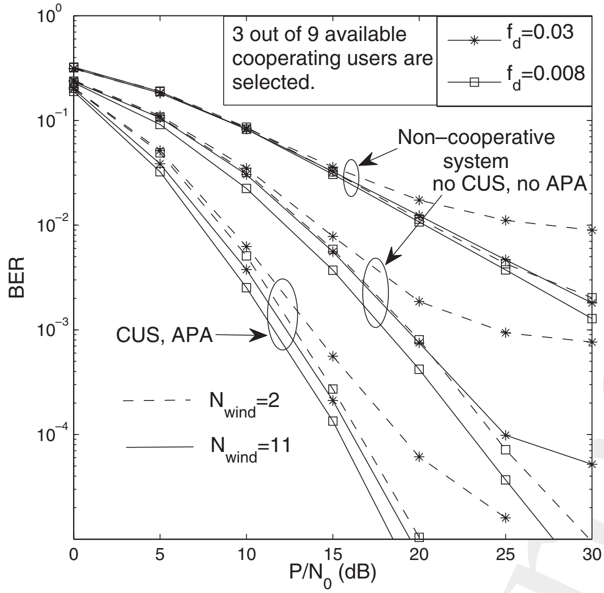

Figure 13.11: Performance improvements achieved by the CUS and APC schemes for a DAF-aided DQPSK-modulated user-cooperative cellular system employing the MSDSD of Section 12.3, where three out of nine cooperating user candidates are activated. All other system parameters are summarized in Table 13.3.

the benchmark system, as demonstrated in Figure 13.12(a). Moreover, besides providing performance gains, the CUS and APC schemes are also capable of achieving a significant complexity reduction in the context of the MSDSD employed by the BS, as seen in Figure 13.12(b), where the complexity imposed by the MSDSD using $N_{wind} = 11$ expressed in terms of the number of the PED evaluations versus P/N_0 is portrayed correspondingly to the four BER curves of Figure 13.12(a). Although the complexity imposed by the MSDSD in all of the four scenarios considered decreases steadily, the transmit SNR increases and then levels out at a certain SNR value around 20 dB. Observe in Figure 13.12(b) that a reduced complexity is imposed when either the CUS or the APC scheme is employed. Remarkably, the complexity imposed by the MSDSD at the BS can be reduced by a factor of about 10 for a wide range of transmit SNRs, when the CUS and APC are amalgamated. By carefully comparing the simulation results of Figures 13.12(a) and 13.12(b), it may be readily observed that the transmit SNR level, which guarantees the BER of 10^{-5}, is roughly the SNR level at which the complexity imposed by the MSDSD starts to level out. Therefore, it is inferred from the above observations that an appropriate cooperative resource allocation expressed in terms of the transmit power control and the appropriate cooperating user selection may significantly enhance the achievable end-to-end BER performance of the DAF-aided cooperative cellular uplink, while substantially reducing the computing power required by the MSDSD at the BS.

In a typical cellular system, the number of users roaming in a cell may also be referred to as the size of the cooperating user candidate pool denoted by $\mathcal{P}_{cand}$ in the scenario of the user-cooperative uplink. In order to investigate its impacts on the end-to-end BER performance of the DAF-aided cooperative system employing the CUS and APC schemes, the BER curves corresponding to different values of $\mathcal{P}_{cand}$ are plotted versus the transmit SNR, P/N_0, against that of the idealized scenario used as a benchmark, where the activated RSs are situated exactly in the optimum locations and have the optimum power control. Again, we assume that $M_r = 3$ RSs are activated, which are selected from the $\mathcal{P}_{cand}$ MSs roaming in the same cell. Interestingly, despite having a fixed number of activated

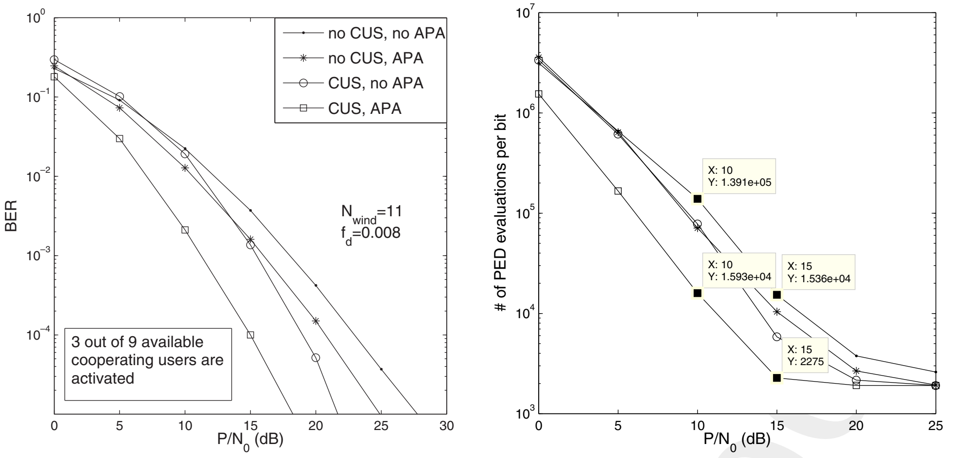

(a) BER performance (b) Complexity imposed by the MSDSD

Figure 13.12: BER performance and the MSDSD complexity reductions achieved by the CUS and APC schemes for DAF-aided DQPSK-modulated user-cooperative cellular uplink, where three out of nine cooperating RS candidates are activated. All other system parameters are summarized in Table 13.3.

cooperating MSs, the end-to-end BER performance of the DAF-aided system steadily improves and approaches that of the idealized benchmark system upon increasing the value of $\mathcal{P}_{cand}$, as observed in Figure 13.13(a). On the other hand, it can be seen in Figure 13.13(b) that the higher the number of cooperating candidates, the lower the computational complexity imposed by the MSDSD at the BS. Specifically, by increasing the size of the candidate pool from $\mathcal{P}_{cand} = 3$ to 9, a performance gain of about 7 dB can be attained, while simultaneously achieving a detection complexity reduction factor of 6.5 at the target BER of 10^{-5}. In comparison with the idealized scenario, where an infinite number of cooperating candidates are assumed to be independently and uniformly distributed between the source MS and the BS, the DAF-aided cooperative system using both the CUS and APC schemes only suffers a negligible performance loss when $\mathcal{P}_{cand} = 9$ cooperating candidates. Therefore, the benefits brought about by the employment of the CUS and APC schemes may be deemed substantial in a typical cellular uplink.

13.3.2 CUS Scheme for DDF Systems with APC

In contrast to the process of obtaining the optimum power and location allocation arrangements discussed in Section 13.3.1 for DAF-aided cooperative systems, the first-order conditions obtained by differentiating the BER bound of a DDF-aided cooperative system formulated in Equations (13.56) and (13.74) for the $M_r = 1$ and $M_r = 2$ scenarios have complicated forms which are impervious to analytical solution. However, their numerical solution is feasible, instead of resorting to Monte Carlo simulations. Explicitly, by taking $M_r = 1$ as an example, the optimum power control can be obtained for a given RS location arrangement by minimizing the worst-case BER of Equation (13.56), yielding

$$\begin{aligned}
&[\hat{P}_s, \{\hat{P}_{r_m}\}_{m=1}^{M_r} \mid \{d_m\}_{m=1}^{M_r}] \\
&\quad = \underset{\check{P}_s, \{\check{P}_{r_m}\}_{m=1}^{M_r}}{\arg\min} \ \{(1 - P_{PLR_1,upper}) P_{BER}^{\Phi_1} + P_{PLR_1,upper} P_{BER}^{\Phi_2}\},
\end{aligned} \tag{13.107}$$

where $P_{PLR_1,upper}$ is the worst-case packet loss ratio at the cooperating MS, which is given by Equation (13.52), while $P_{BER}^{\Phi_1}$ and $P_{BER}^{\Phi_2}$ are given by Equations (13.64) and (13.70), respectively,

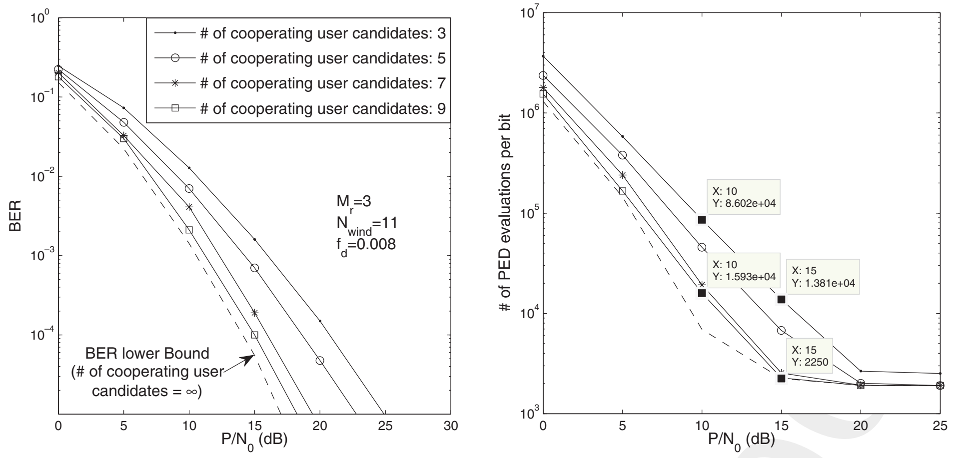

(a) BER performance

(b) Complexity imposed by the MSDSD

Figure 13.13: The effects of the size of the cooperating RS pool on the DAF-aided DQPSK-modulated user-cooperative cellular uplink employing the CUS and APC schemes, where $M_r = 3$ cooperating users are activated. All other system parameters are summarized in Table 13.3.

corresponding to the average BER measured at the BS both with and without the signal forwarded by the RS. In parallel, the optimum location allocation can be obtained for a specific power control arrangement as

$$\begin{aligned}&[\{\hat{d}_m\}_{m=1}^{M_r} \mid P_s, \{P_{r_m}\}_{m=1}^{M_r}] \\ &\quad = \underset{\{\hat{d}_m\}_{m=1}^{M_r}}{\arg\min} \{(1 - P_{PLR_1,upper})P_{BER}^{\Phi_1} + P_{PLR_1,upper}P_{BER}^{\Phi_2}\}.\end{aligned} \tag{13.108}$$

Then, to attain the globally optimum location and activate the available cooperating candidates that happen to be closest to the optimum location, an iterative power versus RS location optimization process identical to that discussed in Section 13.3.1.2 in the context of an AF scheme has to be performed. Again, the rationale of the proposed CUS scheme for the DDF-aided system is based on the observation that the achievable BER is proportional to the distance between the cooperating MS and the optimum location, as will be demonstrated in Section 13.3.2.1.

13.3.2.1 Simulation Results and Discussion

The beneficial effects of cooperative resource allocation, in terms of the transmit power and the cooperating user's location on the achievable BER performance of the DDF-aided cooperative system, are investigated in Figure 13.14. Under the assumption that the channel fluctuates extremely slowly, e.g. for $f_d = 0.0001$, the worst-case BER performances corresponding to Equation (13.56) for $M_r = 1$ and to Equation (13.74) for $M_r = 2$, for the DQPSK-modulated DDF-aided cooperative systems employing either equal power allocation or the optimized power control, are plotted versus the different cooperating users' locations in Figure 13.14(a). The information bit stream is CCITT-4 coded by the source MS in order to carry out the CRC checking at the cooperating MS with the aid of a 32-bit CRC sequence. Hence, to maintain a relatively high effective throughput, two different transmission packet lengths are used, namely $L_f = 128$ and $L_f = 64$ DQPSK symbols. All other system parameters are summarized in Table 13.3. Observe in Figure 13.14(a) that the end-to-end BER performance can be substantially enhanced by employing the optimized power control, if the cooperating MS is not roaming in the neighbourhood of the source MS. Similar to the observation obtained for its DAF-aided counterparts

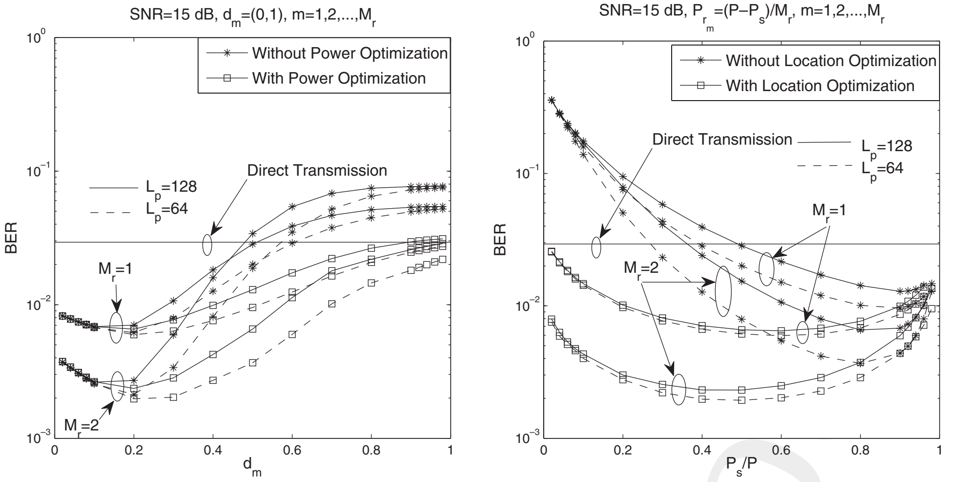

(a) Adaptive power control (b) Relay location optimization

Figure 13.14: Power and relay location optimization for the DQPSK-modulated DDF-aided cooperative cellular systems having M_r activated cooperating MSs. All other system parameters are summarized in Table 13.4. ©IEEE Wang & Hanzo 2007 [8]

Table 13.4: Summary of system parameters.

System parameters	Choice
System	User-cooperative cellular uplink
Cooperative protocol	DDF
Number of relay nodes	M_r
Number of subcarriers	$D = 1024$
Modulation	DQPSK
CRC code	CCITT-4
Detection	MSDSD ($N_{wind} = 11$)
Packet length	L_f
Normalized Doppler freq.	f_d
Path-loss exponent	Typical urban area, $v = 3$ [608]
Channel model	Typical urban, refer to Table 12.1
Noise variance at MS and BS	N_0

characterized in Figure 13.9(a) of Section 13.3.1.3, the higher the number of active cooperating MSs, M_r, the more significant the performance gain attained by optimizing the power control for the DDF-aided system. However, due to the difference between the relaying mechanisms employed by the two above-mentioned cooperative systems, it is interesting to observe that the trends seen in Figure 13.14(a) are quite different from those emerging from Figure 13.9(a). Specifically, recall from the results depicted in Figure 13.9(a) that it is desirable to choose multiple cooperating users closer to the BS than to the source MS in a DAF-aided cooperative system, especially when employing the optimized power control for sharing the power among the cooperating users. By contrast, Figure 13.14(a) demonstrates that the cooperating MSs roaming in the vicinity of the source MS are preferred for a DDF-aided system in the interest of maintaining a better BER performance. Furthermore, the performance gap between the DAF-aided systems employing both the equal and optimized power allocations becomes wider as the cooperating MS moves closer to the optimum location corresponding to the horizontal coordinate of the lowest-BER point in Figure 13.9(a). By contrast, only a negligible performance improvement can be achieved by optimizing the power control, if the cooperating MS is close to the optimum location corresponding also to the horizontal coordinate of the lowest-BER point in Figure 13.14(a). In other words, the DDF-aided system suffers a relatively modest performance loss by employing the simple equal power allocation, if the multiple cooperating MSs are closer to their desired locations. Additionally, recall from Figure 13.9(a) recorded for the DAF-aided system that the worst-case BER performance was encountered by having no cooperating user closer to the optimum locations, regardless of whether the optimum power control is used or not, but the performance of this RS-aided DAF system was still slightly better than that of the conventional direct transmission system. By contrast, the DDF-aided system employing equal power allocation may unfortunately be outperformed by the direct-transmission-based non-cooperative system, if the cooperating MSs are located nearer to the BS than to the source MS. Finally, in contrast to the DAF-assisted system, the performance achieved by the DDF-aided system is dependent on the specific packet length, L_f, due to the potential relaying deactivation controlled by the CRC check carried out at the cooperating MS. To be specific, the shorter the packet length L_f, the lower the resultant BER.

In parallel, the BER performance of the above-mentioned DDF-aided systems is depicted versus P_s/P in Figure 13.14(b). Here, the transmit power of $(P - P_s)$ is assumed to be equally shared across multiple cooperating users. Again, similar to the results recorded for the DAF-aided system in Figure 13.9(b), a significant performance gain can be attained by locating the cooperating MS at the optimum position rather than in the middle of the source MS and BS path. This performance gain is expected to become even higher as the number of actively cooperating MSs, M_r, increases, as seen in Figure 13.14(b). By contrast, for optimum cooperating user location, instead of allocating the majority of the total transmit power to the source MS – as was suggested by Figure 13.9(b) for the DAF-aided system in the interest of achieving an improved BER performance – the results of Figure 13.14(b) suggest that only about half of the total power has to be assigned to the source MS, if the DDF scheme is used. Furthermore, the mild sensitivity of the BER performance observed in Figure 13.14(b) for the DDF-aided system benefiting from the optimum cooperating user location as far as the power control is concerned coincides with the trends seen in Figure 13.14(a), i.e. a desirable BER performance can still be achieved without optimizing the power control, provided that all the cooperating MSs roam in the vicinity of their optimum locations. Interestingly, in contrast to the conclusions inferred from Figure 13.14(a) for the DAF-aided system, the originally significant performance differences caused by the different packet lengths of $L_f = 128$ and $L_f = 64$ can be substantially reduced for the DDF-aided system, provided that the cooperating user is situated at the optimum location. Finally, as observed in Figure 13.14(b), when no active RS can be found in the vicinity of the optimum cooperating user locations, the DDF-aided system might be outperformed by its more simple direct transmission counterpart in the presence of deficient power control imposed by high power control errors.

Observe for the $M_r = 1$ scenario by merging Figures 13.14(a) and 13.14(b) that the globally optimum cooperative resource allocation characterized in terms of the transmit power control and RS selection regime can be visualized as the horizontal coordinates of the lowest point of the resultant 3D BER surface portrayed in Figure 13.15(a), where the 3D BER surface corresponding to different L_f values is plotted versus P_s/P and $d_1 = D_{sr_1}/D_{sd}$ for the DDF-aided cooperative system. The smaller the packet length L_f, the lower the BER. This is because the likelihood that the activated cooperating MS improves the signal relaying is inversely proportional to the packet length L_f. However, observe in Figure 13.15(a) that the gap between the different BER curves of 3D surface becomes relatively small in the vicinity of the globally optimum BER point, as predicted by Figures 13.14(a) and 13.14(b). On the other hand, similar to the results of Figure 13.10(b) recorded for the DAF-aided cooperative system, we plot the power-optimized curve versus d_1, while drawing the location-optimized curve versus P_s/P for the DDF-aided system associated with $M_r = 1$ in Figure 13.15(b), where the intersection of the two curves is the globally optimum solution corresponding to the projection of the lowest BER point onto the horizontal plane in Figure 13.15(a). The globally optimum solution can be found by the joint power–location iterative optimization process discussed in Section 13.3.1.2. Furthermore, the globally

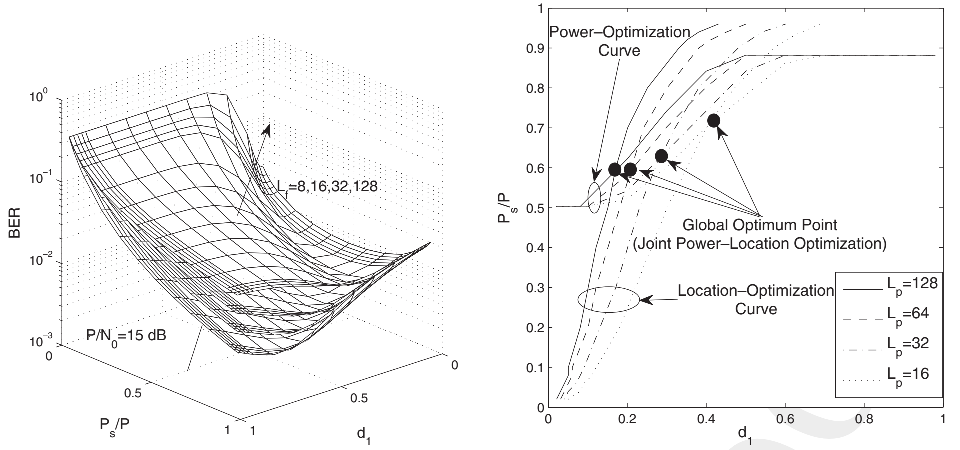

(a) BER surface (b) Globally optimum point

Figure 13.15: Optimum cooperative resource allocation for the DQPSK-modulated DDF-aided cooperative cellular systems having a single activated cooperating MS at $\mathrm{SNR} = 15\,$dB. All other system parameters are summarized in Table 13.4.

optimum resource allocation, denoted by the black dot in Figure 13.15(b), changes as the packet length L_f varies. To be more specific, by increasing the packet length L_f, the optimum cooperating user location moves increasingly closer to the source MS, while the percentage of the total transmit power assigned to the source MS gradually decreases. This is not unexpected, since the probability of perfectly recovering all the symbols of the source MS by the cooperating MS is reduced on employing a higher packet length L_f, which has to be increased by choosing a cooperating MS closer to the source MS in the interest of increasing the received SNR at the cooperating MS.

Let us now continue by examining the BER performance improvement achieved by optimizing the resource allocation for the DDF-aided cooperative system in Figure 13.16, where the four subfigures depict the BER performance of the systems both with and without optimized cooperative resource allocation in terms of the transmit power and relay locations, while varying the packet length L_f. As seen in Figure 13.16, significant performance gains can be attained by using an optimum power control among the M_r cooperating users and the source user, as well as by assuming that all the M_r actively cooperating users are situated in their optimum locations, especially when we have a relatively large packet length L_f. Although a better PLR performance is attained when using short packets, the achievable performance gain is reduced, as indicated by the increasingly narrower gap between the BER curves obtained with and without the optimized resource allocation. Consider the $M_r = 2$ scenario as an example, where the originally achievable performance gain of $5\,$dB recorded for $L_f = 128$ is reduced to about $0.5\,$dB for $L_f = 16$ at a BER of 10^{-5}. In fact, this phenomenon coincides with the observation inferred from our previous simulation results, such as for example the 3D BER surface shown in Figure 13.15(a), which can be explained by the fact that the BER and PLR performance loss induced by a high packet length L_f may be significantly reduced by optimizing the cooperative resource allocation. Again for the scenario of $M_r = 2$, a performance loss of $5\,$dB is endured when employing $L_f = 64$ instead of $L_f = 16$ in the absence of resource allocation optimization, whereas the performance loss is reduced to $1.5\,$dB when the cooperative resource allocation is optimized. Furthermore, we also found that, interestingly, the asymptotic theoretical curves based on the worst-case BER expressions of Equation (13.56) and Equation (13.74) for $M_r = 1$ and $M_r = 2$, respectively, become tighter for the DDF-aided system using optimized resource allocation.

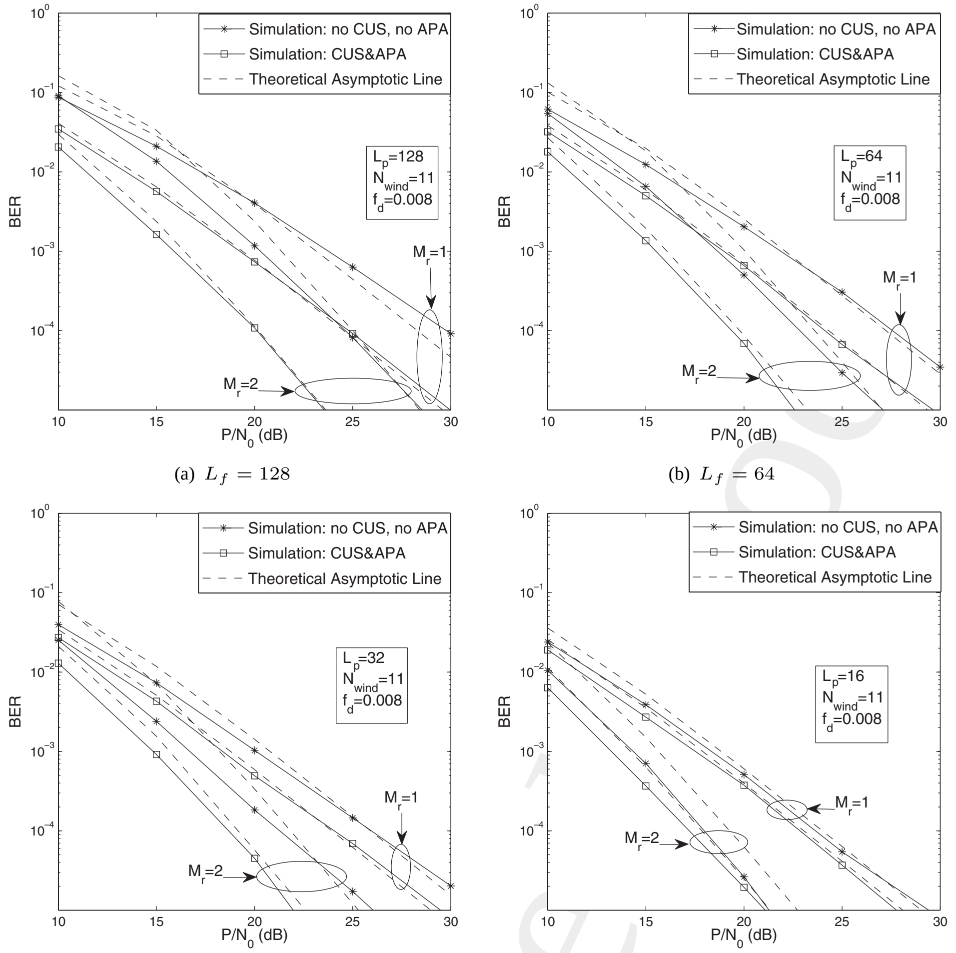

(a) $L_f = 128$

(b) $L_f = 64$

(c) $L_f = 32$

(d) $L_f = 16$

Figure 13.16: Performance improvement achieved by optimizing the cooperative resources for the DQPSK-modulated DDF-aided cooperative cellular systems employing the MSDSD in a relatively fast Rayleigh fading channel, where the M_r activated cooperating users are assumed to be situated at their optimum location. All other system parameters are summarized in Table 13.4.

Figure 13.17 separately investigates the impact of the CUS and that of the APC on the end-to-end BER performance of a DDF-aided cooperative system employing the MSDSD in a relatively rapidly Rayleigh fading channel associated with $f_d = 0.008$, where $N_{wind} = 8$ is employed to combat the performance degradation induced by the time-selective fading channel. Similar to the results of Figure 13.12(a) recorded for the DAF-aided system, a more significant performance improvement can be attained by invoking CUS than APC. However, in contrast to the DAF-aided system, the joint employment of the CUS and APC schemes for the DDF-aided system only leads to a negligible additional performance gain over the scenario where only the CUS is carried out. This is not unexpected, if we recall the observations inferred from Figure 13.14(a), i.e. the additional performance improvement achieved by optimizing the power control gradually erodes as the activated cooperating MS approaches the optimum location. Furthermore, unlike the CUS scheme, which simply selects the cooperating

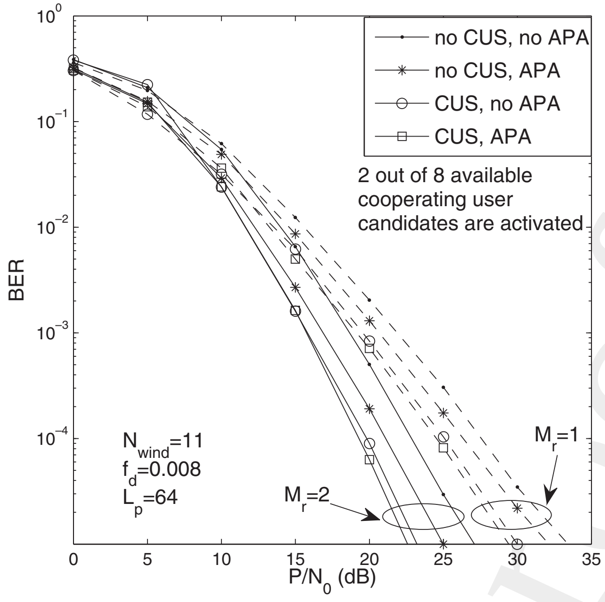

Figure 13.17: Performance improvements achieved by the CUS and APC schemes for the DDF-aided DQPSK-modulated user-cooperative cellular system employing the MSDSD in a relatively fast Rayleigh fading channel, where two out of eight cooperating users are activated. All other system parameters are summarized in Table 13.4.

MS that is closest to the optimum location calculated in an offline manner, the APC scheme, which conducts a real-time search for the optimum power control based on the actual location of the activated cooperating MS, may impose an excessive complexity. Hence, for reducing the complexity, the DDF-aided cooperative system may simply employ equal power allocation, while still being capable of achieving a desirable performance with the aid of the CUS scheme.

13.4 Joint CPS and CUS for the Differential Cooperative Cellular UL Using APC

From our discussions on the performance of the DAF- and DDF-aided cooperative cellular uplink in Sections 13.3.1.3 and 13.3.2.1, respectively, we may conclude that the above-mentioned two scenarios exhibit numerous distinct characteristics due to the employment of different relaying mechanisms. Therefore, the comparison of these two cooperative schemes will be further detailed in Section 13.4.1. Based on the initial comparison of the DAF and DDF schemes, a novel hybrid CPS scheme will be proposed in Section 13.4.2. In conjunction with the CUS and APC arrangements, we will then create a more flexible cooperative system, where the multiple cooperating MSs roaming in different areas might employ different relaying mechanisms to assist in forwarding the source MS's message to the BS to achieve the best possible BER performance. This system may be viewed as a sophisticated hybrid of a BS-aided ad hoc network or – alternatively – as an ad hoc network-assisted cellular network.

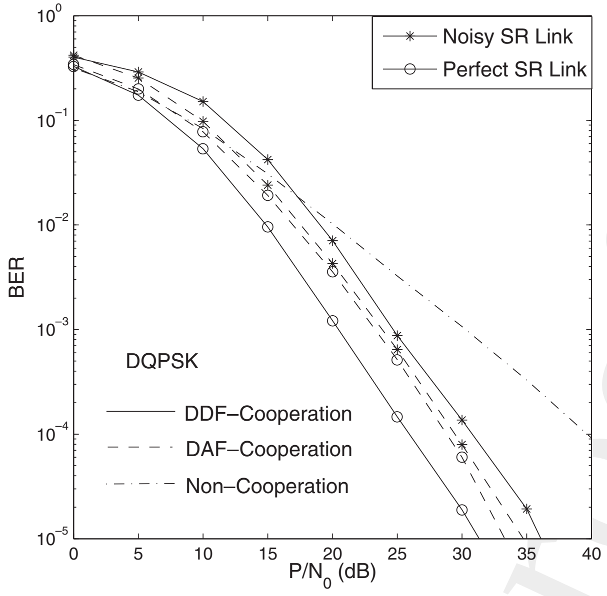

Figure 13.18: Impact of the source–relay link's quality on the end-to-end BER performance of a DQPSK-modulated cooperative system employing $M_r = 1$ cooperating RS roaming about half-way between the source MS and the BS. The CDD is employed by both the RS and the BS in a Rayleigh fading channel having a Doppler frequency of $f_d = 0.001$.

13.4.1 Comparison Between the DAF- and DDF-Aided Cooperative Cellular UL

13.4.1.1 Sensitivity to the Source–Relay Link Quality

The fundamental difference between the DAF and DDF schemes is whether decoding and re-encoding operations are required at the RS or not. Thus, generally speaking, the overall complexity imposed by the DDF-aided cooperative system is expected to be higher than that of its DAF-aided counterpart. However, as a benefit of preventing error propagation by the RS, the DDF-aided system is expected to outperform the DAF-aided one, provided that a sufficiently high source–relay link quality guarantees a near-error-free transmission between the source MS and the RS, as previously indicated by Figure 12.14 of Section 12.3.2.3. For convenience, we repeat these results here in Figure 13.18, where we observe that the sensitivity of the DDF-aided system to the source–relay link quality is significantly higher than that of the DAF-aided system. This is because the CRC employed may suggest to the RS to refrain from participating in forwarding the signal to the BS with a high probability, when the source–relay link is of low quality, which in turn leads to a rapid performance degradation. In practice, a high performance can be achieved for the DDF-aided system by activating the cooperating MSs roaming in the vicinity of the source MS and/or by invoking channel encoding.

13.4.1.2 Effect of the Packet Length

In contrast to the DAF-aided system, where the achievable performance is independent of the packet length L_f employed in the absence of the channel encoding, the DDF-aided system's performance is sensitive to the packet length L_f, as was previously demonstrated for example by Figure 13.16 of Section 13.3.2.1. This trend is not unexpected, since in the absence of the channel coding the PLR increases proportional to the value of L_f. This in turn may precipitate errors in the context of a DDF-

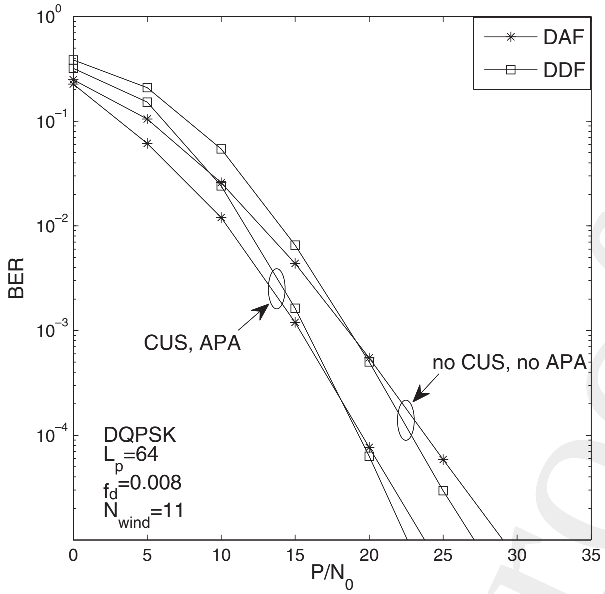

Figure 13.19: Performance comparison between the DAF- and DDF-aided DQPSK-modulated user-cooperative cellular systems employing the MSDSD, where two out of eight cooperating user candidates are activated. All other system parameters are summarized in Table 13.3.

aided system. However, this performance degradation can be substantially reduced by invoking the CUS of Section 13.3.2, as evidenced by Figure 13.14.

13.4.1.3 Cooperative Resource Allocation

As demonstrated by the simulation results of Sections 13.3.1.3 and 13.3.2.1, significant performance gains can be attained for both the DAF- and DDF-aided cellular uplink by optimizing the associated cooperative resource allocation with the aid of the CUS and APC schemes of Section 13.3. More explicitly, the BER performance of both the above-mentioned systems operating with and without the CUS and APC schemes is contrasted in Figure 13.19, where it is assumed that the $M_r = 2$ out of the $\mathcal{P}_{cand} = 8$ available cooperating MS candidates are activated and the MSDSD of Section 12.3 using $N_{wind} = 11$ is employed in order to eliminate the detrimental effects of the fading having a Doppler frequency of $f_d = 0.008$. Moreover, the variance of the noise added at each terminal of the cooperative system is assumed to be identical, namely N_0. Indeed, as seen in Figure 13.19, the performance of both the DAF and DDF systems is significantly enhanced by the employment of the CUS and APC schemes. We also note that the DAF-assisted system exhibits a better performance than the DDF-aided one, when the SNR of P/N_0 is relatively low, while the former is expected to be outperformed by the latter, as the SNR of P/N_0 is in excess of 20 dB. Again, this trend is not unexpected, since the sensitivity of the BER performance to the source–relay link's quality leads to a more rapid BER decrease upon increasing the SNR of P/N_0.

On the other hand, we also observed in Table 13.5 that, due to the distinct relaying mechanisms which lead to different levels of sensitivity to the quality of the source–relay link, the desirable cooperative resource allocation arrangement for the DAF-aided system may be quite different from that of its DDF-aided counterpart. As indicated by the RS's location arrangement of $[d_1, d_2, \ldots, d_{M_r}]$ seen in Table 13.5, the cooperating MSs roaming in the area near the BS are expected to be activated for the DAF-aided cooperative uplink, while those roaming in the neighbourhood of the source MS should be

Table 13.5: Cooperative resource allocation for DAF- and DDF-aided uplinks.

M_r	P/N_0 (dB)	DAF-aided uplink $[P_s, P_{r_1}, \ldots, P_{r_{M_r}}]$	DAF-aided uplink $[d_1, d_2 \ldots, d_{M_r}]$	DDF-aided uplink ($L_f = 64$) $[P_s, P_{r_1}, \ldots, P_{r_{M_r}}]$	DDF-aided uplink ($L_f = 64$) $[d_1, d_2, \ldots, d_{M_r}]$
1	10	$[0.882, 0.118]$	$[0.811]$	$[0.582, 0.418]$	$[0.192]$
	20	$[0.882, 0.118]$	$[0.871]$	$[0.622, 0.378]$	$[0.231]$
	30	$[0.882, 0.118]$	$[0.891]$	$[0.622, 0.378]$	$[0.231]$
2	10	$[0.76, 0.2, 0.04]$	$[0.74, 0.88]$	$[0.602, 0.202, 0.196]$	$[0.26, 0.26]$
	20	$[0.76, 0.2, 0.04]$	$[0.82, 0.91]$	$[0.602, 0.202, 0.196]$	$[0.31, 0.31]$
	30	$[0.78, 0.2, 0.02]$	$[0.85, 0.94]$	$[0.602, 0.202, 0.196]$	$[0.31, 0.31]$
3	10	$[0.88, 0.04, 0.04, 0.04]$	$[0.89, 0.89, 0.89]$	$[0.502, 0.102, 0.202, 0.194]$	$[0.31, 0.21, 0.26]$
	20	$[0.88, 0.04, 0.04, 0.04]$	$[0.92, 0.92, 0.92]$	$[0.502, 0.102, 0.202, 0.194]$	$[0.36, 0.26, 0.26]$
	30	$[0.88, 0.04, 0.04, 0.04]$	$[0.93, 0.93, 0.93]$	$[0.702, 0.102, 0.102, 0.094]$	$[0.41, 0.41, 0.41]$

selected for its DDF-aided counterpart in the interest of achieving the best possible BER performance. It is also indicated in Table 13.5 that the increase of the SNR, P/N_0, or the number of activated cooperating MSs, M_r, will move the desirable RS's location slightly further away from the source MS towards the BS for both the DAF- and DDF-aided scenarios. As for the optimized power control, the majority of the total transmit power P, i.e. about 88%, should be allocated to the source MS for the DAF-aided system, as revealed by the optimized power control arrangement of $[P_s, P_{r_1}, \ldots, P_{r_{M_r}}]$ seen in Table 13.5. By contrast, only about 60% of the power should be assigned to the source MS for the DDF-aided system. It is noteworthy that the optimized transmit power assigned to the M_r RSs as well as their optimum locations are not expected to be identical in both the DAF- and DDF-aided scenarios, as revealed in Table 13.5.

Furthermore, by comparing Figure 13.12(a) of Section 13.3.1.3 and Figure 13.17 of Section 13.3.2.1, we observe that a significant performance degradation may occur if the DAF-aided system dispenses with either the CUS or the APC scheme. By contrast, only a negligible performance loss is imposed when the DDF-aided system dispenses with the APC scheme rather than with the CUS scheme. Additionally, the CUS scheme of Section 13.3.2 is carried out by selecting the cooperating MSs roaming in the area closest to the optimum locations which may be determined offline, i.e. before initiating a voice call or data session. By contrast, the APC scheme of Section 13.3.2 may impose a relatively high real-time complexity, when calculating the optimum power control arrangement based on the current location of the activated RS. Hence, to minimize the complexity imposed by the cooperative resource allocation process, the DDF-aided system employing the CUS scheme may dispense with APC, simply opting for the equal power allocation arrangement at the expense of a moderate performance loss. In contrast to the DDF scheme, the DAF-aided system has to tolerate a high BER performance degradation if it dispenses with the APC scheme. It is also noteworthy that in contrast to the DAF-aided cooperative system, the DDF-assisted scheme employing neither the CUS nor the APC may be outperformed by the classic non-cooperative system, as observed in Figure 13.14, which is a consequence of its sensitivity to the quality of the source–relay link.

13.4.2 Joint CPS and CUS Scheme for the Cellular UL Using APC

Each cooperative cellular uplink considered so far in the book employed either DAF or DDF principles. As argued in the context of Figure 13.20, they both have their desirable RS area, when the CUS is employed. Generally speaking, the neighbourhood of the BS and that of the source MS are the specific areas where the RS should be activated for the DAF- and DDF-aided scenarios, respectively, again as discussed in Sections 13.3.1 and 13.3.2. Thus, often no available cooperating MS is roaming in the desirable RS location area, and hence a performance loss may be imposed by selecting a cooperating MS roaming far away from the optimum RS location. Furthermore, although the DDF-aided system exhibits a better performance than its DAF-aided counterpart in the presence of a high source–relay link quality, the former may be outperformed by the latter, as the quality of the source–relay link degrades despite imposing a higher overall system complexity. On the other hand, from our comparison of the DAF- and DDF-aided cooperative systems in Section 13.4.1, we realized that the two above-mentioned relaying mechanisms have complementary characteristics, reflected, for example, by their distinct optimum cooperative resource allocations. In light of the complementarity of the two relaying schemes, a more flexible cooperative scenario can be created, where either the DAF or DDF scheme is activated in the interest of enhancing the achievable performance of the cooperative system, while maintaining a moderate complexity. In contrast to the conventional cooperative system employing a single cooperative mechanism, the cooperating MSs roaming in different areas between the source MS and the BS may be activated and the relay schemes employed by each activated RS may be adaptively selected, to achieve the best possible performance.

For the sake of simplicity, let us now consider the hybrid cooperative cellular uplink employing the joint CPS and CUS scheme, as portrayed in Figure 13.20, where $M_r = 2$ cooperating MSs roaming in the preferred DDF- and the DAF-RS-area are activated, in order to forward the source MS's information to the BS. The particular cooperative protocol employed by the activated RSs is determined according to the specific area in which they happen to be situated. In order to make the most of the complementarity of the DAF and DDF schemes, it may be assumed that one of the cooperating MSs is activated in the preferred area of the DAF-RS, while the other is from the 'DDF-area', although, naturally, there may be more than one cooperating MS roaming within a specific desirable area. Finally, under the assumption that the first selected cooperating MS is roaming in the 'DDF-area', while the second one is roaming in the 'DAF-area', the MRC scheme employed by the BS, which combines the signals received from the source MS and the cooperating MSs, can be expressed as

$$y = a_0(y_{sd}[n-1])^* y_{sd}[n] + \sum_{m=1}^{2} a_m (y_{r_m d}[n+mL_f-1])^* y_{r_m d}[n+mL_f], \tag{13.109}$$

where L_f is the length of the transmission packet, while the coefficients a_0 and a_m $(m = 1, 2)$ are given by

$$a_0 = a_1 = \frac{1}{N_0} \tag{13.110}$$

and

$$a_2 = \frac{P_s\sigma_{sr_2}^2 + N_0}{N_0(P_s\sigma_{sr_2}^2 + P_{r_2}\sigma_{r_2d}^2 + N_0)}. \tag{13.111}$$

In order to determine the optimum RS areas for the hybrid cooperative system employing $M_r = 2$ cooperating users, the worst-case BER expression will first be derived in a similar manner to that derived for the DDF-aided system of Section 13.2.1 in our following discourse.

First of all, let us define the scenario Φ_1 as the situation when the cooperating MS employing the DDF scheme perfectly recovers the information from the source MS and then transmits the differentially remodulated signal to the BS, which is formulated as

$$\Phi_1 \triangleq \{P_{r_1} \neq 0\}. \tag{13.112}$$

By contrast, the scenario Φ_2 is defined as the situation, when the cooperating MS using the DDF scheme fails to correctly decode the signal received from the source MS and keeps silent during the relay phase, which can be formulated as

$$\Phi_2 \triangleq \{P_{r_1} = 0\}. \tag{13.113}$$

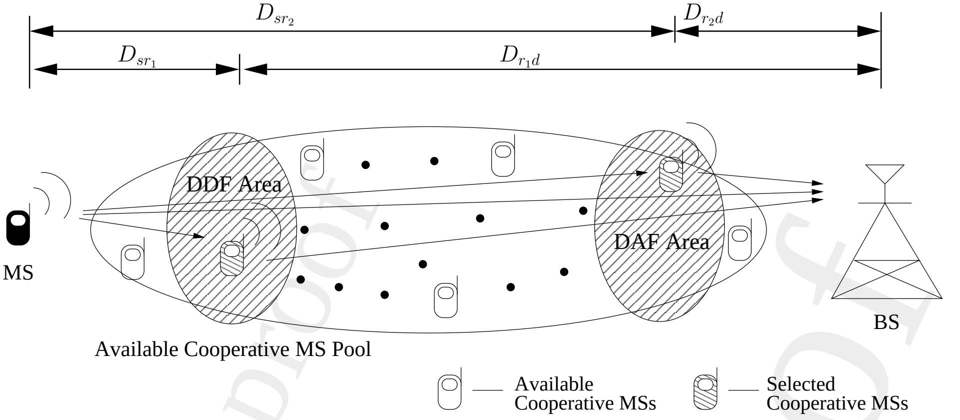

Figure 13.20: Cooperation-aided uplink systems using the joint CPS and CUS scheme.

Then, based on the differentially encoded conditional BER of Equation (13.59) invoked in Section 13.2.2, the unconditional BER observed at the BS is the scenario of Φ_1 can be expressed as

$$P_{BER}^{\Phi_1} = \frac{1}{2^{2L}\pi} \int_{-\pi}^{\pi} f(a, b, L = 3, \theta) \int_{-\infty}^{\infty} e^{-\alpha(\theta)\gamma_{\Phi_1}^b} p_{\gamma_{\Phi_1}^b}(\gamma)\, d\gamma\, d\theta \tag{13.114}$$

$$= \frac{1}{2^{2L}\pi} \int_{-\pi}^{\pi} f(a, b, L = 3, \theta) \mathcal{M}_{\gamma_{\Phi_1}^b}(\theta)\, d\theta, \tag{13.115}$$

where $\gamma_{\Phi_1}^b$ denotes the received SNR per bit after MRC combining, which can be written as

$$\gamma_{\Phi_1}^b = \gamma_{sd}^b + \gamma_{r_1 d}^b + \gamma_{r_2 d}^d. \tag{13.116}$$

Then, the joint MGF, $\mathcal{M}_{\gamma_{\Phi_1}^b}(\theta)$, of the received SNR per bit experienced at the BS in the scenario Φ_1 is expressed as

$$\mathcal{M}_{\gamma_{\Phi_1}^b}(\theta) = \int_{-\infty}^{\infty} e^{-\alpha(\theta)\gamma_{\Phi_1}^b} p_{\gamma_{\Phi_1}^b}(\gamma)\, d\gamma \tag{13.117}$$

$$= \int_{-\infty}^{\infty} \int_{-\infty}^{\infty} \int_{-\infty}^{\infty} e^{-\alpha(\theta)(\gamma_{sd}^b + \gamma_{r_1 d}^b + \gamma_{r_2 d}^b)} \times p_{\gamma_{sd}^b}(\gamma_{sd}) p_{\gamma_{r_1 d}^b}(\gamma_{r_1 d}) p_{\gamma_{r_2 d}^b}(\gamma_{r_2 d})\, d\gamma_{sd}\, d\gamma_{r_1 d}\, d\gamma_{r_2 d} \tag{13.118}$$

$$= \mathcal{M}_{\gamma_{sd}^b}(\theta) \mathcal{M}_{\gamma_{r_1 d}^b}(\theta) \mathcal{M}_{\gamma_{r_2 d}^b}(\theta), \tag{13.119}$$

where

$$\mathcal{M}_{\gamma_{sd}^b}(\theta) = \frac{N_0}{N_0 + \alpha(\theta) P_s \sigma_{sd}^2}, \tag{13.120}$$

$$\mathcal{M}_{\gamma_{r_1 d}^b}(\theta) = \frac{N_0}{N_0 + \alpha(\theta) P_{r_1} \sigma_{r_1 d}^2}, \tag{13.121}$$

$$\mathcal{M}_{\gamma_{r_2 d}^b}(\theta) = \frac{1}{1 + k_{sr_2}(\theta)} \left(1 + \frac{k_{sr_2}(\theta)}{1 + k_{sr_2}(\theta)} \frac{P_s \sigma_{sr_2}^2 + N_0}{P_{r_2}} \frac{1}{\sigma_{r_2 d}^2} Z_{r_2}(\theta) \right), \tag{13.122}$$

and $k_{r_2 d}(\theta)$ and $Z_{r_2}(\theta)$ are given by Equations (13.34) and (13.35), respectively.

Table 13.6: Cooperative resource allocation for the hybrid cooperative uplink.

M_r	P/N_0 (dB)	$[P_s, P_{r_1}, \ldots, P_{r_{M_r}}]$	$[d_1, d_2, \ldots, d_{M_r}]$
2	10	$[0.702, 0.202, 0.096]$	$[0.26, 0.86]$
	20	$[0.702, 0.202, 0.096]$	$[0.31, 0.86]$
	30	$[0.702, 0.202, 0.096]$	$[0.31, 0.91]$

In parallel, the unconditional BER corresponding to the scenario Φ_2 can be formulated as

$$P_{BER}^{\Phi_2} = \frac{1}{2^{2L}\pi} \int_{-\pi}^{\pi} f(a, b, L = 2, \theta) \int_{-\infty}^{\infty} e^{-\alpha(\theta)\gamma_{\Phi_2}^b} p_{\gamma_{\Phi_2}^b}(\gamma)\, d\gamma\, d\theta \tag{13.123}$$

$$= \frac{1}{2^{2L}\pi} \int_{-\pi}^{\pi} f(a, b, L = 2, \theta) \mathcal{M}_{\gamma_{\Phi_2}^b}(\theta)\, d\theta, \tag{13.124}$$

where $\gamma_{\Phi_2}^b$ denotes the received SNR per bit after MRC combining, which can be expressed as

$$\gamma_{\Phi_2}^b = \gamma_{sd}^b + \gamma_{r_2 d}^d, \tag{13.125}$$

and hence the MGF of the received SNR per bit recorded at the BS for the scenario Φ_2 is written as

$$\mathcal{M}_{\gamma_{\Phi_2}^b}(\theta) = \int_{-\infty}^{\infty} e^{-\alpha(\theta)\gamma_{\Phi_2}^b} p_{\gamma_{\Phi_2}^b}(\gamma)\, d\gamma \tag{13.126}$$

$$= \int_{-\infty}^{\infty} \int_{-\infty}^{\infty} e^{-\alpha(\theta)(\gamma_{sd}^b + \gamma_{r_2 d}^b)} p_{\gamma_{sd}^b}(\gamma_{sd}) p_{\gamma_{r_2 d}^b}(\gamma_{r_2 d})\, d\gamma_{sd}\, d\gamma_{r_2 d}, \tag{13.127}$$

$$= \mathcal{M}_{\gamma_{sd}^b}(\theta) \mathcal{M}_{\gamma_{r_2 d}^b}(\theta), \tag{13.128}$$

where $\mathcal{M}_{\gamma_{sd}^b}(\theta)$ and $\mathcal{M}_{\gamma_{r_2 d}^b}(\theta)$ are given by Equations (13.120) and (13.122), respectively.

Finally, based on the worst-case packet loss ratio of $P_{PLR_1,upper}$ given by Equation (13.52), the average end-to-end BER upper bound, $P_{BER,upper}^{CPS}$, is obtained by the summation of the average BERs of two scenarios as

$$P_{BER,upper}^{CPS} = (1 - P_{PLR_1,upper}) P_{BER}^{\Phi_1} + P_{PLR_1,upper} P_{BER}^{\Phi_2}. \tag{13.129}$$

Hence, when using the minimum BER criterion, the desirable RS area can be located by finding the globally optimum RS locations using the iterative power versus RS location optimization process of Sections 13.3.2 or 13.3.2. Considering the $M_r = 2$ scenario as an example, the globally optimum power and distance allocation arrangements are summarized in Table 13.6 under the assumption that the first cooperating MS is activated in the DDF mode. As expected, the figures shown in Table 13.6 reveal that the 'DDF-area' and the 'DAF-area' are still located in the vicinity of the source MS and the BS, respectively. Additionally, the majority of the total transmit power, i.e. about 70%, should be allocated to the source MS, while two-thirds of the remaining power should be assigned to the cooperating MS roaming in the 'DDF-area'.

The BER performance of the hybrid cooperative cellular uplink, where $M_r = 2$ out of $\mathcal{P}_{cand} = 8$ cooperating MSs are activated, is portrayed in comparison with that of its DAF- and DDF-aided counterparts in Figure 13.21. Remarkably, as demonstrated by Figure 13.21, the hybrid cooperative system outperforms both the DAF- and DDF-aided systems, regardless of whether the joint CPS–CUS–APC scheme is employed. These conclusions remain valid across a wide SNR range of our interest, although the performance advantage of the hybrid scheme over the latter two systems decreases in the context of the joint CPS–CUS–APC scheme. Furthermore, as the SNR increases, the DDF-aided system is expected to become superior to the other two systems, since the DDF-aided system

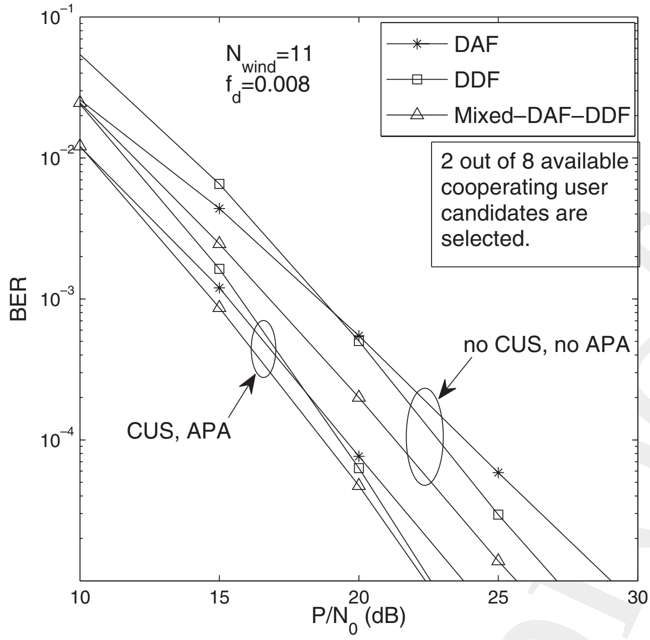

Figure 13.21: Performance improvement by the joint CPS and CUS for the DQPSK-modulated user-cooperative cellular uplink employing the MSDSD, where two out of eight cooperating user candidates are activated. All other system parameters are summarized in Table 13.3.

performs best when error-free transmissions can be assumed between the source MS and the RS. By contrast, if the SNR is low, the DAF-aided system performs best among the three. In addition to the performance advantage of the joint CPS–CUS–APC hybrid cooperative system, the overall system complexity becomes moderate in comparison with that of the DDF-aided system, since only half of the activated MSs have to decode and re-encode the received signal prior to forwarding it. Therefore, the proposed hybrid cooperative system employing the joint CPS–CUS–APC scheme is capable of achieving an attractive performance, despite maintaining a moderate overall system complexity.

13.5 Chapter Conclusions

In this chapter, CUS schemes and APC schemes designed for both the DAF- and DDF-aided cooperative systems were investigated based on our theoretical performance analysis. Significant performance gains can be achieved with the aid of the optimized resource allocation arrangements for both the DAF- and DDF-aided systems. Owing to the different levels of sensitivity to the quality of the source–relay link, the optimum resource allocation arrangements corresponding to the two above-mentioned systems were shown to be quite different. Specifically, it is desirable that the activated cooperating MSs are roaming in the vicinity of the source MS for the DDF-aided system, while the cooperating MSs roaming in the neighbourhood of the BS are preferred for the DAF-aided counterpart. In comparison with the former system, a larger portion of the total transmit power should be allocated to the source MS in the context of a DAF-aided system. Apart from achieving an enhanced BER performance, the complexity imposed by the MSDSD of Chapter 12 may also be significantly reduced by employing the CUS and APC schemes, even in the context of rapidly fading channels. Based on the simulation results throughout this chapter, the natures of the DAF- and DDF-aided systems are summarized and compared in Table 13.7.

Table 13.7: Comparison between the DAF- and DDF-aided cooperative cellular uplinks.

	DAF-aided uplink	DDF-aided uplink	References
Overall performance	Better when SR link quality is poor	Better when SR link quality is good	Figure 13.19
Overall complexity	Relatively low, no decoding at RSs	Relatively high, decoding and re-encoding at RSs	
Performance's sensitivity to source–relay link quality	Relatively moderate	Strong	Figures 12.19 12.23, 13.19
Performance's sensitivity to packet length L_f	Insensitive	Strong without CUS, minor with CUS	Figures 13.14, 13.16
Desirable RS locations	Near the BS	Near the source MS	Table 13.5
Desirable transmit power for the source MS	About 88% of the total power	About 60% of the total power	Table 13.5
Worst-case performance (Inappropriate resource allocation)	Slightly better than the non-cooperative system	Significantly worse than the non-cooperative system	Figures 13.9, 13.14
Importance of CUS and APC	Equally important	CUS is significantly more important	Figures 13.12(a), 13.17

Table 13.8: Summary of the resource-optimized cooperative systems investigated in Chapter 12.

Performance gains achieved by various two-relay-aided differential cooperative systems with and without cooperative resource optimization					
Target BER	System type	Power control $[P_s, P_{r_1}, P_{r_2}]$	Relay selection $[d_{r_1}, d_{r_2}]$	SNR (dB)	Gain (dB)
10^{-3}	Direct transmission	N/A	N/A	27.3	—
	DAF-aided	[0.33, 0.33, 0.33]	[0.5,0.5]	18.8	8.5
	Cooperative System	[0.76, 0.2, 0.04]	[0.81, 0.9]	15.4	11.9
	DDF-aided	[0.33, 0.33, 0.33]	[0.5,0.5]	18.9	8.4
	Cooperative system	[0.602, 0.202, 0.196]	[0.29, 0.29]	15.8	11.5
	Hybrid DAF/DDF	[0.33, 0.33, 0.33]	[0.5,0.5]	16.9	10.4
	Cooperative system	[0.702, 0.202, 0.096]	[0.28, 0.86]	14.9	12.4
10^{-5}	Direct transmission	N/A	N/A	50	—
	DAF-aided	[0.33, 0.33, 0.33]	[0.5,0.5]	29	21
	Cooperative system	[0.76, 0.2, 0.04]	[0.82, 0.91]	23.7	26.3
	DDF-aided	[0.33, 0.33, 0.33]	[0.5,0.5]	27	23
	Cooperative system	[0.602, 0.202, 0.196]	[0.31, 0.31]	22.5	27.5
	Hybrid DAF/DDF	[0.33, 0.33, 0.33]	[0.5,0.5]	25.7	24.3
	Cooperative system	[0.702, 0.202, 0.096]	[0.31, 0.86]	22.3	27.7

Furthermore, in order to make the most of the complementarity of the two above-mentioned cooperative systems, a more flexible resource-optimized adaptive hybrid cooperation-aided system was proposed in this chapter, where the cooperative protocol employed by a specific cooperating MS may also be adaptively selected in the interest of achieving the best possible BER performance.

Finally, we quantitatively summarize and compare the performance gains achieved by the DAF-aided, the DDF-aided as well as the hybrid cooperative systems over the direct-transmission-based system in Table 13.8, based on the simulation results obtained throughout the chapter. Observe in Table 13.8 that, given a target BER of 10^{-3}, the DAF-aided cooperative system is capable of achieving a slightly higher performance gain than that attained by its DDF-aided counterpart, regardless of the employment of the optimized resource allocation. However, given a target BER of 10^{-5}, the latter becomes capable of achieving performance gains of 2 and 1.2 dB over the former for the non-optimized and optimized resource allocation arrangements, respectively, as seen in Table 13.8. Furthermore, among the three types of cooperative systems investigated in this chapter, the adaptive hybrid DAF/DDF cooperative system performs the best for a wide range of SNRs. Remarkably, as observed in Table 13.8, the hybrid cooperative system is capable of achieving performance gains over its direct-transmission-based counterpart, which are as high as 12.4 and 27.7 dB for the BER targets of 10^{-3} and 10^{-5}, respectively, when the optimized resource allocation is employed.

Bibliography

[1] M. Jiang, S. Ng, and L. Hanzo, "Hybrid iterative multiuser detection for channel coded space division multiple access OFDM systems," *IEEE Transactions on Vehicular Technology*, vol. 55, pp. 115–127, Jan. 2006.

[2] M. Jiang and L. Hanzo, "Multi-user MIMO-OFDM Systems Using Subcarrier Hopping," *IEE Proceedings on Communications*, vol. 153, pp. 802–809, Dec. 2006.

[3] M. Jiang, J. Akhtman, and L. Hanzo, "Iterative Joint Channel Estimation and Multi-User Detection for Multiple-Antenna Aided OFDM Systems," *IEEE Transactions on Wireless Communications*, vol. 6, pp. 2904–2914, August 2007.

[4] L. Wang, O. Alamri, and L. Hanzo, "Sphere packing modulation in the SDMA uplink using k-best sphere detection," *IEEE Signal Processing Letters*, vol. 16, pp. 291–294, Apr. 2009.

[5] M. Tuchler, A. C. Singer, and R. Koetter, "Minimum mean squared error equalization using a priori information," *IEEE Transactions on Acoustics, Speech, and Signal Processing*, vol. 50, pp. 673–683, Mar. 2002.

[6] L. Xu, S. Tan, and L. Hanzo, "MBER Turbo Multiuser Beamforming Aided QPSK Receiver Design Using EXIT Chart Analysis," *IEEE*, 2006.

[7] L. Wang and L. Hanzo, "The amplify-and-forward cooperative uplink using multiple-symbol differential sphere-detection," *IEEE Signal Processing Letters*, vol. 16, pp. 913–916, Oct. 2009.

[8] L. Wang and L. Hanzo, "The resource-optimized differentially modulated hybrid AF/DF cooperative cellular uplink using multiple-symbol differential sphere detection," *IEEE Signal Processing Letters*, vol. 16, pp. 965–968, Nov. 2009.

[9] J. Akhtman, A. Wolfgang, S. Chen, and L. Hanzo, "An optimized-hierarchy-aided approximate log-MAP detector for MIMO systems," *IEEE Transactions on Wireless Communications*, vol. 6, pp. 1900–1909, May 2007.

[10] J. A. C. Bingham, "Multicarrier modulation for data transmission: an idea whose time has come," *IEEE Communications Magazine*, vol. 28, pp. 5–14, May 1990.

[11] L. Hanzo, W. Webb, and T. Keller, *Single- and Multi-carrier Quadrature Amplitude Modulation*. West Sussex, England: IEEE Press - John Wiley & Sons Ltd., 2nd ed., 2000. ISBN 0471492396.

[12] L. Hanzo, M. Münster, B. J. Choi, and T. Keller, *OFDM and MC-CDMA for Broadband Multi-user Communications, WLANs and Broadcasting*. IEEE Press - John Wiley & Sons Ltd., 2003.

[13] R. V. Nee and R. Prasad, *OFDM for wireless multimedia communications*. London, UK: Artech House Publishers, 2000.

[14] J. L. Holsinger, "Digital Communication over Fixed Time-Continuous Channels with Memory - with Special Application to Telephone Channels," Technical Report No. 366, MIT - Lincoln Laboratory, Cambridge, Massachusetts, USA, October 1964.

[15] J. M. Cioffi, *A Multicarrier Primer*, November 1991. ANSI T1E1.4/91-157.

[16] ANSI Committee T1-Telecommunications, *A Technical Report on High-Bit-Rate Digital Subscriber Lines (HDSL)*, February 1994. Technical Report No. 28.

[17] *Very-high-speed Digital Subscriber Lines: System Requirements*, September 1998. ANSI T1E1.4 VDSL SR: 98-043R5.

[18] European Telecommunication Standard Institute, *Transmission and Multiplexing (TM);Access transmission systems on metallic access cables;Very high speed Digital Subscriber Line (VDSL);Part 1: Functional requirements*, June 1998. ETSI TS 101 270-1 V1.1.2.

[19] European Telecommunication Standard Institute, *Digital Audio Broadcasting (DAB);DAB to mobile, portable and fixed Receivers*, February 1995. ETSI ETS 300 401 ed.1.

[20] European Telecommunication Standard Institute, *Digital Video Broadcasting (DVB);Framing structure, channel coding and modulation for digital terrestrial television (DVB-T)*, March 1997. ETSI ETS 300 744 ed.1.

[21] European Telecommunication Standard Institute, *Digital Video Broadcasting (DVB);Transmission System for Handheld Terminals (DVB-H)*, November 2004. ETSI EN 302 304 V1.1.1.

[22] European Telecommunication Standard Institute, *Radio Equipment and Systems (RES);HIgh PErformance Radio Local Area Network (HIPERLAN) Type 1;Functional specification*, October 1996. ETSI ETS 300 652 ed.1.

[23] European Telecommunication Standard Institute, *Broadband Radio Access Networks (BRAN);Inventory of broadband radio technologies and techniques*, May 1998. ETSI TR 101 173 V1.1.1.

[24] Institute of Electrical and Electronics Engineers, *IEEE Standard 802.11: Wireless Lan Medium Access Control (MAC) And Physical Layer (PHY) Specifications*, 18 November 1997.

[25] Institute of Electrical and Electronics Engineers, *IEEE Standard 802.16: Air Interface for Fixed Broadband Wireless Access Systems*, 2004.

[26] M. Doelz, E. Heald, and D. Martin, "Binary data transmission techniques for linear systems," *Proceedings of the IRE*, vol. 45, pp. 656–661, May 1957.

[27] R. W. Chang, "Synthesis of Band-Limited Orthogonal Signals for Multichannel Data Transmission," *Bell System Technical Journal*, vol. 45, pp. 1775–1796, December 1966.

[28] B. R. Saltzberg, "Performance of an Efficient Parallel Data Transmission System," *IEEE Transactions on Communications*, vol. 15, pp. 805–811, December 1967.

[29] R. W. Chang and R. A. Gibby, "A Theoretical Study of Performance of an Orthogonal Multiplexing Data Transmission Scheme," *IEEE Transactions on Communications*, vol. 16, pp. 529–540, August 1968.

[30] R. W. Chang, *U.S. Patent No. 3,488,445: Orthogonal Frequency Division Multiplexing*, filed November 14, 1966, issued January 6, 1970.

[31] S. B. Weinstein and P. M. Ebert, "Data Transmission by Frequency-Division Multiplexing Using the Discrete Fourier Transform," *IEEE Transactions on Communications*, vol. 19, pp. 628–634, October 1971.

[32] A. Peled and A. Ruiz, "Frequency domain data transmission using reduced computational complexity algorithms," in *IEEE International Conference on Acoustics, Speech, and Signal Processing (ICASSP '80)*, vol. 5, (Denver, USA), pp. 964–967, 9-11 April 1980.

[33] L. Hanzo, S. X. Ng, T. Keller, and W. T. Webb, *Quadrature Amplitude Modulation: From Basics to Adaptive Trellis-Coded, Turbo-Equalised and Space-Time Coded OFDM, CDMA and MC-CDMA Systems*. West Sussex, England: IEEE Press - John Wiley & Sons Ltd., 3rd ed., 2004.

[34] W. E. Keasler, D. L. Bitzer, and P. T. Tucker, *U.S. Patent No. 4,206,320: High-speed Modem Suitable for Operating with a Switched Network*, filed August 21, 1978, issued June 3, 1980.

[35] B. Hirosaki, "An Analysis of Automatic Equalizers for Orthogonally Multiplexed QAM Systems," *IEEE Transactions on Communications*, vol. 28, pp. 73–83, January 1980.

[36] B. Hirosaki, "An Orthogonally Multiplexed QAM System Using the Discrete Fourier Transform," *IEEE Transactions on Communications*, vol. 29, pp. 982–989, July 1981.

[37] B. Hirosaki, S. Hasegawa, and A. Sabato, "Advanced Groupband Data Modem Using Orthogonally Multiplexed QAM Technique," *IEEE Transactions on Communications*, vol. 34, pp. 587–592, June 1986.

[38] L. J. Cimini Jr., "Analysis and Simulation of a Digital Mobile Channel Using Orthogonal Frequency Division Multiplexing," *IEEE Transactions on Communications*, vol. 33, pp. 665–675, July 1985.

[39] I. Kalet, "The Multitone Channel," *IEEE Transactions on Communications*, vol. 37, pp. 119–124, February 1989.

[40] M. Alard and R. Lassalle, "Principles of modulation and channel coding for digital broadcasting for mobile receivers," *EBU Technical Review*, pp. 168–190, August 1987.

[41] K. Fazel and G. Fettweis, *Multi-carrier Spread Spectrum and Related Topics*. Kluwer, 2000. ISBN 0-7923-9973-0.

[42] T. Keller and L. Hanzo, "Adaptive multicarrier modulation: a convenient framework for time-frequency processing in wireless communications," *Proceedings of the IEEE*, vol. 88, pp. 611–640, May 2000.

[43] L. Hanzo, B. J. Choi, and M. Münster, "A Stroll Along Multi-Carrier Boulevard towards Next-Generation Plaza - OFDM Background and History," *IEEE VTS News*, vol. 51, pp. 4–10, November 2004.

[44] L. Hanzo, B. J. Choi, and M. Münster, "A Stroll Along Multi-Carrier Boulevard towards Next-Generation Plaza - Space-Time Coded Adaptive OFDM and MC-CDMA Comparison," *IEEE VTS News*, vol. 51, pp. 10–19, November 2004.

[45] R. Steele and L. Hanzo, *Mobile Radio Communications: Second and Third Generation Cellular and WATM Systems*. New York, USA: IEEE Press - John Wiley & Sons Ltd., 2nd ed., 1999.

[46] A. J. Viterbi, *CDMA: Principles of Spread Spectrum Communication*. Addison-Wesley Publishing Company, 1995.

[47] L. Hanzo, L.-L. Yang, E.-L. Kuan, and K. Yen, *Single- and Multi-Carrier DS-CDMA: Multi-User Detection, Space-Time Spreading, Synchronisation and Standards*. IEEE Press - John Wiley & Sons Ltd., 2003.

[48] K. Zigangirov, *Theory of Code Division Multiple Access Communication*. IEEE Press - John Wiley & Sons Ltd., 2004. ISBN 0-471-45712-4.

[49] L. E. Miller and J. S. Lee, *CDMA Systems Engineering Handbook*. London, UK: Artech House, 1998.

[50] J. S. Lee, "Overview of the technical basis of QUALCOMM's CDMA cellular telephone system design: A view of North American TIA/EIA IS-95," in *International Conference on Communications Systems (ICCS)*, (Singapore), pp. 353–358, 1994.

[51] I. Koffman and V. Roman, "Broadband Wireless Access Solutions Based on OFDM Access in IEEE 802.16," *IEEE Communications Magazine*, vol. 40, pp. 96–103, April 2002.

[52] R. Laroia, S. Uppala, and J. Li, "Designing a Mobile Broadband Wireless Access Network," *IEEE Signal Processing Magazine*, vol. 21, pp. 20–28, September 2004.

[53] P. Xia, S. Zhou, and G. B. Giannakis, "Bandwidth- and Power-Efficient Multicarrier Multiple Access," *IEEE Transactions on Communications*, vol. 51, pp. 1828–1837, November 2003.

[54] Z. Cao, U. Tureli, and Y. Yao, "Deterministic Multiuser Carrier-Frequency Offset Estimation for Interleaved OFDMA Uplink," *IEEE Transactions on Communications*, vol. 52, pp. 1585–1594, September 2004.

[55] R. Bercovich, "OFDM Enhances the 3G High-speed Data Access," in *GSPx 2004 Conference*, (Santa Clara, USA), 27-30 September 2004. http://www.techonline.com/pdf/pavillions/gspx/2004/1084.pdf.

[56] T. May, H. Rohling, and V. Engels, "Performance analysis of Viterbi decoding for 64-DAPSK and 64-QAM modulated OFDM signals," *IEEE Transactions on Communications*, vol. 46, pp. 182–190, February 1998.

[57] L. Lin, L. J. Cimini Jr., and C.-I. Chuang, "Comparison of convolutional and turbo codes for OFDM with antenna diversity in high-bit-rate wireless applications," *IEEE Communications Letters*, vol. 9, pp. 277–279, September 2000.

[58] P. H. Moose, "A technique for orthogonal frequency division multiplexing frequency offset correction," *IEEE Transactions on Communications*, vol. 42, pp. 2908–2914, October 1994.

[59] Institute of Electrical and Electronics Engineers, *IEEE Standard 802.11a: Wireless LAN Medium Access Control (MAC) and Physical Layer (PHY) specifications: high-speed physical layer in the 5 GHz band*, 1999.

[60] Institute of Electrical and Electronics Engineers, *IEEE Standard 802.11g: Wireless LAN Medium Access Control (MAC) and Physical Layer (PHY) specifications*, 2003.

[61] "OFDM for Mobile Data Communications," White Paper, Flarion Technologies, Inc., Bedminster, USA, March 2003.

[62] "FLASH-OFDM for 450MHz - Advanced Mobile Broadband Solution for 450MHz Operators," White Paper, Flarion Technologies, Inc., Bedminster, USA, November 2004.

[63] "IEEE Standard for Local and Metropolitan Area Networks - Part 16: Air Interface for Fixed Broadband Wireless Access Systems (Revision of 802.16-2001)," 2004. IEEE 802.16d-2004.

[64] "Draft IEEE Standard for Information Technology - Telecommunications and Information Exchange Between Systems - Local and Metropolitan Area Networks - Specific Requirements - Part 11: Wireless LAN Medium Access Control (MAC) and Physical Layer (PHY) Specifications - Amendment 4: Enhancements for Higher Throughput," 2008. IEEE P802.11n/D4.

[65] 3GPP, http://www.3gpp.org/.

[66] M. Jiang and L. Hanzo, "Multi-user mimo-ofdm for next-generation wireless," *Proceedings of the IEEE*, vol. 95, pp. 1430 –1469, July 2007.

[67] L. Hanzo and B. Choi, "Near-instantaneously adaptive hsdpa-style ofdm and mc-cdma transceivers for wifi, wimax and next-generation systems," *Proceedings of the IEEE*, vol. 95, pp. 2368–2392, December 2007.

[68] W. D. Warner and C. Leung, "OFDM/FM frame synchronization for mobile radio data communication," *IEEE Transactions on Vehicular Technology*, vol. 42, pp. 302–313, August 1993.

[69] T. Pollet, M. V. Bladel, and M. Moeneclaey, "BER sensitivity of OFDM systems to carrier frequency offset and Wiener phase noise," *IEEE Transactions on Communications*, vol. 43, pp. 191–193, February/March/April 1995.

[70] A. E. Jones, T. A. Wilkinson, and S. K. Barton, "Block coding scheme for reduction of peak to mean envelope power ratio of multicarrier transmission schemes," *Electronics Letters*, vol. 30, pp. 2098–2099, December 1994.

[71] S. J. Shepherd, P. W. J. V. Eetvelt, C. W. Wyatt-Millington, and S. K. Barton, "Simple coding scheme to reduce peak factor in QPSK multicarrier modulation," *Electronics Letters*, vol. 31, pp. 1131–1132, July 1995.

[72] D. Wulich, “Reduction of peak to mean ratio of multicarrier modulation using cyclic coding,” *Electronics Letters*, vol. 32, pp. 432–433, February 1996.

[73] D. Wulich, “Peak factor in orthogonal multicarrier modulation with variable levels,” *Electronics Letters*, vol. 32, pp. 1859–1861, September 1996.

[74] X. Li and L. J. Cimini Jr., “Effects of clipping and filtering on the performance of OFDM,” in *Proceedings of the IEEE 47th Vehicular Technology Conference, 1997 (VTC 1997 Spring)*, vol. 3, pp. 1634–1638, 4-7 May 1997.

[75] X. Li and L. J. Cimini Jr., “Effects of clipping and filtering on the performance of OFDM,” *IEEE Communications Letters*, vol. 2, pp. 131–133, May 1998.

[76] S. Hara and R. Prasad, “Overview of Multicarrier CDMA,” *IEEE Communications Magazine*, vol. 35, pp. 126–133, December 1997.

[77] Y. Li, L. J. Cimini Jr., and N. R. Sollenberger, “Robust channel estimation for OFDM systems with rapid dispersive fading channels,” *IEEE Transactions on Communications*, vol. 46, pp. 902–915, July 1998.

[78] Y. Li and N. R. Sollenberger, “Adaptive antenna arrays for OFDM systems with cochannel interference,” *IEEE Transactions on Communications*, vol. 47, pp. 217–229, February 1999.

[79] S. Armour, A. Nix, and D. Bull, “Pre-FFT equaliser design for OFDM,” *Electronics Letters*, vol. 35, pp. 539–540, April 1999.

[80] S. Armour, A. Nix, and D. Bull, “Performance analysis of a pre-FFT equalizer design for DVB-T,” *IEEE Transactions on Consumer Electronics*, vol. 45, pp. 544–552, August 1999.

[81] S. Armour, A. Nix, and D. Bull, “Complexity evaluation for the implementation of a pre-FFT equalizer in an OFDM receiver,” *IEEE Transactions on Consumer Electronics*, vol. 46, pp. 428–437, August 2000.

[82] B. Y. Prasetyo and A. H. Aghvami, “Simplified frame structure for MMSE-based fast burst synchronisation in OFDM systems,” *Electronics Letters*, vol. 35, pp. 617–618, April 1999.

[83] B. Y. Prasetyo, F. Said, and A. H. Aghvami, “Fast burst synchronisation technique for OFDM-WLAN systems,” *IEE Proceedings - Communications*, vol. 147, pp. 292–298, October 2000.

[84] C. Y. Wong, R. S. Cheng, K. B. Lataief, and R. D. Murch, “Multiuser OFDM with Adaptive Subcarrier, Bit, and Power Allocation,” *IEEE*

Journal on Selected Areas in Communications, vol. 17, pp. 1747–1758, October 1999.

[85] B. Lu, X. Wang, and K. R. Narayanan, "LDPC-based space-time coded OFDM systems over correlated fading channels: performance analysis and receiver design," in *Proceedings of the 2001 IEEE International Symposium on Information Theory*, vol. 1, p. 313, 24-29 June 2001.

[86] B. Lu, X. Wang, and K. R. Narayanan, "LDPC-based space-time coded OFDM systems over correlated fading channels: Performance analysis and receiver design," *IEEE Transactions on Communications*, vol. 50, pp. 74–88, January 2002.

[87] B. Lu, X. Wang, and Y. Li, "Iterative receivers for space-time block coded OFDM systems in dispersive fading channels," in *IEEE Global Telecommunications Conferenc (GLOBECOM '01)*, vol. 1, pp. 514–518, 25-29 November 2001.

[88] B. Lu, X. Wang, and Y. Li, "Iterative receivers for space-time block-coded OFDM systems in dispersive fading channels," *IEEE Transactions on Wireless Communications*, vol. 1, pp. 213–225, April 2002.

[89] O. Simeone, Y. Bar-Ness, and U. Spagnolini, "Pilot-based channel estimation for OFDM systems by tracking the delay-subspace," *IEEE Transactions on Wireless Communications*, vol. 3, pp. 315–325, January 2004.

[90] J. Zhang, H. Rohling, and P. Zhang, "Analysis of ICI cancellation scheme in OFDM systems with phase noise," *IEEE Transactions on Broadcasting*, vol. 50, pp. 97–106, June 2004.

[91] M. C. Necker and G. L. Stüber, "Totally blind channel estimation for OFDM on fast varying mobile radio channels," *IEEE Transactions on Wireless Communications*, vol. 3, pp. 1514–1525, September 2004.

[92] A. Doufexi, S. Armour, A. Nix, P. Karlsson, and D. Bull, "Range and throughput enhancement of wireless local area networks using smart sectorised antennas," *IEEE Transactions on Wireless Communications*, vol. 3, pp. 1437–1443, September 2004.

[93] E. Alsusa, Y. Lee, and S. McLaughlin, "Channel-adaptive sectored multicarrier packet based systems," *Electronics Letters*, vol. 40, pp. 1194–1196, September 2004.

[94] C. Williams, M. A. Beach, and S. McLaughlin, "Robust OFDM timing synchronisation," *Electronics Letters*, vol. 41, pp. 751–752, June 2005.

[95] R. Fischer and C. Siegl, "Performance of peak-to-average power ratio reduction in single- and multi-antenna ofdm via directed selected

mapping," *IEEE Transactions on Communications*, vol. 57, pp. 3205–3208, Nov. 2009.

[96] G. Mileounis, N. Kalouptsidis, and P. Koukoulas, "Blind identification of hammerstein channels using qam, psk, and ofdm inputs," *IEEE Transactions on Communications*, vol. 57, pp. 3653–3661, December 2009.

[97] S. Huang and C. Hwang, "Improvement of active interference cancellation: avoidance technique for ofdm cognitive radio," *IEEE Transactions on Wireless Communications*, vol. 8, pp. 5928–5937, December 2009.

[98] H. Chen, W. Gao, and D. Daut, "Spectrum sensing for ofdm systems employing pilot tones," *IEEE Transactions on Wireless Communications*, vol. 8, December 2009.

[99] S. Talbot and B. Farhang-Boroujeny, "Time-varying carrier offsets in mobile ofdm," *IEEE Transactions on Communications*, vol. 57, pp. 2790–2798, September 2009.

[100] J. H. Winters, "Optimum Combining in Digital Mobile Radio with Cochannel Interference," *IEEE Journal on Selected Areas in Communications*, vol. 2, pp. 528–539, July 1984.

[101] J. H. Winters, *U.S. Patent No. 4,639,914: Wireless PBX/LAN System With Optimum Combining*, filed December 6, 1984, issued January 27, 1987.

[102] J. Salz, "Digital transmission over cross-coupled linear channels," *AT&T Technical Journal*, vol. 64, pp. 1147–1159, July-August 1985.

[103] J. H. Winters, "On the Capacity of Radio Communication Systems with Diversity in a Rayleigh Fading Environment," *IEEE Journal on Selected Areas in Communications*, vol. 5, pp. 871–878, June 1987.

[104] J. H. Winters, "Optimum Combining for Indoor Radio Systems with Multiple Users," *IEEE Transactions on Communications*, vol. 35, pp. 1222–1230, November 1987.

[105] S. Cheng and S. Verdu, "Gaussian multiaccess channels with ISI: capacity region and multiuser water-filling," *IEEE Transactions on Information Theory*, vol. 39, pp. 773–785, May 1993.

[106] A. Duel-Hallen, "Equalizers for multiple input/multiple output channels and PAM systems with cyclostationary input sequences," *IEEE Journal on Selected Areas in Communications*, vol. 10, pp. 630–639, April 1992.

[107] J. H. Winters, J. Salz, and R. D. Gitlin, “The impact of antenna diversity on the capacity of wireless communication systems,” *IEEE Transactions on Communications*, vol. 5, pp. 1740–1751, February/March/April 1994.

[108] J. Yang and S. Roy, “On joint transmitter and receiver optimization for multiple-input-multiple-output (MIMO) transmission systems,” *IEEE Transactions on Communications*, vol. 42, pp. 3221–3231, December 1994.

[109] J. Yang and S. Roy, “Joint transmitter-receiver optimization for multi-input multi-output systems with decision feedback,” *IEEE Transactions on Information Theory*, vol. 40, pp. 1334–1347, September 1994.

[110] J. H. Winters, “The diversity gain of transmit diversity in wireless systems with Rayleigh fading,” *IEEE Transactions on Vehicular Technology*, vol. 47, pp. 119–123, February 1998.

[111] J. H. Winters and J. Salz, “Upper bounds on the bit-error rate of optimum combining in wireless systems,” *IEEE Transactions on Communications*, vol. 46, pp. 1619–1624, December 1998.

[112] G. G. Raleigh and J. M. Cioffi, “Spatio-temporal coding for wireless communications,” in *IEEE Global Telecommunications Conference, 1996 (GLOBECOM ’96)*, vol. 3, pp. 1809–1814, 18-22 November 1996.

[113] G. J. Foschini, “Layered Space-Time Architecture for Wireless Communication in a Fading Environment When Using Multi-Element Antennas,” *Bell Labs Technical Journal*, vol. Autumn, pp. 41–59, 1996.

[114] G. G. Raleigh and J. M. Cioffi, “Spatio-temporal coding for wireless communication,” *IEEE Transactions on Communications*, vol. 46, pp. 357–366, March 1998.

[115] G. J. Foschini and M. J. Gans, “On limits of wireless communications in a fading environment when using multiple antennas,” *Wireless Personal Communications*, vol. 6, pp. 311–335, March 1998.

[116] G. J. Foschini, G. D. Golden, R. A. Valenzuela, and P. W. Wolniansky, “Simplified processing for high spectral efficiency wireless communication employing multi-element arrays,” *IEEE Journal on Selected Areas in Communications*, vol. 17, pp. 1841–1852, November 1999.

[117] B. Lu and X. Wang, “Iterative receivers for multiuser space-time coding systems,” *IEEE Journal on Selected Areas in Communications*, vol. 18, pp. 2322–2335, November 2000.

[118] S. Y. Kung, Y. Wu, and X. Zhang, “Bezout space-time precoders and equalizers for MIMO channels,” *IEEE Transactions on Signal Processing*, vol. 50, pp. 2499–2514, October 2002.

[119] F. Petré, G. Leus, L. Deneire, M. Engels, M. Moonen, and H. D. Man, “Space-time block coding for single-carrier block transmission DS-CDMA downlink,” *IEEE Journal on Selected Areas in Communications*, vol. 21, pp. 350–361, April 2003.

[120] L. Zhang, L. Gui, Y. Qiao, and W. Zhang, “Obtaining diversity gain for DTV by using MIMO structure in SFN,” *IEEE Transactions on Broadcasting*, vol. 50, pp. 83–90, March 2004.

[121] X. Zhu and R. D. Murch, “Layered space-frequency equalization in a single-carrier MIMO system for frequency-selective channels,” *IEEE Transactions on Wireless Communications*, vol. 3, pp. 701–708, May 2004.

[122] M. R. McKay and I. B. Collings, “Capacity and performance of MIMO-BICM with zero-forcing receivers,” *IEEE Transactions on Communications*, vol. 53, pp. 74–83, January 2005.

[123] J. Hoadley, “Building Future Networks with MIMO and OFDM.” http://telephonyonline.com/wireless/technology/mimo_ofdm_091905/, 19 September 2005. Telephonyonline.com.

[124] A. J. Paulraj, D. A. Gore, R. U. Nabar, and H. Bölcskei, “An overview of MIMO communications - a key to gigabit wireless,” *Proceedings of the IEEE*, vol. 92, pp. 198–218, February 2004.

[125] “Using MIMO-OFDM Technology To Boost Wireless LAN Performance Today,” White Paper, Datacomm Research Company, St. Louis, USA, June 2005.

[126] H. Sampath, S. Talwar, J. Tellado, V. Erceg, and A. J. Paulraj, “A fourth-generation MIMO-OFDM broadband wireless system: design, performance, and field trial results,” *IEEE Communications Magazine*, vol. 40, pp. 143–149, September 2002.

[127] Airgo Networks, http://www.airgonetworks.com/.

[128] Institute of Electrical and Electronics Engineers, *IEEE Candidate Standard 802.11n: Wireless LAN Medium Access Control (MAC) and Physical Layer (PHY) specifications*, 2004. http://grouper.ieee.org/groups/802/11/Reports/tgn_update.htm.

[129] H. Bölcskei, D. Gesbert, and A. J. Paulraj, “On the capacity of OFDM-based spatial multiplexing systems,” *IEEE Transactions on Communications*, vol. 50, pp. 225–234, February 2002.

[130] A. Ganesan and A. M. Sayeed, “A virtual input-output framework for transceiver analysis and design for multipath fading channels,” *IEEE Transactions on Communications*, vol. 51, pp. 1149–1161, July 2003.

[131] R. S. Blum, Y. Li, J. H. Winters, and Q. Yan, "Improved space-time coding for MIMO-OFDM wireless communications," *IEEE Transactions on Communications*, vol. 49, pp. 1873–1878, November 2001.

[132] H. E. Gamal, R. Hammons, Y. Liu, M. P. Fitz, and O. Y. Takeshita, "On the design of space-time and space-frequency codes for MIMO frequency-selective fading channels," *IEEE Transactions on Information Theory*, vol. 49, pp. 2277–2292, September 2003.

[133] P. Dayal, M. Brehler, and M. K. Varanasi, "Leveraging coherent space-time codes for noncoherent communication via training," *IEEE Transactions on Information Theory*, vol. 50, pp. 2058–2080, September 2004.

[134] W. Su, Z. Safar, M. Olfat, and K. J. R. Liu, "Obtaining full-diversity space-frequency codes from space-time codes via mapping," *IEEE Transactions on Signal Processing*, vol. 51, pp. 2905–2916, November 2003.

[135] W. Su, Z. Safar, and K. J. R. Liu, "Full-rate full-diversity space-frequency codes with optimum coding advantage," *IEEE Transactions on Information Theory*, vol. 51, pp. 229–249, January 2005.

[136] J. H. Moon, Y. H. You, W. G. Jeon, K. W. Kwon, and H. K. Song, "Peak-to-average power control for multiple-antenna HIPERLAN/2 and IEEE802.11a systems," *IEEE Transactions on Consumer Electronics*, vol. 49, pp. 1078–1083, November 2003.

[137] Y. L. Lee, Y. H. You, W. G. Jeon, J. H. Paik, and H. K. Song, "Peak-to-average power ratio in MIMO-OFDM systems using selective mapping," *IEEE Communications Letters*, vol. 7, pp. 575–577, December 2003.

[138] S. H. Han and J. H. Lee, "An overview of peak-to-average power ratio reduction techniques for multicarrier transmission," *IEEE Wireless Communications*, vol. 12, pp. 56–65, April 2005.

[139] Y. Li, "Simplified Channel Estimation for OFDM Systems with Multiple Transmit Antennas," *IEEE Transactions on Wireless Communications*, vol. 1, pp. 67–75, January 2002.

[140] I. Barhumi, G. Leus, and M. Moonen, "Optimal training design for MIMO OFDM systems in mobile wireless channels," *IEEE Transactions on Signal Processing*, vol. 51, pp. 1615–1624, June 2003.

[141] M. Shin, H. Lee, and C. Lee, "Enhanced Channel-estimation Technique for MIMO-OFDM Systems," *IEEE Transactions on Vehicular Technology*, vol. 53, pp. 262–265, January 2004.

[142] Y. Li, J. H. Winters, and N. R. Sollenberger, "MIMO-OFDM for Wireless Communications: Signal Detection with Enhanced Channel Estimation," *IEEE Transactions on Communications*, vol. 50, pp. 1471–1477, September 2002.

[143] L. Giangaspero, L. Agarossi, G. Paltenghi, S. Okamura, M. Okada, and S. Komaki, "Co-channel interference cancellation based on MIMO OFDM systems," *IEEE Wireless Communications*, vol. 9, pp. 8–17, December 2002.

[144] J. Li, K. B. Letaief, and Z. Cao, "Co-channel interference cancellation for space-time coded OFDM systems," *IEEE Transactions on Wireless Communications*, vol. 2, pp. 41–49, January 2003.

[145] S. Y. Park and C. G. Kang, "Complexity-reduced iterative MAP receiver for interference suppression in OFDM-based spatial multiplexing systems," *IEEE Transactions on Vehicular Technology*, vol. 53, pp. 1316–1326, September 2004.

[146] G. L. Stüber, J. R. Barry, S. W. McLaughlin, Y. Li, M. A. Ingram, and T. G. Pratt, "Broadband MIMO-OFDM wireless communications," *Proceedings of the IEEE*, vol. 92, pp. 271–294, February 2004.

[147] C. Dubuc, D. Starks, T. Creasy, and Y. Hou, "A MIMO-OFDM prototype for next-generation wireless WANs," *IEEE Communications Magazine*, vol. 42, pp. 82–87, December 2004.

[148] R. J. Piechocki, P. N. Fletcher, A. Nix, N. Canagarajah, and J. P. McGeehan, "Performance evaluation of BLAST-OFDM enhanced Hiperlan/2 using simulated and measured channel data," *Electronics Letters*, vol. 37, pp. 1137–1139, August 2001.

[149] S. Catreux, V. Erceg, D. Gesbert, and R. W. Heath Jr., "Adaptive modulation and MIMO coding for broadband wireless data networks," *IEEE Communications Magazine*, vol. 40, pp. 108–115, June 2002.

[150] R. Piechocki, P. Fletcher, A. Nix, N. Canagarajah, and J. McGeehan, "A measurement based feasibility study of space-frequency MIMO detection and decoding techniques for next generation wireless LANs," *IEEE Transactions on Consumer Electronics*, vol. 48, pp. 732–737, August 2002.

[151] A. F. Molisch, M. Z. Win, and J. H. Winters, "Space-time-frequency (STF) coding for MIMO-OFDM systems," *IEEE Communications Letters*, vol. 6, pp. 370–372, September 2002.

[152] A. Stamoulis, S. N. Diggavi, and N. Al-Dhahir, "Intercarrier interference in MIMO OFDM," *IEEE Transactions on Signal Processing*, vol. 50, pp. 2451–2464, October 2002.

[153] A. Doufexi, M. Hunukumbure, A. Nix, M. A. Beach, and S. Armour, "COFDM performance evaluation in outdoor MIMO channels using space/polarisation-time processing techniques," *Electronics Letters*, vol. 38, pp. 1720–1721, December 2002.

[154] H. Bölcskei, M. Borgmann, and A. J. Paulraj, "Impact of the propagation environment on the performance of space-frequency coded MIMO-OFDM," *IEEE Journal on Selected Areas in Communications*, vol. 21, pp. 427–439, April 2003.

[155] J. Cai, W. Song, and Z. Li, "Doppler spread estimation for mobile OFDM systems in Rayleigh fading channels," *IEEE Transactions on Consumer Electronics*, vol. 49, pp. 973–977, November 2003.

[156] G. Leus and M. Moonen, "Per-tone equalization for MIMO OFDM systems," *IEEE Transactions on Signal Processing*, vol. 51, pp. 2965–2975, November 2003.

[157] R. J. Piechocki, A. Nix, J. P. McGeehan, and S. M. D. Armour, "Joint blind and semi-blind detection and channel estimation," *IEE Proceedings - Communications*, vol. 150, pp. 419–426, December 2003.

[158] P. Xia, S. Zhou, and G. B. Giannakis, "Adaptive MIMO-OFDM based on partial channel state information," *IEEE Transactions on Signal Processing*, vol. 52, pp. 202–213, January 2004.

[159] D. Huang and K. B. Letaief, "Symbol-based space diversity for coded OFDM systems," *IEEE Transactions on Wireless Communications*, vol. 3, pp. 117–127, January 2004.

[160] M. R. G. Butler and I. B. Collings, "A zero-forcing approximate log-likelihood receiver for MIMO bit-interleaved coded modulation," *IEEE Communications Letters*, vol. 8, pp. 105–107, February 2004.

[161] B. Lu, G. Yue, and X. Wang, "Performance analysis and design optimization of LDPC-coded MIMO OFDM systems," *IEEE Transactions on Signal Processing*, vol. 52, pp. 348–361, February 2004.

[162] A. V. Zelst and T. C. W. Schenk, "Implementation of a MIMO OFDM-based wireless LAN system," *IEEE Transactions on Signal Processing*, vol. 52, pp. 483–494, February 2004.

[163] A. Pascual-Iserte, A. I. Pérez-Neira, and M. A. Lagunas, "On power allocation strategies for maximum signal to noise and interference ratio in an OFDM-MIMO system," *IEEE Transactions on Wireless Communications*, vol. 3, pp. 808–820, May 2004.

[164] Y. Zeng and T. S. Ng, "A Semi-blind Channel Estimation Method for Multiuser Multiantenna OFDM Systems," *IEEE Transactions on Signal Processing*, vol. 52, pp. 1419–1429, May 2004.

[165] B. Alien, R. Brito, M. Dohler, and A. H. Aghvami, “Performance comparison of spatial diversity array topologies in an OFDM based wireless LAN,” *IEEE Transactions on Consumer Electronics*, vol. 50, pp. 420–428, May 2004.

[166] J. Tan and G. L. Stüber, “Multicarrier delay diversity modulation for MIMO systems,” *IEEE Transactions on Wireless Communications*, vol. 3, pp. 1756–1763, September 2004.

[167] X. Wang, Y. R. Shayan, and M. Zeng, “On the code and interleaver design of broadband OFDM systems,” *IEEE Communications Letters*, vol. 8, pp. 653–655, November 2004.

[168] Y. Pan, K. B. Letaief, and Z. Cao, “Dynamic spatial subchannel allocation with adaptive beamforming for MIMO/OFDM systems,” *IEEE Transactions on Wireless Communications*, vol. 3, pp. 2097–2107, November 2004.

[169] C. Tepedelenlioĝlu and R. Challagulla, “Low-complexity multipath diversity through fractional sampling in OFDM,” *IEEE Transactions on Signal Processing*, vol. 52, pp. 3104–3116, November 2004.

[170] M. S. Baek, M. J. Kim, Y. H. You, and H. K. Song, “Semi-blind channel estimation and PAR reduction for MIMO-OFDM system with multiple antennas,” *IEEE Transactions on Broadcasting*, vol. 50, pp. 414–424, December 2004.

[171] G. Barriac and U. Madhow, “Space-time communication for OFDM with implicit channel feedback,” *IEEE Transactions on Information Theory*, vol. 50, pp. 3111–3129, December 2004.

[172] J. Zhang, A. Kavcic, and K. M. Wong, “Equal-diagonal QR decomposition and its application to precoder design for successive-cancellation detection,” *IEEE Transactions on Information Theory*, vol. 51, pp. 154–172, January 2005.

[173] Y. Yao and G. B. Giannakis, “Blind carrier frequency offset estimation in SISO, MIMO, and multiuser OFDM systems,” *IEEE Transactions on Communications*, vol. 53, pp. 173–183, January 2005.

[174] K. Zheng, L. Huang, W. Wang, and G. Yang, “TD-CDM-OFDM: Evolution of TD-SCDMA toward 4G,” *IEEE Communications Magazine*, vol. 43, pp. 45–52, January 2005.

[175] H. Yang, “A road to future broadband wireless access: MIMO-OFDM-Based air interface,” *IEEE Communications Magazine*, vol. 43, pp. 53–60, January 2005.

[176] Y. Zhang and K. B. Letaief, "An efficient resource-allocation scheme for spatial multiuser access in MIMO/OFDM systems," *IEEE Transactions on Communications*, vol. 53, pp. 107–116, January 2005.

[177] X. Ma, M. K. Oh, G. B. Giannakis, and D. J. Park, "Hopping pilots for estimation of frequency-offset and multiantenna channels in MIMO-OFDM," *IEEE Transactions on Communications*, vol. 53, pp. 162–172, January 2005.

[178] M. Fozunbal, S. W. McLaughlin, and R. W. Schafer, "On space-time-frequency coding over MIMO-OFDM systems," *IEEE Transactions on Wireless Communications*, vol. 4, pp. 320–331, January 2005.

[179] S. Nanda, R. Walton, J. Ketchum, M. Wallace, and S. Howard, "A high-performance MIMO OFDM wireless LAN," *IEEE Communications Magazine*, vol. 43, pp. 101–109, February 2005.

[180] K. J. Kim, J. Yue, R. A. Iltis, and J. D. Gibson, "A QRD-M/Kalman Filter-based Detection and Channel Estimation Algorithm for MIMO-OFDM Systems," *IEEE Transactions on Wireless Communications*, vol. 4, pp. 710–721, March 2005.

[181] Y. Qiao, S. Yu, P. Su, and L. Zhang, "Research on An Iterative Algorithm of LS Channel Estimation in MIMO OFDM Systems," *IEEE Transactions on Broadcasting*, vol. 51, pp. 149–153, March 2005.

[182] H. Sampath, V. Erceg, and A. Paulraj, "Performance analysis of linear precoding based on field trials results of MIMO-OFDM system," *IEEE Transactions on Wireless Communications*, vol. 4, pp. 404–409, March 2005.

[183] F. Rey, M. Lamarca, and G. Vazquez, "Robust power allocation algorithms for MIMO OFDM systems with imperfect CSI," *IEEE Transactions on Signal Processing*, vol. 53, pp. 1070–1085, March 2005.

[184] Y. Sun, Z. Xiong, and X. Wang, "EM-based iterative receiver design with carrier-frequency offset estimation for MIMO OFDM systems," *IEEE Transactions on Communications*, vol. 53, pp. 581–586, April 2005.

[185] A. Lodhi, F. Said, M. Dohler, and A. H. Aghvami, "Performance comparison of space-time block coded and cyclic delay diversity MC-CDMA systems," *IEEE Wireless Communications*, vol. 12, pp. 38–45, April 2005.

[186] Z. Wang, Z. Han, and K. J. R. Liu, "A MIMO-OFDM Channel Estimation Approach Using Time of Arrivals," *IEEE Transactions on Wireless Communications*, vol. 4, pp. 1207–1213, May 2005.

[187] C. K. Wen, Y. Y. Wang, and J. T. Chen, “A low-complexity space-time OFDM multiuser system,” *IEEE Transactions on Wireless Communications*, vol. 4, pp. 998–1007, May 2005.

[188] W. Su, Z. Safar, and K. J. R. Liu, “Towards maximum achievable diversity in space, time, and frequency: performance analysis and code design,” *IEEE Transactions on Wireless Communications*, vol. 4, pp. 1847–1857, July 2005.

[189] M. Tan, Z. Latinović, and Y. Bar-Ness, “STBC MIMO-OFDM peak-to-average power ratio reduction by cross-antenna rotation and inversion,” *IEEE Communications Letters*, vol. 9, pp. 592–594, July 2005.

[190] K. W. Park and Y. S. Cho, “An MIMO-OFDM technique for high-speed mobile channels,” *IEEE Communications Letters*, vol. 9, pp. 604–606, July 2005.

[191] L. Shao and S. Roy, “Rate-one space-frequency block codes with maximum diversity for MIMO-OFDM,” *IEEE Transactions on Wireless Communications*, vol. 4, pp. 1674–1687, July 2005.

[192] T. C. W. Schenk, X. Tao, P. F. M. Smulders, and E. R. Fledderus, “On the influence of phase noise induced ICI in MIMO OFDM systems,” *IEEE Communications Letters*, vol. 9, pp. 682–684, August 2005.

[193] M. Borgmann and H. Bölcskei, “Noncoherent space-frequency coded MIMO-OFDM,” *IEEE Journal on Selected Areas in Communications*, vol. 23, pp. 1799–1810, September 2005.

[194] A. Tarighat and A. H. Sayed, “MIMO OFDM Receivers for Systems With IQ Imbalances,” *IEEE Transactions on Signal Processing*, vol. 53, pp. 3583–3596, September 2005.

[195] Y. Jiang, J. Li, and W. W. Hager, “Joint transceiver design for MIMO communications using geometric mean decomposition,” *IEEE Transactions on Signal Processing*, vol. 53, pp. 3791–3803, October 2005.

[196] J. Choi and R. W. Heath Jr., “Interpolation Based Transmit Beamforming for MIMO-OFDM With Limited Feedback,” *IEEE Transactions on Signal Processing*, vol. 53, pp. 4125–4135, November 2005.

[197] M. S. Baek, H. J. Kook, M. J. Kim, Y. H. You, and H. K. Song, “Multi-Antenna Scheme for High Capacity Transmission in the Digital Audio Broadcasting,” *IEEE Transactions on Broadcasting*, vol. 51, pp. 551–559, December 2005.

[198] M. Fakhereddin, M. Sharif, and B. Hassibi, “Reduced feedback and random beamforming for ofdm mimo broadcast channels,” *IEEE*

Transactions on Communications, vol. 57, pp. 3827–3835, December 2009.

[199] P. De, T. Chang, and C. Chi, "Linear prediction based semiblind channel estimation for multiuser ofdm with insufficient guard interval," *IEEE Transactions on Wireless Communications*, vol. 8, pp. 5728–5736, December 2009.

[200] L. Haring, S. Bieder, and A. Czylwik, "Fine frequency synchronization in the uplink of multiuser ofdm systems," *IEEE Transactions on Communications*, vol. 57, pp. 3743–3752, December 2009.

[201] P. Vandenameele, L. V. D. Perre, and M. Engels, *Space Division Multiple Access for Wireless Local Area Networks*. London, UK: Kluwer, 2001.

[202] I. P. Kovalyov, *SDMA for Multipath Wireless Channels: Limiting Characteristics and Stochastic Models*. Springer, 1st ed., 2004. ISBN 3-540-40225-X.

[203] D. Tse and P. Viswanath, *Fundamentals of Wireless Communication*. Cambridge, UK: Cambridge University Press, 2005. ISBN-13 978-0-521-84527-4.

[204] M. Cooper and M. Goldburg, "Intelligent Antennas: Spatial Division Multiple Access," *ArrayComm: Annual Review of Communications*, pp. 999–1002, 1996.

[205] P. Vandenameele, L. V. D. Perre, M. Engels, B. Gyselinckx, and H. D. Man, "A Novel Class of Uplink OFDM/SDMA Algorithms: A Statistical Performance Analysis," in *Proceedings of the IEEE Vehicular Technology Conference, 1999 (VTC 1999 Fall)*, vol. 1, (Amsterdam, Netherlands), pp. 324–328, IEEE, 19-22 September 1999.

[206] P. Vandenameele, L. V. D. Perre, M. Engels, B. Gyselinckx, and H. D. Man, "A Combined OFDM/SDMA Approach," *IEEE Journal on Selected Areas in Communications*, vol. 18, pp. 2312–2321, November 2000.

[207] S. Thoen, L. V. D. Perre, M. Engels, and H. D. Man, "Adaptive loading for OFDM/SDMA-based wireless networks," *IEEE Transactions on Communications*, vol. 50, pp. 1798–1810, November 2002.

[208] S. Thoen, L. Deneire, L. V. D. Perre, M. Engels, and H. D. Man, "Constrained Least Squares Detector for OFDM/SDMA-based Wireless Networks," *IEEE Transactions on Wireless Communications*, vol. 2, pp. 129–140, January 2003.

[209] A. T. Alastalo and M. Kahola, “Smart-antenna operation for indoor wireless local-area networks using OFDM,” *IEEE Transactions on Wireless Communications*, vol. 2, pp. 392–399, March 2003.

[210] M. Y. Alias, A. K. Samingan, S. Chen, and L. Hanzo, “Multiple Antenna Aided OFDM Employing Minimum Bit Error Rate Multiuser Detection,” *Electronics Letters*, vol. 39, pp. 1769–1770, November 2003.

[211] X. Dai, “Carrier frequency offset estimation for OFDM/SDMA systems using consecutive pilots,” *IEE Proceedings - Communications*, vol. 152, pp. 624–632, October 2005.

[212] Y. S. Yeh and D. Reudink, “Efficient Spectrum Utilization for Mobile Radio Systems Using Space Diversity,” *IEEE Transactions on Communications*, vol. 30, pp. 447–455, March 1982.

[213] K. T. Ko and B. Davis, “A Space-Division Multiple-Access Protocol for Spot-Beam Antenna and Satellite-Switched Communication Network,” *IEEE Journal on Selected Areas in Communications*, vol. 1, pp. 126–132, January 1983.

[214] S. C. Swales, M. A. Beach, and D. J. Edwards, “Multi-beam adaptive base-station antennas for cellular land mobile radio systems,” in *Proceedings of the IEEE 39th Vehicular Technology Conference, 1989 (VTC 1989 Spring)*, vol. 1, pp. 341–348, 1-3 May 1989.

[215] S. C. Swales, M. A. Beach, D. J. Edwards, and J. P. McGeehan, “The performance enhancement of multibeam adaptive base-station antennas for cellular land mobile radio systems,” *IEEE Transactions on Vehicular Technology*, vol. 39, pp. 56–67, February 1990.

[216] B. G. Agee, S. V. Schell, and W. A. Gardner, “Spectral self-coherence restoral: a new approach to blind adaptive signal extraction using antenna arrays,” *Proceedings of the IEEE*, vol. 78, pp. 753–767, April 1990.

[217] S. Anderson, M. Millnert, M. Viberg, and B. Wahlberg, “An adaptive array for mobile communication systems,” *IEEE Transactions on Vehicular Technology*, vol. 40, pp. 230–236, February 1991.

[218] P. Balaban and J. Salz, “Optimum diversity combining and equalization in digital data transmission with applications to cellular mobile radio. Part I: Theoretical considerations,” *IEEE Transactions on Communications*, vol. 40, pp. 885–894, May 1992.

[219] P. Balaban and J. Salz, “Optimum diversity combining and equalization in digital data transmission with applications to cellular mobile radio. Part II: Numerical results,” *IEEE Transactions on Communications*, vol. 40, pp. 895–907, May 1992.

[220] G. Xu, H. Liu, W. J. Vogel, H. P. Lin, S. S. Jeng, and G. W. Torrence, “Experimental studies of space-division-multiple-access schemes for spectral efficient wireless communications,” in *IEEE International Conference on Communications, 1994 (ICC 1994)*, vol. 2, (New Orleans, USA), pp. 800–804, 1-5 May 1994.

[221] S. Talwar, M. Viberg, and A. Paulraj, “Blind estimation of multiple co-channel digital signals using an antenna array,” *IEEE Signal Processing Letters*, vol. 1, pp. 29–31, February 1994.

[222] A. J. V. D. Veen, S. Talwar, and A. Paulraj, “Blind estimation of multiple digital signals transmitted over FIR channels,” *IEEE Signal Processing Letters*, vol. 2, pp. 99–102, May 1995.

[223] B. H. Khalaj, A. Paulraj, and T. Kailath, “Spatio-temporal channel estimation techniques for multiple access spread spectrum systems with antenna arrays,” in *IEEE International Conference on Communications, 1995 (ICC 1995)*, vol. 3, (Seattle, USA), pp. 1520–1524, 18-22 June 1995.

[224] K. Anand, G. Mathew, and V. U. Reddy, “Blind separation of multiple co-channel BPSK signals arriving at an antenna array,” *IEEE Signal Processing Letters*, vol. 2, pp. 176–178, September 1995.

[225] H. Liu and G. Xu, “Smart Antennas in Wireless Systems: Uplink Multiuser Blind Channel and Sequence Detection,” *IEEE Transactions on Communications*, vol. 45, pp. 187–199, February 1997.

[226] G. Tsoulos, M. A. Beach, and J. McGeehan, “Wireless personal communications for the 21st century: European technological advances in adaptive antennas,” *IEEE Communications Magazine*, vol. 35, pp. 102–109, September 1997.

[227] L. Deneire and D. T. M. Slock, “Blind channel identification based on cyclic statistics,” *IEE Proceedings - Radar, Sonar and Navigation*, vol. 145, pp. 58–62, February 1998.

[228] G. Tsoulos, J. McGeehan, and M. A. Beach, “Space division multiple access (SDMA) field trials. Part I: Tracking and BER performance,” *IEE Proceedings - Radar, Sonar and Navigation*, vol. 145, pp. 73–78, February 1998.

[229] G. Tsoulos, J. McGeehan, and M. A. Beach, “Space division multiple access (SDMA) field trials. Part II: Calibration and linearity issues,” *IEE Proceedings - Radar, Sonar and Navigation*, vol. 145, pp. 79–84, February 1998.

[230] V. A. N. Barroso, J. M. F. Moura, and J. Xavier, “Blind array channel division multiple access (AChDMA) for mobile communications,” *IEEE Transactions on Signal Processing*, vol. 46, pp. 737–752, March 1998.

[231] F. Demmerle and W. Wiesbeck, “A biconical multibeam antenna for space-division multiple access,” *IEEE Transactions on Antennas and Propagation*, vol. 46, pp. 782–787, June 1998.

[232] B. Lindmark, S. Lundgren, J. R. Sanford, and C. Beckman, “Dual-polarized array for signal-processing applications in wireless communications,” *IEEE Transactions on Antennas and Propagation*, vol. 46, pp. 758–763, June 1998.

[233] B. Suard, G. Xu, H. Liu, and T. Kailath, “Uplink channel capacity of space-division-multiple-access schemes,” *IEEE Transactions on Information Theory*, vol. 44, pp. 1468–1476, July 1998.

[234] S. S. Jeng, G. Xu, H. P. Lin, and W. J. Vogel, “Experimental studies of spatial signature variation at 900 MHz for smart antenna systems,” *IEEE Transactions on Antennas and Propagation*, vol. 46, pp. 953–962, July 1998.

[235] P. Petrus, R. B. Ertel, and J. H. Reed, “Capacity enhancement using adaptive arrays in an AMPS system,” *IEEE Transactions on Vehicular Technology*, vol. 47, pp. 717–727, August 1998.

[236] J. M. F. Xavier, V. A. N. Barroso, and J. M. F. Moura, “Closed-form Blind Channel Identification and Source Separation in SDMA Systems Through Correlative Coding,” *IEEE Journal on Selected Areas in Communications*, vol. 16, pp. 1506–1517, October 1998.

[237] C. Farsakh and J. A. Nossek, “Spatial covariance based downlink beamforming in an SDMA mobile radio system,” *IEEE Transactions on Communications*, vol. 46, pp. 1497–1506, November 1998.

[238] G. V. Tsoulos, “Smart antennas for mobile communication systems: benefits and challenges,” *Electronics and Communication Engineering Journal*, vol. 11, pp. 84–94, April 1999.

[239] F. Piolini and A. Rolando, “Smart channel-assignment algorithm for SDMA systems,” *IEEE Transactions on Microwave Theory and Techniques*, vol. 47, pp. 693–699, June 1999.

[240] G. M. Galvan-Tejada and J. G. Gardiner, “Theoretical blocking probability for SDMA,” *IEE Proceedings - Communications*, vol. 146, pp. 303–306, October 1999.

[241] G. M. Galvan-Tejada and J. G. Gardiner, “Theoretical model to determine the blocking probability for SDMA systems,” *IEEE Transactions on Vehicular Technology*, vol. 50, pp. 1279–1288, September 2001.

[242] G. V. Tsoulos, "Experimental and theoretical capacity analysis of space-division multiple access (SDMA) with adaptive antennas," *IEE Proceedings - Communications*, vol. 146, pp. 307–311, October 1999.

[243] U. Vornefeld, C. Walke, and B. Walke, "SDMA techniques for wireless ATM," *IEEE Communications Magazine*, vol. 37, pp. 52–57, November 1999.

[244] P. Djahani and J. M. Kahn, "Analysis of infrared wireless links employing multibeam transmitters and imaging diversity receivers," *IEEE Transactions on Communications*, vol. 48, pp. 2077–2088, December 2000.

[245] F. Shad, T. D. Todd, V. Kezys, and J. Litva, "Dynamic slot allocation (DSA) in indoor SDMA/TDMA using a smart antenna basestation," *IEEE/ACM Transactions on Networking*, vol. 9, pp. 69–81, February 2001.

[246] R. Kuehner, T. D. Todd, F. Shad, and V. Kezys, "Forward-link capacity in smart antenna base stations with dynamic slot allocation," *IEEE Transactions on Vehicular Technology*, vol. 50, pp. 1024–1038, July 2001.

[247] S. S. Jeon, Y. Wang, Y. Qian, and T. Itoh, "A novel smart antenna system implementation for broad-band wireless communications," *IEEE Transactions on Antennas and Propagation*, vol. 50, pp. 600–606, May 2002.

[248] S. Bellofiore, C. A. Balanis, J. Foutz, and A. S. Spanias, "Smart-antenna systems for mobile communication networks. Part 1: Overview and antenna design," *IEEE Antennas and Propagation Magazine*, vol. 44, pp. 145–154, June 2002.

[249] S. Bellofiore, C. A. Balanis, J. Foutz, and A. S. Spanias, "Smart-antenna systems for mobile communication networks. Part 2: Beam-forming and network throughput," *IEEE Antennas and Propagation Magazine*, vol. 44, pp. 106–114, August 2002.

[250] X. Fang, "More realistic analysis for blocking probability in SDMA systems," *IEE Proceedings - Communications*, vol. 149, pp. 152–156, June 2002.

[251] A. Arredondo, K. R. Dandekar, and G. Xu, "Vector channel modeling and prediction for the improvement of downlink received power," *IEEE Transactions on Communications*, vol. 50, pp. 1121–1129, July 2002.

[252] C. M. Walke and T. J. Oechtering, "Analytical expression for uplink C/I-distribution in interference-limited cellular radio systems," *Electronics Letters*, vol. 38, pp. 743–744, July 2002.

[253] T. Zwick, C. Fischer, and W. Wiesbeck, “A stochastic multipath channel model including path directions for indoor environments,” *IEEE Journal on Selected Areas in Communications*, vol. 20, pp. 1178–1192, August 2002.

[254] S. A. Zekavat, C. R. Nassar, and S. Shattil, “Oscillating-beam smart antenna arrays and multicarrier systems: achieving transmit diversity, frequency diversity, and directionality,” *IEEE Transactions on Vehicular Technology*, vol. 51, pp. 1030–1039, September 2002.

[255] J. L. Pan and P. M. Djurić, “Multibeam cellular mobile communications with dynamic channel assignment,” *IEEE Transactions on Vehicular Technology*, vol. 51, pp. 1252–1258, September 2002.

[256] C. C. Cavalcante, F. R. P. Cavalcanti, and J. C. M. Mota, “Adaptive blind multiuser separation criterion based on log-likelihood maximisation,” *Electronics Letters*, vol. 38, pp. 1231–1233, September 2002.

[257] H. Yin and H. Liu, “Performance of space-division multiple-access (SDMA) with scheduling,” *IEEE Transactions on Wireless Communications*, vol. 1, pp. 611–618, October 2002.

[258] M. Rim, “Multi-user downlink beamforming with multiple transmit and receive antennas,” *Electronics Letters*, vol. 38, pp. 1725–1726, December 2002.

[259] I. Bradaric, A. P. Pertropulu, and K. I. Diamantaras, “Blind MIMO FIR Channel Identification Based on Second-order Spectra Correlations,” *IEEE Transactions on Signal Processing*, vol. 51, pp. 1668–1674, June 2003.

[260] Q. H. Spencer, A. L. Swindlehurst, and M. Haardt, “Zero-forcing methods for downlink spatial multiplexing in multiuser MIMO channels,” *IEEE Transactions on Signal Processing*, vol. 52, pp. 461–471, February 2004.

[261] J. Li, K. B. Letaief, and Z. Cao, “A reduced-complexity maximum-likelihood method for multiuser detection,” *IEEE Transactions on Communications*, vol. 52, pp. 289–295, February 2004.

[262] L. U. Choi and R. D. Murch, “A pre-BLAST-DFE technique for the downlink of frequency-selective fading MIMO channels,” *IEEE Transactions on Communications*, vol. 52, pp. 737–743, May 2004.

[263] W. Ajib and D. Haccoun, “An overview of scheduling algorithms in MIMO-based fourth-generation wireless systems,” *IEEE Network*, vol. 19, pp. 43–48, September-October 2005.

[264] K. M. Nasr, F. Costen, and S. K. Barton, “A Wall Imperfection Channel Model for Signal Level Prediction and its Impact on Smart Antenna Systems for Indoor Infrastructure WLAN,” *IEEE Transactions on Antennas and Propagation*, vol. 53, pp. 3767–3775, November 2005.

[265] L. Hanzo, M. Münster, B. J. Choi, and T. Keller, *OFDM and MC-CDMA for Broadband Multi-User Communications, WLANs and Broadcasting*. John Wiley and IEEE Press, 2003. 992 pages.

[266] A. Goldsmith, S. A. Jafar, N. Jindal, and S. Vishwanath, “Capacity limits of MIMO channels,” *IEEE Journal on Selected Areas in Communications*, vol. 21, pp. 684–702, June 2003.

[267] P. Höher, S. Kaiser, and P. Robertson, “Pilot-symbol-aided channel estimation in time and frequency,” in *IEEE Global Telecommunications Conference: The Mini-Conference*, (Phoenix, AZ), pp. 90–96, November 1997.

[268] P. Höher, S. Kaiser, and P. Robertson, “Two-dimensional pilot-symbol-aided channel estimation by Wiener filtering,” in *IEEE International Conference on Acoustics, Speech and Signal Processing*, (Munich, Germany), pp. 1845–1848, April 1997.

[269] O. Edfords, M. Sandell, J.-J. van de Beek, S. Wilson, and P. Börjesson, “OFDM channel estimation by singular value decomposition,” *IEEE Transactions on Communications*, vol. 46, pp. 931–939, July 1998.

[270] Y. Li, L. Cimini, and N. Sollenberger, “Robust channel estimation for OFDM systems with rapid dispersive fading channels,” *IEEE Transactions on Communications*, vol. 46, pp. 902–915, April 1998.

[271] Y. Li, “Pilot-symbol-aided channel estimation for OFDM in wireless systems,” *IEEE Transactions on Vehicular Technology*, vol. 49, pp. 1207–1215, July 2000.

[272] B. Yang, Z. Cao, and K. Letaief, “Analysis of low-complexity windowed DFT-based MMSE channel estimation for OFDM systems,” *IEEE Transactions on Communications*, vol. 49, pp. 1977–1987, November 2001.

[273] M. Münster and L. Hanzo, “Rls-adaptive parallel interference cancellation assisted decision-directed channel estimation for ofdm,” in *Wireless Communications and Networking, 2003. WCNC 2003. 2003 IEEE*, vol. 1, pp. 50–54vol.1, 16-20 March 2003.

[274] R. Otnes and M. Tüchler, “Iterative channel estimation for turbo equalization of time-varying frequency-selective channels,” *IEEE Transactions on Wireless Communications*, vol. 3, no. 6, pp. 1918–1923, 2004.

[275] M. Münster, *Antenna Diversity-Assisted Adaptive Wireless Multiuser OFDM Systems*. PhD thesis, University of Southampton, UK, 2002.

[276] M. Morelli and U. Mengali, "A Comparison of Pilot-Aided Channel Estimation Methods for OFDM Systems," *IEEE Transactions on Signal Processing*, vol. 49, pp. 3065–3073, December 2001.

[277] M.-X. Chang and Y. Su, "Model-based channel estimation for OFDM signals in Rayleigh fading," *IEEE Transactions on Communications*, vol. 50, pp. 540–544, April 2002.

[278] J.-J. van de Beek, O. Edfors, M. Sandell, S. Wilson, and P. Börjesson, "On channel estimation in OFDM systems," in *Proceedings of Vehicular Technology Conference*, vol. 2, (Chicago, IL USA), pp. 815–819, IEEE, July 1995.

[279] V. Mignone and A. Morello, "A novel demodulation scheme for fixed and mobile receivers," *IEEE Transactions on Communications*, vol. 44, pp. 1144–1151, September 1996.

[280] Y. Li and N. Sollenberg, "Clustered OFDM with channel estimation for high rate wireless data," *IEEE Transactions on Communications*, vol. 49, pp. 2071–2076, December 2001.

[281] M. Münster and L. Hanzo, "Second-order channel parameter estimation assisted cancellation of channel variation-induced inter-subcarrier interference in ofdm systems," in *EUROCON'2001, Trends in Communications, International Conference on.*, vol. 1, pp. 1–5vol.1, 4-7 July 2001.

[282] M. Münster and L. Hanzo, "MMSE channel prediction assisted symbol-by-symbol adaptive OFDM," in *Proceedings of IEEE International Conference on Communications*, vol. 1, pp. 416–420, 28 April-2 May 2002.

[283] M. Sandell, C. Luschi, P. Strauch, and R. Yan, "Iterative channel estimation using soft decision feedback," in *Global Telecommunications Conference, 1998. GLOBECOM 98. The Bridge to Global Integration. IEEE*, vol. 6, (Sydney,NSW), pp. 3728–3733, 1998.

[284] M. Valenti, "Iterative channel estimation for turbo codes over fading channels," in *Wireless Communications and Networking Conference, 2000. WCNC. 2000 IEEE*, vol. 3, pp. 1019–1024vol.3, 23-28 Sept. 2000.

[285] B.-L. Yeap, C. Wong, and L. Hanzo, "Reduced complexity in-phase/quadrature-phase m-QAM turbo equalization using iterative channel estimation," *IEEE Transactions on Wireless Communications*, vol. 2, no. 1, pp. 2–10, 2003.

[286] S. Song, A. Singer, and K.-M. Sung, "Turbo equalization with an unknown channel," in *Acoustics, Speech, and Signal Processing, 2002. Proceedings. (ICASSP '02). IEEE International Conference on*, vol. 3, 2002.

[287] S. Song, A. Singer, and K.-M. Sung, "Soft input channel estimation for turbo equalization," *Signal Processing, IEEE Transactions on [see also Acoustics, Speech, and Signal Processing, IEEE Transactions on]*, vol. 52, pp. 2885–2894, 2004.

[288] R. Otnes and M. Tüchler, "Soft iterative channel estimation for turbo equalization: comparison of channel estimation algorithms," in *Communication Systems, 2002. ICCS 2002. The 8th International Conference on*, vol. 1, pp. 72–76, 2002.

[289] N. Seshadri, "Joint data and channel estimation using blind trellis search techniques," *IEEE Transactions on Communications*, vol. 42, pp. 1000–1011, February/March/April 1994.

[290] A. Knickenberg, B.-L. Yeap, J. Hàmorskỳ, M. Breiling, and L. Hanzo, "Non-iterative Joint Channel Equalisation and Channel Decoding," *IEE Electronics Letters*, vol. 35, pp. 1628–1630, 16 September 1999.

[291] C. Cozzo and B. Hughes, "Joint channel estimation and data detection in space-time communications," *IEEE Transactions on Communications*, vol. 51, pp. 1266–1270, Aug. 2003.

[292] T. Cui and C. Tellambura, "Joint channel estimation and data detection for OFDM systems via sphere decoding," in *Proceedings of IEEE Global Telecommunications Conference*, vol. 6, pp. 3656–3660, 29 Nov.-3 Dec. 2004.

[293] T. Cui and C. Tellambura, "Joint data detection and channel estimation for OFDM systems," *IEEE Transactions on Communications*, vol. 54, no. 4, pp. 670–679, 2006.

[294] C. Antón-Haro, J. Fonolossa, and J. Fonolossa, "Blind channel estimation and data detection using hidden Markov models," *IEEE Transactions on Signal Processing*, vol. 45, pp. 241–247, January 1997.

[295] D. Boss, K. Kammeyer, and T. Petermann, "Is blind channel estimation feasible in mobile communication systems?; a study based on GSM," *IEEE JOurnal on Selected Areas of Communications*, vol. 16, pp. 1479–1492, October 1998.

[296] T. Endres, S. Halford, C. Johnson, and G. Giannakis, "Blind adaptive channel equalization using fractionally-spaced receivers: A comparison

study," in *Proceedings of the Conference on Information Sciences and Systems*, (Princeton, USA), 20–22 March 1996.

[297] G. Giannakis and S. Halford, "Asymptotically optimal blind fractionally spaced channel estimation and performance results," *IEEE Transactions on Signal Processing*, vol. 45, pp. 1815–1830, July 1997.

[298] S. Zhou and G. Giannakis, "Finite-alphabet based channel estimation for OFDM and related multicarrier systems," *IEEE Transactions on Communications*, vol. 49, pp. 1402–1414, August 2001.

[299] M. Necker and G. Stüber, "Totally Blind Channel Estimation for OFDM over Fast Varying Mobile Channels," in *Proceedings of International Conference on Communications*, (New York, NY USA), IEEE, April 28 - May 2 2002.

[300] S. Haykin, *Adaptive Filter Theory*. Englewood Cliffs, NJ, USA: Prentice-Hall, 1996.

[301] D. Schafhuber and G. Matz, "MMSE and adaptive prediction of time-varying channels for OFDM systems," *IEEE Transactions on Wireless Communications*, vol. 4, pp. 593–602, March 2005.

[302] P. Vandenameele, L. van der Perre, M. Engels, B. Gyselinckx, and H. D. Man, "A combined OFDM/SDMA approach," *IEEE Journal on Selected Areas in Communications*, vol. 18, pp. 2312–2321, Nov. 2000.

[303] V. Jungnickel, T. Haustein, E. Jorswieck, V. Pohl, and C. von Helmolt, "Performance of a MIMO system with overlay pilots," in *Global Telecommunications Conference, 2001. GLOBECOM '01. IEEE*, vol. 1, pp. 594–598vol.1, 25-29 Nov. 2001.

[304] H. Bolcskei, R. Heath, and A. Paulraj, "Blind channel identification and equalization in OFDM-based multiantenna systems," *Signal Processing, IEEE Transactions on [see also Acoustics, Speech, and Signal Processing, IEEE Transactions on]*, vol. 50, pp. 96–109, Jan 2002.

[305] H. Zhu, B. Farhang-Boroujeny, and C. Schlegel, "Pilot embedding for joint channel estimation and data detection in MIMO communication systems," *Communications Letters, IEEE*, vol. 7, pp. 30–32, Jan 2003.

[306] Y. Li, N. Seshardi, and S. Ariyavisitakul, "Channel estimation for OFDM systems with transmitt diversity in mobile wireless channels," *IEEE Journal on Selected Areas in Communications*, vol. 17, pp. 461–471, March 1999.

[307] Y. Li, "Simplified channel estimation for OFDM systems with multiple transmit antennas," *IEEE Transactions on Wireless Communications*, vol. 1, pp. 67–75, January 2002.

[308] Y. Li, J. Winters, and N. Sollenberger, "MIMO-OFDM for wireless communications: signal detection with enhanced channel estimation," *IEEE Transactions on Communications*, vol. 50, no. 9, pp. 1471–1477, 2002.

[309] X. Deng, A. Haimovich, and J. Garcia-Frias, "Decision directed iterative channel estimation for MIMO systems," in *Proceedings of IEEE International Conference on Communications*, vol. 4, pp. 2326–2329, 11-15 May 2003.

[310] M. Münster and L. Hanzo, "Multi-user ofdm employing parallel interference cancellation assisted decision-directed channel estimation," in *Vehicular Technology Conference, 2002. Proceedings. VTC 2002-Fall. 2002 IEEE 56th*, vol. 3, pp. 1413–1417vol.3, 24-28 Sept. 2002.

[311] M. Münster and L. Hanzo, "Parallel-interference-cancellation-assisted decision-directed channel estimation for ofdm systems using multiple transmit antennas," *Wireless Communications, IEEE Transactions on*, vol. 4, pp. 2148–2162, Sept. 2005.

[312] A. Grant, "Joint decoding and channel estimation for linear MIMO channels," in *Wireless Communications and Networking Conference, 2000. WCNC. 2000 IEEE*, vol. 3, pp. 1009–1012vol.3, 23-28 Sept. 2000.

[313] H. Mai, Y. Zakharov, and A. Burr, "Iterative B-spline channel estimation for space-time block coded systems in fast flat fading channels," in *Vehicular Technology Conference, 2005. VTC 2005-Spring. 2005 IEEE 61st*, vol. 1, pp. 476–480, 30 May-1 June 2005.

[314] X. Qiao, Y. Cai, and Y. Xu, "Joint iterative decision feedback channel estimation for turbo coded v-BLAST MIMO-OFDM systems," in *IEEE International Symposium on Communications and Information Technology*, vol. 2, pp. 1384–1388, 2005.

[315] S. Yatawatta and A. Petropulu, "Blind channel estimation in MIMO OFDM systems with multiuser interference," *Signal Processing, IEEE Transactions on [see also Acoustics, Speech, and Signal Processing, IEEE Transactions on]*, vol. 54, pp. 1054–1068, March 2006.

[316] G. Stüber, J. Barry, S. McLaughlin, Y. Li, M. Ingram, and T. Pratt, "Broadband MIMO-OFDM wireless communications," *Proceedings of the IEEE*, vol. 92, pp. 271–294, Feb 2004.

[317] H. Mai, A. Burr, and S. Hirst, "Iterative channel estimation for turbo equalization," in *Personal, Indoor and Mobile Radio Communications, 2004. PIMRC 2004. 15th IEEE International Symposium on*, vol. 2, pp. 1327–1331, 2004.

[318] G. Foschini Jr. and M. Gans, "On limits of wireless communication in a fading environment when using multiple antennas," *Wireless Personal Communications*, vol. 6, pp. 311–335, March 1998.

[319] A. van Zelst, R. van Nee, and G. Awater, "Space Division Multiplexing (SDM) for OFDM systems," in *Proceedings of Vehicular Technology Conference*, vol. 2, (Tokyo, Japan), pp. 1070–1074, IEEE, May 15-18 2000.

[320] G. Foschini, "Layered Space-Time Architecture for Wireless Communication in a Fading Environment when using Multi-Element Antennas"," *Bell Labs Technical Journal*, vol. Autumn, pp. 41–59, 1996.

[321] J. Blogh and L. Hanzo, *Third-Generation Systems and Intelligent Networking*. John Wiley and IEEE Press, 2002. (For detailed contents, please refer to http://www-mobile.ecs.soton.ac.uk.).

[322] L. Hanzo, T. H. Liew, and B. L. Yeap, *Turbo Coding, Turbo Equalisation and Space-Time Coding*. Chichester, UK; Piscataway, NJ, USA: John Wiley and IEEE Press, 2002. 766 pages. (For detailed contents, please refer to http://www-mobile.ecs.soton.ac.uk.).

[323] S. X. Ng, B. L. Yeap, and L. Hanzo, "Full-rate, full-diversity adaptive space time block coding for transmission over Rayleigh fading channels," in *Proceedings of the IEEE VTC'05 Fall*, (Dallas, Texas), 25-28, September 2005. To be published.

[324] S. Alamouti, "A Simple Transmit Diversity Technique for Wireless Communications," *IEEE Journal on Selected Areas in Communications*, vol. 16, pp. 1451–1458, October 1998.

[325] V. Tarokh, N. Seshadri, and A. Calderbank, "Space-Time Codes for High Data Rate Wireless Communication: Performance Criterion and Code Construction," *IEEE Transactions on Information Theory*, vol. 44, pp. 744–765, March 1998.

[326] V. Tarokh, A. Naguib, N. Seshadri, and A. Calderbank, "A Space-Time Coding Modem for High-Data-Rate Wireless Communications," *IEEE Journal on Selected Areas in Communications*, vol. 16, pp. 1459–1477, October 1998.

[327] V. Tarokh, A. Naguib, N. Seshadri, and A. Calderbank, "Space-Time Codes for High Data Rate Wireless Communication: Performance Criteria in the Presence of Channel Estimation Errors, Mobility and Multiple Paths," *IEEE Transactions on Communications*, vol. 47, pp. 199–207, February 1999.

[328] V. Tarokh, H. Jafarkhani, and A. Calderbank, "Space-Time Block Coding for Wireless Communications: Performance Results," *IEEE Transactions on Communications*, vol. 17, pp. 451–460, March 1999.

[329] V. Tarokh, A. Naguib, N. Seshadri, and A. R. Calderbank, "Combined array processing and space-time coding," *IEEE Transactions on Information Theory*, vol. 45, pp. 1121–1128, May 1999.

[330] V. Tarokh, H. Jafarkhani, and A. Calderbank, "Space-Time Block Codes from Orthogonal Designs," *IEEE Transactions on Information Theory*, vol. 45, pp. 1456–1467, July 1999.

[331] V. Tarokh and H. Jafarkhani, "A Differential Detection Scheme for Transmit Diversity," *IEEE Journal on Selected Areas in Communications*, vol. 18, pp. 1169–1174, July 2000.

[332] S. Ariyavisitakul, J. Winters, and I. Lee, "Optimum space-time processors with dispersive interference: Unified analysis and required filter span," *IEEE Transactions on Communications*, vol. 47, pp. 1073–1083, July 1999.

[333] S. Ariyavisitakul, J. Winters, and N. Sollenberger, "Joint Equalization and Interference Suppression for High Data Rate Wireless Systems," *IEEE Journal on Selected Areas in Communications*, vol. 18, pp. 1214–1220, July 2000.

[334] G. Golden, G. Foschini, R. Valenzuela, and P. Wolniansky, "Detection Algorithms and Initial Laboratory Results using V-BLAST Space-Time Communication Architecture," *IEE Electronics Letters*, vol. 35, pp. 14–16, January 1999.

[335] C. Hassell-Sweatman, J. Thompson, B. Mulgrew, and P. Grant, "A Comparison of Detection Algorithms including BLAST for Wireless Communication using Multiple Antennas," in *Proceedings of International Symposium on Personal, Indoor and Mobile Radio Communications*, vol. 1, (Hilton London Metropole Hotel, London, UK), pp. 698–703, IEEE, September 18-21 2000.

[336] D. E. Goldberg, *Genetic Algorithms in Search, Optimization, and Machine Learning*. Reading, Massachusetts: Addison-Wesley, 1989.

[337] M. J. Juntti, T. Schlösser, and J. O. Lilleberg, "Genetic algorithms for multiuser detection in synchronous CDMA," in *IEEE International Symposium on Information Theory – ISIT'97*, (Ulm, Germany), p. 492, 1997.

[338] S. M. Kay, *Fundamentals of Statistical Signal Processing*. Englewood Cliffs, NJ, USA: Prentice-Hall, 1998.

[339] R. van Nee, A. van Zelst, and G. Awater, "Maximum Likelihood Decoding in a Space-Division Multiplexing System," in *Proceedings of Vehicular Technology Conference*, vol. 1, (Tokyo, Japan), pp. 6–10, IEEE, May 15-18 2000.

[340] G. Awater, A. van Zelst, and R. van Nee, "Reduced Complexity Space Division Multiplexing Receivers," in *Proceedings of Vehicular Technology Conference*, vol. 1, (Tokyo, Japan), pp. 11–15, IEEE, May 15-18 2000.

[341] U. Fincke and M. Pohst, "Improved method for calculating vector of short length in a lattice, including a complexity analysis," *Math. Comput.*, vol. 44, pp. 463–471, April 1985.

[342] M. O. Damen, A. Chkeif, and J.-C. Belfiore, "Lattice code decoder for space-time codes," *IEEE Commun. Letters*, pp. 161–163, May 2000.

[343] B. Hochwald and S. ten Brink, "Achieving near-capacity on a multiple-antenna channel," *IEEE Transactions on Communications*, vol. 51, no. 3, pp. 389–399, 2003.

[344] M. O. Damen, H. E. Gamal, and G. Caier, "On maximum-likelihood detection and the search for closest lattice point," *IEEE Transactions on Information Theory*, vol. 49, pp. 2389–2402, October 2003.

[345] D. Pham, K. R. Pattipati, P. K. Willet, and J. Luo, "An improved complex sphere decoder for V-BLAST Systems," *IEEE Signal Processing Letters*, vol. 11, pp. 748–751, September 2004.

[346] T. Cui and C. Tellambura, "Approximate ML detection for MIMO systems using multistage sphere decoding," *IEEE Signal Processing Letters*, vol. 12, pp. 222–225, March 2005.

[347] M. Damen, K. Abed-Meraim, and J.-C. Belfiore, "Generalised sphere decoder for asymmetrical space-time communication architecture," *Electronics Letters*, vol. 36, no. 2, pp. 166–167, 2000.

[348] T. Cui and C. Tellambura, "An efficient generalized sphere decoder for rank-deficient MIMO systems," *IEEE Communications Letters*, vol. 9, no. 5, pp. 423–425, 2005.

[349] Z. Yang, C. Liu, and J. He, "A new approach for fast generalized sphere decoding in mimo systems," *Signal Processing Letters, IEEE*, vol. 12, pp. 41–44, Jan. 2005.

[350] W. Zhao and G. Giannakis, "Sphere decoding algorithms with improved radius search," *IEEE Transactions on Communications*, vol. 53, no. 7, pp. 1104–1109, 2005.

[351] R. Wang and G. Giannakis, “Approaching MIMO channel capacity with soft detection based on hard sphere decoding,” *IEEE Transactions on Communications*, vol. 54, pp. 587–590, April 2006.

[352] H. Vikalo, B. Hassibi, and T. Kailath, “Iterative decoding for mimo channels via modified sphere decoding,” *IEEE Transactions on Wireless Communications*, vol. 3, pp. 2299–2311, Nov. 2004.

[353] C. Berrou, A. Glavieux, and P. Thitimajshima, “Near shannon limit error-correcting coding and decoding: Turbo codes,” in *Proceedings of IEEE International Conference on Communications*, (Geneva, Switzerland), pp. 1064–1070, IEEE, May 1993.

[354] S. Bug, C. Wengerter, I. Gaspard, and R. Jakoby, “Channel model based on comprehensive measurements for DVB-T mobile applications,” in *IEEE Instrumentation and Measurements Technology Conference*, (Budapest, Hungary), May 21-23 2001.

[355] M. Failli, “Digital land mobile radio communications COST 207,” tech. rep., European Commission, 1989.

[356] R. Steele and L. Hanzo, eds., *Mobile Radio Communications*. New York, USA: John Wiley and IEEE Press, 2nd ed., 1999. 1090 pages.

[357] W. Jakes Jr., ed., *Microwave Mobile Communications*. New York, USA: John Wiley & Sons, 1974.

[358] M. C. Jeruchim, P. Balaban, and K. S. Shanmugan, *Simulation of Communication Systems*. Kluwer Academic, 2000. 2nd edition.

[359] L. Hanzo, C. Wong, and M. Yee, *Adaptive Wireless Transceivers*. John Wiley and IEEE Press, 2002. (For detailed contents, please refer to http://www-mobile.ecs.soton.ac.uk.).

[360] M.-S. Alouini and A. J. Goldsmith, “Capacity of Rayleigh fading channels under different adaptive transmission and diversity-combining techniques,” *IEEE Transactions on Vehicular Technology*, vol. 49, pp. 1165–1181, July 1999.

[361] L. Zheng and N. Tse, “Diversity and multiplexing: A fundamental tradeoff in multiple-antenna channels,” *IEEE Transactions on Information Theory*, vol. 49, pp. 1073–1096, May 2003.

[362] C. E. Shannon, “A mathematical theory of communication,” *Bell System Technical Journal*, vol. 27, pp. 379–423 and 623–656, June and October 1948.

[363] B. Yang, “Projection approximation subspace tracking,” *IEEE Transactions on Signal Processing*, vol. 43, pp. 95–107, January 1995.

[364] W. C. Chung, N. J. August, and D. S. Ha, "Signaling and multiple access techniques for ultra wideband 4G wireless communication systems," *IEEE Wireless Communications*, vol. 12, pp. 46–55, April 2005.

[365] "Wi-Fi Brand Awareness and Consumer Affinity Continues to Grow Worldwide," September 2008. http://www.wi-fi.org/pressroom_overview.php?newsid=711/.

[366] "IEEE Standard for Information Technology - Telecommunications and Information Exchange Between Systems - Local and Metropolitan Area Networks - Specific Requirements - Part 11: Wireless LAN Medium Access Control (MAC) and Physical Layer (PHY) Specifications," 1997. IEEE 802.11-1997.

[367] "IEEE Standard for Information Technology - Telecommunications and Information Exchange Between Systems - Local and Metropolitan Area Networks - Specific Requirements - Part 11: Wireless LAN Medium Access Control (MAC) and Physical Layer (PHY) Specifications," 1999. IEEE 802.11-1999.

[368] "Supplement to IEEE Standard for Information Technology - Telecommunications and Information Exchange Between Systems - Local and Metropolitan Area Networks - Specific Requirements - Part 11: Wireless LAN Medium Access Control (MAC) and Physical Layer (PHY) Specifications: High-speed Physical Layer in the 5 GHz Band," 1999. IEEE 802.11a-1999.

[369] "Supplement to IEEE Standard for Information Technology - Telecommunications and Information Exchange Between Systems - Local and Metropolitan Area Networks - Specific Requirements - Part 11: Wireless LAN Medium Access Control (MAC) and Physical Layer (PHY) Specifications: Higher-speed Physical Layer Extension in the 2.4 GHz Band," 1999. IEEE 802.11b-1999.

[370] "IEEE Standard for Information Technology - Telecommunications and Information Exchange Between Systems - Local and Metropolitan Area Networks - Specific Requirement - Part 11: Wireless LAN Medium Access Control (MAC) and Physical Layer (PHY) Specification - Amendment 3: Specifications for Operation in Additional Regulatory Domains," 2001. IEEE 802.11d-2001.

[371] "IEEE Standard for Information Technology - Telecommunications and Information Exchange Between Systems - Local and Metropolitan Area Networks - Specific Requirements - Part 11: Wireless LAN Medium Access Control (MAC) and Physical Layer (PHY) Specifications -

Amendment 4: Further Higher Data Rate Extension in the 2.4 GHz Band," 2003. IEEE 802.11g-2003.

[372] "IEEE Standard for Information Technology - Telecommunications and Information Exchange Between Systems - Local and Metropolitan Area Networks - Specific Requirements - Part 11: Wireless LAN Medium Access Control (MAC) and Physical Layer (PHY) Specifications - Amendment 5: Spectrum and Transmit Power Management Extensions in the 5 GHz band in Europe," 2003. IEEE 802.11h-2003.

[373] "IEEE Standard for Information Technology - Telecommunications and Information Exchange Between Systems - Local and Metropolitan Area Networks - Specific Requirements - Part 11: Wireless LAN Medium Access Control (MAC) and Physical Layer (PHY) Specifications - Amendment 6: Medium Access Control (MAC) Security Enhancements," 2004. IEEE 802.11i-2004.

[374] "IEEE Standard for Information Technology - Telecommunications and Information Exchange Between Systems - Local and Metropolitan Area Networks - Specific Requirements - Part 11: Wireless LAN Medium Access Control (MAC) and Physical Layer (PHY) Specifications - Amendment 7: 4.9 GHz-5 GHz Operation in Japan," 2004. IEEE 802.11j-2004.

[375] "IEEE Standard for Information Technology - Telecommunications and Information Exchange Between Systems - Local and Metropolitan Area Networks - Specific Requirements - Part 11: Wireless LAN Medium Access Control (MAC) and Physical Layer (PHY) Specifications - Amendment 8: Medium Access Control (MAC) Quality of Service Enhancements," 2005. IEEE 802.11e-2005.

[376] "IEEE Standard for Information Technology - Telecommunications and Information Exchange Between Systems - Local and Metropolitan Area Networks - Specific Requirements - Part 11: Wireless LAN Medium Access Control (MAC) and Physical Layer (PHY) Specifications," 2007. IEEE 802.11-2007.

[377] "IEEE Standard for Information Technology - Telecommunications and Information Exchange Between Systems - Local and Metropolitan Area Networks - Specific Requirements - Part 11: Wireless LAN Medium Access Control (MAC) and Physical Layer (PHY) Specifications - Amendment 1: Radio Resource Measurement of Wireless LANs (Amendment to IEEE 802.11-2007)," 2008. IEEE 802.11k-2008.

[378] "IEEE Standard for Information Technology - Telecommunications and Information Exchange Between Systems - Local and Metropolitan Area

Networks - Specific Requirements - Part 11: Wireless LAN Medium Access Control (MAC) and Physical Layer (PHY) Specifications - Amendment 2: Fast Basic Service Set (BSS) Transition (Amendment to IEEE 802.11-2007 and IEEE 802.11k-2008),” 2008. IEEE 802.11r-2008.

[379] “Draft IEEE Standard for Information Technology - Telecommunications and Information Exchange Between Systems - Local and Metropolitan Area Networks - Specific Requirements - Part 11: Wireless LAN Medium Access Control (MAC) and Physical Layer (PHY) Specifications - Amendment 3: 3650-3700 MHz Operation in USA (Draft Amendment to IEEE 802.11-2007),” 2008. IEEE P802.11y/D10.

[380] “UTRA-UTRAN Long Term Evolution (LTE) and 3GPP System Architecture Evolution (SAE),” May 2008. http://www.3gpp.org/Highlights/LTE/LTE.htm.

[381] “Overview of 3GPP Release 6: Summary of all Release 6 Features (Version TSG #33),” 2006. 3GPP Rel-6.

[382] E. Dahlman, S. Parkvall, J. Sköld, and P. Beming, *3G EVOLUTION: HSPA AND LTE FOR MOBILE BROADBAND*. Academic Press, 2007.

[383] “3rd Generation Partnership Project; Technical Specification Group Radio Access Network; Physical layer aspects for evolved Universal Terrestrial Radio Access (UTRA) (Release 7),” September 2006. 3GPP TR 25.814 V7.1.0.

[384] J. G. Andrews, A. Ghosh, and R. Muhamed, *Fundamentals of WiMAX: Understanding Broadband Wireless Networking*. Prentice Hall, 2007.

[385] S. A. M. Ilyas, *WiMAX Applications*. CRC Press, 2007.

[386] “Frequently Asked Questions.” http://www.wimaxforum.org/technology/faq/.

[387] “IEEE Standard for Local and Metropolitan Area Networks - Part 16: Air Interface for Fixed Broadband Wireless Access Systems,” 2001. IEEE 802.16-2001.

[388] “IEEE Standard for Local and Metropolitan Area Networks - Part 16: Air Interface for Fixed Broadband Wireless Access Systems - Amendment 1: Detailed System Profiles for 10-66 GHz,” 2002. IEEE 802.16c-2002.

[389] “IEEE Standard for Local and Metropolitan Area Networks - Part 16: Air Interface for Fixed Broadband Wireless Access Systems - Amendment 2: Medium Access Control Modifications and Additional Physical Layer Specifications for 2-11 GHz,” 2003. IEEE 802.16a-2003.

[390] “IEEE Standard for Local and Metropolitan Area Networks - Part 16: Air Interface for Fixed and Mobile Broadband Wireless Access

Systems - Amendment 2: Physical and Medium Access Control Layers for Combined Fixed and Mobile Operation in Licensed Bands and Corrigendum 1," 2005. IEEE 802.16e-2005.

[391] "IEEE Standard for Local and Metropolitan Area Networks - Part 16: Air Interface for Fixed Broadband Wireless Access Systems - Amendment 1: Management Information Base," 2005. IEEE 802.16f-2005.

[392] "IEEE Standard for Local and Metropolitan Area Networks Media Access Control (MAC) Bridges - Amendment 5: Bridging of IEEE 802.16," 2007. IEEE 802.16k-2007.

[393] "IEEE Standard for Local and Metropolitan Area Networks - Part 16: Air Interface for Fixed and Mobile Broadband Wireless Access Systems - Amendment 3: Management Plane Procedure and Services," 2007. IEEE 802.16g-2007.

[394] "Draft IEEE Standard for Local and Metropolitan Area Networks - Part 16: Air Interface for Fixed and Mobile Broadband Wireless Access Systems: Improved Coexistence Mechanisms for License-Exempt Operation (Amendment to IEEE 802.16d-2004)," 2008. IEEE P802.16h/D7.

[395] "Draft IEEE Standard for Local and Metropolitan Area Networks - Part 16: Air Interface for Fixed and Mobile Broadband Wireless Access Systems Multihop Relay Specification," 2008. IEEE P802.16j/D5.

[396] G. S. V. R. K. Rao and G. Radhamani, *WiMAX - A Wireless Technology Revolution*. Auerbach Publications, 2007.

[397] "Draft IEEE Standard for Local and Metropolitan Area Networks - Part 16: Air Interface for Broadband Wireless Access Systems (Revision of IEEE 802.16d-2004 and consolidates material from IEEE 802.16e-2005, IEEE 802.16d-2004/Cor1-2005, IEEE 802.16f-2005 and IEEE 802.16g-2007)," 2008. IEEE P802.16Rev2/D5.

[398] "WirelessHUMAN Tutorial," July 2000. IEEE 802.16h-00/08.

[399] L. Nuaymi, *WiMAX: Technology for Broadband Wireless Access*. John Wiley & Sons Ltd., 2007.

[400] "IEEE Standard for Local and metropolitan area networks - Media Access Control (MAC) Bridges," 2004. IEEE 802.1D-2004.

[401] M. Hancock, "WiMAX Questions and Answers," July 2008. http://www.wimaxforum.org/news/wimax_faq_10-2007.pdf.

[402] "ETSI HiperMAN." http://www.etsi.org/WebSite/Technologies/HiperMAN.aspx.

[403] "The Relationship Between WiBro and Mobile WiMAX," 2006. http://www.wimaxforum.org/technology/downloads/.

[404] C. Koo, “2.3GHz Portable Internet - WiBro,” July 2004. http://www.knom.or.kr/tutorial/Tutorial2004/knom_T_1.pdf.

[405] S. Y. Yoon, “Introduction to WiBro Technology,” September 2004. http://www.itu.int/ITU-D/imt-2000/documents/Busan/Session3_Yoon.pdf.

[406] “Mobile WiMAX - Part I: A Technical Overview and Performance Evaluation,” February 2006. http://www.wimaxforum.org/technology/downloads/.

[407] H. Yaghoobi, “Scalable OFDMA Physical Layer in IEEE 802.16 WirelessMAN,” *Intel Technology Journal*, vol. 8, pp. 201–212, August 2004.

[408] S. M. Alamouti, “A Simple Transmit Diversity Technique for Wireless Communications,” *IEEE Journal on Selected Areas in Communications*, vol. 16, pp. 1451–1458, October 1998.

[409] “Draft report on requirements related to technical system performance for IMT-Advanced radio interface(s) [IMT.TECH],” June 2008. ITU-R Document 5D/TEMP/89r1Cleanv2.

[410] S. Ortiz, “4G Wireless Begins to Take Shape,” *Computer*, vol. 40, pp. 18–21, November 2007.

[411] “IEEE 802.16m System Requirements,” October 2007. IEEE 802.16m-07/002r4.

[412] “WiMAX Forum Mobile System Profile, Release 1.0 Approved Specification (Revision 1.4.0: 19 2007-05-02),” May 2007. http://www.wimaxforum.org/technology/documents/.

[413] “Draft IEEE Standard for Local and Metropolitan Area Networks: Media Independent Handover Services),” 2008. IEEE P802.21/D13.

[414] “IEEE 802.16m System Description Document,” July 2008. IEEE 802.16m-08/003r4.

[415] R. B. Marks, M. Lynch, and K. McCabe, “IEEE 802.16 WirelessMAN Standard enters IMT-2000 Family for International Mobile Telecommunications,” October 2007. http://standards.ieee.org/announcements/PR_802.16MT2000.html.

[416] “WiMAX Forum WiMAX Technology Forecast (2007-2012),” June 2008. http://www.wimaxforum.org/technology/downloads/.

[417] “WiMAX Forum announces first certified MIMO 2.5 GHz Mobile WiMAX products,” June 2008. http://www.wimaxforum.org/news/.

[418] P. Chaudhury, W. Mohr, and S. Onoe, "The 3GPP Proposal for IMT-2000," *IEEE Communications Magazine*, vol. 37, pp. 72–81, December 1999.

[419] B. Glance and L. Greestein, "Frequency-selective fading effects in digital mobile radio with diversity combining," *IEEE Transactions Communications*, vol. COM-31, pp. 1085–1094, September 1983.

[420] F. Adachi and K. Ohno, "BER performance of QDPSK with postdetection diversity reception in mobile radio channels," *IEEE Transactions on Vehicular Technology*, vol. 40, pp. 237–249, February 1991.

[421] V. Tarokh, H. Jafarkhani, and A. R. Calderbank, "Space-time Block Codes from Orthogonal Designs," *IEEE Transactions on Information Theory*, vol. 45, pp. 1456–1467, May 1999.

[422] V. Tarokh, H. Jafarkhani, and A. R. Calderbank, "Space-Time Block Coding for Wireless Communications: Performance Results," *IEEE Journal on Selected Areas in Communications*, vol. 17, pp. 451–460, March 1999.

[423] V. Tarokh, N. Seshadri, and A. R. Calderbank, "Space-Time Codes for High Data Rate Wireless Communication: Performance Criterion and Code Construction," *IEEE Transactions on Information Theory*, vol. 44, pp. 744–765, March 1998.

[424] V. Tarokh, A. Naguib, N. Seshadri, and A. R. Calderbank, "Space-Time Codes for High Data Rate Wireless Communication: Performance Criteria in the Presence of Channel Estimation Errors, Mobility, and Multile Paths," *IEEE Transactions on Communications*, vol. 47, pp. 199–207, February 1999.

[425] V. Tarokh, A. Naguib, N. Seshadri, and A. Calderbank, "Space-time codes for high data rate wireless communications: Mismatch analysis," in *Proceedings of IEEE International Conference on Communications '97*, vol. 1, (Montreal, Canada), pp. 309–313, June 1997.

[426] N. Seshadri, V. Tarokh, and A. Calderbank, "Space-Time Codes for High Data Rate Wireless Communications: Code Construction," in *Proceedings of the IEEE Vehicular Technology Conference, 1997 (VTC 1997 Spring)*, vol. 2, (Phoenix, Arizona), pp. 637–641, May 1997.

[427] R. Gallager, "Low Density Parity Check Codes," *IEEE Transactions on Information Theory*, vol. 8, pp. 21–28, January 1962.

[428] C. Berrou, A. Glavieux, and P. Thitimajshima, "Near Shannon Limit Error-Correcting Coding and Decoding: Turbo Codes," in

Proceedings of the International Conference on Communications, (Geneva, Switzerland), pp. 1064–1070, May 1993.

[429] C. Berrou and A. Glavieux, “Near optimum error correcting coding and decoding: Turbo codes,” *IEEE Transactions on Communications*, vol. 44, pp. 1261–1271, October 1996.

[430] G. Bauch, “Concatenation of Space-Time Block Codes and Turbo-TCM,” in *Proceedings of IEEE International Conference on Communications*, vol. 2, (Vancouver, Canada), pp. 1202–1206, June 1999.

[431] W. Koch and A. Baier, “Optimum and Sub-Optimum Detection of Coded Data Distributed by Time-Varying Inter-Symbol Interference,” in *Proceedings of IEEE Globecom ’90*, vol. 3, pp. 1679–1684, 2-5 December 1990.

[432] J. Erfanian, S. Pasupathy, and G. Gulak, “Reduced Complexity Symbol Detectors with Parallel Structures for ISI Channels,” *IEEE Transactions on Communications*, vol. 42, pp. 1661–1671, February/March/April 1994.

[433] P. Robertson, E. Villebrun, and P. Höher, “A Comparison of Optimal and Sub-Optimal MAP Decoding Algorithms Operating in the Log Domain,” in *Proceedings of the International Conference on Communications*, (Seattle, USA), pp. 1009–1013, June 1995.

[434] D. J. C. Mackay and R. M. Neal, “Near Shannon Limit Performance of Low Density Parity Check Codes,” *Electronics Letters*, vol. 33, pp. 457–458, March 1997.

[435] M. G. Luby, M. Mitzenmacher, M. A. Shokrollahi, and D. A. Spielman, “Improved Low Density Parity Check Codes Using Irregular Graphs and Belief Propagations,” in *Proceedings of the IEEE International Symposium on Information Theory*, p. 117, IEEE, 1998.

[436] M. C. Davey, *Error-Correction Using Low Density Parity Check Codes*. PhD thesis, University of Cambridge, UK, 1999.

[437] M. Chiani, A. Conti, and A. Ventura, “Evaluation of Low-Density Parity-Check Codes over Block Fading Channels,” *IEEE ICC’2000*, vol. 3, pp. 1183–1187, 2000.

[438] J. Hou, P. H. Siegel, and L. B. Milstein, “Performance Analysis and Code Optimization of Low Density Parity-Check Codes on Rayleigh Fading Channels,” *IEEE Journal on Selected Areas in Communications*, vol. 19, pp. 924–934, May 2001.

[439] F. Guo, S. X. Ng, and L. Hanzo, “LDPC Assisted Block Coded Modulation for Transmission over Rayleigh Fading Channels,” in

Proceedings of IEEE VTC '03 Spring, vol. 3, (Jeju, Korea), pp. 1867–1871, IEEE, April 2003.

[440] J. Hagenauer, E. Offer, and L. Papke, "Iterative decoding of binary block and convolutional codes," *IEEE Transactions on Information Theory*, vol. 42, pp. 429–445, March 1996.

[441] M. Y. Alias, F. Guo, S. X. Ng, T. H. Liew, and L. Hanzo, "LDPC and Turbo Coding Assisted Space-Time Block Coded OFDM," in *Proceedings of IEEE VTC '03 Spring*, vol. 4, (Jeju, Korea), pp. 2309–2313, IEEE, April 2003.

[442] G. Ungerböeck, "Channel Coding with Multilevel/Phase Signals," *IEEE Transactions on Information Theory*, vol. IT-28, pp. 55–67, January 1982.

[443] P. Robertson and T. Wörz, "Bandwidth Efficient Turbo Trellis-Coded Modulation Using Punctured Component Codes," *IEEE Journal on Selected Area on Communications*, vol. 16, pp. 206–218, February 1998.

[444] E. Zehavi, "8-PSK trellis codes for a Rayleigh fading channel," *IEEE Transactions on Communications*, vol. 40, pp. 873–883, May 1992.

[445] X. Li and J. A. Ritcey, "Bit-interleaved coded modulation with iterative decoding using soft feedback," *Electronics Letters*, vol. 34, pp. 942–943, May 1998.

[446] Z. Guo and W. Zhu, "Performance study of OFDMA vs. OFDM/SDMA," in *VTC-Spring 2002*, vol. 2, pp. 565–569, 6-9 May 2002.

[447] S. Verdu, *Multiuser Detection*. Cambridge University Press, 1998.

[448] C. Z. W. H. Sweatman, J. S. Thompson, B. Mulgrew, and P. M. Grant, "A Comparison of Detection Algorithms including BLAST for Wireless Communication using Multiple Antennas," in *Proceedings of International Symposium on Personal, Indoor and Mobile Radio Communications*, vol. 1, (Hilton London Metropole Hotel, London, UK), pp. 698–703, IEEE, 18-21 September 2000.

[449] M. Münster and L. Hanzo, "Co-Channel Interference Cancellation Techniques for Antenna Array Assisted Multiuser OFDM Systems," in *Proceedings of 3G '2000 Conference*, vol. 1, (London, Great Britain), pp. 256–260, IEE, 27-29 March 2000.

[450] M. Sellathurai and S. Haykin, "A Simplified Diagonal BLAST Architecture with Iterative Parallel-Interference Cancellation Receivers," in *Proceedings of International Conference on Communications*, vol. 10, (Helsinki, Finnland), pp. 3067–3071, IEEE, 11-14 June 2001.

[451] M. Münster and L. Hanzo, "Performance of SDMA Multiuser Detection Techniques for Walsh-Hadamard-Spread OFDM Schemes," in *Proceedings of IEEE VTC '01 Fall*, vol. 4, (Atlantic City, USA), pp. 2319–2323, IEEE, 7-11 October 2001.

[452] "COST207, Digital Land Mobile Radio Communications," final report, Commission of the European Communities, Luxembourg, 1989.

[453] U. Fincke and M. Pohst, "Improved method for calculating vector of short length in a lattice, including a complexity analysis," *Mathematics of Computation*, vol. 44, pp. 463–471, April 1985.

[454] E. Viterbo and J. Boutros, "A universal lattice code decoder for fading channels," *IEEE Transactions on Information Theory*, vol. 45, pp. 1639–1642, July 1999.

[455] M. O. Damen, A. Chkeif, and J.-C. Belfiore, "Lattice code decoder for space-time codes," *IEEE Communications Letters*, vol. 4, pp. 161–163, May 2000.

[456] B. M. Hochwald and S. ten Brink, "Achieving Near-Capacity on a Multiple-Antenna Channel," *IEEE Transactions on Communications*, vol. 51, pp. 389–399, March 2003.

[457] L. Brunel, "Multiuser Detection Techniques Using Maximum Likelihood Sphere Decoding in Multicarrier CDMA Systems," *IEEE Transactions on Wireless Communications*, vol. 3, pp. 949–957, May 2004.

[458] D. Pham, K. R. Pattipati, P. K. Willet, and J. Luo, "An Improved Complex Sphere Decoder for V-BLAST Systems," *IEEE Signal Processing Letters*, vol. 11, pp. 748–751, September 2004.

[459] T. Cui and C. Tellambura, "Approximate ML Detection for MIMO Systems Using Multistage Sphere Decoding," *IEEE Signal Processing Letters*, vol. 12, pp. 222–225, March 2005.

[460] P. W. Wolniansky, G. J. Foschini, G. D. Golden, and R. A. Valenzuela, "V-BLAST: an architecture for realizing very high data rates over the rich-scattering wireless channel," in *URSI International Symposium on Signals, Systems, and Electronics, 1998 (ISSSE '98)*, (Pisa, Italy), pp. 295–300, 29 September-2 October 1998.

[461] J. Holland, *Adaptation in Natural and Artificial Systems*. Ann Arbor, Michigan: University of Michigan Press, 1975.

[462] M. Mitchell, *An Introduction to Genetic Algorithms*. Cambridge, Massachusetts: MIT Press, 1996.

[463] D. Whitley, “A Genetic Algorithm Tutorial,” *Statistics and Computing*, vol. 4, pp. 65–85, June 1994.

[464] S. Forrest, “Genetic Algorithms: Principles of Natural Selection Applied to Computation,” *Science*, vol. 261, pp. 872–878, August 1993.

[465] M. J. Juntti, T. Schlösser, and J. O. Lilleberg, “Genetic Algorithms for Multiuser Detection in Synchronous CDMA,” in *IEEE International Symposium on Information Theory (ISIT’97)*, (Ulm, Germany), p. 492, 29 June-4 July 1997.

[466] X. F. Wang, W.-S. Lu, and A. Antoniou, “A genetic-algorithm-based multiuser detector for multiple-access communications,” in *Proceedings of the 1998 IEEE International Symposium on Circuits and Systems*, vol. 4, (Monterey, California, USA), pp. 534–537, 31 May-3 June 1998.

[467] C. Ergün and K. Hacioglu, “Multiuser Detection Using a Genetic Algorithm in CDMA Communications Systems,” *IEEE Transactions on Communications*, vol. 48, pp. 1374–1383, August 2000.

[468] K. Yen and L. Hanzo, “Antenna-diversity-assisted genetic-algorithm-based multiuser detection schemes for synchronous CDMA systems,” *IEEE Transactions on Communications*, vol. 51, pp. 366–370, March 2003.

[469] K. Yen and L. Hanzo, “Genetic Algorithm Assisted Joint Multiuser symbol Detection and Fading Channel Estimation for Synchronous CDMA Systems,” *IEEE Journal on Selected Areas in Communications*, vol. 19, pp. 985–998, June 2001.

[470] S. Abedi and R. Tafazolli, “Genetically modified multiuser detection for code division multiple access systems,” *IEEE Journal on Selected Areas in Communications*, vol. 20, pp. 463–473, February 2002.

[471] U. Fawer and B. Aazhang, “A Multiuser Receiver for Code Division Multiple Access Communications over Multipath Channels,” *IEEE Transactions on Communications*, vol. 43, pp. 1556–1565, February-April 1995.

[472] T. Blickle and L. Thiele, “A Comparison of Selection Schemes used in Evolutionary Algorithms,” *Evolutionary Computation*, vol. 4, pp. 361–394, January 1996.

[473] E. Zitzler and L. Thiele, “Multiobjective Evolutionary Algorithms: A Comparative Case Study and the Strength Pareto Approach,” *IEEE Transactions on Evolutionary Computation*, vol. 3, pp. 257–271, November 1999.

[474] A. E. Eiben, R. Hinterding, and Z. Michalewicz, “Parameter Control in Evolutionary Algorithms,” *IEEE Transactions on Evolutionary Computation*, vol. 3, pp. 124–141, July 1999.

[475] J. G. Proakis, *Digital Communications*. McGraw-Hill International Edition, 4th ed., 2001.

[476] W. Ledermann and E. Lloyd, *Handbook of Applicable Mathematics, Volume II: Probability*, vol. 2. John Wiley & Sons Ltd., 1980.

[477] M. K. Simon, J. K. Omura, R. A. Scholtz, and B. K. Levitt, *Spread Spectrum Communications: Volume I*. Maryland, USA: Computer Science Press, 1985.

[478] M. K. Simon, J. K. Omura, R. A. Scholtz, and B. K. Levitt, *Spread Spectrum Communications: Volume II*. Maryland, USA: Computer Science Press, 1985.

[479] M. K. Simon, J. K. Omura, R. A. Scholtz, and B. K. Levitt, *Spread Spectrum Communications: Volume III*. Maryland, USA: Computer Science Press, 1985.

[480] R. E. Ziemer and R. L. Peterson, *Digital Communications and Spread Spectrum System*. New York, USA: Macmillan Publishing Company, 1985.

[481] G. Einarsson, “Address Assignment for a Time-Frequency-Coded, Spread-Spectrum System,” *Bell System Technical Journal*, vol. 59, pp. 1241–1255, September 1980.

[482] D. J. Goodman, P. S. Henry, and V. K. Prabhu, “Frequency-Hopped Multilevel FSK for Mobile Radio,” *Bell System Technical Journal*, vol. 59, pp. 1257–1275, September 1980.

[483] A. W. Lam and D. P. Sarwate, “Time-Hopping and Frequency-Hopping Multiple-Access Packet Communications,” *IEEE Transactions on Communications*, vol. 38, pp. 875–888, June 1990.

[484] U. Fiebig, “Iterative Interference Cancellation for FFH/MFSK MA Systems,” *IEE Proceedings - Communications*, vol. 143, pp. 380–388, December 1996.

[485] L.-L. Yang and L. Hanzo, “Slow Frequency-Hopping Multicarrier DS-CDMA for Transmission over Nakagami Multipath Fading Channels,” *IEEE Journal on Selected Areas In Communications*, vol. 19, pp. 1211–1221, July 2001.

[486] L.-L. Yang and L. Hanzo, “Blind Joint Soft-Detection Assisted Slow Frequency-Hopping Multicarrier DS-CDMA,” *IEEE Transactions on Communications*, vol. 48, pp. 1520–1529, September 2000.

[487] E. A. Geraniotis, "Coherent Hybrid DS-SFH Spread-Spectrum Multiple-Access Communications," *IEEE Journal on Selected Area on Communications*, vol. 3, pp. 695–705, September 1985.

[488] J. Wang and H. Huang, "Multicarrier DS/SFH-CDMA Systems," *IEEE Transactions on Vehicular Technology*, vol. 51, pp. 867–876, September 2002.

[489] M. Jankiraman and R. Prasad, "A novel solution to wireless multimedia application: the hybrid OFDM/CDMA/SFH approach," in *The 11th IEEE International Symposium on Personal, Indoor and Mobile Radio Communications, 2000. PIMRC 2000*, vol. 2, pp. 1368–1374, 18-21 September 2000.

[490] K. Hamaguchi and L. Hanzo, "Time-Frequency Spread OFDM/FHMA," in *Proceedings of the IEEE Vehicular Technology Conference, 2003 (VTC 2003 Spring)*, vol. 2, pp. 1248–1252, 22-25 April 2003.

[491] E. A. Geraniotis, "Noncoherent Hybrid DS-SFH Spread-Spectrum Multiple-Access Communications," *IEEE Transactions on Communications*, vol. 34, pp. 862–872, September 1986.

[492] Y. Li and N. R. Sollenberger, "Clustered OFDM with Channel Estimation for High Rate Wireless Data," *IEEE Transactions on Communications*, vol. 49, pp. 2071–2076, December 2001.

[493] B. Daneshrad, L. J. Cimini Jr., M. Carloni, and N. Sollenberger, "Performance and Implementation of Clustered OFDM for Wireless Communications," *ACM Journal on Mobile Networks and Applicaitons (MONET) special issue on PCS*, vol. 2, no. 4, pp. 305–314, 1997.

[494] H. Niu, M. Shen, J. A. Ritcey, and H. Liu, "Performance of Clustered OFDM with Low Density Parity Check Codes over Ddispersive Channels," in *Conference Record of the Thirty-Sixth Asilomar Conference on Signals, Systems and Computers*, pp. 1852–1856, November 2002.

[495] G. Parsaee and A. Yarali, "OFDMA for the 4th Generation Cellular Networks," in *Canadian Conference on Electrical and Computer Engineering*, vol. 4, pp. 2325–2330, 2-5 May 2004.

[496] H. Sari and G. Karam, "Orthogonal frequency-division multiple access and its application to CATV network," *European Transactions on Telecommunications*, vol. 9, p. 507C516, November/December 1998.

[497] J. Jang and K. B. Lee, "Transmit Power Adaptation for Multiuser OFDM Systems," *IEEE Journal on Selected Areas in Communications*, vol. 21, pp. 1747–1758, February 2003.

[498] C. Y. W. amd C. Y. Tsui, R. S. Cheng, and K. B. Lataief, "A Real-time Sub-carrier Allocation Scheme for Multiple Access Downlink OFDM Transmission," in *Proceedings of the IEEE 50th Vehicular Technology Conference, 1999 (VTC 1999 Fall)*, vol. 2, pp. 1124–1128, 19-22 September 1999.

[499] D. Kivanc, G. Li, and H. Liu, "Computationally Efficient Bandwidth Allocation and Power Control for OFDMA," *IEEE Transactions on Wireless Communications*, vol. 2, pp. 1150–1158, November 2003.

[500] D. Kivanc and H. Liu, "Subcarrier Allocation and Power Control for OFDMA," in *Proceedings of the 34th Asilomar Conference on Signals, Systems and Computers, 2000*, vol. 1, pp. 147–151, 29 October-1 November 2000.

[501] I. Kim, H. L. Lee, B. Kim, and Y. H. Lee, "On the use of linear programming for dynamic subchannel and bit allocation in multiuser OFDM," in *Proceedings of the IEEE Global Telecommunications Conference, 2001 (GLOBECOM 2001)*, vol. 6, pp. 3648–3652, 25-29 November 2001.

[502] W. Rhee and J. M. Cioffi, "Increase in capacity of multiuser OFDM system using dynamic subchannel allocation," in *Proceedings of the IEEE 51st Vehicular Technology Conference, 2000 (VTC 2000 Spring)*, vol. 2, (Tokyo, Japan), pp. 1085–1089, 15-18 May 2000.

[503] S. Das and G. D. Mandyam, "An efficient sub-carrier and rate allocation scheme for M-QAM modulated uplink OFDMA transmission," in *Proceedings of the 37th Asilomar Conference on Signals, Systems and Computers, 2003*, vol. 1, pp. 136–140, 9-12 November 2003.

[504] S. Pietrzyk and G. J. M. Janssen, "Multiuser subcarrier allocation for QoS provision in the OFDMA systems," in *Proceedings of the IEEE 56th Vehicular Technology Conference, 2002 (VTC 2002 Fall)*, vol. 2, pp. 1077–1081, 24-28 September 2002.

[505] Z. Hu, G. Zhu, Y. Xia, and G. Liu, "Multiuser subcarrier and bit allocation for MIMO-OFDM systems with perfect and partial channel information," in *Proceedings of the IEEE Wireless Communications and Networking Conference, 2004 (WCNC 2004)*, vol. 2, pp. 1188–1193, 21-25 March 2004.

[506] S. Zhou, G. B. Giannakis, and A. Scaglione, "Long codes for generalized FH-OFDMA through unknown multipath channels," *IEEE Transactions on Communications*, vol. 49, pp. 721–733, April 2001.

[507] Z. Cao, U. Tureli, and P. Liu, "Optimum subcarrier assignment for OFDMA uplink," in *The Thrity-Seventh Asilomar Conference on Signals, Systems and Computers*, vol. 1, pp. 708–712, 9-12 November 2003.

[508] Y. H. Kim, K. S. Kim, and J. Y. Ahn, "Iterative estimation and decoding for an LDPC-coded OFDMA system in uplink environments," in *IEEE International Conference on Communications*, vol. 4, pp. 2478–2482, 20-24 June 2004.

[509] H. Sari, Y. Levy, and G. Karam, "An analysis of orthogonal frequency-division multiple access," in *IEEE Global Telecommunications Conference*, vol. 3, pp. 1635–1639, 3-8 November 1997.

[510] T. Kurt and H. Delic, "Collision avoidance in space-frequency coded FH-OFDMA," in *IEEE International Conference on Communications*, vol. 1, pp. 269–273, 20-24 June 2004.

[511] H. H. Chen, Y. C. Yeh, C. H. Tsai, and W. H. Chang, "Uplink synchronisation control technique and its environment-dependent performance analysis," *Electronics Letters*, vol. 39, pp. 1755–1757, November 2003.

[512] J.-J. V. D. Beek, P. O. Börjesson, M.-L. Boucheret, D. Landström, J. M. Arenas, P. Ödling, C. Östberg, M. Wahlqvist, and S. K. Wilson, "A time and frequency synchronization scheme for multiuser OFDM," *IEEE Journal on Selected Areas in Communications*, vol. 17, pp. 1900–1914, November 1999.

[513] M. Pompili, S. Barbarossa, and G. B. Giannakis, "Channel-independent non-data aided synchronization of generalized multiuser OFDM," in *2001 IEEE International Conference on Acoustics, Speech, and Signal Processing (ICASSP '01)*, vol. 4, pp. 2341–2344, 7-11 May 2001.

[514] S. T. Wu and K. C. Chen, "Programmable multiuser synchronization for OFDM-CDMA," in *Proceedings of the IEEE 53rd Vehicular Technology Conference, 2001 (VTC 2001 Spring)*, vol. 2, pp. 830–834, 6-9 May 2001.

[515] S. Lipschutz and M. L. Lipson, *Schaum's Outline of Theory and Problems of Probability*. Schaum's Outline Series, USA: McGraw-Hill Inc., second ed., 2000.

[516] M. K. Simon, J. K. Omura, R. A. Scholtz, and B. K. Levitt, *Spread Spectrum Communications: Volume I, II, III*. Maryland, USA: Computer Science Press, 1985.

[517] A. Papoulis, *Probability, Random Variables, and Stochastic Processes*. New York, USA: McGraw-Hill, 2nd ed., 1984.

[518] J. Lee and K. B. Bae, “Numerically stable fast sequential calculation for projection approximation subspace tracking,” in *Proceedings of the 1999 IEEE International Symposium on Circuits and Systems*, vol. 3, pp. 484–487, 30 May–2 June 1999.

[519] H. Holma and A. Toskala, eds., *WCDMA for UMTS : Radio Access for Third Generation Mobile Communications*. John Wiley and Sons, Ltd., 2000.

[520] B. Yang, K. Letaief, R. Cheng, and Z. Cao, “Channel estimation for OFDM transmission in multipath fading channels based on parametric channel modeling,” *IEEE Transactions on Communications*, vol. 49, pp. 467–479, March 2001.

[521] J. Yang and M. Kaveh, “Adaptive eigensubspace algorithm for direction or frequency estimation and tracking,” *IEEE Transactions on Acoustics, Speech and Signal Processing*, vol. 36, pp. 241–251, 1988.

[522] S. L. Marple, *Digital spectral analysis with applications*. Englewood Cliffs, NJ, USA: Prentice Hall, 1987.

[523] D. Schafhuber, G. Matz, and F. Hlawatsch, “Adaptive prediction of time-varying channels for coded OFDM systems,” in *Proceedings of the IEEE International Conference on Acoustics, Speech, and Signal Processing*, vol. 3, pp. III–2549 – III–2552, May 2002.

[524] J. Xavier, V. A. N. Barroso, and J. M. F. Moura, “Closed-form correlative coding (CFC2) blind identification of MIMO channels: isometry fitting to second order statistics,” *IEEE Transactions on Signal Processing*, vol. 49, pp. 1073–1086, May 2001.

[525] W. Nabhane and H. V. Poor, “Blind Joint Equalization and Multiuser Detection in Dispersive MC-CDMA/MC-DS-CDMA/MT-CDMA Channels,” in *Proceedings MILCOM 2002*, vol. 2, pp. 814–819, 7-10 October 2002.

[526] Y. Li, N. Seshadri, and S. Ariyavisitakul, “Channel Estimation for OFDM Systems With Transmitter Diversity in Mobile Wireless Channels,” *IEEE Journal on Selected Areas in Communications*, vol. 17, pp. 461–471, March 1999.

[527] H. Minn, D. I. Kim, and V. K. Bhargava, “A Reduced Complexity Channel Estimation for OFDM Systems With Transmit Diversity in Mobile Wireless channels,” *IEEE Transactions on Communications*, vol. 50, pp. 799–807, May 2002.

[528] F. W. Vook and T. A. Thomas, “MMSE Multi-user Channel Estimation for Broadband Wireless Communications,” in *IEEE Global*

Telecommunications Conference, 2001 (GLOBECOM '01), vol. 1, (San Antonio, USA), pp. 470–474, 25-29 November 2001.

[529] K. J. Kim and R. A. Iltis, "Joint Detection and Channel Estimation Algorithms for QS-CDMA Signals Over Time-varying Channels," *IEEE Transactions on Communications*, vol. 50, pp. 845–855, May 2002.

[530] F. Horlin and L. V. D. Perre, "Optimal Training Sequences for Low Complexity ML Multi-channel Estimation in Multi-user MIMO OFDM-based Communications," in *2004 IEEE International Conference on Communications*, vol. 4, pp. 2427–2431, 20-24 June 2004.

[531] T. Cui and C. Tellambura, "Joint channel estimation and data detection for OFDM systems via sphere decoding," in *IEEE Global Telecommunications Conference, 2004 (GLOBECOM '04)*, vol. 6, pp. 3656–3660, 29 November-3 December 2004.

[532] H. Zhu, B. Farhang-Boroujeny, and C. Schlegel, "Pilot Embedding for Joint Channel Estimation and Data Detection in MIMO Communication Systems," *IEEE Communications Letters*, vol. 7, pp. 30–32, January 2003.

[533] J. Wang and K. Araki, "Pilot-symbol Aided Channel Estimation in Spatially Correlated Multiuser MIMO-OFDM Channels," in *Proceedings of the IEEE 60th Vehicular Technology Conference, 2004 (VTC 2004 Fall)*, vol. 1, pp. 33–37, 26-29 September 2004.

[534] J. Siew, J. Coon, R. J. Piechocki, A. Dowler, A. Nix, M. A. Beach, S. Armour, and J. McGeehan, "A channel estimation algorithm for MIMO-SCFDE," *IEEE Communications Letters*, vol. 8, pp. 555–557, September 2004.

[535] S. Chen and Y. Wu, "Maximum likelihood joint channel and data estimation using genetic algorithms," *IEEE Transactions on Signal Processing*, vol. 46, pp. 1469–1473, May 1998.

[536] Y. S. Zhang, Y. Du, W. Zhang, X. Z. Wang, and J. Li, "A data-aided time domain channel estimation method," in *Proceedings of the 2004 Joint Conference of the 10th Asia-Pacific Conference on Communications and the 5th International Symposium on Multi-Dimensional Mobile Communications*, vol. 1, pp. 469–473, 29 August-1 September 2004.

[537] C. E. Tan and I. J. Wassell, "Near-optimum training sequences for OFDM systems," in *The 9th Asia-Pacific Conference on Communications (APCC 2003)*, vol. 1, pp. 119–123, 21-24 September 2003.

[538] K. Yen and L. Hanzo, “Genetic-algorithm-assisted multiuser detection in asynchronous CDMA communications,” *IEEE Transactions on Vehicular Technology*, vol. 53, pp. 1413–1422, September 2004.

[539] X. Wu, T. C. Chuah, B. S. Sharif, and O. R. Hinton, “Adaptive robust detection for CDMA using a genetic algorithm,” *IEE Proceedings - Communications*, vol. 150, pp. 437–444, 10 December 2003.

[540] J. Akhtman and L. Hanzo, “Reduced-Complexity Maximum-Likelihood Detection in Multiple-Antenna-Aided Multicarrier Systems,” in *Proceedings of the 5th International Workshop on Multi-Carrier Spread Spectrum Communications*, (Oberpfaffenhofen, Germany), 14-16 September 2005. Available at http://www.ecs.soton.ac.uk/˜mj02r/t/mcss-05.pdf.

[541] J. Akhtman and L. Hanzo, “Novel Optimized-Hierarchy RSA-aided Space-Time Processing Method,” Mobile VCE Core 3 Programme - Wireless Enablers 2.2: ICR-WE2.2.1, University of Southampton, Southampton, UK, May 2005.

[542] N. Seshadri, “Joint data and channel estimation using blind trellis search techniques,” *IEEE Transactions on Communications*, vol. 42, pp. 1000–1011, February-April 1994.

[543] R. Raheli, A. Polydoros, and C. K. Tzou, “Per-Survivor Processing: a general approach to MLSE in uncertain environments,” *IEEE Transactions on Communications*, vol. 43, pp. 354–364, February-April 1995.

[544] R. L. Haupt and S. E. Haupt, *Practical Genetic Algorithms*. New Jersey, USA: John Wiley & Sons, Ltd, 2nd ed., 2004. ISBN 0-471-45565-2.

[545] Z. Michalewicz, *Genetic Algorithms + Data Structures = Evolution Programs*. New York, USA: Springer-Verlag, 2nd ed., 1994.

[546] T. K. Moon and W. C. Stirling, *Mathematical Methods and Algorithms for Signal Processing*. Prentice Hall, 2002.

[547] S. Kay, *Fundamentals of Statistical Signal Processing, Estimation Theory*. New Jersey, USA: Prentice Hall, 1993.

[548] L. Hanzo, M. Munster, B. J. Choi, and T. Keller, *OFDM and MC-CDMA for Broadband Multi-User Communications, WLANs and Broadcasting*. IEEE Press, 2003.

[549] U. Fincke and M. Pohst, “Improved method for calculating vector of short length in a lattice, including a complexity analysis,” in *Math. Comput.*, vol. 44, pp. 463–471, April 1985.

[550] E. Viterbo and J. Boutros, “A universal lattice code decoder for fading channels,” *IEEE Transactions on Information Theory*, vol. 45, pp. 1639–1642, July 1999.

[551] A. M. Chan and I. Lee, “A new reduced-complexity sphere decoder for multiple antenna systems,” *Communications, 2002. ICC 2002. IEEE International Conference on*, vol. 1, pp. 460–464, April 2002.

[552] K. Su and I. J. Wassell, “A new ordering for efficient sphere decoding,” in *Communications, 2005. ICC 2005. 2005 IEEE International Conference on*, vol. 3, pp. 1906–1910, May 2005.

[553] D. Pham, K. R. Pattipati, P. K. Willett, and J. Luo, “An improved complex sphere decoder for v-BLAST systems,” *IEEE Signal Processing Letters*, vol. 11, pp. 748–751, Sept. 2004.

[554] Q. Liu and L. Yang, “A novel method for initial radius selection of sphere decoding,” *2004. VTC2004-Fall. 2004 IEEE 60th Vehicular Technology Conference*, vol. 2, pp. 1280–1283, Sept. 2004.

[555] Z. Guo and P. Nilsson, “Algorithm and implementation of the K-best sphere decoding for MIMO detection,” *IEEE Journal on Selected Areas in Communications*, vol. 24, pp. 491–503, Mar. 2006.

[556] K. Wong, C. Tsui, R. Cheng, and W. Mow, “A VLSI architecture of a K-best lattice decoding algorithm for MIMO channels,” *IEEE International Symposium on Circuits and Systems, 2002. ISCAS 2002.*, vol. 3, May 2002.

[557] J. Pons and P. Duvaut, “New approaches for lowering path expansion complexity of k-best MIMO detection algorithms,” in *Communications, 2009. ICC ’09. IEEE International Conference on*, (Dresden), pp. 1–6, June 2009.

[558] B. Kim, H. Kim, and K. Choi, “An adaptive k-best algorithm without SNR estimation for MIMO systems,” in *Vehicular Technology Conference, 2008. VTC Spring 2008. IEEE*, (Singapore), pp. 817–821, May 2008.

[559] B. M. Hochwald and S. ten Brink, “Achieving near-capacity on a multiple-antenna channel,” *IEEE Transactions on Communications*, vol. 51, pp. 389–399, Mar. 2003.

[560] M. Pohst, “On the Computation of Lattice Vectors of Minimal Length, Successive Minima and Reduced Bases With Applications,” *Proc. ACMSIGSAM*, pp. 37–44, 1981.

[561] U. Fincke and M. Pohst, “Improved methods for calculating vectors of short length in a lattice, including a complexity analysis,” *Mathematics of Computation*, vol. Vol. 44, pp. 463–471, April 1985.

[562] M. O. Damen, K. Abed-Meraim, and J. C. Belfiore, “Generalised sphere decoder for asymmetrical space-time communication architecture,” *Electronics Letters*, vol. 36, pp. 166–167, Jan. 2000.

[563] T. Cui and C. Tellambura, “An efficient generalized sphere decoder for rank-deficient MIMO systems,” *2004. VTC2004-Fall. 2004 IEEE 60th Vehicular Technology Conference*, vol. 5, pp. 3689–3693, Sept. 2004.

[564] M. O. Damen, K. Abed-Meraim, and M. S. Lemdani, “Further results on the sphere decoder,” *Proceedings. 2001 IEEE International Symposium on Information Theory, 2001.*, June 2001.

[565] J. Li and Y. Yang, “Ordered sphere detector for high rate spatial multiplexing architecture,” *Emerging Technologies: Frontiers of Mobile and Wireless Communication, 2004. Proceedings of the IEEE 6th Circuits and Systems Symposium on*, vol. 2, pp. 417–420, May 2004.

[566] O. Damen, A. Chkeif, and J. C. Belfiore, “Lattice code decoder for space-time codes,” *IEEE Communications Letters*, vol. 4, pp. 161–163, May 2000.

[567] G. D. Golden, C. J. Foschini, R. A. Valenzuela, and P. W. Wolniansky, “Detection algorithm and initial laboratory results using v-BLAST space-time communication architecture,” *Electronics Letters*, vol. 35, pp. 14–16, Jan. 1999.

[568] J. Akhtman and L. Hanzo, “An optimized-hierarchy-aided maximum likelihood detector for MIMO-OFDM,” *2006. VTC 2006-Spring. IEEE 63rd Vehicular Technology Conference*, vol. 3, pp. 1526–1530, 2006.

[569] C. Berrou, A. Glavieux, and P. Thitimajshima, “Near shannon limit error-correcting coding and decoding: Turbo-codes. 1,” in *Communications, 1993. ICC 93. Geneva. Technical Program, Conference Record, IEEE International Conference on*, vol. 2, (Geneva), pp. 1064–1070, May 1993.

[570] C. Berrou and A. Glavieux, “Near optimum error correcting coding and decoding: turbo-codes,” *IEEE Transactions on Communications*, vol. 44, pp. 1261–1271, Oct. 1996.

[571] S. Benedetto, D. Divsalar, G. Montorsi, and F. Pollara, “Analysis, design, and iterative decoding of double serially concatenated codes with interleavers,” *IEEE Journal on Selected Areas in Communications*, vol. 16, pp. 231–244, Feb. 1998.

[572] J. Li, K. B. Letaief, and Z. Cao, “Space-time turbo multiuser detection for coded MC-CDMA,” *IEEE Transactions on Wireless Communications*, vol. 4, pp. 538–549, March 2005.

[573] L. Hanzo, C. H. Wong, and M. S. Yee, *Adaptive Wireless Transceivers*. IEEE Press, 2002.

[574] S. Baro, J. Hagenauer, and M. Witzke, "Iterative detection of MIMO transmission using a list-sequential (LISS) detector," *Communications, 2003. ICC '03. IEEE International Conference on*, vol. 4, pp. 2653–2657, May 2003.

[575] M. S. Yee, "Max-log-MAP sphere decoder," *Acoustics, Speech, and Signal Processing, 2005. Proceedings. (ICASSP '05). IEEE International Conference on*, vol. 3, Mar. 2005.

[576] L. Xu, S. Tan, S. Chen, and L. Hanzo, "Iterative minimum bit error rate multiuser detection in multiple antenna aided OFDM," *2006. WCNC 2006. IEEE Wireless Communications and Networking Conference*, vol. 3, pp. 1603–1607, Apr. 2006.

[577] J. Wang, S. X. Ng, L. L. Yang, and L. Hanzo, "Combined serially concatenated codes and MMSE equalization: An EXIT chart aided perspective," *Vehicular Technology Conference, 2006. VTC-2006 Fall. 2006 IEEE 64th*, pp. 1–5, Sept. 2006.

[578] J. Wang, S. X. Ng, A. Wolfgang, L. L. Yang, S.Chen, and L. Hanzo, "Near-Capacity Three-Stage MMSE Turbo Equalization Using Irregular Convolutional Codes," *in the 4th International Symposium on Turbo Codes in connection with 6th International ITG-Conference on Source and Channel Coding / ISTC'06, Munich, Germany*, April 2006.

[579] J. Kliewer, S. X. Ng, and L. Hanzo, "Efficient computation of exit functions for non-binary iterative decoding," *IEEE Transactions on Communications*, vol. 54, pp. 2133–2136, Dec. 2006.

[580] J. Kliewer, A. Huebner, and D. J. Costello, "On the achievable extrinsic information of inner decoders in serial concatenation," in *Proceedings of the IEEE International Symposium on Information Theory*, (Seattle, WA, USA), pp. 2680–2684, July 2006.

[581] S. X. Ng, J. Wang, and L. Hanzo, "Unveiling near-capacity code design: The realization of shannon's communication theory for mimo channels," *IEEE International Conference on Communications, 2008*, pp. 1415–1419, May 2008.

[582] M. Tüchler and J. Hagenauer, "Exit charts of irregular codes," *in Proceedings of Conference on the Information Science and Systems [CDROM], Princeton University*, pp. 20–22, March 2002.

[583] M. Tüchler, "Design of serially concatenated systems depending on the block length," *IEEE Transactions on Communications*, vol. 52, pp. 209–218, Feb. 2004.

[584] R. W. Heath and A. J. Paulraj, "Switching between diversity and multiplexing in MIMO systems," *IEEE Transactions on Communications*, vol. 53, pp. 962–968, June 2005.

[585] J. H. Conway and N. J. A. Sloane, *Sphere Packings, Lattices and Groups*. third edition, Springer-Verlag, 1999.

[586] W. F. Su, Z. Safar, and K. J. R. Liu, "Space-time signal design for time-correlated Rayleigh fading channels," *IEEE International Conference on Communications 2003.*, vol. 5, pp. 3175–3179, May 2003.

[587] S. M. Alamouti, "A simple transmit diversity technique for wireless communications," *IEEE Journal on Selected Areas in Communications*, vol. 16, pp. 1451–1458, Oct. 1998.

[588] V. Tarokh, H. Jafarkhani, and A. R. Calderbank, "Space-time block codes from orthogonal designs," *IEEE Transactions on Information Theory*, vol. 45, pp. 1456–1467, July 1999.

[589] W. Su and X. G. Xia, "On space-time block codes from complex orthogonal designs," *Wirel. Pers. Commun.*, vol. 25, pp. 1–26, apr 2003.

[590] A. F. Naguib, N. Seshadri, and A. R. Calderbank, "Applications of space-time block codes and interference suppression for high capacity and high data rate wireless systems," *The Thirty-Second Asilomar Conference on Signals, Systems & Computers*, vol. 2, pp. 1803–1810, Nov. 1998.

[591] X.-B. Liang and X.-G. Xia, "On the nonexistence of rate-one generalized complex orthogonal designs," *IEEE Transactions on Information Theory*, vol. 49, pp. 2984–2988, Nov. 2003.

[592] O. R. Alamri, B. L. Yeap, and L. Hanzo, "A turbo detection and sphere-packing-modulation-aided space-time coding scheme," *IEEE Transaction on Vehicular Technology*, vol. 56, pp. 575–582, Mar. 2007.

[593] M. El-Hajjar, "Multi-functional MIMO schemes employing iterative detected multi-dimensional sphere packing modulation," *Mini Thesis submitted in partial fulfilment of the requirements for the award of Doctor of Philosophy at University of Southampton*, Aug. 2007.

[594] S. ten Brink, "Convergence behavior of iteratively decoded parallel concatenated codes," *IEEE Transactions on Communications*, vol. 49, pp. 1727–1737, Oct. 2001.

[595] L. Hanzo, L.-L. Yang, E.-L. Kuan, and K. Yen, *Single and Multi-Carrier DS-CDMA: Multi-User Detection, Space-Time Spreading, Synchronisation, Networking and Standards*. Wiley-IEEE Press, 2003.

[596] G. J. Foschini and M. J. Gans, “On limits of wireless communications in a fading environment when using multiple antennas,” *Wireless Personal Communications*, vol. 6, pp. 311–335, Mar. 1998.

[597] J. N. Laneman, D. N. C. Tse, and G. W. Wornell, “Cooperative diversity in wireless networks: Efficient protocols and outage behavior,” *IEEE Transaction on Information Theory*, vol. 50, pp. 3062–3080, Dec. 2004.

[598] L. Hanzo, O. Alamri, M. El-Hajjar, and N. Wu, *Near-Capacity Multi-Functional MIMO Systems: sphere-packing, iterative detection, and cooperation*. First Edition, John Wiley & Sons Ltd, 2009.

[599] L. Lampe, R. Schober, V. Pauli, and C. Windpassinger, “Multiple-symbol differential sphere decoding,” *IEEE Transactions on Communications*, vol. 12, pp. 1981–1985, Dec. 2005.

[600] V. Pauli, L. Lampe, and R. Schober, ““Turbo DPSK” using soft multiple-symbol differential sphere decoding,” *IEEE Transactions on Information Theory*, vol. 52, pp. 1385–1398, April 2006.

[601] V. Pauli, L. Lampe, and J. Huber, “Differential space-frequency modulation and fast 2-d multiple-symbol differential detection for MIMO-OFDM,” *IEEE Transactions on Vehicular Technology*, vol. 57, pp. 297–310, Jan. 2008.

[602] V. Pauli and L. Lampe, “Multiple-symbol differential sphere decoding for unitary space-time modulation,” *IEEE Global Telecommunications Conference*, vol. 3, p. 6, Nov. 2005.

[603] D. Divsalar and M. K. Simon, “Multiple-symbol differential detection of mpsk,” *IEEE Transaction on Communications*, vol. 38, pp. 300–308, March 1900.

[604] D. Divsalar and M. K. Simon, “Maximum-likelihood differential detection of uncoded and trellis-coded amplitude phase modulation over awgn and fading channels–metrics and performance,” *IEEE Transaction on Communications*, vol. 42, pp. 76–89, Jan. 1994.

[605] M. O. Damen, H. E. Gamal, and G. Caire, “On maximum-likelihood detection and the search for the closest lattice point,” *IEEE Transactions on Information Theory*, vol. 49, pp. 2389–2402, Oct. 2003.

[606] T. Himsoon, W. Su, and K. J. R. Liu, “Differential transmission for amplify-and-forward cooperative communications,” *IEEE Signal Processing Letters*, vol. 12, pp. 597–600, Sept. 2005.

[607] T. Himsoon, W. P. Siriwongpairat, W. Su, and K. J. R. Liu, “Differential modulation with threshold-based decision combining for cooperative

communications," *IEEE Transaction on Signal Processing*, vol. 55, pp. 3905–3923, July 2007.

[608] T. S. Rappaport, *Wireless Communications Principles and Practise*. Pearson Education Asia Limited and Publishing House of Electronics Industry, second ed., 2002.

[609] M. K. Simon and M. S. Alouini, "A unified approach to the probability of error for noncoherent and differentially coherent modulations over generalized fading channels," *IEEE Transactions on Communications*, vol. 46, pp. 1625–1638, Dec. 1998.

[610] T. Himsoon, W. P. Siriwongpairat, W. Su, and K. J. R. Liu, "Differential modulations for multinode cooperative communications," *IEEE Transactions on Signal Processing*, vol. 56, pp. 2941–2956, July 2008.

[611] I. S. Gradshteyn and I. M. Ryzhik, *Table of Integrals, Series, and Products*. Seventh Edition, Springer-Verlag, 2007.

[612] Q. T. Zhang and X. W. Cui, "A closed-form expression for the symbol-error rate of M-ary DPSK in fast rayleigh fading," *IEEE Transaction on Communications*, vol. 53, pp. 1085–1087, July 2005.

[613] S. X. Ng, Y. Li, and L. Hanzo, "Distributed turbo trellis coded modulation for cooperative communications," in *Communications, 2009. ICC '09. IEEE International Conference on*, (Dresden), pp. 1–5, June 2009.

[614] K. Lee and L. Hanzo, "Iterative detection and decoding for hard-decision forwarding aided cooperative spatial multiplexing," in *Communications, 2009. ICC '09. IEEE International Conference on*, (Dresden), pp. 1–5, June 2009.

[615] T. L. Marzetta and B. M. Hochwald, "Capacity of a mobile multiple-antenna communication link in rayleigh flat fading," *IEEE Transactions on Information Theory*, vol. 45, pp. 139–157, Jan. 1999.

[616] L. Z. Zheng and D. N. C. Tse, "Communication on the grassmann manifold: a geometric approach to the noncoherent multiple-antenna channel," *IEEE Transactions on Information Theory*, vol. 48, pp. 359–383, Feb. 2002.

[617] Y. Liang and V. V. Veeravalli, "Capacity of noncoherent time-selective rayleigh-fading channels," *IEEE Transactions on Information Theory*, vol. 50, pp. 3095–3110, Dec. 2004.

[618] T. M. Cover and J. A. Thomas, *Elements of Information Theory*. Second Edition, John Wiley & Sons, Inc., 2006.

[619] R. R. Chen, R. Koetter, U. Madhow, and D. Agrawal, “Joint noncoherent demodulation and decoding for the block fading channel: a practical framework for approaching shannon capacity,” *IEEE Transactions on Communications*, vol. 51, pp. 1676–1689, Oct. 2003.

[620] A. Ashikhmin, G. Kramer, and S. ten Brink, “Extrinsic information transfer functions: model and erasure channel properties,” *IEEE Transactions on Information Theory*, vol. 50, pp. 2657–2673, Nov. 2004.

[621] B. Zhao and M. C. Valenti, “Distributed turbo coded diversity for relay channel,” *Electronics Letters*, vol. 39, pp. 786–787, May 2003.

[622] J. Kliewer, A. Huebner, and D. J. Costello, “On the achievable extrinsic information of inner decoders in serial concatenation,” in *Information Theory, 2006 IEEE International Symposium on*, (Seattle, WA), pp. 2680–2684, July 2006.

[623] Y. Fan, C. Wang, J. Thompson, and H. V. Poor, “Recovering multiplexing loss through successive relaying using repetition coding,” *IEEE Transactions on Wireless Communications*, vol. 6, pp. 4484–4493, Dec. 2007.

[624] T. Moon and W. Stirling, *Mathematical Methods and Algorithms for Signal Processing.* Prentice Hall, 2000.

[625] P. W. Wolniansky, G. J. Foschini, G. D. Golden, and R. A. Valenzuela, “V-BLAST: An architecture for realizing very high data rates over the rich scattering wireless channels,” in *Proceedings of the IEEE ISSSE-98*, (Pisa, Italy), September 1998. Invited Paper.

[626] A. Bhargave, R. Figueiredo, and T. Eltoft, “A Detection Algorithm for the V-BLAST System,” in *Proceedings of Global Telecommunications Conference*, vol. 1, (San Antonio, Texas, USA), pp. 494–498, IEEE, November 25-29 2001.

[627] L. Hanzo, L.-L. Yang, E.-L. Kuan, and K. Yen, *Single- and Multi-Carrier DS-CDMA.* John Wiley and IEEE Press, 2003. 430 pages.

[628] X. F. Wang, W. S. Lu, and A. Antoniou, “A genetic algorithm-based multiuser detector for multiple-access communications,” in *IEEE International Symposium on Circuits and System – ISCAS’98*, (Monterey, California, USA), pp. 534–537, 1998.

[629] R. Wang and G. Giannakis, “Approaching MIMO channel capacity with reduced-complexity soft sphere decoding,” in *Proceedings of IEEE Wireless Communications and Networking Conference*, vol. 3, pp. 1620–1625, 21-25 March 2004.

[630] J. E. Gentle, *Numerical Linear Algebra for Applications in Statistics*. Berlin: Springer-Verlag, 1998.

[631] M. K. Varanasi, “Decision feedback multiuser detection: A systematic approach,” *IEEE Transactions on Information Theory*, vol. 45, pp. 219–240, January 1999.

[632] G. Valiente, *Algorithms on Trees and Graphs*. New York: Springer, 2002.

[633] A. Viterbi, *CDMA: Principles of Spread Spectrum Communication*. Reading MA, USA: Addison-Wesley, June 1995. ISBN 0201633744.

[634] R. D. Schafer, *An Introduction to Nonassociative Algebras*. New York: Dover, 1996.

[635] J. Hagenauer, E. Offer, and L. Papke, “Iterative decoding of binary block and convolutional codes,” *IEEE Transactions on Information Theory*, vol. 42, pp. 429–445, March 1996.

[636] C. Berrou and A. Glavieux, “Near optimum error-correcting coding and decoding: Turbo codes,” *IEEE Transactions on Communications*, vol. 44, pp. 1261–1271, October 1996.

[637] C. Berrou, “Some Clinical Aspects of Turbo Codes,” in *Proceedings of the International Symposium on Turbo Codes & Related Topics*, (Brest, France), pp. 26–31, 3-5 September 1997.

[638] S. Benedetto, R. Garello, and G. Montorsi, “A search for good convolutional codes to be used in the construction of turbo codes,” *IEEE Transactions on Communications*, vol. 46, pp. 1101–1105, September 1998.

[639] G. Battail, “A conceptual framework for understanding turbo codes,” *IEEE Journal on Selected Areas in Communications*, vol. 16, no. 2, pp. 245–254, 1998.

[640] O. Açikel and W. Ryan, “Punctured turbo-codes for BPSK/QPSK channels,” *IEEE Transactions on Communications*, vol. 47, pp. 1315–1323, September 1999.

[641] IEEE LAN/MAN Standards Committee, *Wireless LAN Medium Access Control (MAC) and Physical Layer (PHY) specifications*, IEEE 802.11g ed., 2003.

[642] H. Vikalo, B. Hassibi, and T. Kailath, “Iterative decoding for MIMO channels via modified sphere decoding,” *IEEE Transactions on Wireless Communications*, vol. 3, pp. 2299–2311, Nov. 2004.

[643] T. Bäck, *Evolutionary Algorithms in Theory and Practice: Evolution Strategies, Evolutionary Programming, Genetic Algorithms*. New York, USA: Oxford University Press, 1996.

[644] D. B. Fogel, "An Introduction to Simulated Evolutionary Optimization," *IEEE Transactions on Neural Networks*, vol. 5, pp. 3–14, January 1994.

[645] S. Haykin, *Neural Networks*. Prentice Hall, second ed., 1999.

[646] L. Fausett, *Fundamentals of Neural Networks: Architectures, Algorithms and Applications*. Prentice-Hall, 1994.

[647] V. W. Porto and D. B. Fogel, "Alternative Neural Network Training Methods," *IEEE Expert*, vol. 10, pp. 16–22, June 1995.

[648] K. Chellapilla and D. Fogel, "Evolving an expert checkers playing program without using human expertise," *IEEE Transactions on Evolutionary Computation*, vol. 5, pp. 422–428, August 2001.

[649] G. Kechriotis, E. Zervas, and E. S. Manolakos, "Using Recurrent Neural Networks for Adaptive Communication Channel Equalization," *IEEE Transactions on Neural Networks*, vol. 5, pp. 267–278, March 1994.

[650] R. Parisi, E. D. D. Claudio, G. Orlandi, and B. D. Rao, "Fast Adaptive Digital Equalization by Recurrent Neural Networks," *IEEE Transactions on Signal Processing*, vol. 45, pp. 2731–2739, November 1997.

[651] M. D. Buhmann, *Radial Basis Functions: Theory and Implementations*. Cambridge University Press, 2003.

[652] P. V. Yee and S. Haykin, *Regularized Radial Basis Function Networks: Theory and Applications*. USA: John Wiley & Sons Ltd., 2001.

[653] U. Mitra and H. V. Poor, "Neural network techniques for adaptive multiuser demodulation," *IEEE Journal on Selected Areas in Communications*, vol. 12, pp. 1460–1470, December 1994.

[654] K. Ko, S. Choi, C. Kang, and D. Hong, "RBF multiuser detector with channel estimation capability in a synchronous MC-CDMA system," *IEEE Transactions on Neural Networks*, vol. 12, pp. 1536–1539, November 2001.

[655] C. Ahn and I. Sasase, "Adaptive array antenna based on radial basis function network as multiuser detection for WCDMA," *Electronics Letters*, vol. 38, pp. 1208–1210, September 2002.

[656] H. Wei and L. Hanzo, "Reduced-Complexity Genetic Algorithm Aided and Radial Basis Function Assisted Multiuser Detection for Synchronous

CDMA," in *Proceedings of European Signal Processing Conference (EUSIPCO) 2004*, (Vienna, Austria), pp. 157–160, September 2004.

[657] X. Zhou and X. Wang, "Channel Estimation for OFDM Systems Using Adaptive Radial Basis Function Networks," *IEEE Transactions on Vehicular Technology*, vol. 52, pp. 48–59, January 2003.

[658] G. Charalabopoulos, P. Stavroulakis, and A. H. Aghvami, "A frequency-domain neural network equalizer for OFDM," in *IEEE Global Telecommunications Conference 2003 (GLOBECOM '03)*, vol. 2, pp. 571–575, 1-5 December 2003.

[659] S. Lerkvaranyu, K. Dejhan, and Y. Miyanaga, "M-QAM demodulation in an OFDM system with RBF neural network," in *The 2004 47th Midwest Symposium on Circuits and Systems (MWSCAS '04)*, vol. 2, pp. II–581–II–584, 25-28 July 2004.

[660] T. Cui and C. Tellambura, "Channel estimation for OFDM systems based on adaptive radial basis function networks," in *Proceedings of the IEEE 60th Vehicular Technology Conference, 2004 (VTC 2004 Fall)*, vol. 1, (New Orleans, USA), pp. 608–611, 26-29 September 2004.

[661] S. Chen, A. K. Samingan, B. Mulgrew, and L. Hanzo, "Adaptive minimum-BER linear multiuser detection for DS-CDMA signals in multipath channels," *IEEE Transactions on Signal Processing*, vol. 49, pp. 1240–1247, June 2001.

[662] H. Mühlenbein, *Foundations of Genetic Algorithms*. California, USA: G. Rawlins, ed., Morgan Kaufmann, 1991.

[663] J. J. Grefenstette and J. E. Baker, "How Genetic Algorithms Work: A critical look at implicit parallelism," in *Proceedings of the Third International Conference on Genetic Algorithms* (J. D. Schaffer, ed.), (California, USA), pp. 20–27, Morgan Kaufmann, 1989.

[664] B. L. Miller and D. E. Goldberg, "Genetic Algorithms, Selection Schemes and the Varying Effects of Noise," *Evolutionary Computation*, vol. 4, pp. 113–131, Summer 1996.

[665] L. J. Eshelman and J. D. Schaffer, "Preventing premature convergence in Genetic Algorithms by preventing incest," in *Proceedings of the Fourth International Conference on Genetic Algorithms* (R. K. Belew and L. B. Booker, eds.), (California, USA), pp. 115–122, Morgan Kaufmann, 1991.

[666] G. Syswerda, "Uniform Crossover in Genetic Algorithms," in *Proceedings of the Third International Conference on Genetic Algorithms* (J. D. Schaffer, ed.), (California, USA), pp. 2–9, Morgan Kaufmann, 1989.

AUTHOR QUERIES

Please reply to these questions on the relevant page of the proof;
please do not write on this page.

Q1 (page 493):
Please check all notation in the List of Symbols and throughout Part III is as intended